Brunel University London

C1q Classical complement pathway inhibition:

A novel strategy to dampen complement activation and inflammation in Alzheimer's disease

A thesis submitted for the degree of Doctor of Philosophy

By

Christianah Oluwadare

November 2018

Department of Life Sciences,

Brunel University London

Declaration

I hereby declare that the research presented in this thesis is my own work, except where otherwise specified, and has not been submitted for any other degree.

Christianah Oluwadare

ACKNOWLEDGEMENTS

I would like to thank God Almighty for His loving kindness towards me and my family throughout this project. I am forever grateful for His grace and favour.

I would like to thank Dr. Kishore for affording me the opportunity to undertake this project within his group and for his guidance on this project. I would also like to thank Dr Pathan for his patient teaching. I would like to thank Dr Eswari Marri, Dr Terry Roberts, Dr Mat Themis, Dr Christina Sisu, Dr Magdalena Sastre and Professor Kevin O'Byrne for teaching me the techniques necessary to test the hypotheses and carry out the analysis. Finally, I would like to thank Professor Guy Brown for providing me with BV-2 cells without which I could not have completed this project.

To my family, words cannot express my gratitude towards you. Mum, thank you for being such a wonderful mother. You made so many sacrifices, dried up my many tears, never let me give up. You kept me in your constant prayers, even as you were always supportive and encouraging. I will never forget all the times you drove me there and back, and all the late nights and weekends we spent in Uxbridge, while I was trying to conduct an experiment. I only hope I can be a fraction of the mother you are one day. To my brothers and sister thank you for all the support and encouragement. Thank you for all the conversations and the jokes that cheered me up. I'm lucky to have such a wonderful mischievous bunch of siblings. Thanks for the support Dad. I love you all very much.

Finally, to my friends Raguez, Ranya, Goshan, Haroon, Temi, Juhi, Ezgi, Shamoose, Stefan and Sheila. You made this experience entertaining and kept me laughing. You were always there for me, and ready to drop everything at a moment's notice. I will forever be grateful.

ABSTRACT

Alzheimer's disease (AD) is a neurological disorder characterised by memory loss and which affects millions over the age of 65. Due to its multifactorial causality, it has proved difficult to find a cure. The primary pathological hallmark of the disorder is the deposition and impaired clearance of extracellular Amyloid-beta plaques. This in turn triggers a cascade of events such as neuronal loss, chronic neuroinflammation and brain atrophy, which manifest behaviorally as memory loss, and will eventually culminate in death. One promising avenue for future therapeutic benefit is the study of neuro-inflammatory effectors; in particular, the complement system, and its primary recognition subcomponent C1q (composed of the globular heads ghA, ghB and ghC). The complement system is a part of the innate immune system that enhances the body's ability to remove pathogens and aberrant proteins. Once activated, the complement system acts to maintain homeostatic balance within the neuronal milieu by pathogen recognition, opsonisation, inflammatory stimulation, and direct apoptosis through the membrane attack complex of the classical complement pathway. An activated complement system has been implicated in the perpetuation of the chronic inflammatory state observed in AD. C1q the main recognition component binds to Aβ and triggers a whole cascade of events including the activation of the classical complement pathway. which results in the recruitment of microglia and the secretion of inflammatory cytokines. An exaggerated or insufficient activation of the complement system contributes towards the perpetuation of neurotoxicity and neuroinflammation. In this study we cloned mutant homotrimeric forms of the globular heads which are capable of binding to Aβ, but incapable of activating the CCP. We assessed their ability to bind to Aβ via ELISA, and their ability to inhibit complement mediated haemolysis. The homotrimers ghA_3, ghB_3 and ghC_3 bound to Aβ and protected against CCP induced haemolysis in a dose dependent manner. We further demonstrated a downregulation in the mRNA and protein expression of inflammatory mediators via qPCR and western blot post globular head treatment. Finally, we assessed the BV-2 transcriptome post ghB^3 treatment and observed an initial upregulation in the expression of inflammatory genes which was severely downregulated 12 hrs post treatment. Indicating that inhibition of the CCP leads to a faster post inflammatory recovery and therefore may be useful towards the prevention of chronic inflammation.

CONTENTS

Table of Contents

ABBREVIATIONS

Á	Angstrom (Unit Length)
A_{280}	Absorbance at 280 nm
A_{405}	Absorbance at 405 nm
A_{450}	Absorbance at 450 nm
ACh	Acetylcholine
AChE	Acetylcholinesterase
AD	Alzheimer's disease
AICD	APP intracellular domain
APOE	Apolipoprotein E
APP	Amyloid Precursor Protein
Aβ	Amyloid Beta
Aβ40	Amyloid Beta 1-40aa
Aβ42	Amyloid Beta 1-42aa
BACE1	B Secretase 1
BL21	Strain of Escherichia coli (Bacteria)
BSA	Bovine Serum Albumin
BSA	Bovine Serum Albumin
BuChE	Butyrylcholinesterase
C	Complement Component
C-terminal	Carboxyl-terminal
C1q	First Subcomponent of the Classical Complement Pathway
C1q-/-	C1q nul/ Knockout mice
C4BP	C4 binding protein
CH50	The 50% Haemolytic Complement Activity of Serum
CLR	Collagen Like Region
CNS	Central nervous system
COX	Cyclooxygenase
DAB	Diaminobenzidine peroxidase
DAMPs	Danger Associated Molecular Patterns
DEAE	Diethylaminoethanol
DGVB++	Dextrose Gelatin Veronal Buffer

DNA	Deoxyribonucleic acid
DPBS	Dulbecco's Phosphate Buffered Saline
DRG	Dorsal root Ganglion
E	Erythrocytes
E. coli	Escherichia coli (Bacteria)
EA	Antibody Sensitised erythrocytes
ELISA	Enzyme –Linked Immunosorbent Assay
Fc region	Fragment Crystallisable region of IgG
gC1q	Globular Head Region of the C1q Molecule
ghA	C1q Globular Head A
ghA_3	C1q Globular Head A containing SPD neck segment designed to multimerise
ghB	C1q Globular Head B
ghB_3	C1q Globular Head B containing SPD neck segment designed to multimerise
ghC	C1q Globular Head C
ghC_3	C1q Globular Head C containing SPD neck segment designed to multimerise
GWAS	Genome wide association studies
HRP	Horseradish Peroxidase
I- κB	Inhibitor of NF-κB
IgG	Immunoglobin G
IgM	Immunoglobin M
IKK	I- κB kinase
IL-1B	Interleukin-1B
iNOS	Inducible nitric oxide synthase
IPTG	Isopropyl β-D-1-thiogalactopyranoside (Reagent)
kDa	Kilo-Dalton (Unit of Mass)
KO	Knockout
LB	Luria Bertani Medium
LDL	Low Density Liporotein
LOAD	Late onset Alzheimer's disease
LPS	Lipopolysaccharide
LRP-1	Lipoprotein receptor related protein 1

MAPT	Microtubule associated protein tau
MBP	Maltose binding protein
MCI	Mild cognitive Impairment
mghA	Mouse C1q Globular Head A
mghB	Mouse C1q Globular Head B
mghC	Mouse C1q Globular Head C
NBM	Nucleus basilis of Meynert
NF-κB	Nuclear factor kappa-light-chain-enhancer of activated B cells
NFT	Neurofibrillary Tangles
NMDA	N-Methyl D aspartate receptors
NSAID	Non-steroidal anti-inflammatory drug
NSAIDs	Non-steroidal anti infllammatory drugs
PAMPs	Pathogen Associated Molecular Patterns
PBS	Phosphate Buffered Saline
PS1	Presenilin 1
PS2	Presenilin 2
RAGE	Receptor advanced glycation endproducts
RNA	Ribonucleic acid
TGFβ	Transforming growth factor beta
TLR	Toll like receptors
TNFα	Tumour necrosis factor alpha

LIST OF FIGURES

LIST OF TABLES

CHAPTER 1:

INTRODUCTION

1.1 Alzheimer's disease (AD)

From the development of the Smallpox vaccine, to the discovery of Penicillin in 1928, scientific research has led to the effective diagnosis, treatment and cure of diseases that previously killed millions. Due to numerous medical and technological advancements, the average global life expectancy has increased by approximately 23 years in the period between 1960 and 2015 (UN World Population prospects database, 2008). With this ever-increasing global population, and an increased average life -span for each individual compared with 100 years ago comes the advent of age-related diseases that would previously not be evident in the global population. One such age-related phenomenon is Dementia.

Dementia is a broad categorisation defining neurodegenerative diseases of which the principal observable symptom is severe memory loss. It can develop as a result of global brain insults such as brain injury, brain tumours, normal pressure hydrocephalus, chronic alcohol abuse, vitamin B12 deficiency; or as a secondary effect of other medical conditions such as Huntington's disease, Multiple sclerosis, HIV/AIDS, Lyme disease, Parkinson's disease, Pick's disease and Progressive supranuclear palsy. The cause of dementia determines whether the disease is static (non-progressive) or degenerative (progressive). However, most types of dementia such as Alzheimer's disease (AD), vascular dementia, dementia with Lewy bodies and frontotemporal dementia are degenerative.

1.2 History of Alzheimer's Disease

The psychiatrist and neuroscientist Alois Alzheimer first outlined the behavioural and histological hallmarks of this eponymous disorder. Alzheimer recorded the ante-mortem history of his 55-year-old patient Auguste Deter who presented with the behavioural symptoms of impaired memory, aphasia, social incompetence, disorientation and delusion (Ramirez-Bermudez 2012). Deter's cognitive functions further deteriorated with age. After her death in 1906, Alzheimer conducted post-mortem studies in order to identify the neuropathological causes of the patient's behavioural deficits. He identified what we now describe as amyloid β (Aβ) plaques and neurofibrillary tangles (NFT) in her brain and presented these findings later that year and termed the disease presenile dementia. (Zilka, Novak 2006).

1.3 Epidemiology

AD accounts for 60-70% of all dementia cases. Globally an estimated 35.6 million people were living with dementia in 2010, a number that is set to quadruple to 115.4 million by 2050 unless preventative, therapeutic strategies are developed (Brookmeyer et al., 2007). Most cases of AD occur sporadically i.e., there is no identifiable cause. However, age is the most significant risk factor for sporadic AD (**Fig. 1.1**). AD affects approximately 5% of people over the age of 65yrs. The prevalence of AD rises exponentially as the patient's age advances, increasing to approximately 35% in individuals over the age of 85 (Brookmeyer et al., 2002, Kamer et al., 2008, Reitz et al., 2011). Two out of every three AD sufferers are female, though the role Gender plays is as yet unidentified (Global Alzheimer's and Dementia Action Alliance (GADAA) in March 2017).

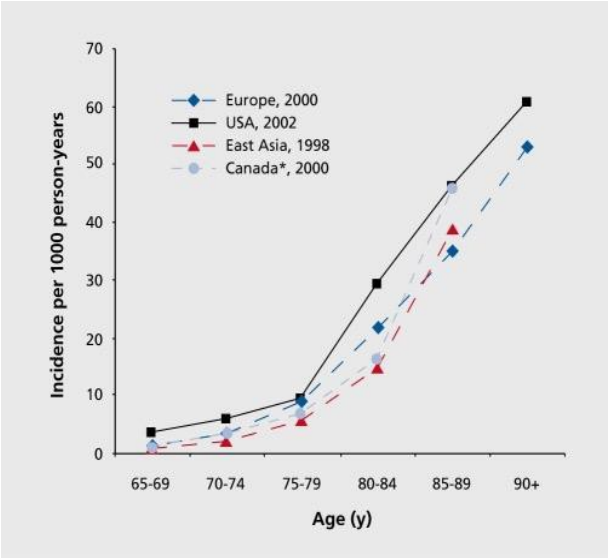

Figure 1.1 Age Specific Incidence of AD. Illustrates the age-specific incidence of Alzheimer's disease (per 1000) across the continents of East Asia, Europe and the countries of USA and Canada.

(Qiu et al., 2009)

It is currently impossible to ascertain whether the incidence reaches a zenith or continues to rise after 85 years of age (Qiu et al., 2009). This question will likely become more important in future if faced with increased longevity in life span. It may enable researchers to further elucidate whether AD is a disease of the "when" i.e. a disease that will eventually become prevalent in a majority of the aged population if the average life span continues to increase; or whether it is a disease of the proportion who will develop the disorder and the proportion that will not.

There is a substantial socioeconomic and financial cost of caring for patients with dementia, and it is thought to amount to £23 Billion a year in the UK alone, and £380

billion worldwide (Mashta, 2007, Mangialasche et al, 2012). Consequently, dementia and its most common form AD hold the potential of an impending global health crisis that is also too costly economically to ignore.

1.4 Risk factors

For a disease as extensively researched as AD, a thorough understanding of a single causative mechanism underlying the disorder has proved elusive. This lack of clarity is due to the interplay between a number of environmental and genetic risk factors that suggest an increased propensity towards AD and contribute towards this disorder of multifactorial causality. Population-based studies have been the primary approach used in the identification of influential risk factors. As previously stated age confers the most risk for the development of AD. Another major risk factor is genetics. About 5% of all AD suffers are genetically predisposed to the disorder. The onset of symptoms for this familial AD often occurs much earlier than sporadic i.e. between 30-65 years (Bird, 2008). Other risk factors for the development of AD include systemic disease, oxidative stress, obesity, reduced physical activity, cerebral hypoperfusion, inflammation, hypoxia, cigarette smoking, excess alcohol consumption, cardiovascular disease, traumatic brain injury, late-life metabolic syndrome and depression (Xu et al., 2013).

1.5 Pathology

Over the past century, post-mortem studies have been the primary method by which to confirm AD diagnosis. The primary pathological hallmarks are deposition of the diffuse and neuritic extracellular beta-amyloid (Aβ)/senile plaques in the parenchyma, cerebral amyloid angiopathy, intracellular NFT composed of the microtubule-associated protein tau, neuropil threads, and dystrophic neurites containing hyperphosphorylated tau (**Fig 1.2, 1.3**) (Crews and Masliah 2010). In addition to these pathological processes, AD sufferers display a characteristic loss of neurons, loss of synaptic function and dendritic arborisation. Moreover an increase in neuroinflammation and brain atrophy in cortical and subcortical regions has been demonstrated (Mayeux and Stern, 2012; Xu et al., 2013). The cerebral

areas most severely impacted are the entorhinal cortex, hippocampus and the basal forebrain.

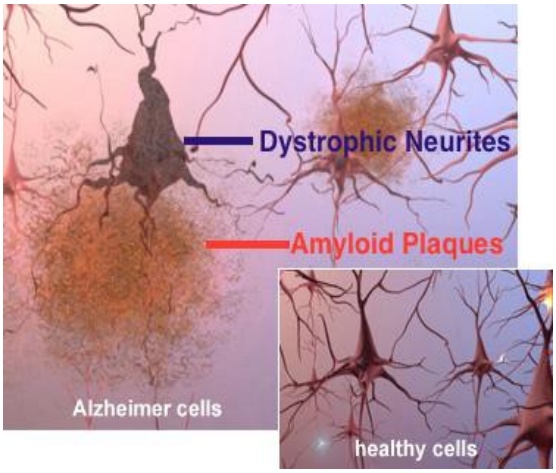

Fig 1.2: Portrays the main neuropathological features of the AD.

In contrast to the healthy cells within the normal brain, AD brains contain extracellular deposits of aggregated Amyloid-Beta known as plaques. Also present in the AD brain are dystrophic neurites caused by the intracellular abnormal aggregation of Hyperphosphorylated tau.

(Modified from https://www.alz.org/espanol/about/brain/10.asp)

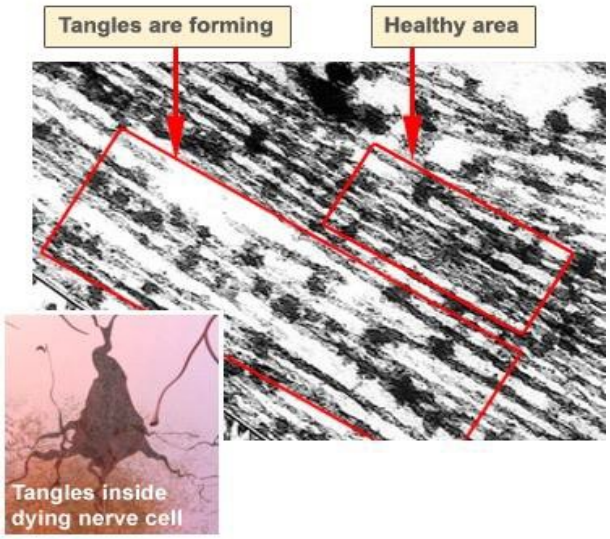

Fig 1.3: Image of a dystrophic neuron taken with an electron microscope

Image shows "healthy areas" within the cell in which the parallel tubular organisation remains intact. In contrast, other regions within the cell show the disintegration of the microtubules, and the apparent location of the aggregated tau tangles.

(https://www.alz.org/espanol/about/brain/12.asp)

AD is hallmarked by a progressive deterioration in multiple cognitive domains, severe enough to result in a global alteration or loss of cognitive ability. This manifests ante-mortem as the following behavioural symptoms; memory impairment, aphasia, temporal and spatial disorientation, poor judgment, delusions, sleep deprivation, weight loss, and changes in mood and personality (Guillot-Sestier and Town; 2013). Behavioural symptoms correlate with regions of pathology and brain atrophy. As is common with all progressive neurodegenerative diseases, behavioural symptoms will worsen as pathology increases.

1.5.1 Production of Amyloid Beta

Amyloid beta is a 36-43 amino acid polypeptide derived from the cleavage of a membrane glycoprotein known as Amyloid Precursor Protein (APP) (Kang et al., 2000). APP is a highly conserved multifunctional protein consisting of a large extracellular N-terminal domain, a transmembrane domain and the APP intracellular domain (AICD) at its C terminus (Rohan De Silva et al., 1997). The APP gene is located on chromosome 21 and consists of 18 exons which span 290 kilobase pairs (kbp) (Bergsdorf et al., 2000). Aβ is encoded by exons 16 and 17 of the APP gene. In humans, alternative splicing of APP mRNA leads to the generation of isoforms which express proteins of between 639-770 aa. The major APP isoforms expressed in the brain are APP^{695}, APP^{751} and APP^{770}. Neurons preferentially express the APP^{695} isoform, whilst APP^{751} is the primary APP isoform outside the CNS (Cirrito et al., 2005). Though each isoform is capable of generating Aβ, its secretion is by far highest by Neurons. Therefore, the APP^{695} isoform is primarily responsible for Aβ production (Cirrito et al., 2005).

A*β* is derived from the sequential proteolysis of APP's luminal domain by the aspartyl membrane bound endoproteases α or β, followed by γ–secretase (Fig 1.4). The first form of APP cleavage produces the protein p3 from sequential cleavages by α- and γ-secretases in what is called the non-amyloidogenic pathway. Whereas in the amyloidogenic pathway, the main neuronal β- secretase known as BACE1 cleaves the N-terminal ectodomain of APP, which leads to the secretion of sAPPβ and the generation of a 99 aa CTFβ (which begins with the N-terminus of Aβ). Subsequent intramembranous cleavage by γ-secretase generates the 4kDa Aβ released into the neuronal milieu (Schaefer et al., 2011) and a 50 amino acid AICD (Kaneko et al., 2007; Edbauer et al. 2003). The isoform of Aβ produced by the amyloidogenic pathway depends on the γ-secretase cleavage location.

In a normally functioning CNS α and β secretase compete to bind APP. However due to the rate limiting aspect of β secretase, generation of Aβ constitutes only 10% of total APP processing, thus preventing the formation and abnormal build-up of amyloid protein. Thus β- and γ-secretase provide prime targets for the development of novel therapeutics for the treatment of Alzheimer's disease.

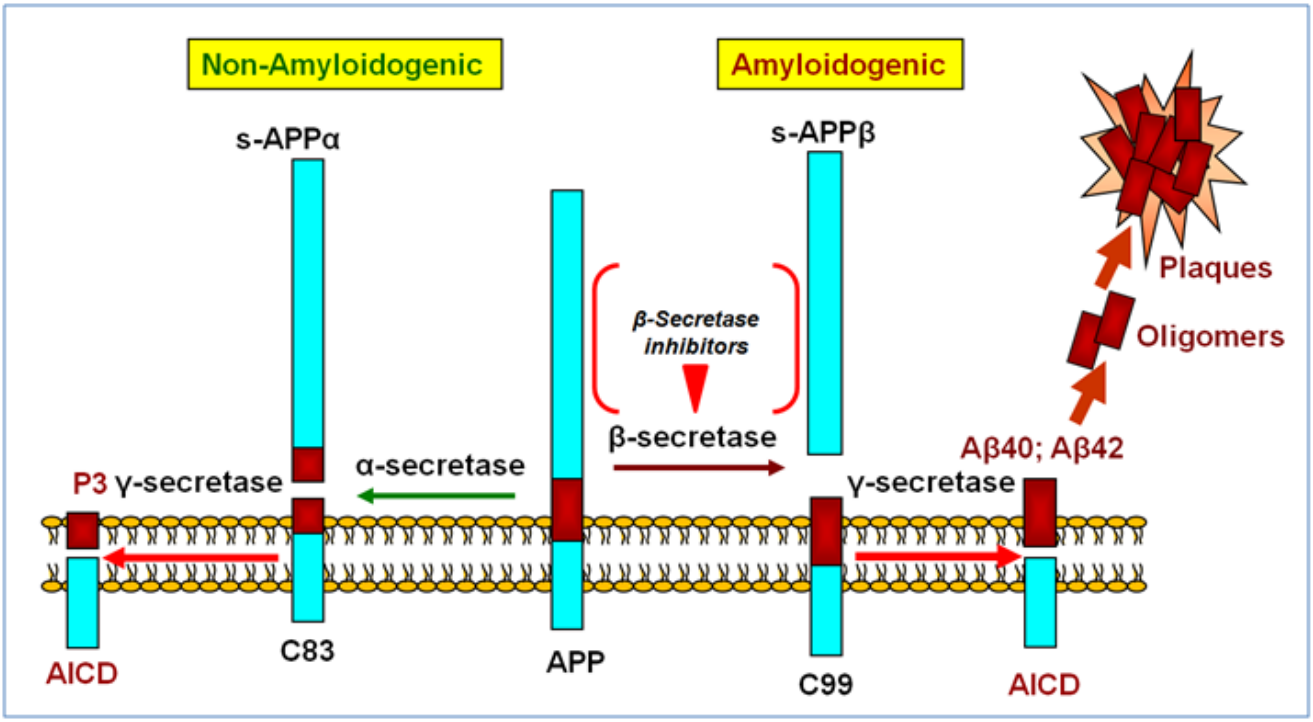

Fig 1.4: Image illustrates the two APP proteolysis pathways.
APP is a transmembrane protein with a large extracellular domain. In the non-amyloidogenic pathway, APP is cleaved in the middle of the Aβ region by α-secretase into an n-terminal s-APPα protein and a transmembrane protein C83. Further cleavage of C83 by γ-secretase results in the production of the protein p3 and the 50 amino acid APP intercellular domain (AICD). In the amyloidogenic pathway β-secretase mediated proteolysis of APP occurs at the n-terminal of the Aβ sequence yielding the s-APPβ fragment and the transmembrane protein C99. Sequential cleavage by γ-secretase generates Aβ and AICD. The isomer of Aβ (Aβ40 or Aβ42) produced depends on the location of γ-secretase cleavage. Aβ42 is more hydrophobic and aggregates into oligomers and plaques more readily than Aβ40.

(Zhang et al. 2007)

1.5.2 Normal function of Amyloid Beta

The function of Aβ has been investigated by numerous researchers. However, it is important to note that Aβ also carries out normal physiological functions, though their role requires further elucidation. Cell culture experiments were conducted by Plant and colleagues, who treated rat and human cortical neurons with inhibitors of γ- or β-secretase as well as an antibody against Aβ. Neuronal viability as measured via an MTT assay was significantly reduced in these experiments, however when cells were co-incubated with Aβ cell viability was restored (Plant et al. 2003). Thus, indicating that one of the primary functions of Aβ is the maintenance of cell viability. However, the exact mechanism by which it maintains cell viability has yet to be clarified. One suggestion is that Aβ functions as

a negative feedback mechanism to modulate neuronal activity (Ting et al. 2007; Kamenetz et al. 2003).

It has also been hypothesised that Aβ plays a role in synaptic plasticity and thus mediates learning and memory formation (Huber et al. 1993). Rodents injected with competitive inhibitors of endogenous Aβ prior to a learning exercise showed a severe disruption in their ability to acquire and retain memory up to 5 days post training, indicating that one major pre-disease function of Aβ is the formation of memories. Further corroborating with this hypothesis, intrahippocampal treatment with Aβ after learning exercises significantly enhanced retention of memories (Garcia-Osta et al., 2009).

1.6 Genetics

Genetics is another risk factor for the development of AD. About 5% of AD sufferers are genetically predisposed towards the disorder due to Mendelian autosomal dominant patterns of inheritance and are thus said to suffer from Familial Alzheimer's disease (Bertram et al., 2010; Philipson et al., 2011; Schellenberg and Montine, 2012). The onset of disease phenotype for these patients is between 40-50 years of age (Zhang et al., 2012)

1.6.1 Early onset Alzheimer's disease

Due to genetic studies of individuals with early-onset familial dementia, it was discovered that a majority of these individuals had mutations in at least one of three genes directly involved in amyloid production. First was the transmembrane amyloid precursor protein (*APP*) on chromosome 21. Sequential cleavage of APP by β- and γ-secretases results in the production of Aβ. The isomer of Aβ produced Aβ40 (40 amino acids) or Aβ42 (42 amino acids) is dependent on the location of the γ-secretase cleavage. The more distal the cut is to the n-terminus of the Aβ protein, the longer the length of the Aβ protein produced. Of the isomers, Aβ42 is more prone to aggregating than Aβ40, and is thus the component that aggregates to form amyloid plaques. It has also been shown to correlate best with neurotoxicity and cognitive dysfunction. As a result, many researchers were led to posit that mutations in the genes coding for both APP, or α, β, and γ–secretases may play a significant role in the development of AD (Xu et al., 2013). Genetic studies, geared towards

unearthing the cause of AD identified mutations in the genes encoding presenilin 1 (PS1) and 2 (PS2), PSEN 1 and PSEN 2 respectively. PS1 and PS2 are proteins, which form the catalytic core of the γ-secretase complex (Goate et al., 1991, Levy-Lahad et al., 1995, Sherrington et al., 1995, Giasson et al., 2003).

1.6.2 Late onset Alzheimer's disease

Remarkably, late-onset AD (LOAD), often defined as sporadic in nature, has been shown to have a strong genetic component. Genome-wide association studies (GWAS) have identified novel loci involved in lipid metabolism, immune response, endocytosis, tau metabolism, axonal development and epigenetics, which contribute towards AD risk. Many of these genetic polymorphisms contribute mild to high AD risk and even more importantly determine the time of onset. The major genetic point of interest for LOAD is Apolipoprotein E (APOE), a regulator of cholesterol transport, involved in neuroplasticity, tau phosphorylation and inflammation. The presence of the ε4 allele of the gene for Apolipoprotein E (APOE) is the largest genetic risk factor for the development of sporadic AD. Between 40 and 80% of people with AD possess at least one APOEε4 allele. "One copy of APOE ε4 increases the risk for AD threefold and two copies further elevate the risk twelvefold" (Corder et al., 1993; Huang and Mucke, 2012).

In AD, APOE binds to Aβ and functions as a catalyst that enhances the proteolysis of Amyloid Beta, and thus prevents its abnormal aggregation (Kim et al., 2009; Castellano et al., 2011). Moreover, binding of APOE to the low-density lipoprotein receptor-related protein 1 (LRP1/CD91/alpha 2-macroglobulin receptor) on the plasma membrane of astrocytes regulates the metabolism of soluble Aβ (Verghese et al., 2013). Neuropathological, Neuroimaging and transgenic mice studies have all shown a higher deposition of Aβ in APOε4 positive carriers than in the ε4 negative counterparts. Despite these facts, APOE is not considered a causative gene, as many develop AD with or without its contribution. Rather it has been suggested that it is a determinant of age of onset.

Several genes associated with neuro-inflammation have been identified in GWAS. Single nucleotide polymorphisms in the gene CR1, which encodes the complement (3b/4b) receptor 1 were identified in individuals with LOAD. The CR1 protein is widely expressed on the surface of erythrocytes, microglia, and neurons. Binding of complement proteins C3b or C4b to CR1 on microglia is responsible for

the phagocytosis of complement opsonised particles. It modulates the effect of APOE *ε4* on brain fibrillar amyloid burden and can bind to C3b and C4b, thus moderating the activity of the complement system (Rogers et al., 2006). Pathological studies have demonstrated that there is a correlation between the elevated expression of CR1 mRNA and AD, which is seemingly at odds with the fact that CR1 facilitates Aβ clearance. However, the identified polymorphisms encode high-expression (1400 copies per cell) and low-expression (<200 copies per cell) alleles in erythrocytes (Krych-Goldberg et al., 2002). High levels of CR1 protein may potentially lead to reduction in complement activation (Fernie-King et al., 2002); whilst lower levels may lead to impaired clearance of Aβ. Thus, the increase in mRNA expressions of either polymorphism may have different effects, which contribute in their own way towards AD pathology and increase the risk of developing the disease.

Other genes of note include Clusterin, an apolipoprotein upregulated in AD which influences fibril formation, Aβ clearance, neurotoxicity and regulates the complement membrane attack complex; ATP-binding cassette transporter A7 (ABCA7), upregulated 10 fold in microglia, modulates microglial phagocytosis of apoptotic cells and Aβ via the complement pathway; CD33 expressed in microglia, which is positively correlated with insoluble Aβ42, plaque burden, cognitive decline and has been postulated to inhibit Aβ phagocytosis; and the Triggering receptor expressed on myeloid cells 2 (TREM2), thought to impair the ability of brain leukocytes to maintain a homeostatic balance of amyloid beta (reviewed in Karch and Goate, 2014).

1.7 Causal Hypothesis

1.7.1 Amyloid cascade hypothesis

The most popular theory is the amyloid cascade hypothesis (Hardy and Allsop 1991; Karran et al., 2011). The initial hypothesis posits that amyloid deposition, results in the initiation of AD with numerous secondary processes - such as the hyper-phosphorylation of the microtubule-associated protein tau (MAPT), and the formation of NFT occurring subsequently. Accumulation of these deposits then leads to neuronal dysfunction and eventually dementia (Selkoe, 1996). Several observations made in the late 1980s and early 90s corroborate with this hypothesis. First, was the detection of Aβ as an important component of the senile plaques (Glenner et al., 1984), which Alzheimer described in 1907. Genetic studies, geared towards the proof of this hypothesis, identified familial mutations in APP on chromosome 21, PS1 and PS2; thus providing an added boost towards the amyloid cascade hypothesis (Goate et al., 1991, Levy-Lahad et al., 1995, Sherrington et al., 1995, Giasson et al., 2003). Furthermore, individuals with Down syndrome - a condition hallmarked by the triplicate of chromosome 21- display many of the same pathological hallmarks and cognitive deficits as those who suffer from AD. Following the amyloid cascade hypothesis, and recent amyloid imaging studies, it is thought that Aβ accumulation begins first (Jack et al., 2011). Aβ exists in a number of different conformations in the CNS such as, monomers, oligomers, protofibrils, fibrils and Aβ plaques. The degree to which they promote pathology differs. Deposition of Aβ is thought to be succeeded by a tau-mediated neuronal injury, brain atrophy, and cognitive decline (Mintun et al., 2006, Bourgeat et al., 2010). Jack and colleagues (1999, 2007, 2011) proposed a hypothetical timeline for the progression of the

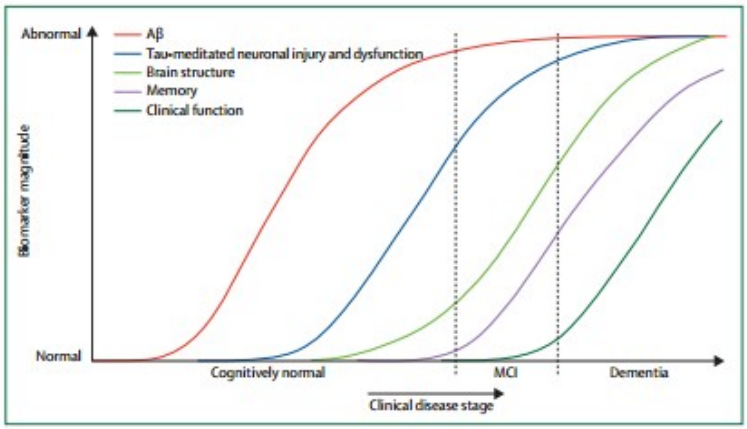

Fig 1.5: Schematic diagram illustrating the preclinical stages of Alzheimer disease.
The horizontal axis indicates the clinical stages and its progression from normal to Mild Cognitive Impairment and AD. The vertical axis indicates biomarker magnitude from its normal value (bottom) to its maximal value. The first 3 curves indicate areas where biomarkers are detecting/can detect AD pathology. (Jack et al., 2010)

disorder based on the use of biomarkers (**Fig 1.5**).

1.7.2 Neuro-inflammatory hypothesis of AD

Neuroinflammation is a chronic inflammation of the central nervous system triggered by trauma and infections to the CNS. Markers of CNS inflammation include increased activation of microglia, pro-inflammatory cytokine concentration, blood-brain-barrier permeability, and leukocyte invasion. Over the past 20 years, inflammation in the CNS has been extensively studied both as a cause of neurodegeneration, though more importantly as a potential target for novel therapeutics.

The hypothesis that post Aβ pathology in AD is caused by neuroinflammation has recently gained traction. The amyloid cascade-inflammatory hypothesis posits that while the abnormal production and aggregation of Aβ acts as a trigger, it is not in itself sufficient to be causative of the disease (McGeer and McGeer, 2013). Rather it is thought that the presence of aberrant deposits of Aβ may induce inflammation. In turn, inflammatory cytokines then enhance tau up-regulation and promote tau aggregation. These postulations are largely due to two major observations non-steroidal anti-inflammatory drugs reduce the risk of developing AD and; several lifestyle/environmental factors which are known risk factors for the development of AD display an inflammatory component. For example, the hypothesis suggests that ageing - the single largest risk factor for the development of AD - is influential due to enhanced chronic inflammation associated with increasing age (Blasko et al., 2004). Moreover, many of the aforementioned risk factors for AD such as obesity and systemic disease have been shown to display an increase in the concentrations of inflammatory mediators. Studies have suggested that systemic and chronic conditions are associated with increased cognitive decline, hippocampal atrophy (Yaffe et al., 2004; Marsland et al., 2008),changes in electroencephalograph readings (Semmler et al., 2013) and an increased risk of Alzheimer's disease (Engelhart et al., 2004; Tan et al., 2008, Bermejo et al., 2008). This cognitive decline was positively correlated with the expression of the pro-inflammatory mediator Tumour Necrosis factor-alpha (TNFα; Holmes et al., 2009).

Numerous recent studies have indicated that the presence of extracellular Aβ deposits is considered to be an important trigger for the chronic neuroinflammation

that has been observed in AD brains. This is based on the observation of activated microglia, increased levels of complement elements, cytokines and chemokines in regions surrounding amyloid plaques. The pro-inflammatory enzyme cyclooxegenase-2 (COX-2) is elevated early in AD progression, and IL-6 and transforming growth factor-β1 (TGF-β1) were also found to be elevated in patients with severe dementia (Luterman et al., 2000; Ho et al., 2001; Pasinetti, 2001). Moreover, a long-term epidemiological study demonstrated that the use of non-steroidal anti-inflammatory drugs (NSAIDs) lowers the risk of AD (Etminan et al., 2003). Ibuprofen and indomethacin have been shown to decrease the levels of secreted Aβ42 in vitro as well as in animal models of AD (Weggen et al., 2001; Eriksen et al., 2003). As the levels of Aβ40 have remained unaffected, it is likely that NSAIDs are causing modulation of either APP or gamma secretase (Kukar et al., 2008).

Not all conventional NSAIDs provide benefits (Aisen et al., 2003; Kukar et al., 2005). Some NSAIDS have been shown to accelerate AD pathogenesis in patients with advanced progression (Breitner et al., 2009). It is therefore apparent that the effects of NSAIDs may provide beneficial or detrimental effects dependent on the progression stage of the disease and the type of NSAID used. This dependence may explain failure of NSAIDS as a treatment for AD in many clinical trials. Therefore, the pathways by which beneficial NSAIDs reduce specific inflammatory mechanisms, and thus how those inflammatory processes contribute to the pathogenesis of AD must be identified.

1.7.3 Cholinergic hypothesis

Acetylcholine (Ach) is a neurotransmitter in the brain synthesised by the enzyme choline acetyltransferase from choline and acetyl-CoA before being released by cholinergic neurons into the synaptic cleft (Hampel et al., 2018). ACh neurotransmitters then activate and mediate transmission to the post synaptic neurons which innervate regions of the cerebral cortex, hippocampus and amygdala. The enzyme acetylcholinesterase inactivates acetylcholine by decomposing it into choline and acetate. Insufficient clearance of ACh results in impaired muscular and neuronal function. There are two cholinesterases; acetylcholinesterase (AChE) and

butyrylcholinesterase (BuChE), but ACh is dominantly decomposed by AChE instead of BuChE.

The cholinergic hypothesis is based on 3 observations. First came the observation that cholinergic antagonists impair memory and may thus be involved in age-related memory degeneration (Drachman and Leavitt, 1974). Healthy individuals who took anticholinergic drugs experienced worse memory recall, and had reduced cortical volume (Risacher et al., 2016). Moreover, there was a significant correlation between long-term use of cholinergic drugs and progression to MCI or Alzheimer's disease (Risacher et al., 2016). Secondly, Bowen and colleagues observed a significant reduction of presynaptic cholinergic markers in the cerebral cortex of senile dementia subjects compared to controls (Bowen et al., 1976). Finally came the observation through retrograde staining that the source of cortical cholinergic innervation– the nucleus basalis of Meynert (NBM) in the basal forebrain undergoes neurodegeneration in Alzheimer's disease (Mesulam, 1976). Perry and colleagues further observed through post mortem studies that NBM neurodegeneration is correlated with an increase in Aβ load (neuritic plaques). In addition, the loss of cholinergic neurons is further thought to exacerbate the pathology of AD by promoting further Aβ deposition (Ramos-Rodriguez et al., 2013). This progressive loss of NBM neurons, leads to a loss of synaptic transmission to the cerebral cortex, hippocampus and amygdala (Sassin et al., 2000); the regions of the brain most involved in memory formation and which show the greatest regional atrophy in AD. Moreover, the cholinergic neurons of the NBM are thought to play a role in the regulation of cerebral blood flow to several cortical areas (Lacombe et al., 1989; Sato and Sato, 1990; Lacombe et al., 1997). This reduction in cerebral blood in addition to the morphological changes in capillary networks induced by Aβ may explain the cerebrovascular disease observed in many AD subjects. It could also further explain the impaired clearance of Aβ. It is therefore evident that the cholinergic system plays an important role in the pathology of AD.

1.8 Current therapeutic strategies for the treatment of AD

Though a thorough understanding of the biochemical cascade leading to AD has yet to be elucidated, slow but sufficient progress has been made to identify hallmarks of disease progression. This has enabled researchers to develop drugs targeted at the identified pathways of the disease in order to slow progression.

The primary therapeutic strategy is to reduce Aβ production by targeting β- and γ-secretase (Vassar and Citron, 2000). Inhibitors of BACE1 (β-secretase 1) in particular have been particularly targeted as it catalyses the rate-limiting reaction in Aβ production. However, there are many reasons why BACE inhibitors have failed to produce a viable treatment option. Physiologically BACE1 plays a role in the regulation of axon myelination, and further regulates the thickness of the myelin sheath (Brinkmann et al., 2008). Moreover, studies of BACE1 deficient mice indicate that the absence of BACE1 plays a role in the development of schizophrenia (Savonenko et al., 2008). Thus, BACE1 may provide an alluring target, but without further investigation into its physiological role it is not a viable option for treatment. The potential side effects of such as hypomyelination, toxic and behavioural effects far outweigh any benefits. Furthermore, due to a large active site which is capable of binding numerous substrates, inhibitors of BACE1 may be unable to cross the BBB (Citron, 2002). Due to the dominance of the amyloid cascade hypothesis as the initiator of AD, researchers developed another therapeutic strategy; the development of antibodies that target Aβ. Despite this, phase 2 and 3 trials of drugs such as bapineuzumab (Kerchner et al., 2010; Salloway et al., 2014) and crenezumab (Cummings et al., 2018) monoclonal antibodies of Aβ failed to show any significant changes in clinical outcomes of mild to moderate AD, minimal cognitive impairment, and in nondemented subjects (Salloway et al., 2014). A more promising drug solanezumab (Siemers et al., 2016), reduced cognitive and functional decline in only mild AD patients when compared to placebo. Indicating that the drug could be efficacious if used for treatment of patients at earlier stages of disease development such as MCI. This correlates with studies that show that though Aβ is important in early stages of the disease, it is not as necessary for the pathogenesis in later stages of the disease (Jack et al., 2009). Thus, until advancements in pre-AD diagnosis, match up with early treatment options, Aβ antibodies may not provide a viable treatment option for the treatment of AD.

The cholinergic pathway has proved most efficacious for the management of AD. Decline of cognitive function which is one of the major hallmarks of AD; is as a result of an abnormal decrease in ACh levels and neurons in the cortex, hippocampus, forebrain Meynert basal ganglia and septal area. Therefore, in order to stall this decline and provide symptomatic relief; drugs were developed with a primary strategy of inhibiting cholinesterase and prolonging the action of ACh neurotransmitters in the synaptic cleft. Cholinergic inhibitors Donepezil (Lee et al., 2015; Birks et al., 2018), Galanthamine (Fulton and Benton, 1996), Rivastigmine (Kandiah et al., 2017) and Memantine (Kishi et al., 2017) are four of only five drugs currently approved for AD (Cummings et al., 2016. These drugs are often paired with the fifth drug, a N- methyl-D-aspartate (NMDA) receptor antagonist. However, the benefits provided by taking both drugs are marginal and unable to slow the progression of AD (Ferreira-Vieira et al., 2016). This is as a result of a 90% decrease in AChE levels due to atrophied cholinergic neurons (Hampel et al., 2018). In order to compensate BuChE decomposes ACh. There are severe downsides to drug use. Previous studies have demonstrated that inhibiting AChE might result in liver injury (Uzunhisarcikli and Kalender, 2011). Therefore, to provide better symptomatic relief inhibitors of BuChE will have to be developed and used in conjunction with AChE inhibitors.

While a number of therapeutic strategies and drugs exist, none have been able to stall AD disease progression in the moderate to latter stages of the disease, nor indeed cure or reverse harmful pathologies. This is largely due to the multifactorial nature of the disorder, the difficulty in identifying early stages and the varying degrees of viability depending on the stage of disease progression. As such it is unlikely that any one drug or treatment mechanism will be able to treat AD, unless it targets the early mechanisms. Therefore, in order to develop a cure or treatment, early mechanisms will need to be understood, detected and targeted for earlier stages; and co-adjuvant therapies incorporating symptomatic and mechanism targets will need to be developed for latter stages of disease progression.

1.9 Cellular components of the Central Nervous System

1.9.1 The blood brain barrier

An optimally functioning CNS is a well-calibrated chemical, ionic and anti-inflammatory environment ideally suited to ensure optimal neuronal function. The blood-brain barrier (BBB) is a physical barrier of phylogenetic origin which restricts molecular transport between peripheral and CNS vasculature, thus protecting the neuronal milieu from peripheral innate and adaptive immune cells, plasma proteins and oscillations in the concentration of inflammatory mediators which would offset the delicate homeostatic balance of the brain (Sharma et al., 2012). Structurally, the BBB defines the tight junctions that connect endothelial cells of the brain capillaries. Endothelial-lined capillaries form a core, which is in turn surrounded by astrocytic end- feet, a basal lamina, and pericytes (Marques et al., 2013). Every neuron is perfused by its one such capillary and a dynamic crosstalk exists between the BBB endothelial cells, glia and neurons thus highlighting how essential a functioning BBB is in the maintenance of neurons and prevention of aberrant disease like states (Abbott et al., 2006). Moreover, degeneration and increased permeability of the BBB has been well characterised in many of the AD-associated risk factors further highlighting its importance.

BBB permeability increases with the progression of age. Similarly, in AD, BBB permeability is more pronounced and grows at an accelerated rate when compared to the progression of permeability in age-matched controls. Post-mortem studies have shown BBB damage in AD including BBB-endothelial cell necrosis, increased exocytosis, cortical and in particular hippocampal accumulation of blood-derived proteins such as immunoglobulins, albumin, fibrinogen, serum amyloid P and thrombin (Fiala et al., 2002; Zipser et al., 2007; Hultman et al., 2013) and degeneration of BBB- pericytes (Sengillo et al., 2013).

The endothelial cells, which form an integral part of the BBB, express receptors for pro-inflammatory mediators on their cell membrane. Exposure to peripheral inflammatory ligands such as TNF, IL-1β and IL-6 may elicit barrier-opening, lead to an influx of inflammatory mediators and may alter the normal response of the brain to various stimuli. High local concentrations of the anti-inflammatory mediators TGF-β, IL- 10, and gangliosides, which are toxic to T cells, make the CNS a robust environment capable of withstanding inflammation to a degree (Irani et al, 1996; Strle

et al., 2001). However, with age and other peripheral systemic states there is an increased BBB permeability. Thus, the BBB becomes more susceptible to inflammation and if damaged enough may lead to an influx of peripheral immune cells into the CNS. Therefore, despite the fact that the CNS is not an immune privileged organ, it may be that systemic triggers lead to receptor activation of a failing BBB and are required to initiate neuroinflammation. Chronic perpetuation of which may result in chronic neuroinflammation and initiate many of the pathogenic neurodegenerative states of the CNS.

A few studies suggest that BBB failure may initiate neuroinflammation and AD due to an inadequate efflux-influx balance. For example, it is thought that the influx of serum amyloid protein and plasma amyloid through the BBB may be the point of origin for Aβ aggregation (Pluta, 2007). The receptor for advanced glycation end products (RAGE) - present on BBB-endothelial cells – is of particular note, as binding to Aβ or its natural ligand AGE can activate it. Ligand binding to RAGE leads to the activation of NF-κB, downstream of which causes changes to the expression of inflammatory mediators and an increase in RAGE expression. In transgenic models of AD and β-amyloidosis, RAGE expression is elevated in neurons, microglia and vasculature proximal to sites of pathology (Yan et al., 2006; Deane et al., 2003). Particularly noteworthy since many individuals living with AD risk factors also display elevated levels of AGE (Vlassara et al., 2002; Goldin et al., 2006). Thus, RAGE activation and the resulting influx of peripheral proteins leads to a chronic cycle of activation and is a likely contributor towards the chronic neuroinflammatory state observed in AD.

Conversely, impaired efflux of Aβ -from the CNS to the peripheral vasculature- has also been observed in human and animal models of AD (Shibata et al., 2000; Kang et al., 2000); Storck et al., 2016). The clearance mechanism is modulated by the binding of Aβ to α2-macroglobulin (alpha 2M). In turn the stable complexes formed bind to LRP-1, and Aβ leaves the CNS through transcytosis across the BBB (Zlokovic et al., 2010; Storck et al., 2016). Expression of LRP-1 is reduced in AD patients (Donahue et al., 2006). Hence, despite the opposing roles of RAGE and LRP-1 it is evident that both contribute towards the homeostatic balance of the CNS. Changes in the expression of both leads to the presence of amyloid protein in the CNS, which sustained may result in the pathogenesis of AD. However, it is unclear from these

studies whether the BBB impairment is causative in nature, or whether it exacerbates a pre-existing neurodegenerative/neuroinflammatory condition.

1.9.2 Neurons

Neuronal apoptosis leading to regional atrophy of the cortical regions is characteristic of neurodegenerative diseases. Originally thought to be unfortunate bystanders and unwitting “victims” in the degenerative process, neurons are capable of producing inflammatory mediators that are damaging to the neuronal milieu. They are one source of complement proteins, COX, IL-1β, IL-6 and TNF-α a majority of which are pro-inflammatory in nature (reviewed in Heneka et al., 2007). Also, neurons have been shown to express iNOS (inducible nitric oxide synthase). In the long-term release of NO - a chemical known to cause neuronal dysfunction and apoptosis - will be damaging (Heneka et al., 2001). It is possible that TNF-α and NO in low concentrations may have a neuroprotective effect, but this theory is not well characterised (Heneka et al., 2007).

1.9.3 Astrocytes

Astrocytes are glial cells with fine elongated processes, giving the cells a star-like appearance (Fig 1.6). Though these are the most abundant cells in the CNS, each cell occupies a distinct territory. A territory contains up to 2,000,000 neuronal synapses - with the only astrocyte- astrocyte interaction occurring between the end-feet of the astrocytic processes (Bushong et al., 2002; Oberheim et al., 2009). This interdigitation forms gap junctions, connecting adjacent astrocytic cells, thus building an entire network with close contact to neurons, synapses and the cerebral vasculature (Sofroniew et al., 2010). Functionally, astrocytes are involved in synaptic formation, maturation and pruning during the developmental stages. Post-development, astrocytes maintain the ionic milieu of the CNS, regulate long-term potentiation, facilitate neurotransmitter release and uptake, modulate the passing of information at the synapse, establish bi-directional communication with neurons, and control the BBB via their perivascular end-feet (Clarke and Barres, 2013).

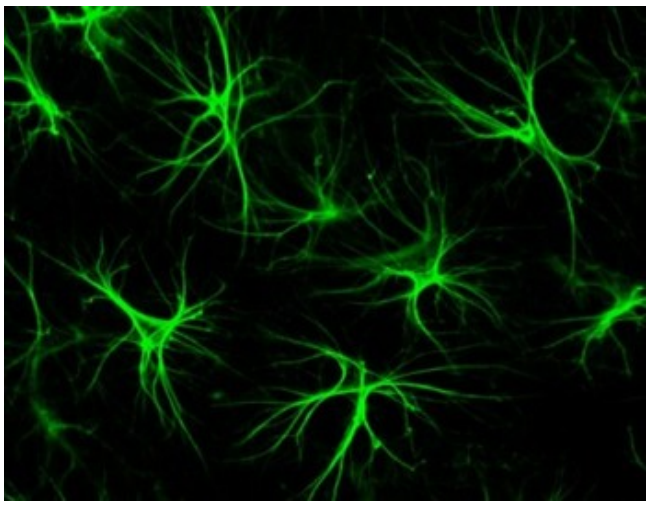

Fig 1.6 Astrocytes from human cell culture.

Astrocytes (Green) are star shaped cells with fine elongated processes which reside in the CNS. Cells were stained for (glial fibrillary acidic protein), which is primarily expressed by Astrocytes in the CNS.

(https://www.astrocyte.info)

Astrogliosis is a process, which results in the conformational change (Hypertrophic soma and processes) of reactive astrocytes, an increase in expression of glial fibrillary acidic protein (GFAP) intermediate filaments and, increased proliferation. Aβ may activate astrocytes, and thus elicit a neuroprotective or neuro-detrimental change in normal function of astrocytes. Post-mortem tissue samples of individuals with AD show activated astrocytes clustered at sites of Aβ deposition and astrogliosis (Wisniewski and Wegiel, 1991). The large group of astrocytes proximal to Aβ deposition sites indicates that once activated astrocytes generate chemotactic molecules, which result in the further recruitment of other astrocytes to the site. A subsequent study found a positive correlation between phagocytosed Aβ within astrocytes of the entorhinal cortex and the amount of AD pathology in the local milieu. ApoE polymorphisms may increase the risk of developing AD by affecting phagocytosis of Aβ (Nino et al., 2001). While there is a definite role for astrocytes in the clearance of Aβ it appears that they may also contribute to the generation of Aβ and thus a neuro-detrimental pathway.

B-Secretase (BACE1) known to result in the cleavage of the Aβ42 isoform, is over- expressed when exposed to chronic stressors. Therefore, it is possible that activation of astrocytes by inflammatory mediators and or Aβ may result in the generation of Aβ thereby perpetuating the condition. Granting credence to this theory, a study tested 3 and 16-month-old transgenic mice overexpressing a mutant form of APP, (APPV717I) for glial activation and amyloid deposition (Heneka et al., 2005). Heneka and colleagues demonstrated CD11b immunostaining of microglia at the 3-month stage, which was undetected in wild

type controls. Whereas, thioflavin S staining detected Aβ deposition only at the 16-month stage. Thus, indicating that transgenic mice display glial activation prior to the local deposition of Aβ (Heneka et al., 2005). Further studies posit a neuro-detrimental role for astrocytes in AD. Oscillations in calcium signaling were observed in those with the Familial AD presenilin 1 (PSEN1) mutation (Haughey and Mattson, 2003). It is likely that aberrant calcium signaling may contribute to much of the neuronal dysfunction, neuronal apoptosis and disintegration of the synapse observed in AD. Finally, when present, astrocytes inhibit the ability of microglia to phagocytose Aβ deposits either by creating a physical barrier or by releasing proteoglycans (Akiyama et al., 2000). Astrocytes express some inflammatory mediators including complement subcomponents and receptors, IL-1β, IL-6, COX, TNF-α and prostaglandins (reviewed in Akiyama et al., 2000).

1.9.4 Microglia

Microglial cells known as the resident macrophages of the CNS are key mediators of the immune response. These cells are derived from progenitors of myeloid origin, which migrate from the periphery and enter the brain during early development. Postnatally, they are found to be disseminated through the brain, primarily in a “resting” ramified phenotype, characterised by a small soma with fine cellular processes. Microglial processes are equipped with neurotransmitter, cytokine, chemokine and pattern recognition receptors which function to sense pathogen-associated molecular patterns (PAMPs) and host-derived danger associated molecular patterns (DAMPs), such as misfolded proteins, mislocalised nucleic acids and protein aggregates as found in AD, and to respond to these signals by activating and adopting a change in morphological and functional phenotype. Brain-derived neurotrophic factor, essential for the formation of learning-dependent synapses and thus the development of memory by long-term potentiation is secreted by microglia.

Microglia play a role that aims for neuroprotection by the elimination of Aβ aggregates via phagocytosis (Heneka et al., 2010). However, microglia tend to have more detrimental than beneficial effects by contributing to neuronal cell death and neurodegeneration. Pathological events such as infection, ischaemia, traumatic injury, tumour invasion, neurodegenerative diseases and changes in the homeostatic balance of the CNS may present some of these DAMPSs and can result

in microglial activation. Activated/Reactive microglia can be characterised by a reduction in cell processes, amoeboid appearance, up-regulation of gene expression of surface receptors and function (Fig 1.7). Persistence of pro-inflammatory mediators - as found in states of chronic neuroinflammation - can cause microglia to remain activated for extended periods, releasing quantities of cytokines and neurotoxic molecules that contribute to long-term neurodegeneration (Liu and Hong, 2003). This functional perturbation of microglia from its normal neuroprotective states may exacerbate the progression of pathogenesis in many neurodegenerative states.

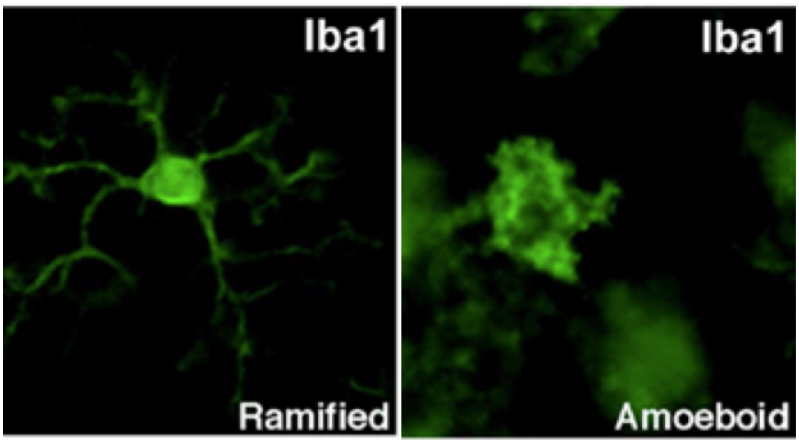

Fig 1.7 Resting and Activated Microglia in the rat brain.

Photomicrographs illustrating the two different states of Microglial activation. The resting state can be characterised by a ramified phenotype whereas the activated state can be characterised by a reduction in ramified processes and a larger soma.

(Ekdahl, 2012)

There is a strong signaling overlap between pathways activated by external pathogen associated molecular patterns (PAMPS) and the host-derived DAMPs, such that microglia may recognize and react to host aggregated proteins with the same exaggerated response as to an invading pathogen. Amyloid β can bind to several innate immune receptors expressed on microglia, such as NOD-like receptor (NLR), CD14, CD36, CD47, α6β1 integrin, class A scavenger receptor, RAGE and toll-like receptors (TLRs) 2, 4, and 6, all of which can lead to activation when triggered. Initial activation of microglia by Aβ results in the chemotaxis and recruitment of more microglial cells to sites of Aβ deposition (Terry and Wisniewski, 1975). In one study AD mice with Cx3cr1 (a chemokine receptor) had high levels of microglial migration; whereas Cx3cr1-/- mice had neither microglial accumulation nor neuronal loss, in addition with low levels of hyperphosphorylated tau (Osherovich, 2008). Knock-out animal models for the scavenger receptors A and B present on microglia which promote Aβ clearance have shown increases in the

amyloid burden. Evidently microglia play a crucial role in the perpetuation of the neurodegenerative and chronic inflammatory state that exists in AD.

Activation of microglia by Aβ also results in the expression of pro-inflammatory cytokines such as IL-1β, and IL-18 in their inactive forms. Cleavage into pro/active forms is controlled by a large molecular signaling complex known as the inflammasome, which has particular significance in the development of chronic inflammation. As such its components, which include the cleavage molecule caspase 1, adaptor protein ASC, the NLRP3 domain (sensor NLR, LRR- and pyrin domain-containing 3); are of particular interest as regions of possible therapeutic benefit.

1.10 The immune system in AD

The human immune system is an intricate system of immune sensors and mediators, which acts as the first line of defence against infection, injury and invasion by pathogens such as viruses, bacteria and fungi. It is composed of the innate and acquired (adaptive) immune responses. Of the two, innate immunity is the phylogenetic predecessor, whereas adaptive immunity is an evolutionary phenomenon that can be attributed only to vertebrates.

Innate immune responses are rapid (0-12 hour) responses to antigens that are reliant on pattern recognition receptors (PRRs) present on innate immune cells (macrophages, neutrophils and dendritic cells); and inflammatory mediators, both passed through the organism's germ line (Murphy, 2012). Immunity of this sort acts in a non-specific manner towards antigens and can neither be acquired nor adapted during an organism's lifetime. Conversely, adaptive immunity is an acquired form of immunity that is developed in response to primary exposure to antigens. Its response is extraordinarily discriminative, and its components "adapt" to the presence of pathogens by activating, proliferating, and creating potent mechanisms for the removal of pathogens. It further differs from the innate immune response by the slow duration of response and its immunological memory.

On presentation of an antigen, components of the innate immune system such as lysozymes, defensins, mucin, lectin, macrophages and the complement system first act to lyse and phagocytose pathogens. In the second phase, PRRs expressed on innate immune cells recognize non-self-motifs on host cells- known

as pathogen-associated molecular patterns and activate. Activation sets off a cascade of effector mechanisms, ultimately resulting in the removal of the pathogen. However, the innate immune system can be overwhelmed or evaded by pathogens. In such a scenario where the first two lines of defence are breached, innate immunity can trigger the adaptive immune system.

1.11 The role of the complement system

The complement system is a crucial component of the innate immune system. Complement first discovered by Jules Bordet is defined as a “heat-labile component of normal plasma. It is comprised of approximately 40 plasma/serum and cell-membrane-associated glycoproteins. Although complement proteins are found predominantly in plasma, a disruption of the blood brain barrier is not required for complement to be present in the CNS. In response to CNS changes microglia, astrocytes and neurons can synthesise complement proteins (Gasque et al., 2000). Their role is to facilitate the removal of pathogenic organisms via four primary functions: recognition, opsonisation, inflammatory stimulation, and direct killing through the membrane attack complex (Maibaum, 2000). The complement membrane attack complex (MAC) forms transmembrane channels that penetrate through the phospholipid bilayer of the target cells, leading to cell lysis and apoptosis.

Initiation of the complement cascade can be achieved by either the Innate or the Adaptive immune system via one of three pathways: the C1q pathway (classical pathway), an amplification loop (alternative complement pathway) and the lectin pathway (**Fig 1.8**). Upon activation of the complement system by several triggers, many inflammatory mediators are produced, initiating inflammatory processes. If unregulated, this cascade will result in an amplification of the inflammatory response and cell apoptosis.

The classical pathway involves the activation of the C1 complex, composed of the glycoproteins C1q, C1r and C1s associated in a calcium-dependent macromolecular complex. C1r and C1s are serine proteases activated primarily by the interaction of C1q protein with antibody-antigen complexes containing IgG or IgM (Kishore and Reid, 1999). Activation can also occur subsequent to the interaction of C1 with molecules such as serum amyloid P, DNA, RNA and C-

reactive protein (Sim and Malhotra, 1994; Gaboriaud et al., 2003). Once a ligand has bound to C1q, a conformational change occurs in the collagen rich region. This change leads to the activation of C1r and eventually C1s. C1s acts to cleave the complement proteins C2 and C4 into C2a, C2b, C4a and C4b respectively, resulting in the formation of a C4bC2a complex known as C3 convertase.

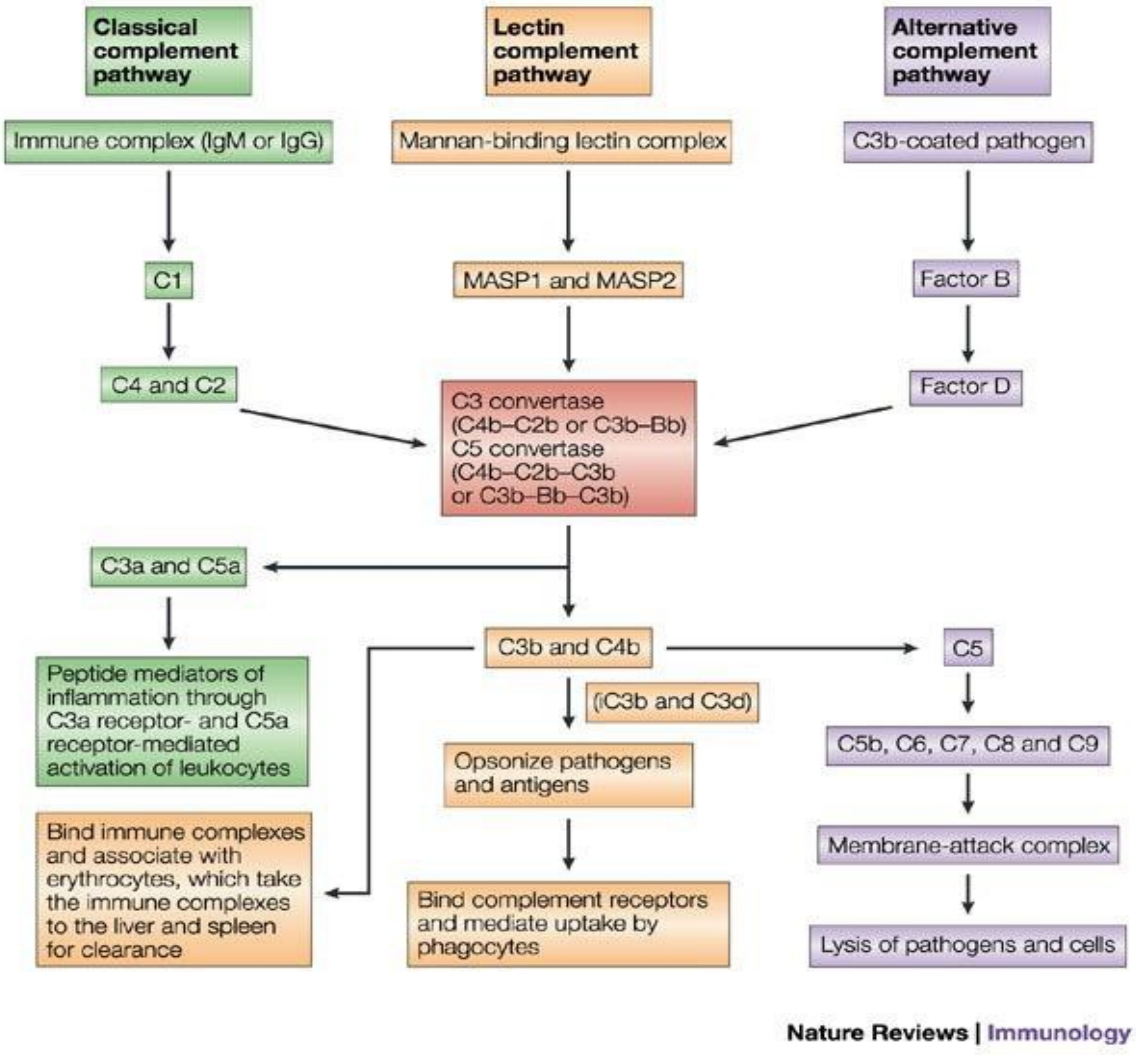

Fig 1.8: Illustrates the three pathways by which the complement cascade can be activated: The Classical complement pathway (green); the Mannose Binding Lectin pathway (orange); and the Alternative pathway (purple). All three pathways converge at the formation of C3 convertase. (Murphy, 2012)

Activation via the lectin pathway occurs when mannose-binding lectin (MBL) or ficolins bind to motifs (mainly carbohydrates) on target surfaces. Once bound, proteases associated with MBL or ficolins known as MBL-associated-serine-proteases (MASPs) can also cleave C2 and C4 complement proteins, resulting in the formation of C3 convertase.

Alternative pathway activation occurs via the spontaneous hydrolysis of C3. This slight conformational change in the protein enables the binding of factor B and results in its subsequent cleavage into subunits Ba and Bb. Similarly, to the classical pathway of complement activation, the result is the production of a C3 convertase complex, this time composed of C3bBb.

All three pathways converge at the formation of C3 convertase. The function of C3 convertase is to cleave and activate component C3, creating C3a and C3b. C3a is a weak chemotaxis agent, with the primary role of microglial and phagocyte recruitment (Kishore et al., 2003). While the C3b fragment attaches to the pathogen's surface and can act as an opsonin for target recognition and subsequent phagocytosis. Also, C3b binds with the C3 convertase to form C5 convertase (C4b2a3b). Subsequently C5-convertase cleaves C5 into the anaphylatoxin C5a and C5b the base for the formation of the MAC (C5-C9 complex). The MAC creates pores in the lipid bilayer of pathogens or host-derived cells in chronic inflammatory states causing cell lysis and apoptosis (Shastri et al., 2013). Amplification and or chronic activation of the complement cascade will inevitably lead to tissue atrophy.

Complement C5a also plays an important role. C5a is a very potent chemotactic agent which binds to a number of receptors- such as C5aR (C5R1, CD88) and C5L2 (gpr77)- which are expressed on macrophages (including microglia), neutrophils and T cells (Monk et al., 2007). The C5a-C5aR interaction in particular, has been shown to lead to microglial activation, microglial recruitment, and the release of proinflammatory mediators (Hernandez et al., 2017[1]). In a recent study, the Arctic AD mouse model was crossed with a C5aR knockout mice. the researchers observed that Arctic/C5aR knockout mice were protected from behavioural deficits, despite no change to local fibrillar amyloid pathology, while those with elevated C5a showed accelerated cognitive decline (Hernandez et al., 2017[1]). Moreover, RNA-Seq analysis identified a decreased expression of inflammatory genes when Arctic/C5aR knockout mice were compared to both wild

type and Arctic AD mice with normal C5aR function (Hernandez et al., 2017[1]). Moreover, in a second study, primary neurons treated with exogenous C5a and fibrillar amyloid showed increased neuronal injury than with just C5a or fibrillar amyloid (Hernandez et al., 2017[2]). These studies therefore indicate that the C5a-C5aR interaction plays a significant role in the neuronal injury observed in AD, and the corresponding behavioural deficits.

1.12 C1q Structure

C1q, the recognition subcomponent of the classical complement pathway, is a 460kDa protein consisting of 18 polypeptide chains of 3 types (6A, 6B and 6C) (Fig 1.9). Chiefly produced by cells of myeloid origin, microglia are the only CNS resident cells capable of synthesising C1q (Lynch et al., 2004). Each chain consists of a 3-9 aa N-terminal region, an 81 aa collagen-like region (CLR) and the approx. 135 aa C-terminal globular head region (gC1q) (Fig 1.9) (Sellar et al., 1991). Interchain disulphide bonds between N-terminal cysteine residues yields dimer subunits of 6 A-B and 3 C-C. The CLRs of the A-B and C-C subunits then bind through covalent and non-covalent bonds to give rise to a triple helical collagen-like unit ABC-CBA. Three of these units bind further via non-covalent bonds to form the hexameric C1q, which has been described as having morphology similar to a" bouquet of tulips" (Reid and Porter, 1976; Kishore and Reid, 1999; Kishore et al., 2003).

The globular gC1q domain (ligand recognition domain) is a heterotrimeric structure, formed from the C-terminal regions of the A, B and C chains (Kishore et al., 2003; Nayak et al., 2010). These modules are denoted globular heads A (ghA), B (ghB) and C (ghC). Proximal to the apex of the gC1q domain lies a calcium ion, which plays a significant role in the binding of C1q to immune complexes (Roumenina et al., 2005). Protein crystallisation studies have also revealed a three-dimensional structural similarity between the gC1q domain and tumour necrosis factor (TNF), hence leading to recognition of a C1q/TNF superfamily. The members of this family are crucial in a range of functions including inflammation, adaptive immunity, energy homeostasis and tissue regeneration (Kishore et al., 2004). The amino acid similarity (ranging from 20-96%) between family members has been found conserving eight invariable residues, critical in the maintenance of the

structural integrity of the gC1q domain. This highlights the importance of jelly roll topology throughout evolution in regard to C1q's various functions (Nayak et al., 2011). On the other hand, C1q overall structural organisation is similar to the MBL, surfactant protein A (SP-A), surfactant protein D (SP-D) and ficolin, which are PPRs belonging to the collectin family. (Nayak et al., 2011). The ability to express these modules as recombinant vectors has been enlightening in the understanding of how C1q is activated by a host of self and non-self-ligands. A study by Kishore and colleagues (1998) revealed that although IgG and IgM seemingly bind with the same affinity to C1q, ghB preferentially binds to IgG. Further studies have elucidated that ghA can bind heat- aggregated IgG, IgM and HIV-1 gp41; ghB binds to heat-aggregated IgG as well as amyloid β and; ghC shows a preference for IgM and HTLV-1 gp21 peptide (Kishore et al., 2004). This is due to differences in the surface expression of charged and hydrophobic residues between the three subunits. For instance, a positive charge cluster of Arginine on the surface of ghB was implicated in the interaction of ghB with IgG (Marqués et al., 1993). Thus, globular heads are not only structurally different but also functionally autonomous. Consequently, the multivalency of C1q's function is due to its heterotrimeric structure.

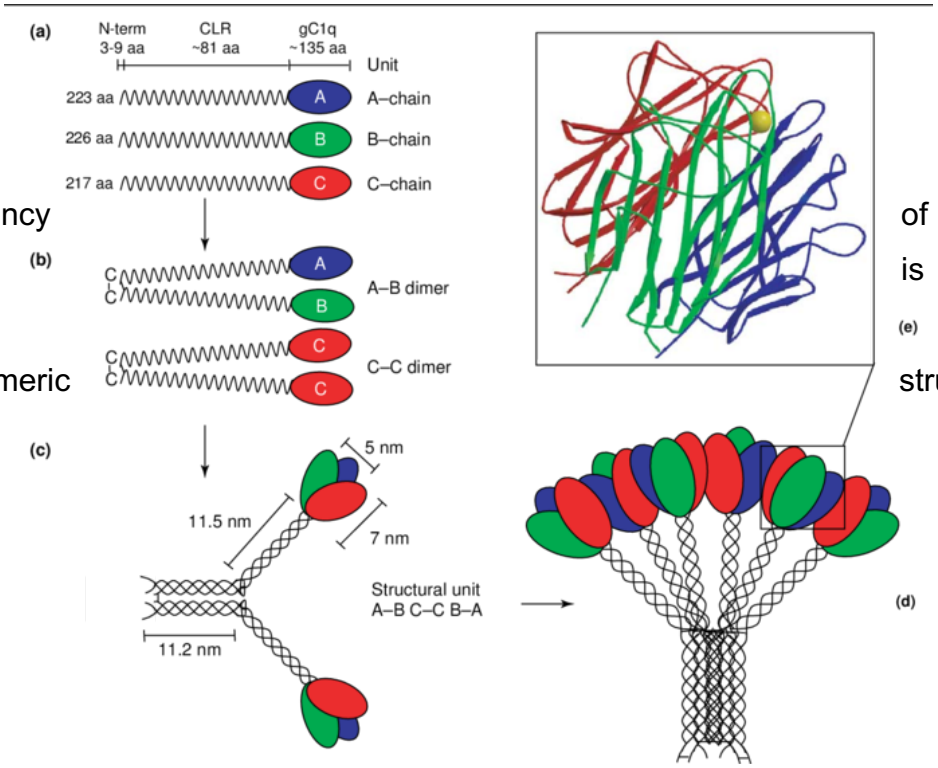

Fig 1.9: Structural organization of the C1q molecule. C1q (460 kDa) is composed of 18 polypeptide chains (6A, 6B and 6C). (a) The A, B and C chains each have a short N-terminal region (containing a half-cysteine residue involved in interchain disulfide bond formation), followed by a collagen region (CLR) of w81 residues and a C-terminal globular region (gC1q domain) ofw135 residues. (b) The interchain disulfide bonding yields 6A–B dimer subunits and 3C-C dimer subunits. The triple-helical collagen region in the A and B chains of an A–B subunit, together with one of the C-chains present in a C–C subunit, form a structural unit (ABC–CBA), which is held together by both covalent and non- covalent bonds (c). Three of these structural units associate, via strong non-covalent bonds in the fibril-like central portion, to yield the hexameric C1q molecule that has a tulip-like structure. Image and legend Reference: Kishore U, Gaboriaud C, Waters P, Shrive A, Greenhough, T, Reid, KBM, Sim RB, Arlaud G; *Trends in Immunology;* vol. 25, No. 10, (2004).

1.13 C1q function

The primary function of C1q is the recognition of charge clusters, thus initiating the classical complement pathway (Kishore et al., 2003). Moreover, it is involved in a varied number of processes such as phagocytosis of bacteria, neutralisation of retroviruses, cell adhesion, modulation of dendritic cells (DC), B cells and fibroblasts, and the clearance of apoptotic cells (Kishore et al., 2004). Due to its ability to be activated by a broad range of self and non-self-ligands - such as IgG, IgM, serum amyloid P, HLTV1, HIV gp41, Lipopolysaccharide, gram-negative bacteria, phospholipids, pentraxins and C-reactive protein- in an extensive range of diseases, it's overall significance is second only to that of complement subcomponent 3b (Nayak et al., 2010).

1.14 Complement system in AD

The two major hallmarks of AD are extracellular plaque deposits of Aβ and the neurofibrillary tangles of the microtubule-associated tau. Copious evidence indicates that C1q and the complement system play a role in the pathophysiology of Alzheimer's disease. However, there has been no interaction observed between tau and complement factors, indicating that complement mediated pathogenesis in AD is due to its interaction with Aβ.

AD and the complement system became linked by the discovery by Rogers et al. 1992 that Aβ binds to complement protein C1q in-vitro. In regions of the brain with a high amyloid load, the expression of C1q is up-regulated 80-fold compared to control levels (Yasojima et al., 1999). C1q synthesis is induced in neurons during ageing, and subsequent to Aβ treatment. In particular the mRNA expression of the B chain of C1q has been shown to be significantly higher in AD than in control. A fact confirmed by the specific affinity of ghB for Aβ (Kishore et al., 2003).

In AD, Aβ aggregates into either inert diffuse plaques or compact neuritic plaques made of β-pleated sheets of fibrillar amyloid. The process of aggregation begins with monomers binding to each other to form dimers or multimers. These aggregates further bind together to form larger oligomers which can form fibrillar amyloid, and in turn neuritic plaques. The greater the aggregative state, the more

potent the neurotoxicity of Aβ (Bruggink et al., 2012). Immunohistochemistry is often used to identify the co-localisation of amyloid associated proteins with Aβ, and its state of aggregation. Thioflavin-S is a stain which detects the B-sheet conformation observed in fibrillar Aβ. Immunohistochemical staining of human and rodent post-mortem samples has shown C1q to be co-localised with fibrillar Aβ (thioflavin-S staining) plaques and detected the presence of the C5b-9 MAC when compared to controls (Tenner and Fonseca, 2006). Although these studies introduce a role for C1q in AD, later studies have only just begun to characterise what this role is and the part it plays in the pathogenesis of AD.

It has been postulated that C1q plays a neurodetrimental role in the CNS. One study identified by Webster and colleagues identified a contribution of C1q towards the aggregation of AB. In-vitro experimentation demonstrated a 7-fold enhancement of Amyloid beta aggregation on co-incubation with C1q (Webster et al., 1994), indicating that C1q may be a trigger for the aggregation of AB into fibrillar amyloid. Previous in-vivo experimentation has shown fibrillar amyloid aggregation, to be one of two major focal points at which clinically significant cognitive decline occurs (Reviewed in Tenner and Fonseca, 2006). Therefore, it can be postulated from this evidence that C1q is a major contributor towards both the pathology (fibrillar amyloid plaques) and the resulting behavioural (cognitive decline) observed in AD.

Corroborating with the studies mentioned above, C1q-/- transgenic mice over- expressing an aberrant form of APP, were created to characterise the role of C1q in AD. When compared to transgenic mutant APP mice with the comprehensive complement system, there was a significant decrease in the observed inflammatory glial markers proximal to the plaques in C1q-/- mice. In addition, the researchers further reported an improvement in the neuronal integrity of APP C1q-/- when compared with APP mice, despite there being no change in the plaque pathology (Fonseca et al., 2004). Furthermore, inhibiting the binding of C1q to Aβ may lead to the protection of hippocampal cells (reviewed in (Shastri et al., 2013). This body of evidence suggests that C1q may exert a detrimental role in AD by contributing towards the aggregation of fibrillar amyloid, causing an increase in inflammation and an activation of the classical complement cascade, the major consequence of which is a loss of neuronal and neurite integrity.

Seemingly at variance with these compelling studies, many researchers have

hypothesised that the role of C1q and the complement system in AD is neuroprotective in nature. Some studies have bolstered this postulation. Foremost were the observations that C1q deficient individuals develop systemic lupus (Botto and Walport., 2002) and APP C1q-/- mice of a particular strain display an SLE-like phenotype, evident in the persistence of glomerulonephritis. The hallmarks of the disorder are multiple apoptotic cell bodies and immune deposits, assessed by immunofluorescence and electron microscopy (Botto et al., 1998). Providing an in-vitro correlate, subsequent experiments have shown that globular head domains of C1q bind to apoptotic cells (Navratil et al., 2001), thus inducing activation of the complement system (Nauta et al., 2002). The stability of the binding between the cells and C1q increases during the latter stages of apoptosis, due to the shedding of complement inhibitors from the cell membrane in early apoptosis (Trouw et al. 2007; Fraser et al. 2010). Moreover, C1q through direct binding and opsonisation of target cells, or by binding IgM on late stage apoptotic cells has been shown to contribute to apoptotic cell clearance (Ogden et al. 2001; Chen et al. 2009), thereby leading to the activation of the complement pathway, recognition by phagocytes such as microglia, and subsequent phagocytic clearance (Trouw et al., 2007). A reduction in inflammation and inflammatory markers was also observed in this study. C1q itself does not induce pro-inflammatory cytokine production. It inhibits the activation of NFkB, an important pro-inflammatory regulator and thus leads to a resolution of inflammation (Fraser et al., 2007). Interestingly, C1q may serve as a reliable marker of microglial activation (CNS resident macrophage), ranging from undetectable levels of C1q biosynthesis in resident microglia to high C1q expression in activated, non-ramified microglia. Microglia added to C1q coated wells or fed apoptotic neurons, or neuronal blebs coated with C1q suppressed the expression of IL- 1α, IL-1β, IL-6 and TNF-α (Fraser et al., 2010).

Wyss-Coray and colleagues reported that "activation of the CCP can attenuate the effects of AB mediated toxicity and may also reduce the amyloid load either by promoting clearance of senile plaques or reducing their accumulation" (Wyss-Coray et al., 2002). Furthermore, it was previously reported that AD mice expressing soluble CR1 an inhibitor of complement protein C3, displayed more AB deposition and further progressed neurodegeneration than age-matched controls (Fonseca et al., 2004). Concurrently, complement inhibitor C4b-binding protein (C4BP) was found to be present on apoptotic cells and in AB plaques in-vivo (Trouw

et al., 2008). C4BP is a cofactor in factor I mediated cleavage of C4b and C3b and thus inhibiting the formation of C3 convertase and accelerating its decay. Additionally, C4BP binds to pathogenic proteins, apoptotic and necrotic cells, which prevents opsonisation of cells and phagocytic clearance. Thus, C1q activation and the subsequent formation of the MAC play a decisive role in the induction of neuronal apoptosis and phagocytic clearance in AD (Trouw et al., 2008).

1.15 Regulators of complement activation

Regulation of the complement system does not solely rely on the expression of the complement proteins. In order to complete its full innate immune role it relies on the efficacious binding to its receptor components which are present on many CNS cells. One such example of disruption of normal complement function is the decreased concentration of CR1 (also known as C3b/C4b or CD35 receptor) encoded by the previously described CR1 gene in AD. Due to a gene variant, which produces a low copy number of the protein, the proportion of C3b opsonised immune complexes that are phagocytosed will be significantly lower than in an age- matched control. As such inflammation will persist in a chronic state, as the toxic species continue to reside in the CNS milieu. C4BP, Factor H, CD46 CD55 are inhibitors of C3b, which prevent formation of the MAC, with the former residing on the surface of apoptotic membranes thus inhibiting phagocytosis and ensuring the persistence of necrotic cells (Trouw et al., 2008).

Insufficiency or deficiency of complement inhibitors may also play a significant role in the pathogenesis of AD. CD59, which prevents MAC by forming a complex with C5b-8, has been shown to be significantly decreased in the frontal cortex and hippocampus of AD compared with non-demented elderly patients (Yang et al., 2000), whereas C9, the terminal component of MAC, is significantly increased. Aβ-peptide can down-regulate CD59 expression at the mRNA level, suggesting a partial explanation for CD59 deficit in the AD brain (Kolev et al., 2009).

The evidence presented for either a neuroprotective role or a neurodetrimental role for C1q in AD, though seemingly contradictory are equally compelling. Both streams of research implicate C1q as an important regulator of internal homeostasis.

We postulate that the different roles observed are due in large part to the presence of fibrillar amyloid and its activation of the complement system. In the absence of fibrillar amyloid we suggest that CCP activation, opsonisation and phagocytic clearance will occur. However, in its presence activation of the CCP will occur, but due to inhibitors of downstream complement factors such as C4BP, Crry, formation of the MAC will be diminished. As a result, apoptotic cells will persist within the CNS parenchyma and inflammation will be perpetuated. In order to combat this, two streams of action may be taken. One such option would be to increase the amount of C1q. However, we suggest this would likely have minimal effect, as C1q is already upregulated in AD. Hence, the more likely avenue for treatment would be the creation of recombinant proteins, to provide competitive binding for Aβ, thus reducing CCP activation and the recruitment of microglia to the target site.

1.16 Hypotheses

From the experimental evidence shown above it is evident that C1q, the complement pathway and the MAC play a role in the perpetuation of chronic inflammatory state observed in AD. Whether through direct binding to Aβ and the neuronal membrane, impairment of microglial phagocytosis, the indirect contribution to amyloid aggregation; the detrimental effects of C1q far outweigh its innate immune protection. As such we posit that the complement pathway and its primary recognition component C1q are viable targets, which when inhibited may have therapeutic implications either as a sole therapy or as a co-adjuvant to currently existing therapies.

The objective of this study is to create recombinant C1q recombinant proteins capable of trimerizing in solution, in order to mimic the globular heads of C1q. We will be able to study the role of the individual globular head modules (A, B or C) of the complement system in Alzheimer's disease and test their viability as inhibitors of the CCP. First, we will investigate whether the monomers and homotrimers of C1q activate (consume) complement in human serum. If serum consumption occurs then the monomers and homotrimers will not be useful as competitive inhibitors, as they are capable of activating the complement system. Secondly, we will investigate the ability of the recombinant peptides to inhibit haemolysis (erythrocyte lysis) caused by the terminal membrane attack complex of the CCP. Thirdly we will investigate the ability of monomers and homotrimers to bind to Amyloid Beta. Once that is characterised, we will examine their ability to act as competitive inhibitors to the C1q-Aβ mediated activation of BV-2 cell microglia mouse model and the corresponding release of inflammatory mediators. Finally, we will examine the transcriptome (the total mRNA) molecules expressed by the BV-2 cells, and assess the differential expression of mRNA transcripts in response to challenge by Aβ in the absence and presence of globular head monomers or trimers.

CHAPTER 2:

MATERIALS AND METHODS

2.1 Constructs of vectors for the intracellular expression of the globular head region of C1q A, B, and C chains as fusion proteins

The plasmid pMal-c2 (New England Biolabs, Beverly, MA), which codes for maltose-binding protein (MBP) under the Tac polymerase (P_{tac}) promoter, was used as a vector for expression of C-terminal globular region of C1q A, B and C, designated ghA, ghB and ghC respectively.

Further details concerning the primers, restriction enzymes and the expressed polypeptide sequence have been described earlier (Kishore et al., 2003).

2.2 Constructs of mouse globular head C1q A, B and C chains as fusion proteins

The constructs were provided by Dr Ahishek Shastri according to the protocol below. Sequence information can be found in the Appendix.The plasmid used for protein expression was pMal-c (New England Biolabs, Beverley, MA), which codes for maltose-binding protein under the Ptac promoter (de Boer, Comstock, 1983, PNAS). The primers used to amplify the DNA sequences of each of the globular heads were: ghA forward primer (FP) 5'-GGGGAATTCAGGGACCAGCCCCGGCC-3' and ghA reverse primer (RP) 3'-GGGAAGCTTTCAGGCCGAGGGGAAAATGAGGAAT-5'; ghB FP 5'-GGGGAATTCGGGGCTACACAGAAAGTCGCCT-3' and ghB RP 3'-GGGAAGCTTTTACGCATCCATGTCAGGGAAAAGCA-5'; ghC FP 5'-GGGGAATTCAAACAGAAGCACCAGTCGGTATTCACA-3' and ghC RP 3'-GGGAAGCTTCTAGTCGGGAAACAGTAGGAAACCA-5'. Plasmid pMal-c was double digested with *EcoRI* and *HindIII* and each PCR product was cloned as a *EcorI-HindIII* fragment. The polypeptide sequence thus expressed corresponded to residues of mghA, of mghB and of mghC.

2.3 Construction of plasmid encoding the neck region of human SP-D and globular head homotrimer

The expression vector pCRT7/NT-TOPO (Life Technologies, Paisley, UK) which contains delta SPD, was cut with SacI and BamHI to remove the SPD globular head, but retain the trimerising neck region. Each of the globular domains of C1q was inserted into the above plasmid with SacI and BamHI. Primers used are displayed in table 2.1

ghA FP AglobSacI	ccaggagagctcaaggaccagccgaggccagcc
ghA RP AglobBamHI	tccttcggatcctcaggcagatgggaagatgag
ghB FP BglobSacI	tagggagagctcaaggccacccagaaaatcgcc
ghB RP BglobBamHI	gcagccggatcctcaggcctccatatctggaaa
ghC FP CglobSacI	gagggcgagctcaagcagaaattccagtcagtg
ghC RP CglobBamHI	Catctggatccctagtcggggaagagcaggaa

Table 2.1: Table showing the forward primer (FP) and Reverse primer (RP) design for pCRT7 recombinant vectors of globular heads A, B and C.

PCTR7 constructs were provided by Dr Paddy Waters, and created as previously described (Kishore et al., 2001).

2.4 The expression vector pMal- c5x.

Due to the tendency of pCRT7 to form inclusion bodies when overexpressed, the plasmid pMal-c5x (5677 bp; New England Biolabs, Beverly, MA), which codes for maltose- binding protein (MBP) under the Tac polymerase (Ptac) promoter, was deemed to be more suitable for the expression of the globular head homotrimers ghA, ghB and ghC. The MBP in pMal C has been engineered to bind more tightly to amylose, thus ensuring that a higher proportion of protein is purified. The yield of fusion protein from the affinity purification ranges up to 200 mg/L culture, with typical yields in the range of 10–40 mg/L.

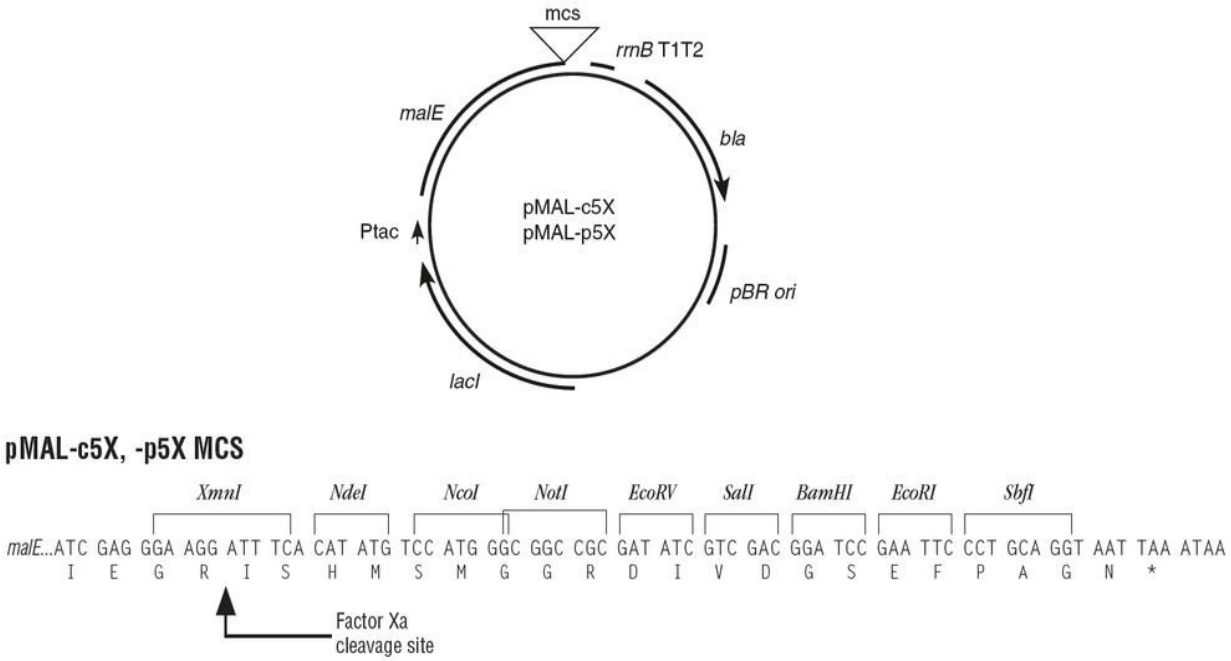

Fig 2.1: The pMAl-c5x vector was used for the expression of ghA3, ghB3, ghC3 as recombinant fusion proteins. The genes were inserted downstream of the malE gene which codes for MBP.

2.5 Amino acid sequence of globular head multimer constructs

The amino acid sequence for the constructs of the multimer constructs can be found below:

ghA^3 amino acid sequence

MDVASLRQQV EALQGQVQHL QAAFSQYKKV ELKDQPRPAF SAIRRNPPMG GNVVIFDTVI INQEEPHQNH SGRFVRTVPG YYYFTFQVLS QWEICLSIVS SSRGQVRRSL GFCDTTNKGL FQVVSGGMVL QLQQGDQVWV EKDPKKGHIY LGSEADSVFS GFLIFPSA

168 aa | Molecular weight ~ 19kDa | Theoretical pI: 8.60| Abs 0.1% (=1 g/l) 0.985

ghB^3 amino acid sequence

MDVASLRQQV EALQGQVQHL QAAFSQYKKV ELKATQKIAF SATRTINVPL RRDQTIRFDH VITNMNNNYE PRSGKFTCKV PGLYYFTYHA SSRGNLCVNL MRGRERAQKV VTFCDYAYNT FQVTTGGMVL KLEQGENVFL QATDKNSLLG MEGANSIFSG FLLFPDMEA

169 aa | Molecular weight ~ 19 kDa | Theoretical pI: 9.19 | Abs 0.1% (=1 g/l) 0.552

ghC^3 amino acid sequence

MDVASLRQQV EALQGQVQHL QAAFSQYKKV ELKQKFQSVF TVTRQTHQPP APNSLIRFNA VLTNPQGDYD TSTGKFTCKV PGLYYFVYHA SHTANLCVLL YRSGVKVVTF CGHTSKTNQV NSGGVLLRLQ VGEEVWLAVN DYYDMVGIQG SDSVFSGFLL FPD

163 aa | Molecular weight ~ 18 kDa | Theoretical pI: 8.43 | Abs 0.1% (=1 g/l) 0.966

2.6 Plasmid extraction

A single colony of TOP10 bacterial cells transformed with pCRT7-ghA$_3$, -ghB$_3$, or -ghC$_3$ was inoculated in 20ml of Lysogeny broth (LB; 10 g/l Tryptone, 5 g/l yeast extract, 10 g/l NaCl, pH 7.0) bacterial growth medium and placed in a shaker for 12-16 hours at a temperature of 37± 2°C. The next morning, the culture was centrifuged at 5000 rpm for 10 minutes. Plasmid was extracted from the pellet using the Qiagen Spin Miniprep Kit (Qiagen, Manchester, UK). Pellet was resuspended in 250ul of buffer P1, followed in quick succession by 250ul of lysis buffer P2 (25^{o}C, 5 mins). 350ul of neutralization buffer N3 was added to the

samples, in order to stop the cell lysis. Cells were mixed by inversion (x12) and left at room temperature for 10 mins. Samples were spun at 13,000 rpm for 10 mins, and the supernatant was transferred to a spin column (provided within the kit) and centrifuged for 30-60s (13,000 rpm). The flow through was discarded and 500ul of binding buffer was added to the column. Column was again spun for 30-60s (13,000 rpm), and flow through discarded. 750ul of wash buffer PE was introduced into the column and the previous step was repeated. In order to ensure that all residual buffers were removed from the column, it was again spun for 30-60s (13,000 rpm). 50ul of kit provided elution buffer was then added to the column. The column was left to stand for 4 mins, and then spun at 13,000 for 60s. Concentration of plasmid obtained was read at A_{260} using the Nanodrop. Composition of all kit buffers can be found on the product page at qiagen.com

2.7 Double digestion of plasmids Pmal-c5x and pCRT7

Nde1 and BamH1 restriction endonucleases (New England Biolabs, Beverly, MA) were chosen to cut the plasmids pMal-c5x and pCRT7, as neither enzyme cut within the gene sequence encoding ghA, ghB and ghC. 1ug of plasmid was double digested in a 50ul reaction (2.5ul Nde1, 2.5ul BamH1, 5ul of 10x cutsmart buffer, pure dH_2O; 37^oC, 2hr). Reaction products were run on a 1% Agarose gel with TAE buffer (40 mM Tris-acetate, 1 mM EDTA). Uncut versions of pCRT7-ghA_3, -ghB_3, and -ghC_3 were run as controls for their corresponding digests. DNA gel stain Gels were run using 1ul gel red (Biotium, UK) as a substitution for EtBr.

Once a gel image was obtained, and the presence of target DNA band (500 bp) for the Nde1-BamH1 fragment (SPd-homotrimer fragment) was confirmed; the bands were excised from the gel with a clean scalpel. Double digested pMal-c5x was also excised from the gel to form the plasmid backbone for the 500bp SPD neck region-ghA_3, -ghB_3, and -ghC_3 fragments.
DNA was then extracted from the excised slice using a Qiagen gel extraction kit. The concentration of the DNA fragments was obtained by A_{260} reading on the nanodrop spectrophotometer. pMal-c5x backbone was ligated to the Nde1-BamH1 fragment at a ratio of 1:3 (plasmid: insert, 2ul T4 ligase buffer, 1ul T4 ligase, pure H_2O to 20ul). A control ligation reaction was also run at a ratio of 1:3 (water: insert,

2ul T4 ligase buffer, 1ul T4 ligase, pure H_2O to 20ul). The ligation reaction was left at room temperature for 20 mins, and stored at -20°C until required for bacterial transformation.

2.8 Bacterial Transformation

A single colony of E. Coli cells (TOP10, BL21 (DES) or BL21 (DE3) pLysS; Life Technologies, Paisley, UK) was inoculated in 5ml of LB bacterial growth medium and placed in a shaker for 12-16 hours at a temperature of 37± 2°C. 500µl of the primary culture was then inoculated in 25mL of LB. A_{600} of the secondary culture was read until the cells reached an optical density value of 0.3. Bacterial cells were then spun at a centrifugal speed of 5000 revolutions per minute (rpm) for 10 minutes. The supernatant was removed, and the pellet was gently suspended in 12.5 mL of 0.1M $CaCl_2$ (O - 4°C). The mixture was left on ice for an hour and underwent further centrifugation. Cells were again re-suspended, in 2mL of 0.1M $CaCl_2$. The cells are now deemed competent i.e. able to take up extracellular DNA from their environment.

2 µl of ligation reaction between recombinant DNA and Pmal-c5x was mixed with 200 µl of competent BL21 cells and incubated on ice for 30 minutes. The cells were then heated at 42°C for 2 minutes and rested on ice for a further 3 minutes. 800 µl of LB was added, and the cells were grown at 37± 2°C for 1 hour. Subsequently, the cells (TOP10 or BL21 (DES)) were plated on LB agar plates containing 100µg/ml ampicillin and grown for 14- 16 hours. BL21 (DE3) pLysS competent cells when used were plated on LB agar plates containing 100µg/ml ampicillin and 100µg/ml chloramphenicol.

2.9 IPTG mediated testing of recombinant protein expression: Pilot scale

A single colony was selected from the plate obtained as a product of the bacterial transformation reaction. It was incubated in 5ml of LB for 14-16 hours (37°C), with a dilution of the resistant antibiotic ampicillin (100µg/ml). 500ul of primary culture obtained for each recombinant protein was grown in 10ml of fresh LB containing ampicillin (100µg/ml) at a dilution of 1:1000 and incubated (37°C)

until A_{600} reached between 0.6-08. Once the desired optical density was reached 1ml of sample (designated the uninduced sample) was saved for subsequent analysis. To the remainder of the secondary culture, 0.4mM isopropyl β-D-thiogalactoside (IPTG, 37oC) was added, to trigger the transcription of the malE gene. After 3 hr 1ml of sample (designated the induced sample) was taken out to test the expression. Both samples underwent centrifugation at 13,000 rpm for 10 mins. The supernatant was discarded, and each crude pellet was re-suspended in 50ul dd.H20 and 50ul 2x leammli buffer (4% SDS, 20% glycerol, 10% 2-mercaptoethanol, 0.004% bromophenol blue and 0.125 M Tris HCl, pH 6.8). All samples were denatured at 100^{o}C on the heatblock for 5-10 mins. Subsequently 20ul of each sample was assessed by SDS-PAGE gel electrophoresis (12% w/v) under reducing conditions to identify whether the fusion proteins MBP-ghA, -ghB and –ghC, are present and expressing. If found to be expressing, 1-3ul of primary culture was taken up with an inoculation loop and spread onto selective LB ampicillin plate.

2.10 Large scale recombinant protein expression

A single colony was selected from the plate obtained as a product of the pilot scale expression. It was incubated in 25ml of LB for 14-16 hours (37°C), with a 1:1000 dilution of the resistant antibiotic.

12.5ml of primary culture obtained for each recombinant protein was then grown (37°C), in 1000ml fresh Luria-Bertani medium containing ampicillin (100µg/ml) at a 1:1000 dilution. When A_{600} reached 0.6, the uninduced sample was taken; the culture was induced with 0.4mM IPTG for 3hr, and then centrifuged (3,000 x g, 4 ^{o}C, 15 min). The pellets were then stored at -20°C, until required for purification by affinity chromatograph.

2.11 MBP fusion protein purification: Amylose affinity chromatography.

The cell pellet was suspended in 20ml of lysis buffer (20 mM Tris-HCl, pH 8.0, 0.5 M NaCl, 0.2% v/v Tween 20, 1 mM EDTA, 5% v/v glycerol, and 0.05% NaN_3) containing lysozyme (100 µg/ml) to lyse the phospholipid membrane and the protease inhibitor Phenylmethanesulfonylfluoride (PMSF (0.1 mM)) and

incubated on a roller at 4°C for 1 h. The cell lysate was then sonicated at 60Hz for 30 s with an interval of 1 min (12 cycles) to disrupt the cells and shear the bacterial chromosomal DNA. After centrifugation (10,000 x g for 15 min), the supernatant was collected and diluted 5-fold using buffer I (20 mM Tris-HCl pH 8.0, 100 mM NaCl, 0.2% v/v Tween 20, 1 mM EDTA, 5% v/v glycerol, and 0.05% NaN_3) and passed through an amylose resin column (15 ml). The column was first washed with buffer I (150 ml), followed by buffer II (20 mM Tris-HCl, 100 mM NaCl, 1 mM EDTA, 5% v/v glycerol, and 0.05% NaN_3) with 1M NaCl. Each fusion protein was then eluted with 50 ml of buffer II containing 10 mM maltose. A280 was read for each fraction and peak fractions (A280>0.3) were pooled. Pooled elution fractions in maltose buffer were dialysed overnight in buffer II in order to exchange the buffer.

2.12 Ion exchange chromatography for further purification of the more anionic protein

In some cases, amylose resin purification was insufficient to remove all proteins obtained from the cell lysate and further cleaning of the elution fractions was required. DEAE Sepharose (Sigma-Aldrich, Dorset, UK) was used for ion exchange chromatography. First, the column was washed with 3 bed volumes of autoclaved d.H_2O, followed by an extensive wash with buffer II $_{1000\ mM\ NaCl}$ (20 mM Tris-HCl, pH 7.5, 1 M NaCl, 2 mM $CaCl_2$, 5% v/v glycerol, and 0.05% NaN_3). Subsequently the column was washed and equilibrated with buffer II (20 mM Tris-HCl, pH 7.5, 100 mM NaCl, 2 mM $CaCl_2$, 5% v/v glycerol, and 0.05% NaN_3). Peak elution fractions of the MBP-fused proteins were passed through the column and followed by a second extensive wash with buffer II. The MBP fused proteins were eluted using a steep NaCl gradient elution with buffer II $_{150\ mM\ NaCl}$ to buffer II $_{1000\ mM\ NaCl}$. A_{280} was read for each fraction and peak fractions (A_{280}>0.3) were pooled.

2.13 Factor Xa digest of MBP-fused protein and post-digest ion exchange chromatography

Factor Xa (New England Biolabs) was added to MBP fusion protein (1U factor Xa per 100 µg of MBP fusion protein) and incubated overnight (4°C). The digest was loaded over a DEAE Sepharose (Sigma-Aldrich, Dorset, UK) column

and washed extensively with Factor Xa buffer. ghA_3, ghB_3, and ghC_3 were eluted using a steep gradient elution 0.15-1M NaCl. A_{280} was read for each fraction and peak fractions (A_{280}>0.1) were pooled.

2.14 Endotoxin Removal

Endotoxins consist of the biologically active Lipopolysaccharides (LPS) and structural components of the outer cell membrane of gram-negative bacteria. Small amounts in recombinant protein preparations can cause side effects, which include endotoxin shock and tissue injury. Removal was carried out using the Pierce High-Capacity Endotoxin Removal Resin Kit (Pierce Biotechnology, Rockford, IL, USA). Subsequently the Limulus amoebocyte assay (LAL; Lonza, Allendale, NJ, USA) was used to measure the endotoxin levels.

2.15 DNA sequencing

To confirm the DNA sequence of the recombinant proteins, the plasmids were applied to Beckman Coulter Genomics (Herts, UK) plasmid DNA sequencer. The forward and reverse primers were determined using BLAST Final DNA sequence was confirmed for each trimer.

2.16 Enzyme Linked Immuno-sorbent assay (ELISA)

Direct binding ELISA experiments were performed by coating flat-bottomed 96 well microtiter plates (Fisher Scientific, UK) with Aβ-42 (1µg/well; Sigma Aldrich, UK. A9810-.1MG), 199µl carbonate bicarbonate buffer (CBB, 0.0125 M Sodium bicarbonate, 0.0875 M Sodium Carbonate). The concentration of the Aβ-42 peptide was diluted down from 1 µg to 0.6 µg. This process was repeated for each protein in triplicate. The plate was covered with foil and was kept in the fridge at 4°C overnight. The following day the plate was blocked with 2% BSA (in PBS). The plate was left to incubate at 37° for 2 hours. The plate was washed with PBST (PBS + 0.02% Tween 20) three times. A solution containing MBP-ghA, -ghB, -ghC, -mghA, -mghB, -mghC, $-ghA_3$, $-ghB_3$ or $-ghC_3$ protein diluted in PBS (5 µg: 100 µl)

was added to wells coated in the different concentrations of Aβ-42 in triplicate. The plate was incubated for 1 hour at 37° first, and then incubated in ice for 1 hour. The plate was washed again with PBST three times. Anti- MBP mAb (1:5000 PBS; 100 µl per well) was used as the primary antibody and added to the wells. A 1-hour incubation at 37° followed. The plate was washed with PBST three times. Goat-anti mouse horse radish peroxidase (1:5000 PBS; 100 µl per well; Sigma Aldrich, UK) was used as the secondary antibody, and added to the plate, followed by 45 minutes incubation at 37°. Finally, colour development occurred using Tetramethylbenzidine (TMB) substrate (Sigma Aldrich, UK. RABTMB1-12ML). Absorbance 450nm was read for each sample. As the proteins utilised in this experiment were MBP fused, MBP was used as a standard while BSA was used as a negative control.

2.17 Binding specificities of MBP-gh to heat aggregated mouse IgG

A direct binding ELISA was performed by coating the wells of 96 well microtiter plate (Fisher Scientific, UK) with MBP-ghA, -ghB, -ghC, -mghA, -mghB, -mghC, -ghA_3, -ghB_3 or -ghC_3 (0.6-20 µg/well) in 200ul of CBB overnight at 4°C. Wells were blocked with 2% BSA in PBS for 2hrs. Subsequently wells were washed with PBST and incubated with heat aggregated IgG (10µg/ml) in a PBS 10mM $CaCl_2$ solution for 2 hrs (100ul). Protein A-HRP (1:5000 PBS; 100 µl) was used to probe for bound IgG. After a 2hr incubation, colour development occurred using the TMB substrate. Absorbance 405nm was read for each sample. As the proteins utilised in this experiment were MBP fused, MBP was used as a standard while BSA was used as a negative control.

2.18 Sensitization of Sheep red blood cells

5 ml of Sheep Blood in Alsever's (Cat SB068; TCS Biosciences ltd., UK) was divided equally between two 50ml centrifuge tubes. The samples were washed with 30ml Dulbecco's PBS (0.9 mM $CaCl_2$, 2.7 mM KCl, 0.5 mM $MgCl_2.2H_2O$, 138 mM NaCl, 8.1 mM Na_2HPO_4, ph. 7.4) and centrifuged at 3000 rpm for 10 mins. Supernatant was discarded, washed and centrifuged a further 3 times. Each crude pellet was re-suspended in 10ml Dulbecco's PBS. To obtain the required cell concentration of 10^9/ml, 100ul was added to 1.4ml of dH_2O and A_{541} was

measured until an OD of 0.7 was obtained. If the OD was much higher than 0.7 then the sample was further diluted with Dulbecco's PBS.

In order to sensitise the cells 10ml of cells at 10^9/ml was incubated with 100ul of haemolysin (H9395-.5MG; Sigma Aldrich, UK.; volume may be increased to increase sensitivity, 37^{o}C, 15 min), and mixed through gentle inversions. The cells were then placed on ice for a further 15 mins. Sensitised cells (EA) cells were then washed once with Dulbecco's PBS, and a further 2 times in $DVGB^{++}$ buffer (0.15 mM $CaCl_2$, 141 mM NaCl, 0.5 mM $MgCl_2$, 1.8 mM sodium barbitone, 3.1 mM barbituric acid, 0.15% w/w gelatine, 2.5% w/v glucose, pH 7.4; per Litre). Each washing step requires centrifugation and re-suspension (2000 rpm, 5-10 mins, 4oC). Supernatant was discarded. EA cells were re- suspended and adjusted to 10^9/ml in $DVGB^{++}$ buffer. Cells were subsequently stored at 4oC until required.

2.19 Haemolytic assay

Haemolytic assays were conducted with the sensitised EA cells to assess the haemolytic activity of human serum. The EA cells and the non-sensitised erythrocytes (E cells) A 1/10 serial-folding dilution of normal human serum (NHS) was performed starting from 1:10 dilution of NHS diluted in $DGVB^{++}$ buffer down up to 1:5120 dilutions (I.e 10 2-fold dilutions). This was performed in duplicate to enable the addition of either 100ul E or 100ul EA cells individually to each sample within one group each of serial dilutions. Two positive controls of undiluted NHS, and ddH_2O were also used. Reactants were incubated (37^{o}C, 1 hr). Cells were then centrifuged (5000 rpm, 5 mins), and 180ul of supernatant was added to a microtiter plate. A_{541} was read with a spectrophotometer.

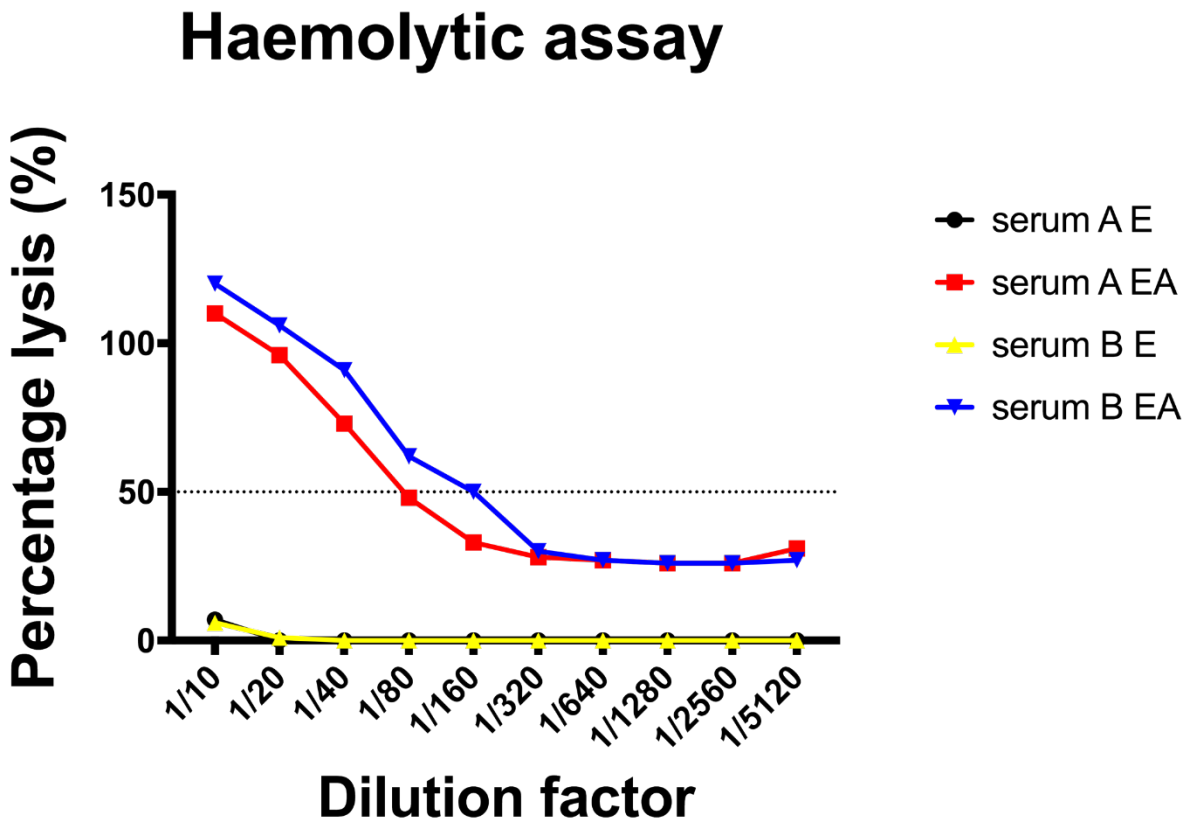

Fig 2.2: Haemolytic assay.
Graph was plotted as percentage lysis observed for each dilution. Two different serums from 2 different individuals was used. The greater the serum dilution factor, the lower the haemolytic activity. From this graph we obtained CH50 values with which to conduct the next set of experiments. CH50 is calculated from the dilution at which 50% lysis occurs.

2.20 Classical complement pathway inhibitory assay

A complement inhibitory assay was conducted in order to investigate the ability of MBP-gh to inhibit C1q dependent haemolysis of EA cells. Globular heads (MBP-ghA, -ghB, -ghC, -mghA, -mghB, -mghC, -ghA$_3$, -ghB$_3$ or -ghC$_3$) (0.6-10ug; 100ul in PBS), or MBP, were incubated with EA cells in a U bottom 96 well microtiter plate (Fisher Scientific, UK) for 1h at 37 °C. Cells were pelleted by centrifugation (3000 rpm, 2 mins). Subsequently cells were washed with DGVB^{2+}, pelleted by centrifugation (3000 rpm, 2 mins) and resuspended in 100 µl of DGVB^{2+}. Cells were then incubated with 1 µg/ well C1q (Millipore, UK), 2.5 µl/well of C1q deficient serum (Millipore, UK), and 96.5 µl/well of DGVB^{2+} for 1hr at 37^{o}C. Subsequent to the incubation, cells were spun down and pelleted (3000rpm, 10 min). 180µl of supernatant was transferred to

a 96 well flat bottom microtiter plate. Amount of haemoglobin released was measured at Absorbance 541nm using a spectrophotometer plate reader. Total Haemolysis (100%) was measured by lysing EA cells with H_2O (100ul:100ul). Spontaneous haemolysis was measured by incubating EA cells with $DGVB^{2+}$ buffer (100ul:100ul). MBP was used as a negative control for the experiment. Percentage lysis was calculated by:

$$\% \text{ lysis} = \frac{OD_{540} \text{ test} - OD_{540} \text{ (Blank)}}{OD_{540} \text{ (total lysis} - OD_{540} \text{ (Blank)}} \times 100$$

Results were plotted as concentration of MBP-gh vs percentage lysis.

2.21 Classical complement system consumption assays

Complement consumption assays were conducted in order to ensure that ghA, ghB, ghC, ghA^3, ghB^3 and ghC^3 are incapable of activating the classical complement pathway. Globular head proteins ghA, ghB, ghC, ghA^3, ghB^3 and ghC^3, and C1q at concentrations of 0.6, 1.25, 2.5, 5 and 10ug/well; 100ul in PBS were incubated with C1q deficient serum (1:80 dilution) in a 96 well microtiter plate (Fisher Scientific, UK) for 1h at 37 °C. C1q was used as a positive control. After an 1hr, excess precipitate complexes with gh were removed by centrifugation (2500 rpm, 10 mins). Subsequetly the supernatants of each sample was then transferred to a fresh 96 well plate and incubated with 100 µl of EA (108 cells/ml in $DGVB^{2+}$) in U bottom 96 well microtiter plates for 1hr at 37°C. Subsequent to the incubation, cells were spun down (2500 rpm, 10 min). The supernatant was then transferred to a 96 well flat bottom microtiter plate. Amount of haemoglobin released was measured at Absorbance 541nm using a spectrophotometer plate reader. Complement consumption per recombinant protein at each concentration was then calculated as a percentage of C1q consumption at the same concentration.

2.22 Statistical Analysis

Data analysis was performed with GraphPad Prism version 8.01. We utilised 2-Way ANOVA and unpaired t-test. qPCR and mRNA expression values were normalized to β-Actin expression values.

CHAPTER 3:

Cloning, expression and purification of individual homotrimer globular heads ghA3, ghB3 and ghC3

3.1 Introduction

C1q, the recognition subcomponent of the classical complement pathway, is a 460kDa protein consisting of 18 polypeptide chains of 3 types (6A, 6B and 6C) (Fig 1.9). Chiefly produced by cells of myeloid origin, microglia are the only CNS resident cells capable of synthesising C1q (Lynch et al., 2004). Each chain consists of a 3-9 aa N-terminal region, an 81 aa collagen-like region (CLR) and the approx. 135 aa C-terminal globular head region (gC1q) (Fig 1.9) (Sellar et al., 1991). Interchain disulphide bonds between N-terminal cysteine residues yields dimer subunits of 6 A-B and 3 C-C. The CLRs of the A-B and C-C subunits then bind through covalent and non-covalent bonds to give rise to a triple helical collagen-like unit ABC-CBA. Three of these units bind further via non-covalent bonds to form the hexameric C1q, which has been described as having morphology similar to a" bouquet of tulips" (Reid and Porter, 1976; Kishore and Reid, 1999; Kishore et al., 2003).

The globular gC1q domain (ligand recognition domain) is a heterotrimeric structure, formed from the C-terminal regions of the A, B and C chains (Kishore et al., 2003; Nayak et al., 2010). These modules are denoted globular heads A (ghA), B (ghB) and C (ghC). Proximal to the apex of the gC1q domain lies a calcium ion, which plays a significant role in the binding of C1q to immune complexes (Roumenina et al., 2005).

The ability to express these modules as recombinant proteins has been enlightening in the understanding of how C1q is activated by a host of self and non-self-ligands. A study by Kishore and colleagues (1998) revealed that although IgG and IgM seemingly bind with the same affinity to C1q, ghB preferentially binds to IgG. Further studies have elucidated that ghA can bind heat- aggregated IgG, IgM and HIV-1 gp41; ghB binds to heat-aggregated IgG as well as amyloid β and; ghC shows a preference for IgM and HTLV-1 gp21 peptide (Kishore et al., 2004). This is due to differences in the surface expression of charged and hydrophobic residues between the three subunits. For instance, a positive charge cluster of Arginine on the surface of ghB was implicated in the interaction of ghB with IgG (Marqués et al., 1993). Thus, globular heads are not only structurally different but also functionally autonomous. A multivalency of ligand recognition allows for the

production of proteins that are essentially biologically identical to each of the globular head chains of C1q and are thus able to recognize ligands; but will be unable to activate the complement system. These complement system antagonists would thus be able to prevent the activation of the complement system and stop the perpetuation and exacerbation of chronic conditions and pathologies in neurodegenerative diseases. As such, the objective of this study is to express and characterise recombinant peptides capable of trimerising in solution. As the multimeric forms have a greater binding surface area and therefore higher avidity than their monomeric counterparts, we will be able to study the role of the individual recognition components i.e. globular heads of C1q in Alzheimer's disease and test their viability as inhibitors of the binding of C1q to C1q targets. As a result of the potential inhibition of C1q binding, the constructs will act as competitive inhibitors to complement activation.

Table 3.1: List of globular head constructs expressed and purified

Globular head	Human		Mouse
	Monomer	Multimer	Monomer
A	ghA	ghA^3	mghA
B	ghB	ghB^3	mghB
C	ghC	ghC^3	mghC

All 9 globular heads listed in the table were expressed as MBP linked proteins and purified with Amylose resin to determine which will be most suitable to inhibit complement activation and the generation of the Membrane attack complex. The monomeric constructs ghA, ghB, ghC differ from the multimers ghA^3, ghB^3 and ghC^3 due to a fusion of the trimerizing neck region of surfactant protein D with the globular head region of C1q A, C1q B and C1q C chains respectively. The hypothesis was that trimers would be formed. However, this is unlikely, due to the difficulty - in this study- of separating maltose-binding protein from the recombinant proteins.

3.2 Results

3.2.1 Construction of plasmid encoding the neck region of Human SP-D and globular head using the entry vector pCRT7/NT-TOPO.

The expression vector pCRT7/NT-TOPO (Life Technologies, Paisley, UK) which contains delta SPD, was cut with SacI and BamHI to remove the SPD globular head but retain the trimerising neck region. Each of the globular domains of C1q was inserted into the above plasmid with SacI and BamHI. Primers used are displayed in table 3.2.

ghA FP AglobSacI	ccaggagagctcaaggaccagccgaggccagcc
ghA RP AglobBamHI	tccttcggatcctcaggcagatgggaagatgag
ghB FP BglobSacI	tagggagagctcaaggccacccagaaaatcgcc
ghB RP BglobBamHI	gcagccggatcctcaggcctccatatctggaaa
ghC FP CglobSacI	gagggcgagctcaagcagaaattccagtcagtg
ghC RP CglobBamHI	Catctgggatccctagtcggggaagagcaggaa

Table 3.2: Table showing the forward primer (FP) and Reverse primer (RP) design for pCRT7 recombinant vectors of globular heads A, B and C.

Constructs were provided by Dr. Paddy Waters, and created as previously described (Kishore et al., 2001). We have detailed what few changes above.

3.2.2 Agarose gel electrophoresis of Nde1-BamH1 digested pCRT7 and pMal-c5x

Plasmid pCRT7 containing the gene for the globular head modules, coupled with the SPD neck region was denoted pCRT7-A_3, pCRT7-B_3 or pCRT7-C_3. The plasmids

~3000 bp were double digested by restriction endonucleases BamH1 and Nde1 at 37^{o}C for 2 hours. The digestion was required to separate the plasmid backbone from the 500bp SPD-A, SPD-B or SPD-C DNA fragment. After digestion, the 50ul reaction products for each recombinant plasmid were run on an Agarose gel (**Fig 3.1**). Undigested pCRT7- A_3, pCRT7-B_3 or pCRT7-C_3 was also run adjacent to the corresponding digests, to provide a control/ visual confirmation that a digest had occurred.

Based on the comparison between the uncut plasmid and the double digested plasmid, it is clear that the double digest took place. Target 500bp band were visible for pCRT7-A_3, pCRT7-B_3 and pCRT7-C_3 when viewed through the UV trans illuminator and gel image- doc.

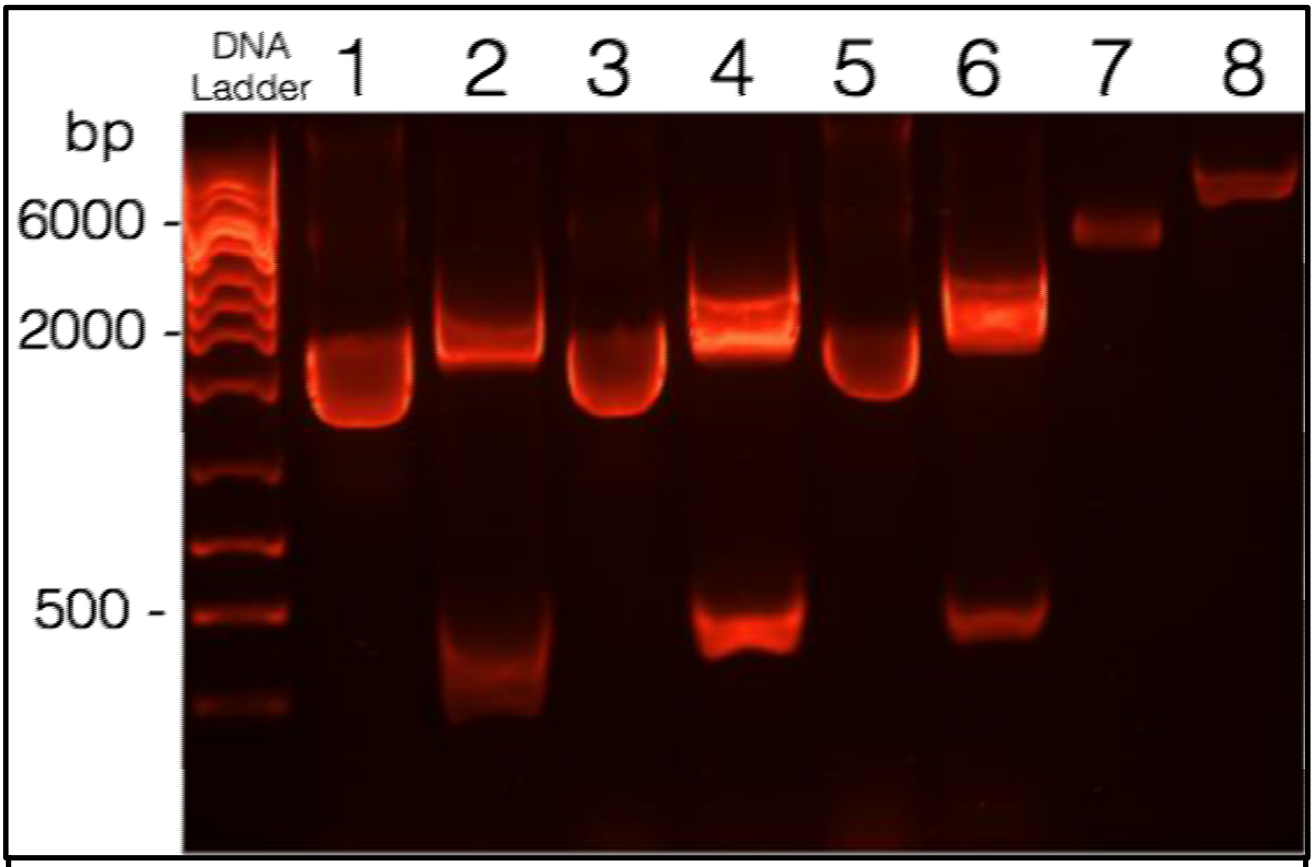

Fig 3. 1 Agarose gel electrophoresis (1.0%, w/v, 0.5ul Gel red) of Nde1-BamH1 digested pMal- c5x, pCRT7-A_3, pCRT7-B_3 or pCRT7-C_3. 1Kb DNA ladder; **Lane 1:** pCRT7-A_3; **Lane 2:** pCRT7-A_3 Nde1 BamH1 digest; **Lane 3:** pCRT7-B_3; **Lane 4:** pCRT7-B_3 Nde1 BamH1 digest; **Lane 5:** pCRT7-C_3; **Lane 6:** pCRT7-C_3 Nde1 BamH1 digest; **Lane 7:** pMal-c5x; **Lane 8:** pMal-c5x Nde1 BamH1 digest.

3.2.3 Insertion of the SPD neck-gh (A, B or C) fragment into the expression vector pMal- c5x PMC-A_3, PMC-B_3 and PMC-C_3

The double digested plasmid backbone of pMal-c5x and the Nde1-BamH1 restriction site bound DNA fragment coding for the SPD neck region - globular head A_3 multimer (ghA_3), B_3 multimer (ghB_3) and C_3 multimer (ghC_3) were ligated with the enzyme T4 ligase. The new plasmid constructs were denoted PMC-A_3, PMC-B_3 and PMC- C_3. The next day, the plasmid (5-10ng) was transformed into BL21 bacterial cells and spread unto selective LB Agar + ampicillin plates.

Agarose gel electrophoresis of the ligation products of PMC-A3 are shown in Fig 3.2. In lanes 1 and 3 the plasmid DNA appears as a weight band of approx. 3000bp in size. Lanes 2 and 4 (Fig 4.) are the reaction products of a Nde1-BamH1 double digestion of PMC-A3. There are two visible bands. The first is approximately 500 bp in size, which corresponds to the size of the fragment insert which codes for the SPD neck region - globular head A3 (ghA3). The second DNA band appears at approximately 6000 bp.

Fig 3.2 illustrates the agarose gel electrophoresis of the ligation products of PMC- B_3 and PMC-C_3. In lanes 1 and 3 corresponding to PMC-B_3 and PMC-C_3 respectively, the plasmid DNA appears as a weight band of approx. 3000bp in size. There was no other observable band within either lane. Lanes 2 and 4 (**Fig 3.3**) are the reaction products of a Nde1-BamH1 double digestion of PMC-B_3 and PMC-C_3 respectively. There are two visible bands. The first is approximately 500 bp in size, which corresponds to the size of the genetic fragment insert which codes for the SPD neck region - globular head B_3 (ghB_3) and SPD neck region - globular head C_3 ghC_3) respectively. The second DNA band appears at approximately 6000 bp in both lanes.

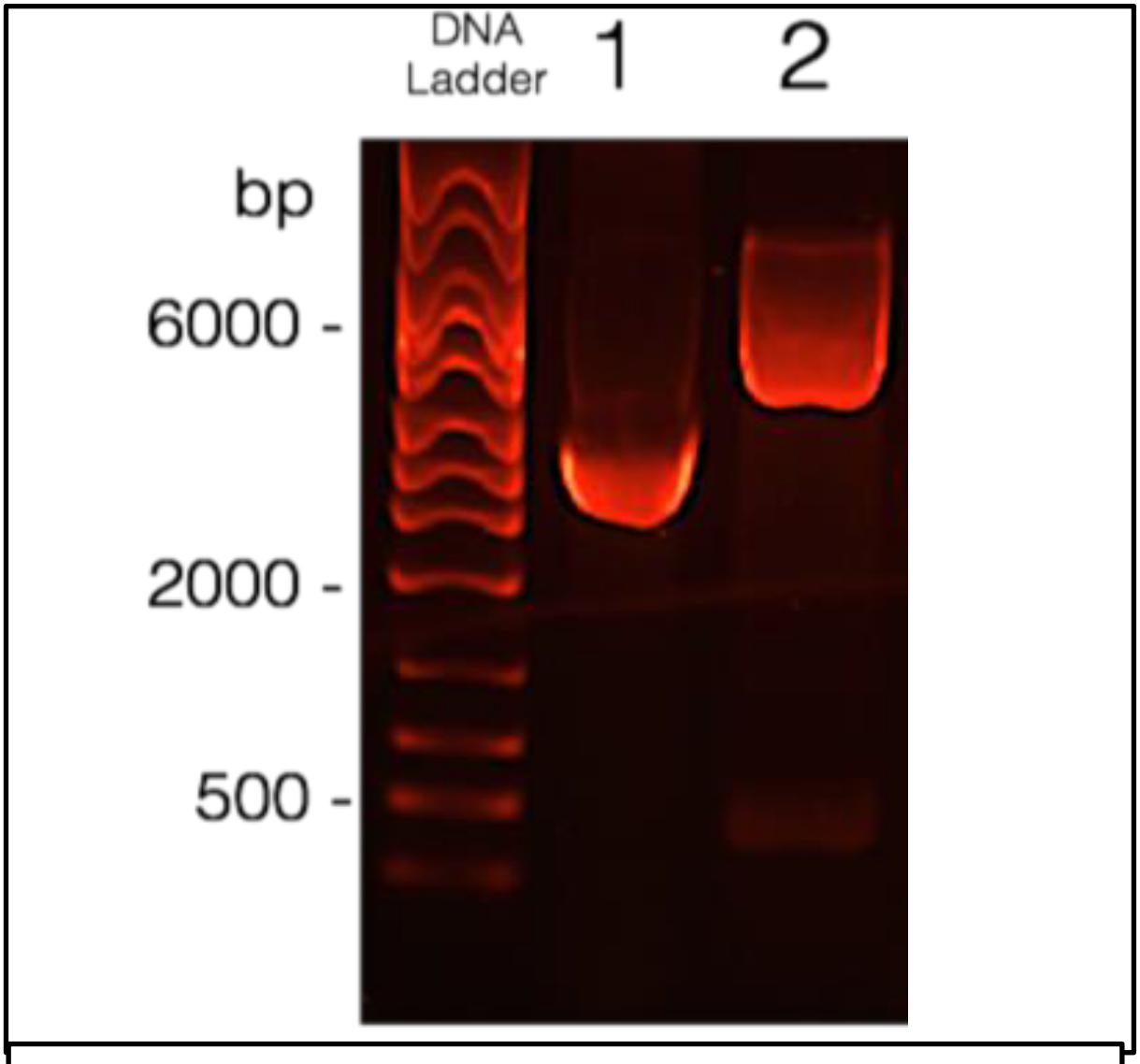

Fig 3.2 Agarose gel electrophoresis (1.0%, w/v, 0.5ul Gel red) of PMC-A_3 plasmid obtained from ligation of Pmalc-5x and SPD-A_3 gene inserts.

1Kbp DNA ladder; Lane 1: PMC-A_3; Lane 2: PMC-A_3 Nde1 BamH1 digest.

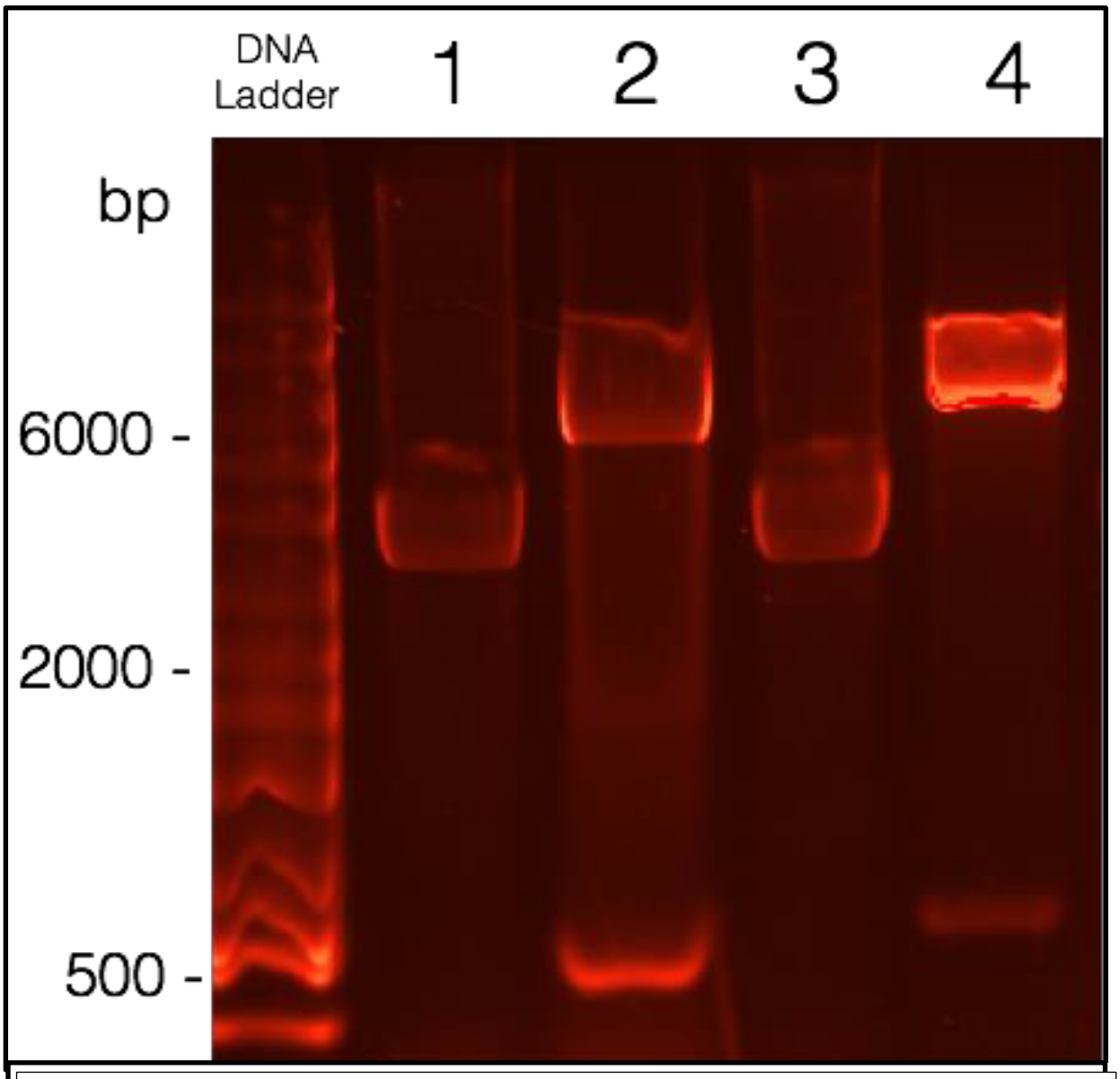

Fig 3.3 Agarose gel electrophoresis (1.0%, w/v, 0.5ul Gel red) of plasmids obtained from ligation of Pmalc-5x, SPD-B_3 and SPD-C_3 gene inserts.

1Kbp DNA ladder; Lane 1: PMC-C_3; Lane 2: PMC-C_3 Nde1 BamH1 digest; Lane 3: PMC-B_3; Lane 4: PMC-B_3 Nde1 BamH1 digest.

3.2.4 Pilot Expression of recombinant fusion proteins MBP-ghA, - ghB and -ghC

The globular head regions of C1q A, B and C chains were expressed as MBP-fused proteins in E. coli BL21 cells containing the recombinant vectors pKBM-A, pKBM-B and pKBM-C, respectively. When expressed, ghA, ghB and ghC sequences linked to MBP, expressed as one segment. MBP has a molecular weight of 42.5kDa but when this is fused to any of the globular head's sequences, the fusion protein molecular weight is expected to be between 55-65kDa. Following induction with 0.4 mM IPTG for 3 hours, each recombinant fusion protein appeared as over-expressed protein band of ~60 KDa in pilot and large-scale expressions, as judged by SDS PAGE under reducing conditions in **Fig 3.4**. Un-induced samples showed lower levels of protein expression whereas the induced sample showed predominant protein expression.

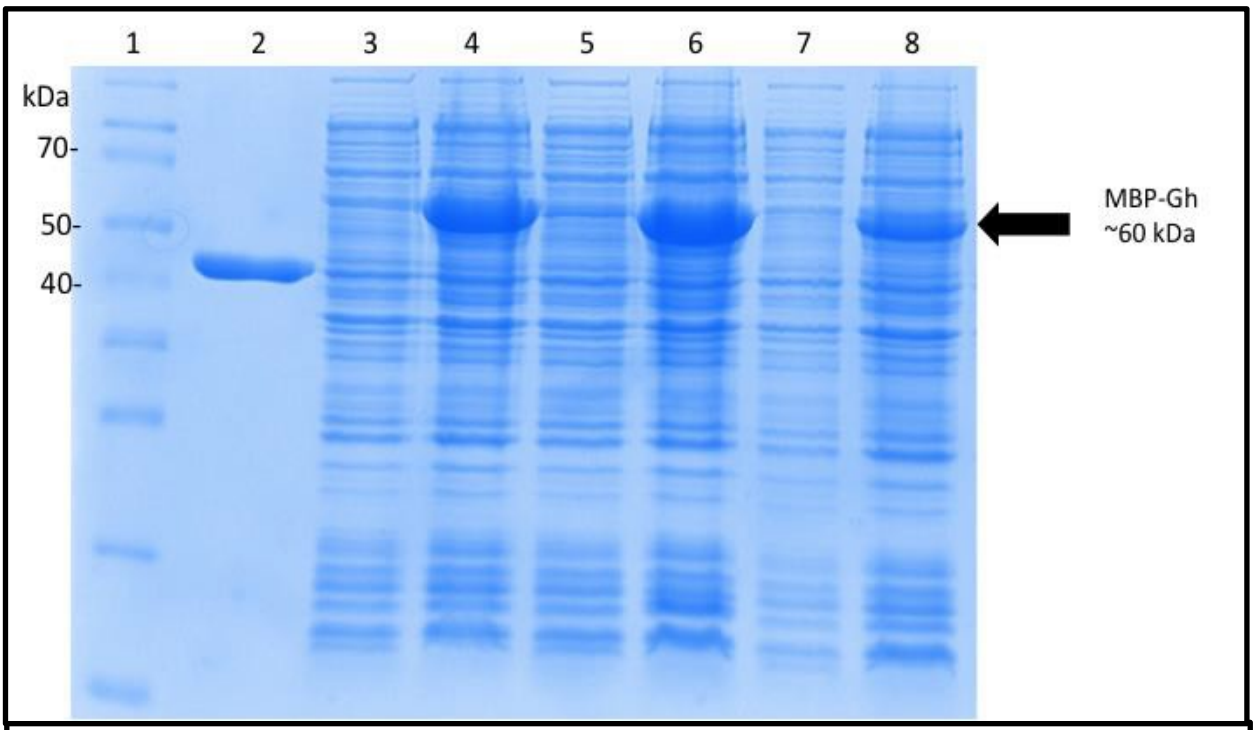

Fig 3.4. SDS-PAGE gel electrophoresis (12% w/v, under reducing conditions) analysis of BL21 E.coli transformed cells containing PKBM-A, PKBM-B and PKBM-C. **Lane 1:** Protein molecular weight marker; **Lane 2:** purified MBP; **Lane 3:** cell lysate of PKBM-A uninduced sample; **Lane 4:** cell lysate of PKBM-A induced sample; **Lane 5**: cell lysate of PKBM-B uninduced sample; **Lane 6:** cell lysate of PKBM-B induced sample; **Lane 7:** cell lysate of PKBM-C uninduced sample; **Lane 8:** cell lysate of PKBM-C induced sample.

The SDS gel electrophoresis image shown in **Fig 3.4** shows a difference in expression between the un-induced samples pKBM-A, pKBM-B and pKBM-C in Lanes 3, 5 and 7 respectively; and their IPTG induced counterparts in Lanes 4, 6 and 8. There is a marked increase in expression in the 50-70 kDa range between the PKBM- A uninduced samples (Lane 3) and the induced sample (Lane 4); PKBM- B uninduced samples (Lane 5) and the induced sample (Lane 6) and the PKBM- C uninduced samples (Lane 7) and the induced sample (Lane 8). The proteins expressed correspond with the molecular size of our expected protein. In addition to the molecular marker, MBP (42.5 kDa; Lane 2) derived from the non-transformed expression of the pMalc plasmid is used as another reference point in order to confirm that the proteins are expressed as MBP fused fractions.

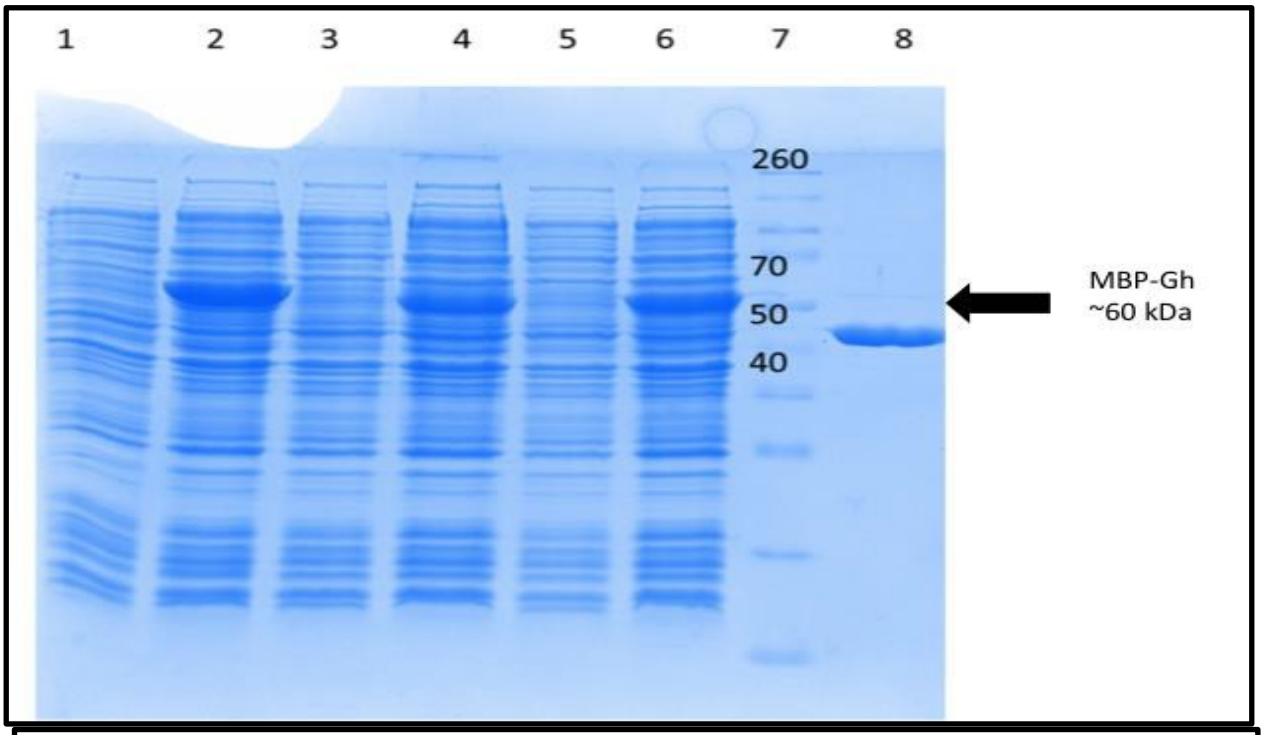

Fig 3.5. SDS-PAGE gel electrophoresis (12% w/v, under reducing conditions) analysis of BL21 E.coli transformed cells containing mghA, mghB and mghC. **Lane 1:** cell lysate of mghA uninduced sample; **Lane 2:** cell lysate of mghA induced sample; **Lane 3:** cell lysate of mghB uninduced sample; **Lane 4:** cell lysate of mghB induced sample; **Lane 5**: cell lysate of mghC uninduced sample; **Lane 6:** cell lysate of mghC induced sample; **Lane 7:** Protein molecular weight marker; **Lane 8:** purified MBP

Fig 3.5 shows the difference in expression between uninduced and induced mghA, mghB and mghC samples. There is an observable increase in expression when the un-induced samples mghA, mghB and mghC in Lanes1, 3, and 5 respectively are compared to their IPTG induced counterparts in Lanes 2, 4 and 6. There is a marked increase in expression in the 50-70 kDa range between the mghA uninduced samples (Lane 1) and the induced sample (Lane 2); mghB uninduced samples (Lane 3) and the induced sample (Lane 4) and the mghC uninduced samples (Lane 5) and the induced sample (Lane 6). The proteins expressed correspond with the molecular size of our expected protein of ~60kDa. In addition to the molecular marker, MBP (42.5 kDa; Lane 8) was used as a reference point.

3.2.5 Purification of recombinant fusion proteins.

Bacterial cultures, which demonstrated a pronounced increase in expression of a 60-61 kDa protein after induction, were up-scaled to large scale protein expression. Cells expressing MBP-ghA^3, -ghB^3 or –ghC^3 were lysed and subsequently sonicated, in order to shear the bacterial chromosomal DNA, spun at 5000 rpm and the soluble fused proteins were purified from the supernatant using an Amylose resin column. MBP has a high affinity for amylose, thus enabling the recombinant fused proteins to be bound to the column, and later eluted with maltose, which has an even greater affinity. Eluted samples were collected in 1ml fractions. The concentration of protein in eluted samples was verified by measuring A_{280} using the nano drop spectrophotometer. Samples with the highest concentration were run on a gel to verify the presence of the MBP-fused protein.

As shown in **Fig 3.6 and 3.7** purification via affinity chromatography removes almost all of the protein contaminants. The presence of the recombinant proteinis verified in the gels below by the presence of a band at 61 kDa for ghA^3, 61 kDa for ghB^3 and 60 kDa for ghC^3. Furthermore, the MBP- ghA^3, ghB^3 and ghC^3 proteins have a higher molecular weight than their monomeric counterparts; which indicates that the gene for the SPD neck region was successfully incorporated into the multimeric constructs.

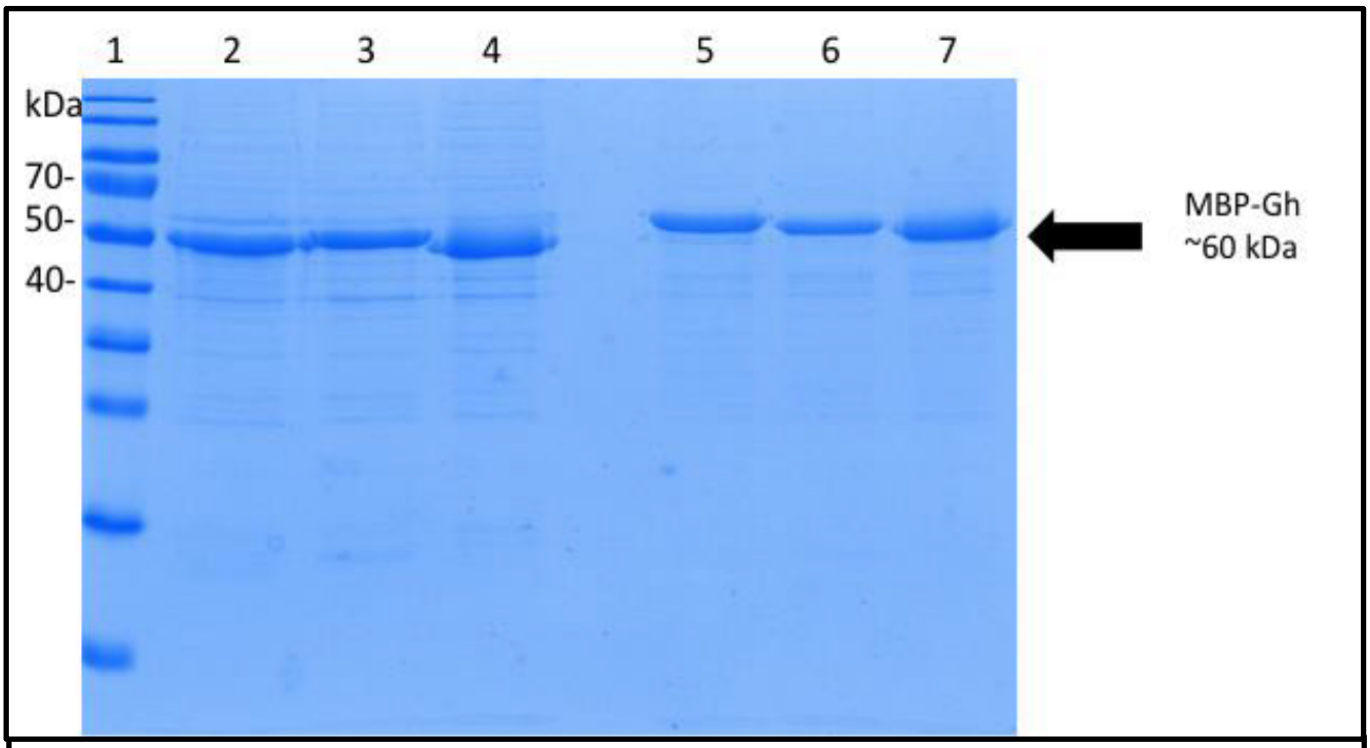

Fig 3.6. SDS-PAGE gel electrophoresis (12% w/v, under reducing conditions) image showing the pooled peak purification fractions of MBP fused recombinant globular heads obtained via amylose resin affinity chromatography. **Lane 1**: Protein molecular weight marker; **Lane 2:** purified MBP-ghA **Lane 3:** purified MBP-ghB; **Lane 4:** purified MBP-ghC; **Lane 5:** purified MBP-ghA^3; **Lane 6**: purified MBP-ghB^3; **Lane 7:** purified MBP-ghC^3.

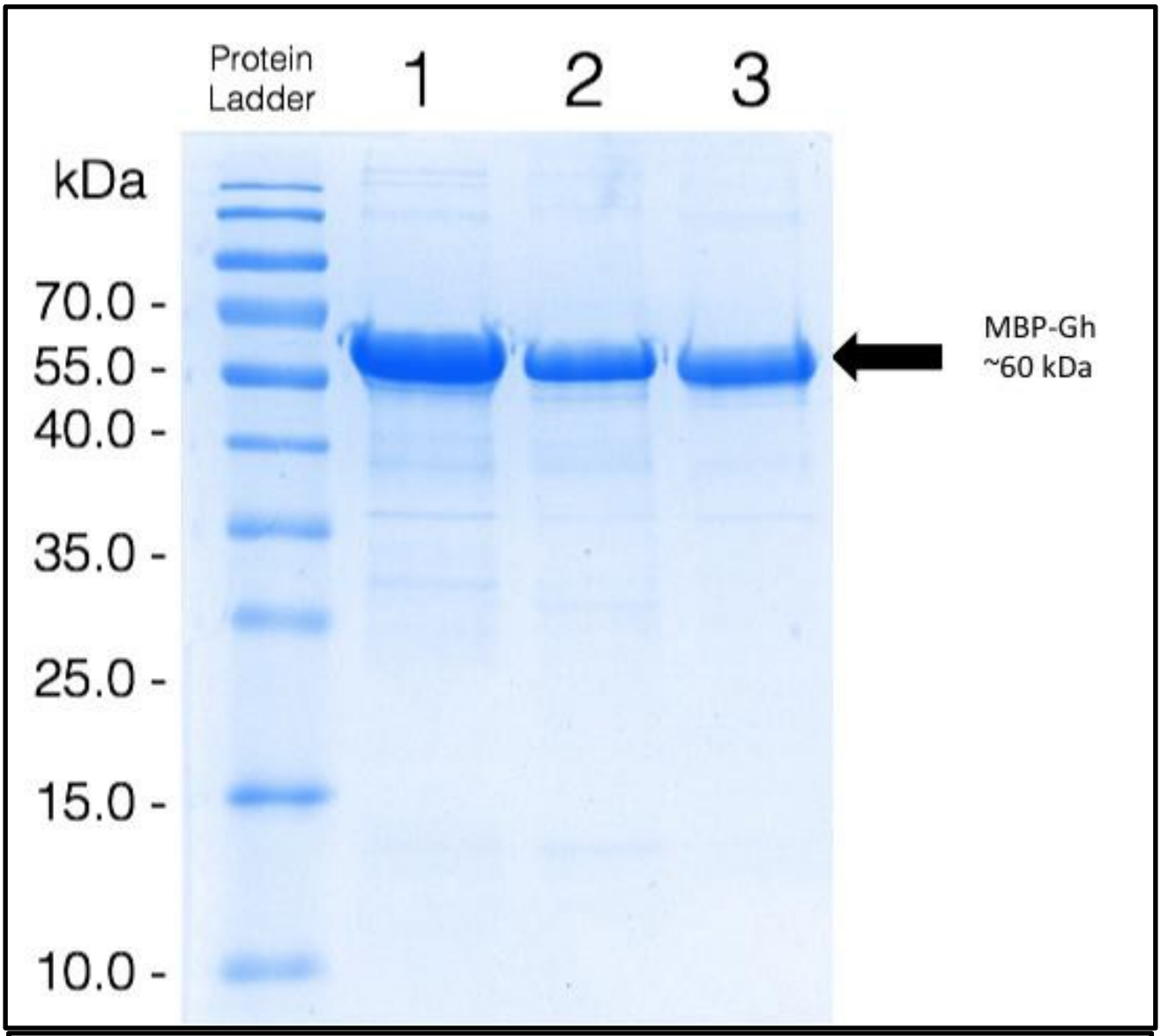

Fig 3.7 SDS-PAGE gel electrophoresis (12% w/v, under reducing conditions) image showing the pooled peak purification fractions of MBP fused recombinant mghA, mghB and mghC obtained via amylose resin affinity chromatography. **Lane 1**: purified fusion protein mghA. **Lane 2**: purified fusion protein mghB. **Lane 3**: purified fusion protein mghC.

3.2.6 Ion exchange chromatography

In order to remove contaminants, peak fractions were passed through the DEAE anion exchange column. Different gradients of NaCl molarity were used (ranging from 0.1 M to 1 M) and the fusion proteins bound at 0.1 M NaCl while peak fractions were eluted at 0.2-0.3 M NaCl for all proteins. However, many of the eluted fractions still retained some contamination, so elutes were dialysed overnight and passed through the DEAE Sepharose column and run through ion exchange again. In order to obtain the pure protein, there was a significant loss of purified protein. Bands are observed at approximately 60 kDa (Fig 3.8-3.9).

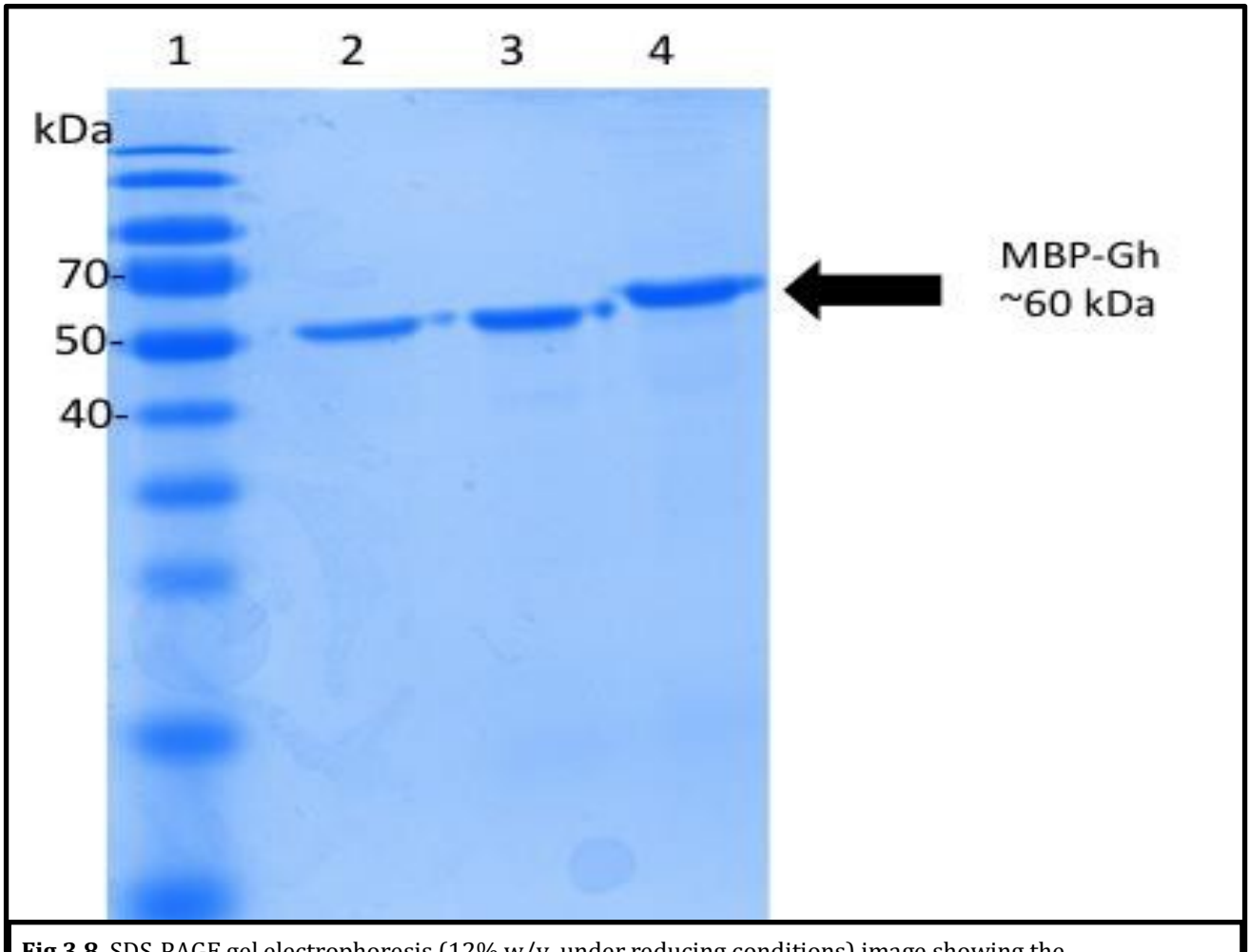

Fig 3.8. SDS-PAGE gel electrophoresis (12% w/v, under reducing conditions) image showing the pooled peak purification fractions of MBP fused recombinant ghA, ghB and ghC obtained via anion exchange chromatography. **Lane 1**: protein molecular weight marker; **Lane 2:** purified fusion protein ghA. **Lane 3**: purified fusion protein ghB. **Lane 4**: purified fusion protein ghC.

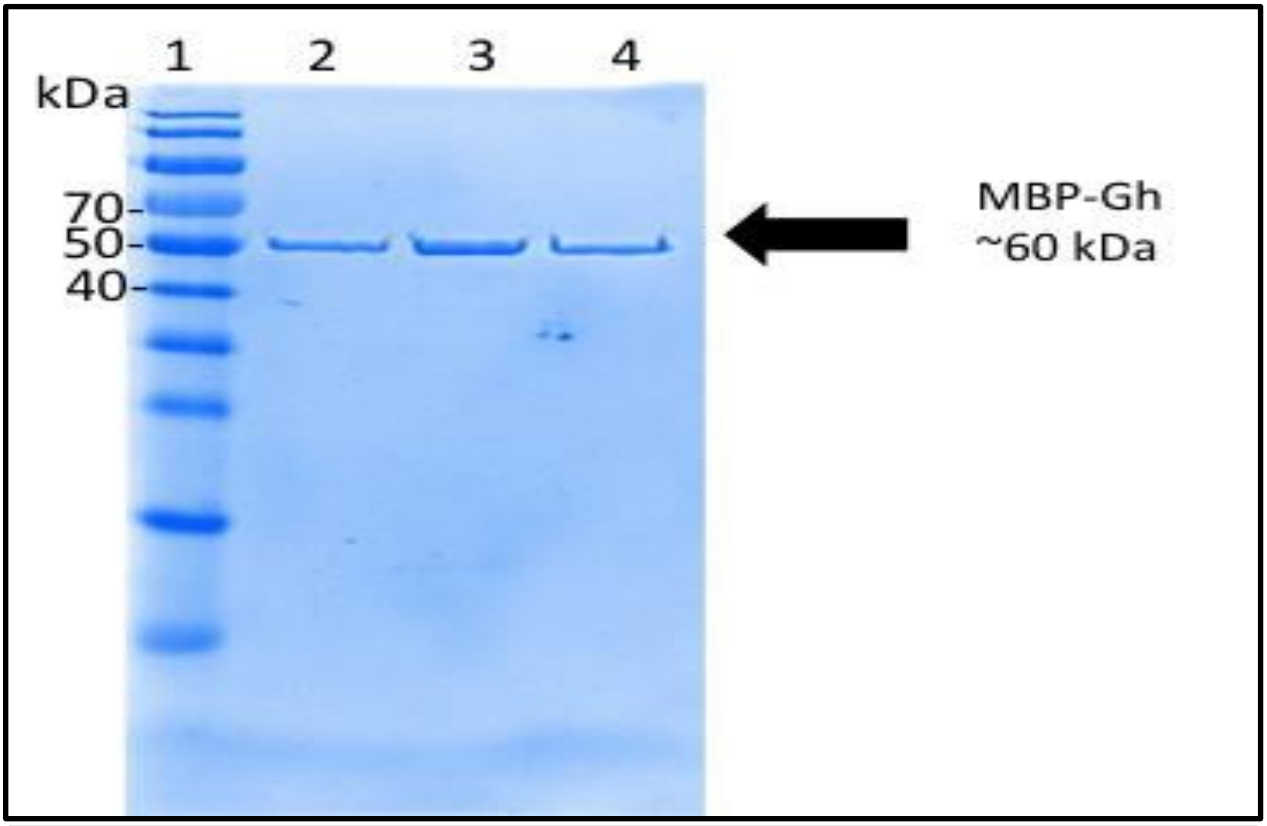

Fig 3.9 SDS-PAGE gel electrophoresis (12% w/v, under reducing conditions) image showing the pooled peak purification fractions of MBP fused recombinant mghA, mghB and mghC obtained via anion exchange chromatography. **Lane 1**: protein molecular weight marker; **Lane 2**: purified fusion protein mghA. **Lane 3**: purified fusion protein mghB. **Lane 4**: purified fusion protein mghC.

3.2.7 Expression PMC-A^3, PMC-B^3 and PMC-C^3

The recombinant proteins ghA^3, ghB^3 and ghC^3 were expressed as MBP-fused proteins in E.coli BL21 cells containing the recombinant vectors PMC-A_3, PMC-B_3 and PMC-C_3, respectively. MBP has a molecular weight of 42.5kDa but when this is fused to the globular head sequences the molecular weight is 61 kDa for ghA^3, 61 kDa for ghB^3 and 60 kDa for ghC^3. Following induction with 0.4 mM IPTG for 3 hours, the SDS gel electrophoresis image shown in **Fig 3.10** shows an increase in expression between the un-induced cell-lysate samples of PMC-A_3, PMC-B_3 and PMC-C_3 in Lanes 2, 4 and 6 respectively and the 3hr IPTG induced counterparts in Lanes 3,5 and 7. Each recombinant fusion protein appeared as an over-expressed protein band of ~60 KDa in pilot and largescale expressions, as judged by SDS PAGE under reducing conditions in **Fig 3.10**.

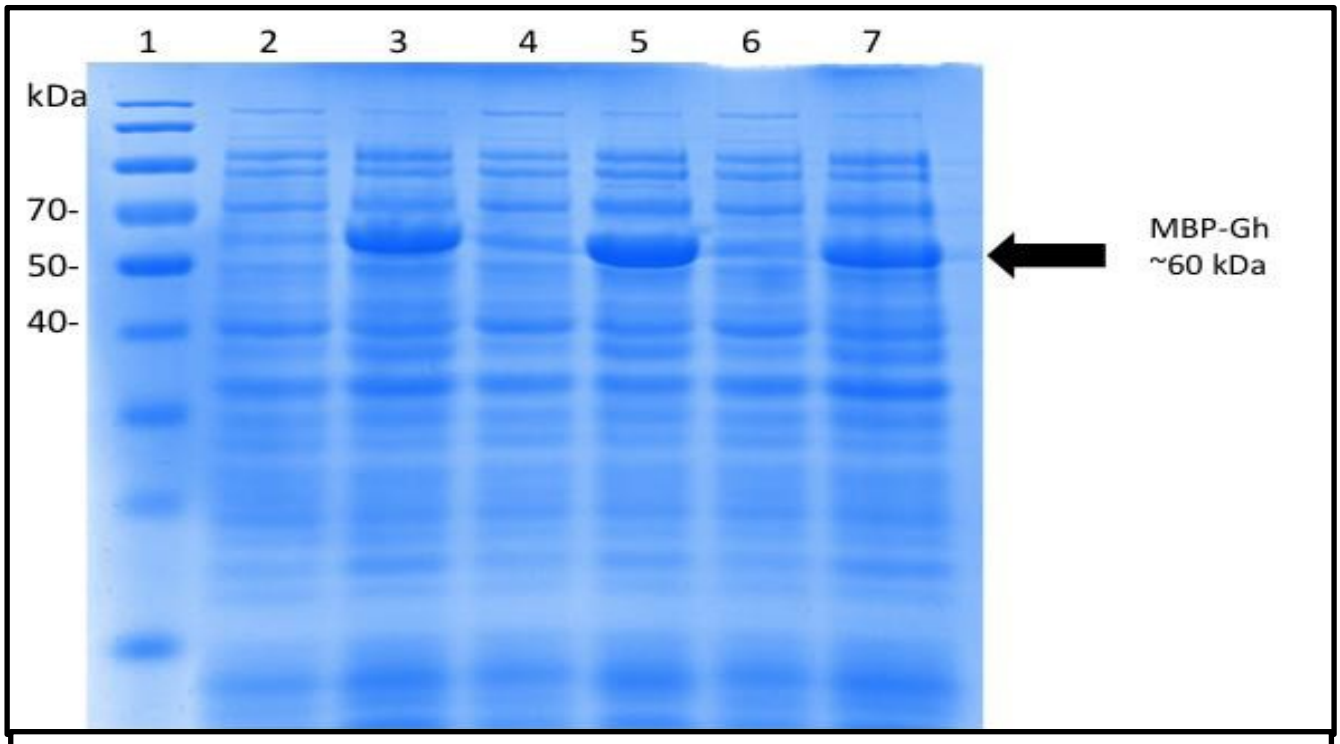

Fig 3.10 SDS-PAGE gel electrophoresis (12% w/v, under reducing conditions) analysis of BL21 E.coli transformed cells containing ghA^3, ghB^3 and ghC^3. **Lane 1**: Protein molecular weight marker; **Lane 2:** cell lysate of ghA^3 uninduced sample; **Lane 3:** cell lysate of ghA3 induced sample; **Lane 4:** cell lysate of ghB3 uninduced sample; **Lane 5:** cell lysate of ghB^3 induced sample; **Lane 6**: cell lysate of ghC^{3}uninduced sample; **Lane 7:** cell lysate of ghC^3 induced sample.

3.2.8 Western blot of Purified MBP-Fusion proteins

In order to confirm whether the eluates of the Amylose Resin column and subsequent Ion exchange were MBP fusion proteins, we conducted a western blot. The western blot image in Fig 1 shows the presence of bound antibody for MBP at approximately 60 kDa, and within the 50-70 kDa range of the protein marker. These bands correspond with the size of the MBP-fusion proteins as characterised in (Kishore et al., 2003). Thus, the eluates of the Amylose resin column and ion exchange purification are the MBP fused recombinant proteins. Moreover, Western blots were used to confirm the less pure fractions in order identify whether the bands were due to protein degeneration or due to minor contaminants. No bands were observed in the 42kDa range for MBP, nor where there any other observable bands present on the western blot. Therefore, indicating the presence of minor E. coli contaminants (which were purified by subsequent DEAE ion exchange chromatography); and not a degeneration of the MBP fusion proteins.

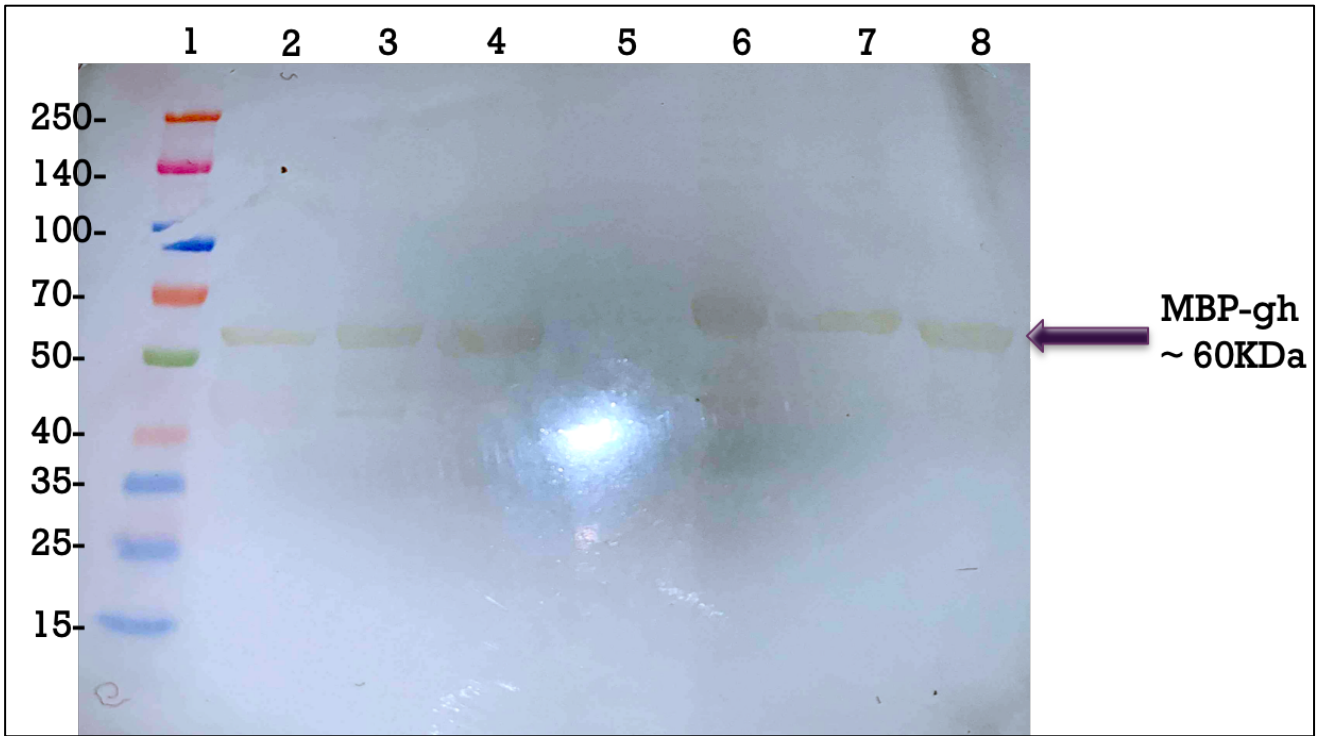

Fig 3.11. Western blot of MBP fused recombinant globular heads probed with anti-MBP.

Lane 1: Protein molecular weight marker Lane 2: MBP-ghA; Lane 3: MBP-ghB; Lane 4: MBP-ghC; Lane 5: Amyloid Beta (Aβ); Lane 6: MBP-ghA[3]; Lane 7: MBP-ghB[3]; Lane 8: MBP-ghC[3]

3.2.9 Factor Xa digest of MBP fused trimers

The pMalc -5x vector contains a short sequence within its multiple cloning site, which codes for an enzyme recognition site allowing, for the separation of MBP from the recombinantly expressed proteins. Once the sequence is recognized by the enzyme Factor Xa, MBP and the recombinant protein will be cleaved apart. Purified fractions of MBP fused ghA^3, ghB^3, and ghC^3 (200µg) were added to 1U of Factor Xa overnight at 4°C. 20µg of the digest were then run on an SDS page gel.

Lanes 1 to 6 (**Fig 3.12.**) have a number of bands present in their digests. The highest weight band is between 55-70 kDa, corresponding to the size of an undigested MBP-fused protein. At approximately 40 kDa there is band present in all lanes corresponding with the size of native MBP. Another band appears between 25-35 kDa in all lanes. The final bands in each lane appear approximately between 18 and 25 kDa corresponding with the size of the monomer units of ghA^3, ghB^3, and ghC^3. ghA^3 (Lanes 1 and 2) appears to be of a larger size than ghB_3 which in turn appears to be of a larger size than ghC^3.

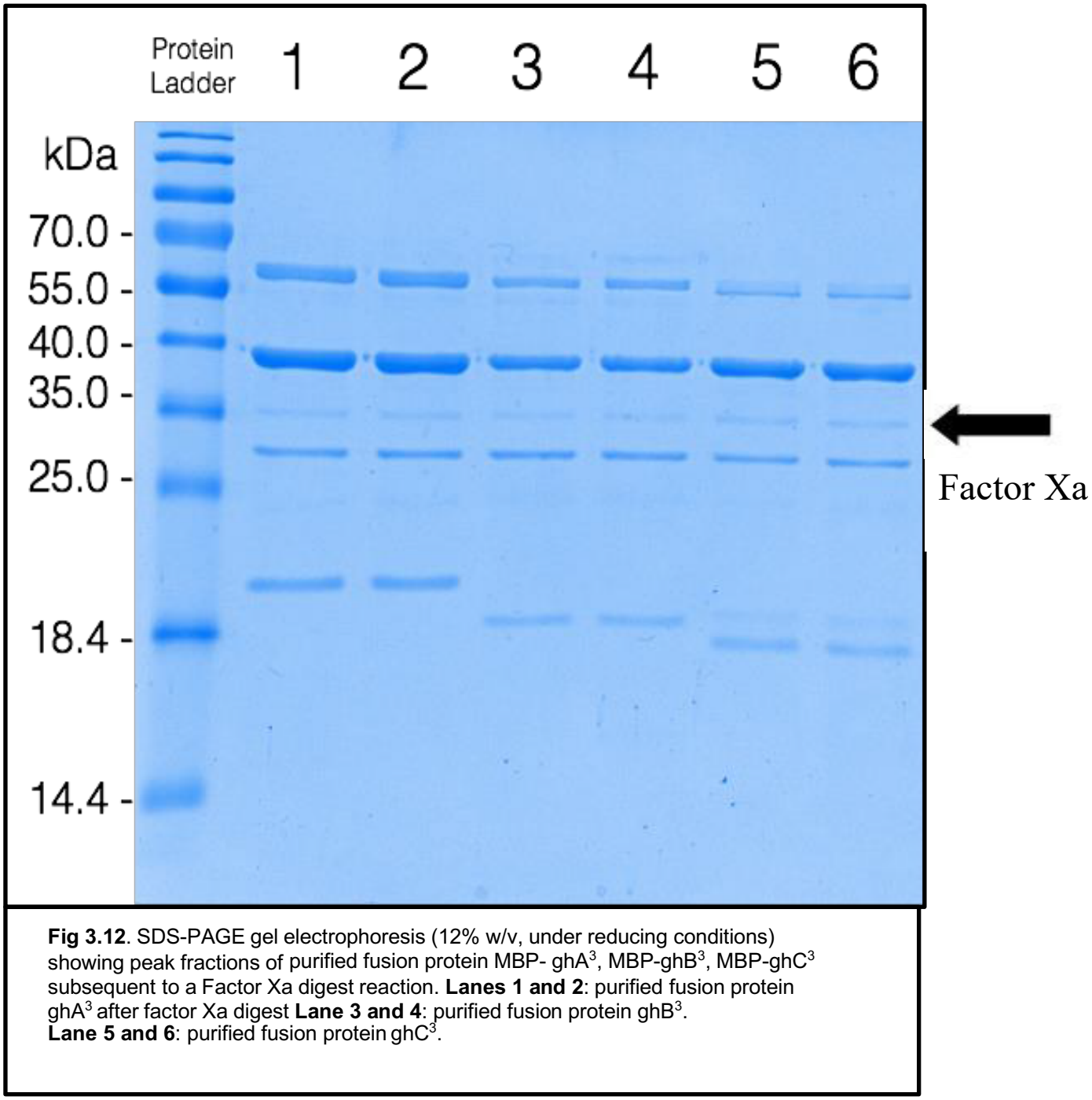

Fig 3.12. SDS-PAGE gel electrophoresis (12% w/v, under reducing conditions) showing peak fractions of purified fusion protein MBP- ghA[3], MBP-ghB[3], MBP-ghC[3] subsequent to a Factor Xa digest reaction. **Lanes 1 and 2**: purified fusion protein ghA[3] after factor Xa digest **Lane 3 and 4**: purified fusion protein ghB[3]. **Lane 5 and 6**: purified fusion protein ghC[3].

3.2.10 Ion exchange chromatography for separation of MBP and recombinant protein

The purpose of this second ion exchange chromatography was to separate MBP, MBP fused protein and the globular head fragment. Factor Xa digests were dialysed overnight and then passed through a DEAE anion exchange column. Different gradients of NaCl molarity were used (ranging from 0.1 M to 1 M) to elute the proteins. Based on previous studies, the expected molarity for drop out of MBP is 200 mM; the uncut globular head 300-400mM and the recombinant ghA[3], ghB[3] or ghC[3] 500-700mM (Kishore et al., 2003). Much of the MBP and MBP fused globular heads eluted between 200-400mM (Fig 3.13), as did some of the cut globular heads. However, the globular heads did not visibly elute within its target eluent range, nor did it fall out through the flow through and thus it was impossible to isolate the target recombinant fragments. To combat this, the following steps were taken at different points in order to troubleshoot. A larger concentration of protein was cut; samples were eluted in 50mM increments which was later reduced to 25mM increments from 0.1-1M NaCl; the gradient range of NaCl was increased to 1.5 M; Different pH ranges were tested; A cation exchange channel was also tested. Finally, the protein was dialysed in 5M UREA and 2% mercaptoethanol to break the multimers down to their monomeric forms and thus make Factor Xa site easier for the enzyme to digest. Despite all these troubleshooting steps, it appears that the uncut protein bound irreversibly to the ion exchange column. The isolated uncut protein that did elute, eluted in such low levels that it was insufficient to be observed on an SDS-PAGE and therefore insufficient to conduct further experiments with. From this point in the study, all experiments were conducted with MBP bound fusion protein.

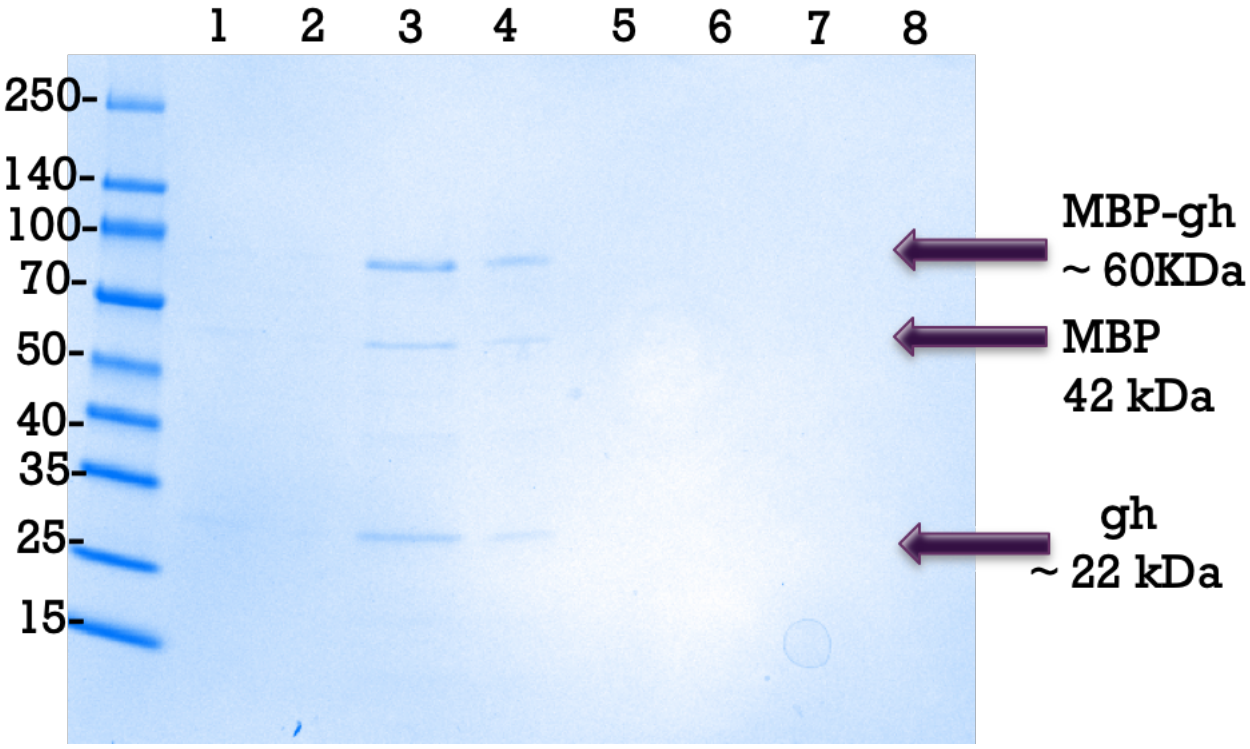

Fig 3.13. SDS-PAGE gel electrophoresis (12% w/v, under reducing conditions) showing peak fractions of eluents from the anion chromatography of Factor Xa Digested samples.

Lane 1: Flow throuh, **Lane 2:** Eluent of 200mM NaCl buffer, **Lane 3:** Eluent of 250mM NaCl buffer, **Lane 4:** Eluent of 300mM NaCl buffer, **Lane 5:** Eluent of 400mM NaCl buffer, **Lane 6:** Eluent of 500mM NaCl buffer, **Lane 7:** Eluent of 600mM NaCl buffer **Lane 8:** Eluent of 700mM NaCl buffer.

3.2.11 C1q recombinant proteins post chromatography yields

Protein	Post amylose resin purification	Post Ion exchange	Post Factor Xa ion exchange
ghA	5.31 mg	1.97 mg	N/A
ghB	6.714 mg	3.32 mg	N/A
ghC	4.476 mg	2.45 mg	N/A
ghA3	8.55 mg	3.383 mg	0.075 mg
ghB3	11.79 mg	4.64 mg	0.102 mg
ghC3	8.74 mg	3.861 mg	0.059 mg
mghA	4.25 mg	2.79 mg	N/A
mghB	4.588 mg	2.65 mg	N/A
mghC	3.864 mg	2.01 mg	N/A

Table 3.3 shows the amounts of protein obtained for ghA, ghB, ghC, ghA^3, ghB^3, ghC^3, mghA, mghB, mghC after the 3 main protein purification stages: amylose resin chromatography, ion exchange chromatography for the removal of contaminants and post Factor Xa ion exchange chromatography to separate the MBP from the cleaved recombinant proteins ghA^3, ghB^3 or ghC^3.

3.2.12 Inhibition of C1-q dependent haemolysis by ghA, ghB, ghC, ghA^3, ghB^3 and ghC^3.

In order to examine the inhibitory effects of MBP-ghA$_3$, -ghB$_3$, and –ghC$_3$ on C1q-dependent haemolysis, sheep erythrocytes were sensitized with haemolysin (anti-sheep erythrocyte antibody) to yield activated erythrocytes EA cells. A serum dilution of 1:80 was used. In order to achieve >50% inhibition, > 10 µg/well of MBP-ghA$_3$, and >5µg/wellof MBP-ghC$_3$ were required, whereas MBP-ghB$_3$ and MBP-gh MBP-ghC$_3$ achieved close to 50% inhibition at a concentration of 1.25 µg/well (Fig 3.14). Both MBP-ghB$_3$ and were capable of inhibiting lysis of sheep erythrocytes by up to 70% at a concentration of 10µg/well. The potencies of the three recombinant proteins as inhibitors of C1q- mediated haemolysis of sheep erythrocytes are in the order ghB $_3$>ghC$_3$>ghA$_3$. MBP did not interfere significantly with C1q-mediated haemolysis. By comparison peak inhibitory 10 µg/well of globular head monomers was sufficient to inhibit only 40% of compliment pathway haemolysis. (Fig 3.15)

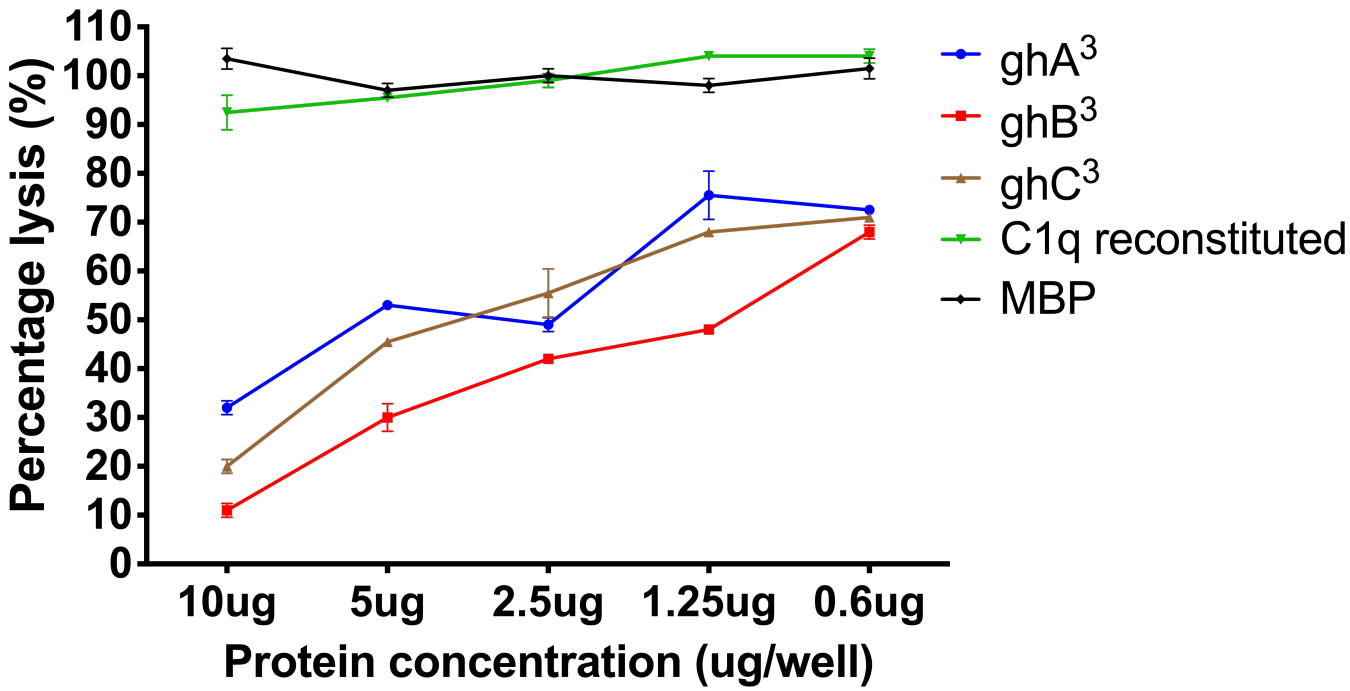

Fig 3.14 Composite graph illustrating inhibition of classical pathway haemolysis of C1q reconstituted serum by MBP fused globular head multimers MBP-ghA^3, - ghB^3 and ghC^3. 0.6, 1,25, 2.5, 5 and 10µg of MBP-ghA^3, ghB^3 and ghC^3 protein respectfully were incubated with activated sheep erythrocytes. BSA was a negative control for the experiment whereas After wash, serum reconstituted with C1q was added. The data are shown as mean±SD of three independent experiments. Percentage lysis is plotted along the vertical axis.

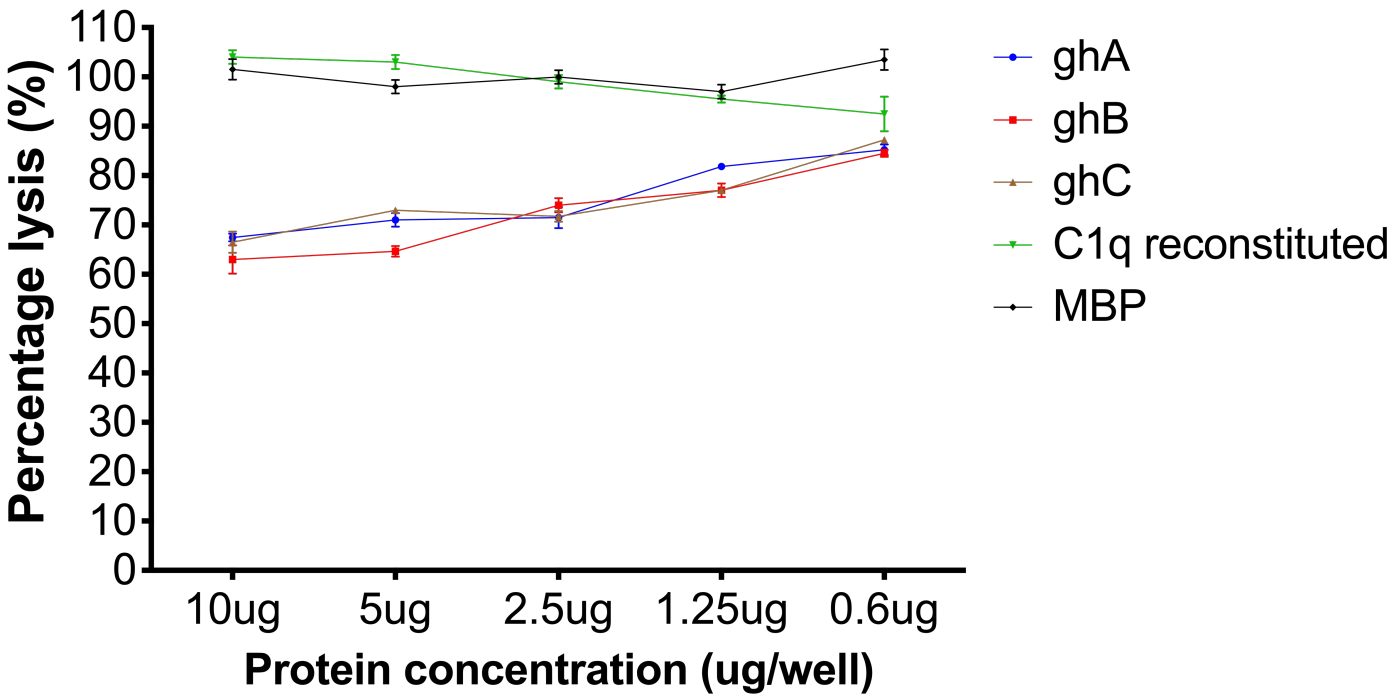

Fig 3.15 Composite graph illustrating inhibition of classical pathway haemolysis of C1q reconstituted serum by MBP fused globular head monomers MBP-ghA, - ghB and ghC. 0.6, 1,25, 2.5, 5 and 10µg of MBP-ghA, ghB and ghC protein respectfully were incubated with activated sheep erythrocytes. BSA was a negative control for the experiment whereas After wash, serum reconstituted with C1q was added. The data are shown as mean±SD of three independent experiments. Percentage lysis is plotted along the vertical axis.

3.2.13 Differential binding of Globular heads to IgG

IgG has been characterised as one of the main ligands of C1q globular heads. We sought to identify whether the human recombinant fragments and the mutant multimers were capable of binding IgG using a direct ELISA. ghA, ghB and ghC coated microtiter wells at different concentrations (0.6,1.25,2.5, 5 and 10 µg/well) were probed with IgG (see section 2.17 for methods). BSA was used as an experimental control, whereas MBP was used as a globular head control. Both controls showed negligible values for optical density at all doses. As shown in Fig 3.16 all three globular heads bound IgG in dose dependent manner indicating that each globular head chain is capable of binding IgG independently. The dose dependent increases were significant (***p<0.001) when compared to controls. Furthermore, ghB demonstrated a higher affinity for IgG than ghA and ghC at every dose (See **Table 3.4**). At almost all doses, no significant change was found between the optical density for ghA and ghC indicating that binding properties are similar Fig 3.16.

IgG concentration (ug/well)	**Optical Density 450 nm**		
	ghA	**ghB**	**ghC**
0.6	0.3493± 0.048	0.721±0.149	0.429±0.028
1.25	0.458± 0.019	0.766±0.012	0.601±0.029
2.5	0.554± 0.049	0.796±0.053	0.777±0.018
5	0.746± 0.025	1.029±0.061	0.859±0.032
10	0.851± 0.049	1.195±0.064	0.909±0.009
20	0.962± 0.032	1.493±0.084	1.072±0.038

Table 3.4: Data showing differential dose dependent binding of C1q globular heads ghA, ghB and ghC to heat aggregated IgG. Data points are presented as the mean±SD.

We further sought to identify whether the human recombinant fragments and the mutant multimers were capable of binding IgG using a direct ELISA. ghA^3, ghB^3 and ghC^3 coated microtiter wells at different concentrations (0.6,1.25,2.5, 5, 10 and 20 µg/well) were probed with IgG. BSA was used as an experimental control, whereas MBP was used as a globular head control. Both controls showed negligible values for optical density at all doses. As shown in Fig 3.b all three multimeric globular heads bound IgG. 0.6 µg of ghB^3 (1.704±0.092), 1.25 µg of ghA^3 (1.564±0.018) and ghC^3 (1.696 ±0.018) was sufficient to bind IgG at a higher optical density than 20 µg of ghB (1.493±0.084). A mild dose dependent increase in binding was also observed with all three monomers. The dose dependent increases were significant (*$p<0.05$) when compared to controls and subsequent concentrations. ghB^3 demonstrated a higher affinity for IgG than ghA^3 and ghC^3 at lowers doses (see **Table 3.5**). At doses of 10 µg and 20 µg there was no significant difference between the optical density (nm) i.e. binding affinity between ghA^3, ghB^3 and ghC^3. This indicates either a plateau of binding affinity at higher doses or more likely the surface area available for binding in the 96 well plates was limited (Fig 3.17).

IgG concentration (ug/well)	**Optical Density 450 nm**		
	ghA^3	**ghB^3**	**ghC^3**
0.6	1.308± 0.097	1.704±0.092	1.378±0.088
1.25	1.564± 0.018	1.740±0.015	1.696±0.018
2.5	1.685± 0.016	1.887 ±0.008	1.805±0.021
5	1.827± 0.043	1.983±0.029	1.930 ±0.042
10	1.977±0.066	2.125±0.075	2.003±0.103
20	2.250±0.136	2.387±0.125	2.242±0.110

Table 3.5: Data showing differential and dose dependent binding of C1q globular heads ghA^3, ghB^3 and ghC^3 to heat aggregated IgG. Data points are presented as the mean±SD.

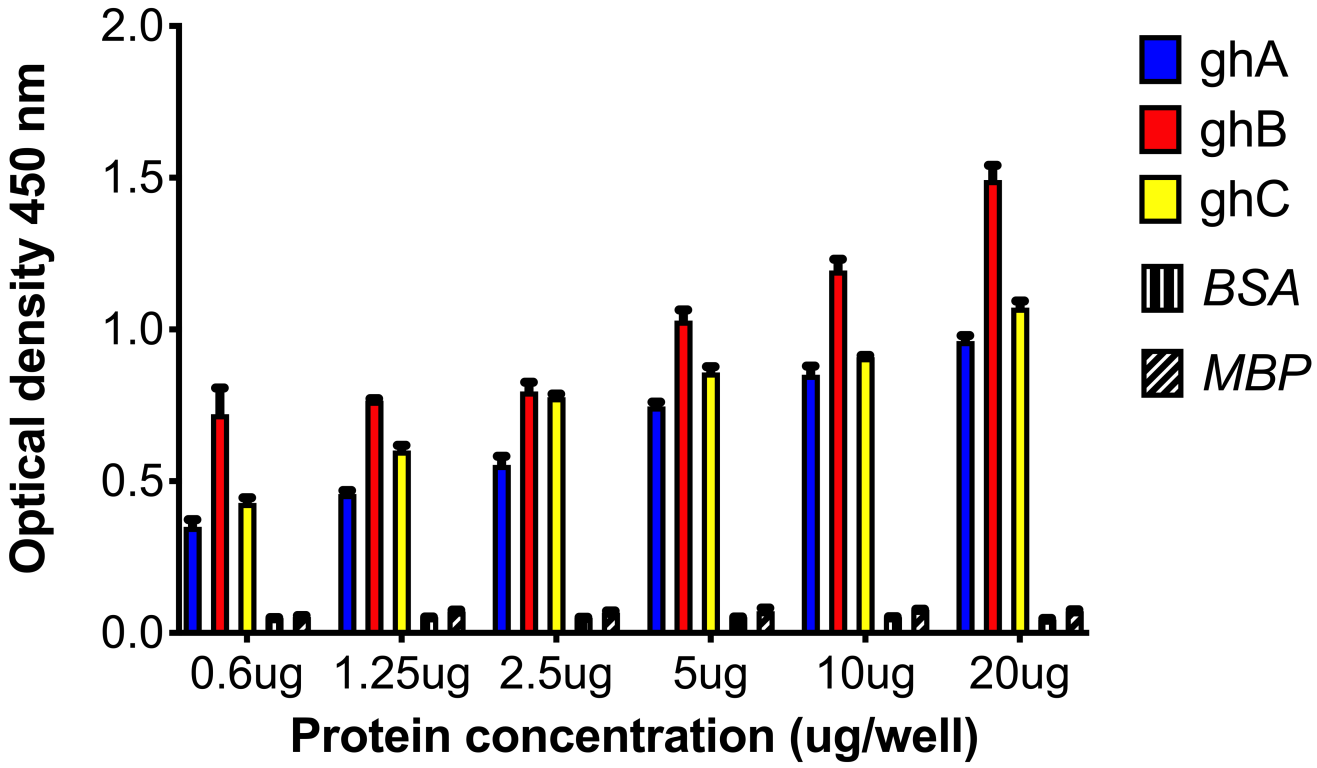

Fig 3.16. Composite graph illustrating the dose dependent binding of recombinant MBP fused globular head A, B and C variants of C1q to IgG. MBP-ghA, MBP-ghB, and MBP-ghC were coated at different concentrations (0.6, 1.25, 20 µg/well) in microtiter wells (1µg/well). IgG (10ug/ul) was added to each well and incubated for 2 hours. Human Protein A-HRP probed the amount of bound IgG. Data points were presented as the mean ± SD of optical density at 450 nanometres on the vertical axis versus the protein concentration in µg/well on the horizontal axis.

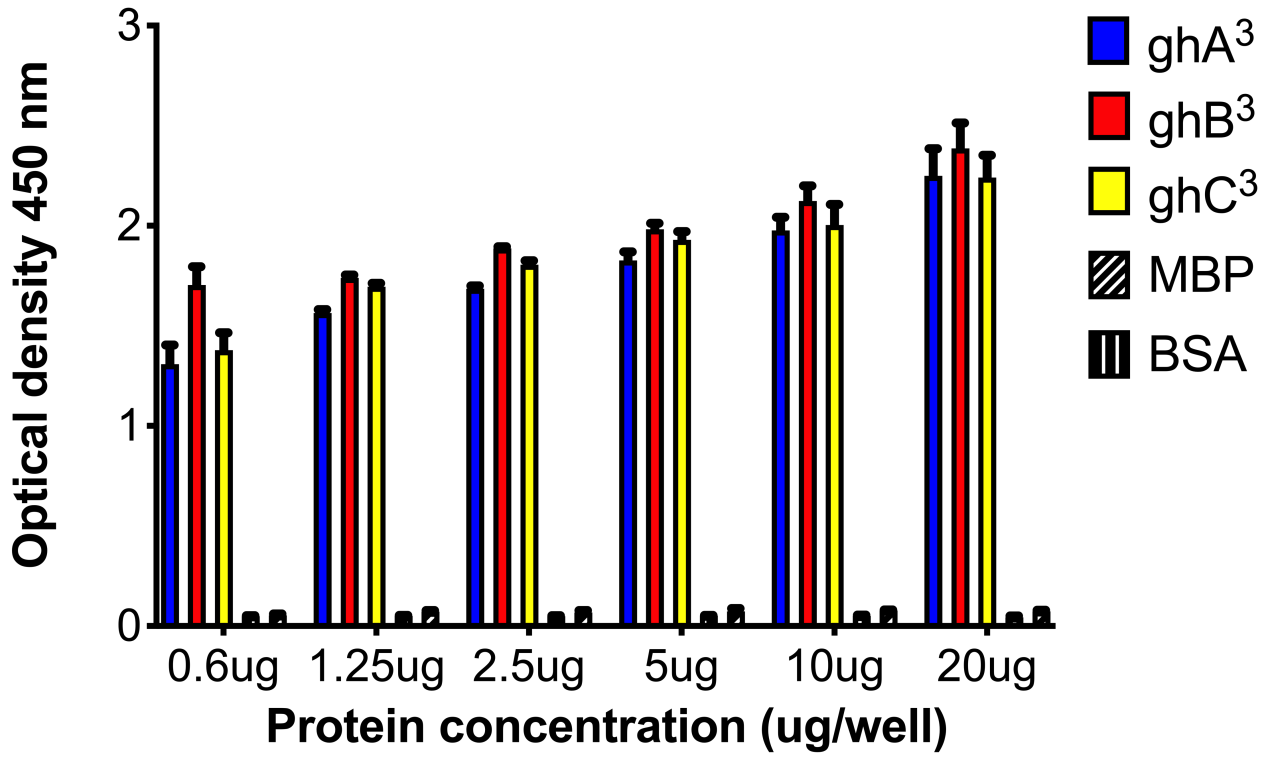

Fig 3.17. Composite graph illustrating the dose dependent binding of recombinant MBP fused globular head multimers A³, B³ and C variants of C1q to IgG. MBP-ghA³, MBP-ghB³, and MBP-ghC³ were coated at different concentrations (0.6, 1.25, 2.5, 10 and 20 µg/well) in microtiter wells (1µg/well). IgG (10µg/µl) was added to each well and incubated for 2 hours. Human Protein A-HRP probed the amount of bound IgG. Data points were presented as the mean ± SD of optical density at 450 nanometres on the vertical axis versus the protein concentration in µg/well on the horizontal axis.

3.2.14 Complement pathway consumption assays using ghA, ghB and ghC

Classical pathway consumption assays were conducted to test the ability of ghA, ghB and ghC to activate the classical complement pathway (refer to section 2.21 for methodology). Different concentrations of the globular head monomer proteins were incubated with a constant concentration/dilution of C1q deficient serum. Fig 3.18 shows that at 0.6 µg/well there was less than 10% consumption of serum with all 3 proteins. Complement consumption did not increase with an increased dose of protein with 1.25, 2.5, 5 and 10 µg/well of protein showing a consistent consumption of approximately 10%. Thus, indicating that the complement consumption observed may be due to background/spontaneous activation. The results therefore indicate that the MBP fused monomers are incapable of activating the classical complement pathway.

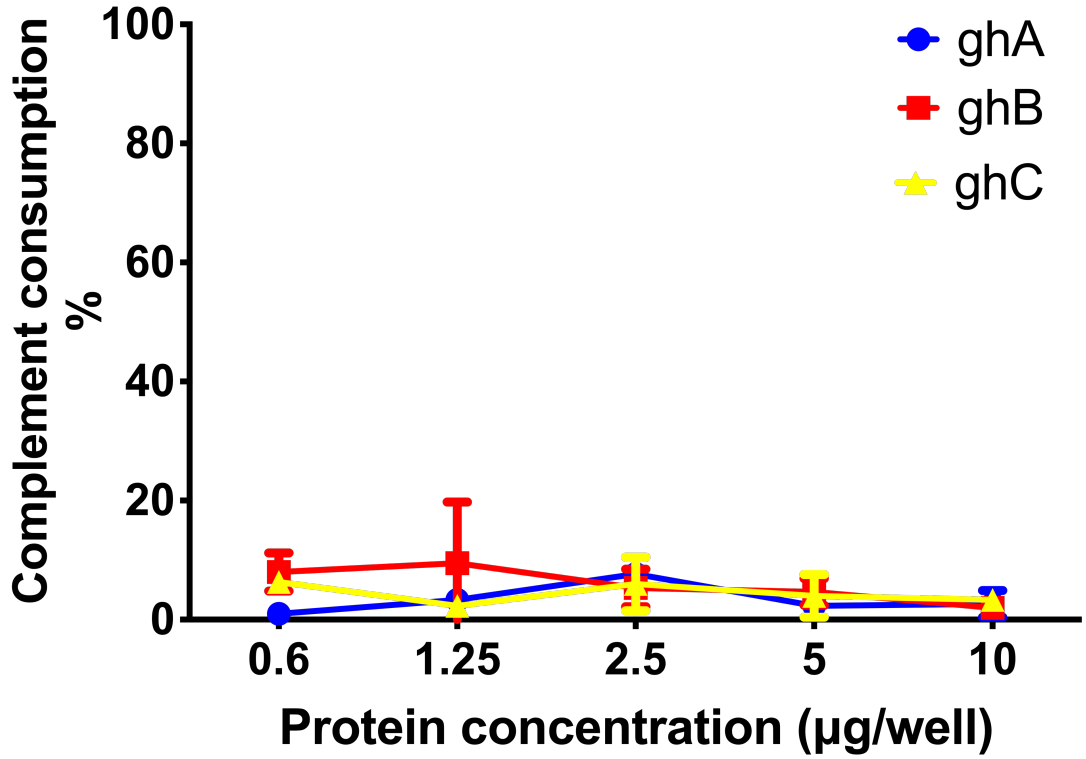

Fig 3.18 Composite graph illustrating classical complement consumption of human serum by MBP globular head monomers.
Haemolytic assay was conducted to determine the complement consumption by ghA, ghB and ghC. 0.6, 1,25, 2.5, 5 and 10µg/well of each protein respectfully was incubated with C1q deficient serum (1:80 dilution) for an hr at 37◦C. The supernatants were then tested via an haemolytic assay. Percentage of complement consumption was calculated as Cgh/CC1q× 100%, where CC1q represents the total haemolytic activity with C1q, and Ci represents the total haemolytic of the recombinant protein. Data points were presented as the mean and SD (n=3) of complement consumption (%) by each protein at different concentrations (µg/well).

3.2.15 Classical Complement pathway consumption assays using ghA^3, ghB^3 and ghC^3.

Classical pathway consumption assays were conducted to test the ability of ghA^3, ghB^3 and ghC^3 to activate the classical complement pathway (refer to section 2.21 for methodology). Different concentrations of the globular head multimer proteins were incubated with a constant concentration/dilution of human serum. Fig 3.19 shows that at 0.6 µg, there was less than 10% consumption of serum with all 3 proteins. Complement consumption did not increase with an increased dose of protein with 1.25, 2.5, 5 and 10 µg/well of protein showing a consistent consumption of approximately 10%. Thus, indicating that the complement consumption observed may be due to background/spontaneous activation. The results therefore indicate that the MBP fused multimers are incapable of activating the classical complement pathway.

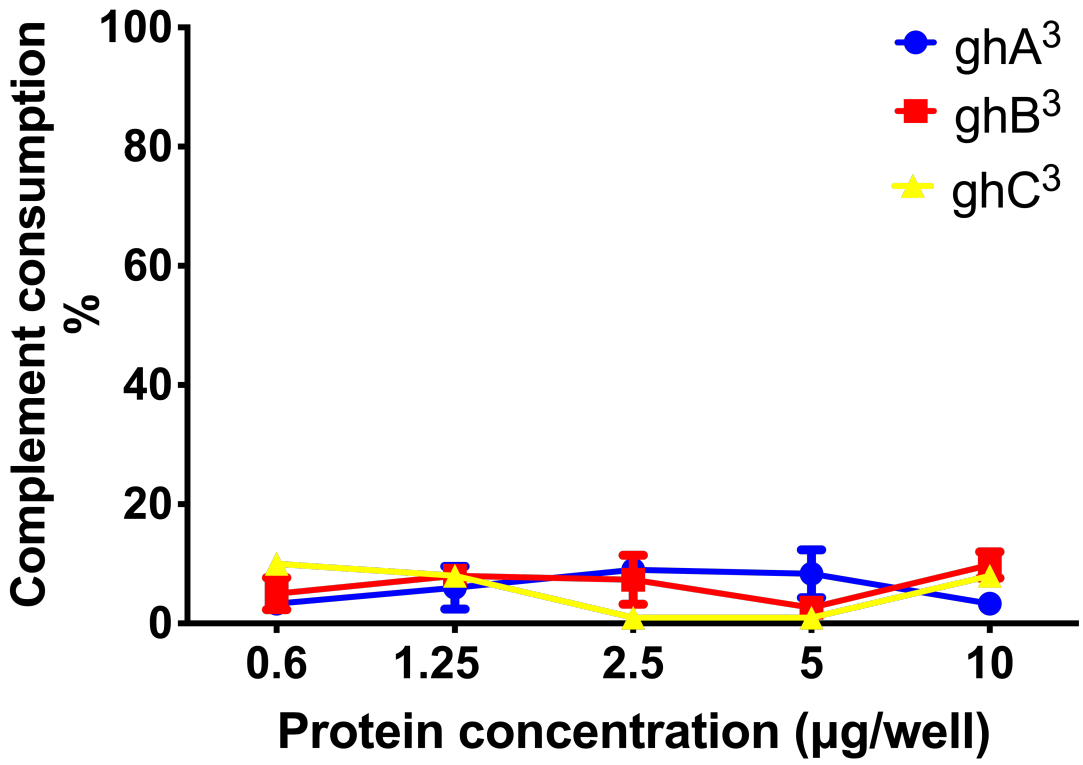

Fig 3.19 Composite graph illustrating classical complement consumption of human serum by MBP globular head multimers.
Haemolytic assay was conducted to determine the complement consumption byC1q, ghA^3, ghB^3 and ghC^3. 0.6, 1,25, 2.5, 5 and 10µg of each protein respectfully was incubated with C1q deficient serum for an hr at 37◦C. The supernatants were then tested via an haemolytic assay. Percentage of complement consumption was calculated as Cgh/CC1q× 100%, where CC1q represents the total haemolytic activity with C1q, and Ci represents the total haemolytic of the recombinant protein. Data points were presented as the mean and SD (n=3) of complement consumption (%) by each protein at different concentrations (µg/well).

3.3 Discussion

C1q is structurally characterized by a heterotrimeric globular domain (gC1q domain). This globular head domain is formed from the C-terminal regions of the A, B and C chains (Kishore et al., 2003; Nayak et al., 2010). These modules are denoted globular heads A (ghA), B (ghB) and C (ghC). Each globular head displays a functional and structural independence characterised by different ligand interactions and binding affinities (Kishore et al., 1998; Kishore et al., 2003). As such, the heterotrimeric C1q which incorporates all 3 globular heads is functionally diverse, and able to engage in a host of ligand interactions. Recombinantly expressed globular head domain regions are able to play a role in ligand binding that does not require activation of the complement pathway. In this way they are capable of acting as inhibitors to the innate immune response and will enable researchers to elucidate the role of C1q and the complement system in many disease states. However, in order to best act as inhibitors, recombinant proteins must at the very least be expressed as trimers in order to compete with the trimeric gC1q. Furthermore, in their trimeric form they must be capable of binding C1q ligands at an equal or higher affinity than C1q in order to be credible competitive inhibitors. As such, they would be best expressed as a recombinant homotrimeric globular domain and targeted towards ligands for which they display the highest binding affinity.

There are biological correlates for a homotrimeric expression of globular head domains. Human type VIII collagen, Human type X collagen, precerebellin, human endothelial cell protein, and Acrp-30 display triple helical carboxy terminal motifs similar to the gC1q module; however, some such as collage type X form a homotrimer (Kishore et al., 2003).

The aim of this study was to express ghA, ghB and ghC proteins with a trimeric neck region that is capable of forming a homotrimer in solution. We denoted these recombinant proteins as ghA^3, ghB^3 and ghC^3. Proteins were expressed as MBP-fused proteins in order to aid expression and ease purification. Once expressed Factor Xa cleavage by factor Xa enzyme was attempted as described in Kishore et al., 2003. However, it was impossible to obtain the protein in large enough quantity to conduct experiments. Previous research by Kishore and colleagues observed that the original constructs formed dimers, trimers and multimers (Kishore et al., 2003). In this research study the aim was that the incorporation of the SPD neck trimerising

region would form trimers as opposed to mixed oligomers. However attempts to isolate cleaved protein via ion exchange chromatography failed for two reasons. During ion exchange chromatography, expected loss of protein by irreversible column binding can range between 30-50 % (as observed by post ion exchange concentration readings). Furthermore, the concentration of cleaved protein was low. So, although there was likely some purification, sample concentration readings obtained from NaCl gradient elution fractions did not demonstrate the presence of any protein. Moreover, SDS page runs of the same samples displayed blank wells indicating no cleavage protein or a concentration so low that it could not be visualised via SDS page. Due to the above reasons we were unable to carry out extensive characterisation of the degree of oligomer formation with these constructs. Had there been sufficient protein this study would have confirmed oligomer formation via Low-Angle Light Scattering (LALS) gel filtration. However, as protein concentration of ghA^3, ghB^3 and ghC^3 was very low (see section…)we decided to proceed experimentally with the MBP-fused proteins.

As hypothesised, both recombinant monomeric and trimeric variants of gC1q inhibited C1q dependent haemolysis in a dose dependent manner. Haemolysis of antibody activated sheep erythrocytes is dependent on C1q. This is corroborated by studies showing no haemolysis in serum devoid/depleted of C1q; and subsequent recovery of haemolysis subsequent to serum reconstitution with C1q. (Kolb et al., 1979). ghB and its trimeric variant had a much more pronounced effect on the inhibition of C1q dependent haemolysis, than the monomeric variants. This is due to functional and structural variance, in the globular head chains leading to differential binding affinities. ghB chain binds to IgG proximal to residues 114–129, whereas ghA and ghC bind at residue 160 (Shapiro et al., 1998). Moreover, ghB has been shown to have a higher binding affinity for IgG than both ghA (Kojouharova et al., 1998), as corroborated by this study. All multimeric variants bound with more IgG at the lowest dose of 0.6 µg, compared to the monomeric variant at 20ug which suggests that the trimeric variants display a higher binding avidity for C1q ligands than the monomeric variants.

Less than 10% consumption by all variants was observed in this study. Indicating, that the globular head proteins are incapable of activating the CCP. This is due to the fact that the globular head variants were cloned and expressed without the collagen like region, through which C1q activates the CCP and binds to

complement receptors (Kishore et al., 2003). Thus, we have successful expressed proteins that bind to C1q ligands, function as competitive inhibitors for the classical complement pathway, and which do not activate the complement system.

CHAPTER 4:

Assessment of the ability of recombinant ghA, ghB, ghC, ghA3, ghB3 and ghC3 to modulate immune functions of microglial cells.

4.1 Introduction

Alzheimer's disease is a chronic debilitating disorder characterised by memory loss, impairment of reasoning and disorientation. Post mortem studies identified the pathological characteristics of this neurodegenerative disorder which include extracellular senile plaques composed of Aβ, intracellular neurofibrillary tangles composed of Tau, cerebrovascular dysfunction, synaptic loss and neuronal atrophy particularly of ACH neurons. Due to studies conducted on early onset/familial AD subjects and subjects with Trisomy 21, researchers identified point mutations in the Amyloid precursor protein (APP), thereby indicating that Aβ which is derived from APP is the initial causative agent in the development of AD. However, the discoveries that plaques also occur in normal aged subjects (albeit in lower numbers), and that the pathology of Aβ precedes development of AD by decades, indicates that though Aβ is required, it is not sufficient to initiate the chronic neurodegeneration observed in this disorder.

Recent studies have identified activated inflammatory proteins colocalised with amyloid plaques in the cerebral milieu of AD subjects. Many of the proteins are components of the classical complement pathway (C1-9); in particular the membrane attack complex (C5b-9) which makes the phospholipid bilayer porous thereby leading to cellular lysis and apoptosis (Bayly-Jones C et al., 2017). The normal function of the complement system is the maintenance and regulation of homeostasis. It achieves this by facilitating the removal of activators (pathogenic organisms, apoptotic cells, tissue debris and molecular aggregates such as Aβ) via four primary functions: recognition, opsonisation, inflammatory stimulation, and direct killing through the membrane attack complex (Maibaum, 2000). For instance, a beneficial effect of the complement system in AD is the binding of opsonins such as C1q, C4b, C3b to Aβ plaques which facilitate the uptake of Aβ via specific receptors found on glial cells. An activated complement system would further lead to the production of chemotactic agents which recruit microglia, and induces the production of pro-inflammatory cytokines; thereby returning a homeostatic balance to the neuronal milieu. In fact, studies have shown that though low levels of complement exist in the brain, when confronted with pathogen and aggregates in the microglia, glial cells and neurons can synthesise complement proteins (Gasque et al., 2000). It is therefore clear that the complement system does indeed play a role.

However, complement activation can also be detrimental and lead to the perpetuation of chronic pathologies, when activated inappropriately or for a prolonged duration. Many neurodegenerative diseases such as AD may require a primary aetiology, but the pathogenic factor that exacerbates the issue is thought to be chronic activation of the complement system and deficiency of complement inhibitors/regulators such as CD59 (Gasque et al., 2000). In the case of AD, additional amyloid associated proteins such as clusterin, and sulphated proteoglycans, shield Aβ from microglial immunosurveillance. This ensures that despite the opsonisation of Aβ deposits by complement proteins, the clearance mechanism is hindered. Unfortunately, this continues a process of chronic activation of the complement system and its membrane attack complex, which directly results or contributes to many or the neurodegenerative pathologies, such as a perpetual recruitment of microglial cells, persistent neuroinflammation due to release of inflammatory cytokines, apoptosis of nearby cells by the MAC.

Based on the studies above, it is clear that though the complement system plays a role in the maintenance of homeostasis, its suggested detrimental role in the pathogenesis of AD far outweigh the benefits. Therefore, in this study we examined the ability of recombinant globular heads of C1q (ghA, ghB and ghC) and the mutant recombinant multimers (ghA^3, ghB^3 and ghC^3) to bind to Aβ42 and therefore act as competitive inhibitors of C1q. We further investigated the ability of the recombinant globular heads to competitively inhibit Aβ activation of microglia and therefore prevent or reduce the complement induced pathologies observed in AD.

4.2 Materials and methods

4.2.1 Cell lines

Microglial cells are the resident effectors of the innate immune system in the brain. The presence of activated microglia within the neuronal milieu is a prominent hallmark of AD. *In vitro* cultures are utilised in the study of microglial function more often than *in vivo* techniques, as an increased yield and homogeneity of cells allows for the generation of more data within a shorter period. Moreover, variations in activation state, cell motility, pro- and anti-inflammatory responses are better examined *in vitro.* Current *in vitro* models for microglial study in neurodegenerative diseases include primary microglia and immortalised cell lines. Whilst primary microglial cultures maintain the phenotype of endogenous cells and are therefore beneficial to study; low cell number and extensive preparation required make this model less attractive compared to Immortalised cell lines.

The mouse microglial cell line BV-2 is most commonly used in published studies. It was originally derived by immortalising murine macrophages obtained from the bone marrow, via transformation with the v-raf and v-my oncogenes of the J2 retrovirus (Blasi et al. 1990). BV-2 cells have been shown to resemble primary microglia morphologically, electrophysiologically and functionally. BV-2 cells phagocytose inactivated yeast cells and latex beads and maintain the constitutive and inducible secretory properties of primary microglia. In addition, this phenotype is maintained over time in *in vitro* culture (Blasi et al. 1990; Bocchini et al. 1992). A more recent study strengthened these original findings, demonstrating that the genes upregulated by LPS in BV-2 microglia mirror those upregulated in primary microglia, although the upregulation in BV-2 cells was often less pronounced (Lund et al. 2006). Thus, magnitude of response has been sacrificed in order to increase feasibility of experiments and reduce preparation time.

4.2.2 Cell culture

The BV-2 mouse microglial cell line (passage 12) was a kind gift from Professor Guy Brown (Department of Biochemistry, Cambridge University, UK). BV-2 microglial cells (Fig 4.1) were maintained in 75cm^2 non-treated culture flasks (Nunc) in cell culture media (Dulbecco's modified Eagle's medium (DMEM; Invitrogen) with 4500 mg.L-1 glucose, supplemented with 10% Foetal Bovine Serum (FBS), 2 mM glutamine, 100 units.ml-1 penicillin, 100 µg.ml-1 streptomycin) at 37°C

in a humidified atmosphere of 5.0% CO2 in air. At confluence, cells were washed with sterile 1x in phosphate-buffered saline pH 7.2 (PBS; Invitrogen) and subsequently harvested using 0.5% trypsin-EDTA (Invitrogen) in PBS (3 min). Fresh DMEM was added to the flasks to allow cell survival.

4.2.3 Thawing cells

Prior to removing frozen cells from liquid nitrogen, fresh media was equilibrated to 37°C in a water bath. Once equilibrated 15ml of fresh media was added to a 75cm^2 flask. Next, a cryovial including the frozen cells, was removed from the liquid nitrogen and thawed in the water bath at 37°C. Once the cell suspension was sufficiently defrosted, the solution was diluted in a falcon tube containing 30ml fresh DMEM and centrifuged at 1500 rpm for 5 minutes. Supernatant was aspirated with a sterile pipette and pellet was resuspended in 1ml of fresh media. The cells were then transferred into the 75cm^2 flask and moved into the incubator overnight to allow the cells to adhere. Cells adhered within 24 hours and reached confluence within 48 hours. At confluence cells were harvested using 0.5% trypsin-EDTA (Invitrogen) in PBS and subcultured in a 1:10 ratio. The remaining cells were cryopreserved.

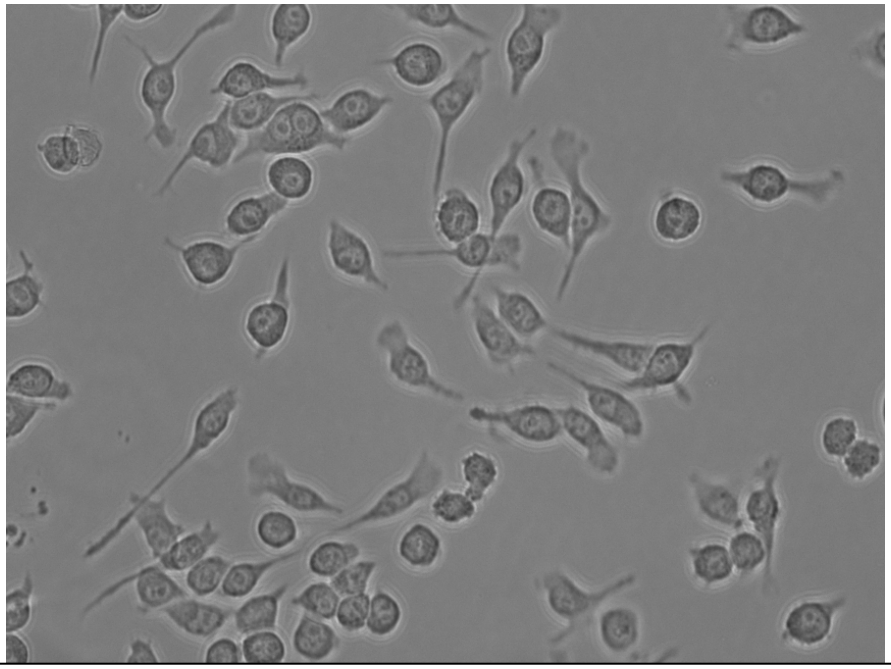

Fig 4.1 White light image of BV-2 cells (26 hours) using the fibre image program. (Westover, Scientific)

4.2.4 Cryopreservation of cells

15ml of media as prepared above was added to trypsinised cells in order to inactivate trypsin. Cells were then centrifuged at 1500 rpm for 5 minutes. The media was then aspirated from the pellet. Subsequently the pellet was resuspended in 5ml of Freezing medium (DMEM, 50% FBS and 10% DMSO). Resuspended cells were then transferred in 1ml suspensions into 1.5 ml cryotubes (Nunc, UK). Cryotubes were then placed into a cell freezing container and placed at -80^{o}C overnight. Once sufficiently frozen the cryotubes were transferred to liquid nitrogen for storage.

4.2.5 Cell counting

In order to calculate the seeding density of cells, and thus accurately conduct cell treatment experiments, the no of cells in suspension need to be counted. 15ml of media as prepared above was added to trypsinised cells in order to inactivate trypsin. Cells were then centrifuged at 1500 rpm for 5 minutes. Subsequent to centrifugation, cells were resuspended in 10ml of DMEM medium. 10 µl of cells were then mixed with 40ul of trypan blue, creating a cell dilution factor of 5. 10ul of this suspension was then pipetted onto a section of a haemocytometer and a clear plastic slide placed on top which would allow the cells to flow by lamina flow. The haemocytometer was placed under the microscope and cells visible within 16 squares were counted with a cell counter. The total amount was multiplied by 10_4 in order to ascertain the no of cells in suspension.

4.2.6 Cell treatments

All cell treatments were conducted in 6 well culture plates (Thermoscientific, UK) with a seeding density of 0.1 x 10^6 in 2ml DMEM (0.5 % FBS). Cells were then incubated at 37◦C with 5% CO_2 atmosphere and left to adhere. The following day cells were treated with PBS (Vehicle/control treatment), 10ug of ghA, ghB, ghC, ghA^3, ghB^3, ghC^3 or MBP, and transferred to an incubator at 37◦C with 5% CO_2 atmosphere for an hour. Cells were removed and 1µM of unaggregated Amyloid Beta 1-42 fragment (Sigma; Stine et al., 2013) was added to wells containing ghA, ghB, ghC, ghA^3, ghB^3, ghC^3 or MBP, Cell treatment was also run with Aβ42 as a positive control. Cells were then harvested at the following time points post Aβ incubation: 3hrs, 6hrs, 9 hrs, 12 hrs and 24hrs. Cells were harvested by aspirating the media from the plate and incubating cells in DMEM, containing 0.025% trypsin/ 0.01% EDTA for 3 mins at 37◦C. Cells were removed using a cell scraper, added to an equal volume of DMEM media and then centrifuged at 1500 rpm for 10 mins. Supernatant was then aspirated, and cell pellets

were used immediately for RNA extraction.

Total RNA was extracted from frozen cell pellets using the Picopure RNA Isolation kit (Thermoscientific). Samples were then treated with DNase I (Sigma-Aldrich) to remove any contaminating DNA. Samples were then heated at 70ºC for 10 min to inactivate both the DNase I and the RNase, and subsequently chilled on ice. The amount of total RNA was measured by determining the optical density at 260nm using the Nanodrop 2000/2000c (Thermo-Fisher Scientific) and the purity of the RNA determined using the ratio of absorbance at 260nm and 280 nm. Complementary DNA (cDNA) was synthesized using High Capacity RNA to cDNA Kit (Applied Biosystems) from a quantity of 2µg of total RNA extract.
Primer sequences were designed and analysed for specificity using the nucleotide Basic Local Alignment Search Tool and Primer-BLAST (http://blast.ncbi.nlm.nih.gov/Blast.cgi). The following primers were used:

Gene name	Forward primer sequence	Reverse primer sequence
18S rRNA	GTAACCCGTTGAACCCCATT	CCATCCAATCGGTAGTAGCG
IL-1β	CAGGCAGGCAGTATCACTCA	TGTCCTCATCCTGGAAGGTC
IL-18	GACTCTTGCGTCAACTTCAAGG	CAGGCTGTCTTTTGTCAACGA
Tgfβ1	CAGCCCTGCTCACCGTCGTG	GGTTTGTGGCTCCCGAGGGC
β-Actin	AGTGTGACGTTGACATCCGT	TGCTAGGAGCCAGAGCAGTA
IL-6	CTCTGGGAAATCGTGGAAAT	CCAGTTTGGTAGCATCCATC
TNF-α	ATGAGAAGTTCCCAAATGGC	CTCCACTTGGTGGTTTGCTA

Table 4.1 qPCR Forward and Reverse Primers inflammatory mediators

PCR was performed on all cDNA samples to assess the quality of the cDNA. The qPCR reactions consisted of 5 µl PowerUp SYBR Green MasterMix (Applied Biosystems), 75 nM of forward and reverse primer, 500 ng template cDNA in a 10 µl final reaction volume. Sequences are described in the above Table 4.1. PCR was performed in a 7900HT Fast Real-Time PCR System (Applied Biosystems). The initial steps were 2 minutes incubation at 50°C followed by 10 minutes incubation at 95°C, the template was then amplified for 40 cycles under these conditions: 15 seconds incubation at 95°C and 1-minute incubation at 60°C. Samples were normalized using the expression of mouse B-Actin mRNA. Data was analysed using Expression (Applied Biosystems). Ct (cycle threshold) values for each target gene were calculated and the relative expression of each cytokine target gene was calculated using the Relative Quantification (RQ) value, using the formula: $RQ = 2^{-\Delta\Delta Ct}$ for each cytokine target gene and comparing relative expression with that of the β-Actin rRNA constitutive gene

product. Assays were carried out twice in triplicate.

Statistical analysis was conducted using GraphPad Prism version 8.0 (GraphPad). A 2- Way ANOVA was used to compare the means of the expressed targets of the timepoints analysed, using the timepoint as calibrator. P values were computed, graphs compiled and analysed.

4.3 Results

4.3.1Globular heads bind in a dose dependent manner to Aβ-42.

Previous studies have shown that Aβ can bind to C1q. In order to study the recombinant globular heads as inhibitors for C1-Aβ mediated damage, we must first confirm the ability of the residues to bind to C1q. We examined the binding ability of MBP-ghA, MBP-ghB and MBP-ghC to 1ug Aβ. MBP was used as a negative control in order to confirm that none of the observed response was MBP mediated. The binding curve is shown in **Fig 4.1a.** In all cases, the binding was dose-dependent. With an increase in the concentration of recombinant proteins added to the ELISA wells, an increased level of binding was detected. We observed a significant difference in absorbance 450nm readings of ghA, ghB, and ghC at all concentrations when compared to MBP. The ligand binding activity of ghB to Aβ was significantly higher than that of ghA, and ghC at all concentrations, reaching approximately 30% more than ghA, and 20% more than ghC at the highest concentration of 10 µg.

We further examined the binding ability of MBP-ghA^3, MBP-ghB^3 and MBP-ghC^3 to 1ug Aβ. MBP was used as a negative control in order to confirm that none of the observed response was MBP mediated. The binding curve is shown in **Fig 4.1b.** In all cases, the binding was dose-dependent. With an increase in the concentration of recombinant proteins added to the ELISA wells, an increased level of binding was detected. We observed a significant difference in absorbance 450nm readings of ghA^3, ghB^3, and ghC^3 at all concentrations when compared to the monomeric variants and MBP. At a concentration of 0.6µg/well we observed that the ligand binding activity of ghA^3, and ghC^3 to Aβ was the same as that of the monomeric variants ghA, ghB and ghC at a concentration of 10µg/well. However, ghB^3 bound more strongly to Aβ than ghA^3, and ghC^3 at all concentrations, reaching approximately 200% more than ghA^3 and ghC^3 at concentrations of 0.6, 1.25 and 2.5 and 5µg/well, thus indicating that the multimeric variants may have a higher binding affinity to Aβ42 than the monomeric variants, and that ghB^3 in particular has a very high affinity at even the lowest concentrations.

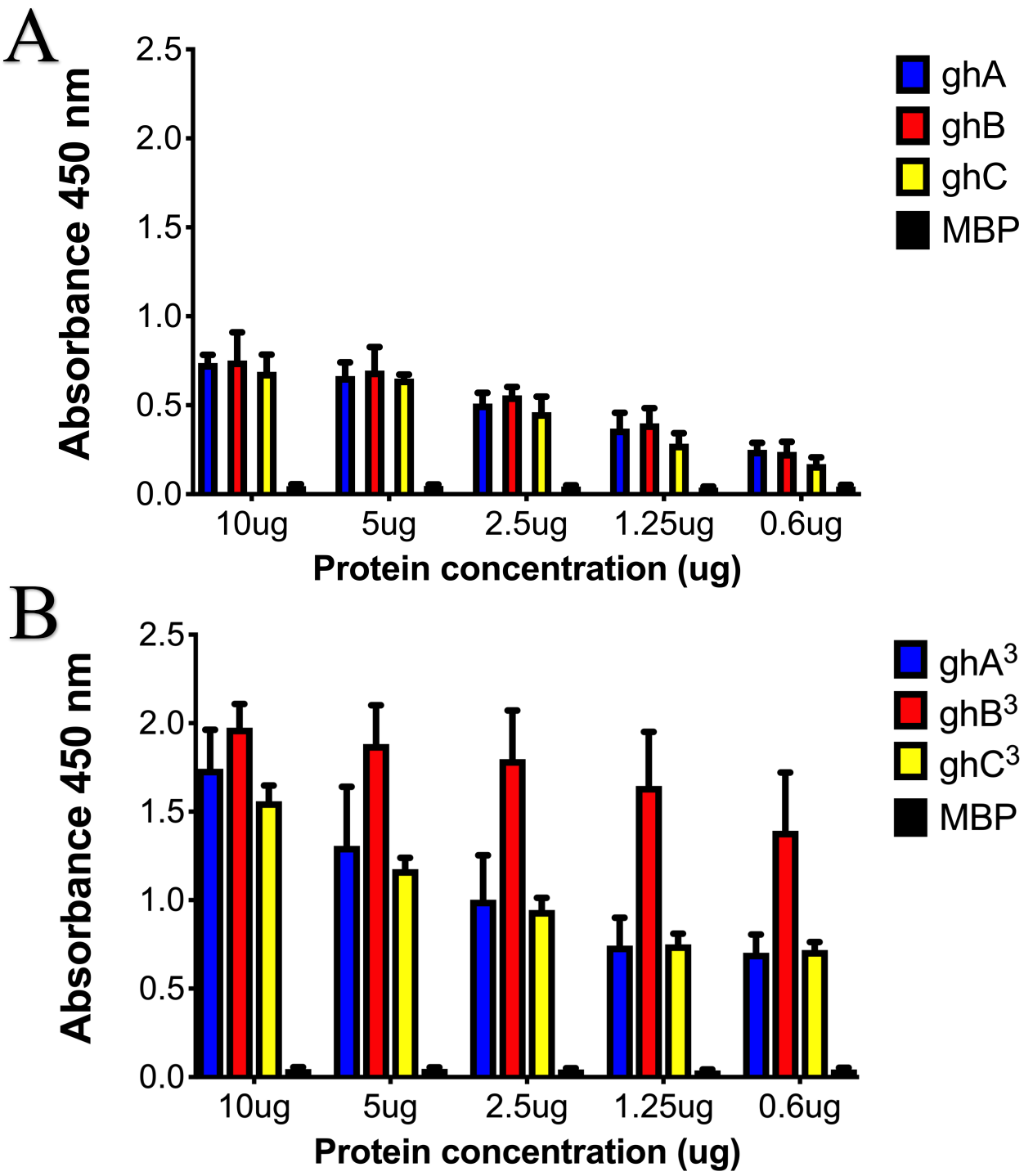

Fig. 4.1 Composite graph illustrating the direct ELISA binding of recombinant globular heads to Aβ.
MBP-ghA, MBP-ghB and MBP-ghC, MBP-ghA^3, MBP-ghB^3 and MBP-ghC^3 and MBP were incubated at different concentrations (0.6, 1.25, 2.5, 5 and 10µg/well) with Aβ coated microtiter wells (1µg/well). Mouse anti-MBP antibodies and rabbit anti- mouse IgG-HRP conjugate probed the amount of bound recombinant protein. MBP was used as a negative control protein. The experiments were conducted at the same time. The data are shown as means ± SD of triplicate measurements. Optical density at 450 nanometres is plotted along the vertical axis. Statistical analysis: Unpaired t-test between MBP and MBP-gh. Significance levels (*p<0.05, **p<0.01, ***p<0.001).

4.3.2 C1q recombinant fusion proteins inhibit the expression of TNF α mRNA.

Gene expression of BV-2 cells incubated with Aβ-42 were studied via qPCR following treatment with or without MBP fusion proteins. This was a cross species study testing human serum proteins on a mouse cell line. Primers as previously described were used. The data (Fig 4.2, 4.3, 4.4, 4.5, 4.6 and 4.7) revealed a significant (***p<0.001) downregulation of TNF-α mRNA expression by MBP fusion protein treated BV-2 cells at all timepoints when compared to cells that received no treatment, thus indicating that the globular head proteins are capable of inhibiting the expression of the pro-inflammatory cytokine TNF-α. Though a significant downregulation was consistent at all time points, the extent of downregulation varied between globular head monomers ghA (Fig 4.2), ghB (Fig 4.4), and ghC (Fig 4.6); and differed across all timepoints which is likely due to the different protein properties of each globular head and their varied binding affinities to Aβ.

The globular head multimers ghA^3 (Fig 4.3), ghB^3 (Fig 4.5), and ghC^3 (Fig 4.7) revealed a significant 2-fold downregulation of expression at all time points compared to the untreated groups (***p<0.001) and the treated globular head monomer groups (**p<0.001). revealing that the multimers have a greater inhibitory effect on mRNA expression of the pro-inflammatory cytokine than the monomers. Moreover, ghB^3 (Fig 4.5) had the largest effect on the downregulation (3-fold) of TNF-α mRNA expression. This downregulation was also significant (**p<0.01) when compared to ghA^3 (Fig 4.3) and ghC^3 (Fig 4.7) at all time points, thus indicating that ghB^3 may have a greater binding affinity and therefore inhibitory effect on the expression of TNFα mRNA than both the globular head multimers. Raw data is included in Appendix sections (1-5).

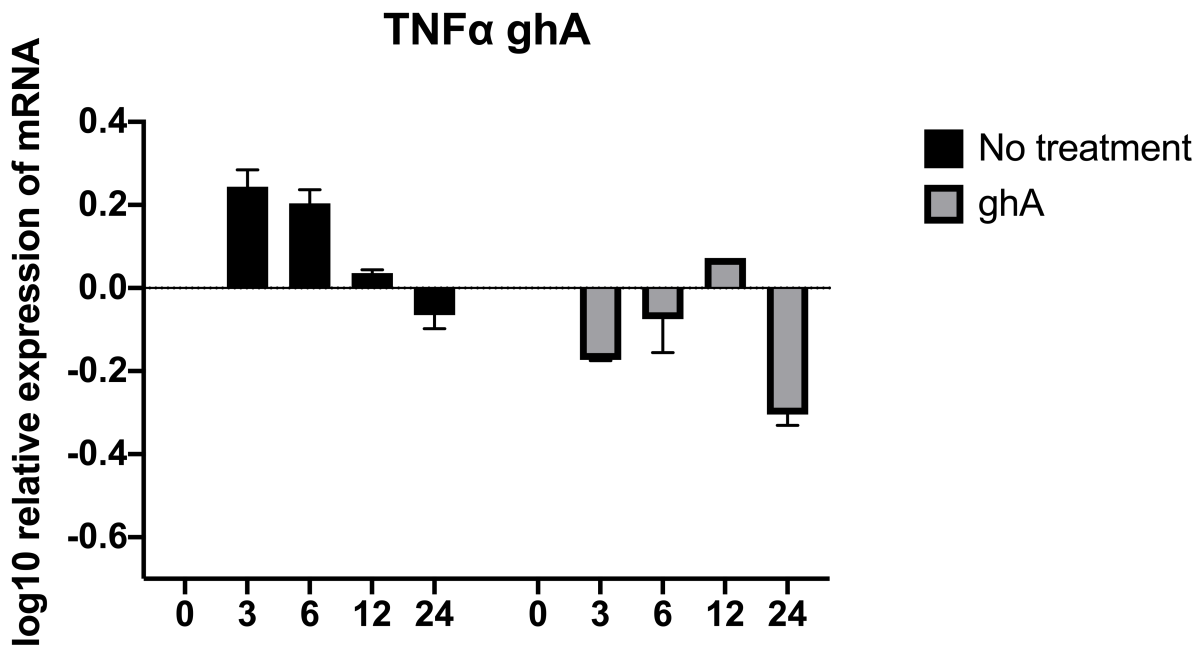

Fig 4:2 Composite Bar graph illustrating the effect of ghA on Amyloid Beta induced expression of TNF-α mRNA.
qPCR analysis of the expression of TNF α mRNA extracted from BV-2 microglia samples at 0, 3, 6, 12, 24hr. All samples were incubated with Aβ42 with or without ghA treatment. Graph plotted represents log10 relative expression levels of gene of interest normalised to an endogenous control of β-actin. Zero hr timepoint was used as the calibrator. Assays were conducted in triplicate. Error bars represent Mean ± standard deviation.

Statistical Analysis: A 2-way ANOVA was performed on the data to determine significant differences in expression between Amyloid Beta challenged BV-2 samples with or without ghA treatment.

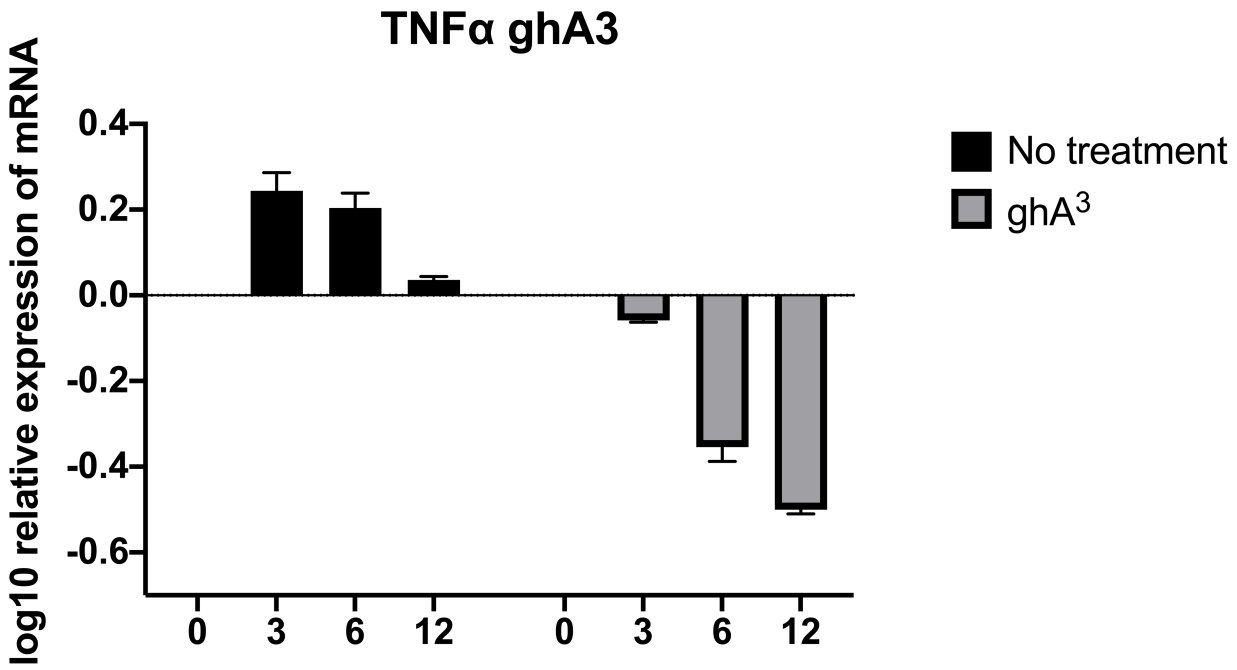

Fig 4:3 Composite Bar graph illustrating the effect of ghA^3 on Amyloid Beta induced expression of TNF-α mRNA.
qPCR analysis of the expression of TNF α mRNA extracted from BV-2 microglia samples at 0, 3, 6, 12 hr timepoints. All samples were incubated with Aβ42 with or without ghA^3 treatment. Graph plotted represents log10 relative expression levels of gene of interest normalised to an endogenous control of β-actin. Zero hr timepoint was used as the calibrator. Assays were conducted in triplicate. Error bars represent Mean ± standard deviation. (n=3)

Statistical Analysis: A 2-way ANOVA was performed on the data to determine significant differences in expression between Amyloid Beta challenged BV-2 samples with or without ghA^3 treatment.

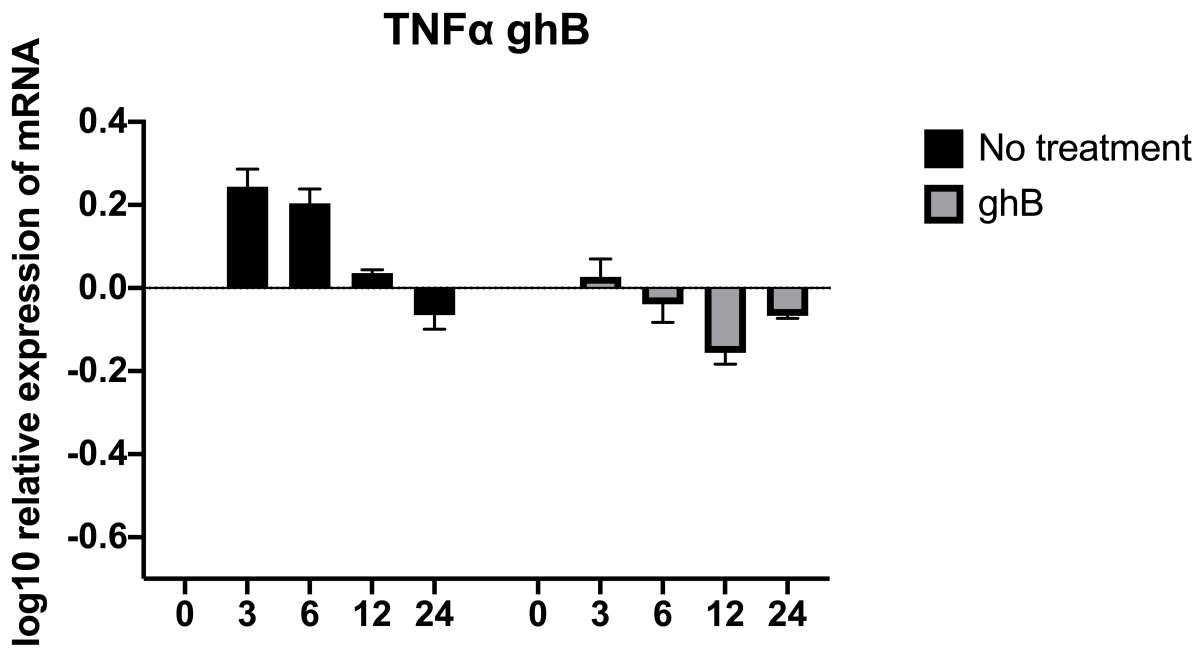

Fig 4:4 Composite Bar graph illustrating the effect of ghB on Amyloid Beta induced expression of TNF-α mRNA.
qPCR analysis of the expression of TNF α mRNA extracted from BV-2 microglia samples at 0, 3, 6, 12, 24hr. All samples were incubated with Aβ42 with or without ghB treatment. Graph plotted represents log10 relative expression levels of gene of interest normalised to an endogenous control of β-actin. Zero hr timepoint was used as the calibrator. Assays were conducted in triplicate. Error bars represent Mean ± standard deviation. (n=3)

Statistical Analysis: A 2-way ANOVA was performed on the data to determine significant differences in expression between Amyloid Beta challenged BV-2 samples with or without ghB treatment.

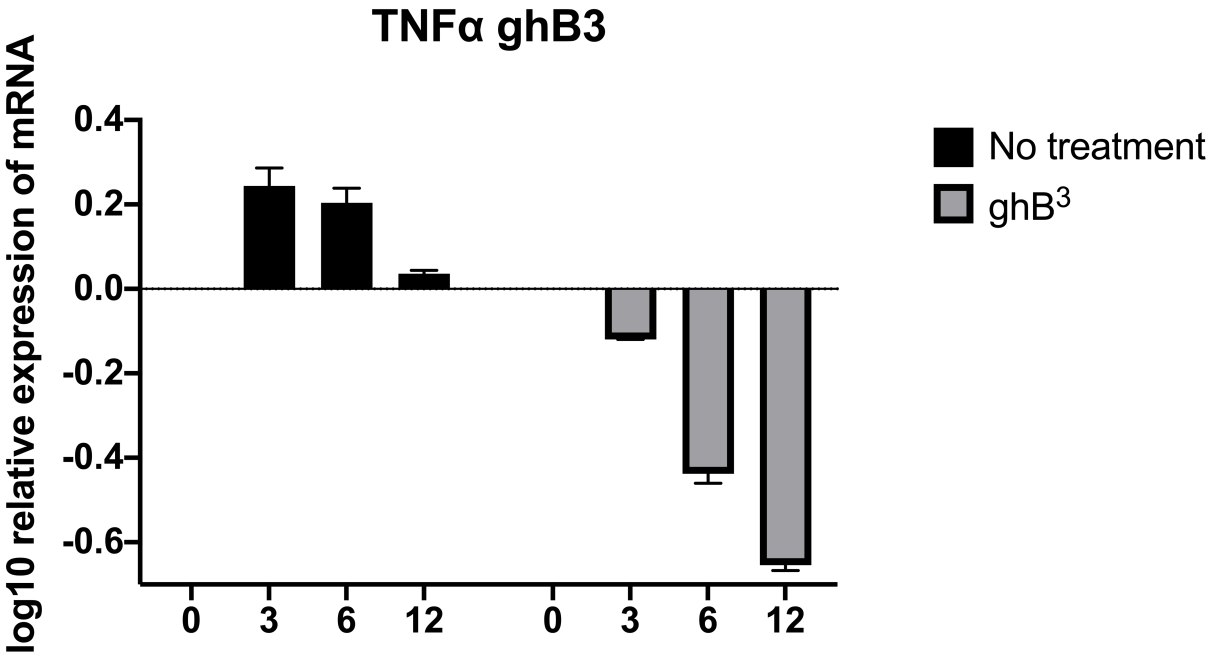

Fig 4:5 Composite Bar graph illustrating the effect of ghB^3 on Amyloid Beta induced expression of TNF-α mRNA.
qPCR analysis of the expression of TNF α mRNA extracted from BV-2 microglia samples at 0, 3, 6, 12 hr timepoints. All samples were incubated with Aβ42 with or without ghB^3 treatment. Graph plotted represents log10 relative expression levels of gene of interest normalised to an endogenous control of β-actin. Zero hr timepoint was used as the calibrator. Assays were conducted in triplicate. Error bars represent Mean ± standard deviation.

Statistical Analysis: A 2-way ANOVA was performed on the data to determine significant differences in expression between Amyloid Beta challenged BV-2 samples with or without ghB^3 treatment.

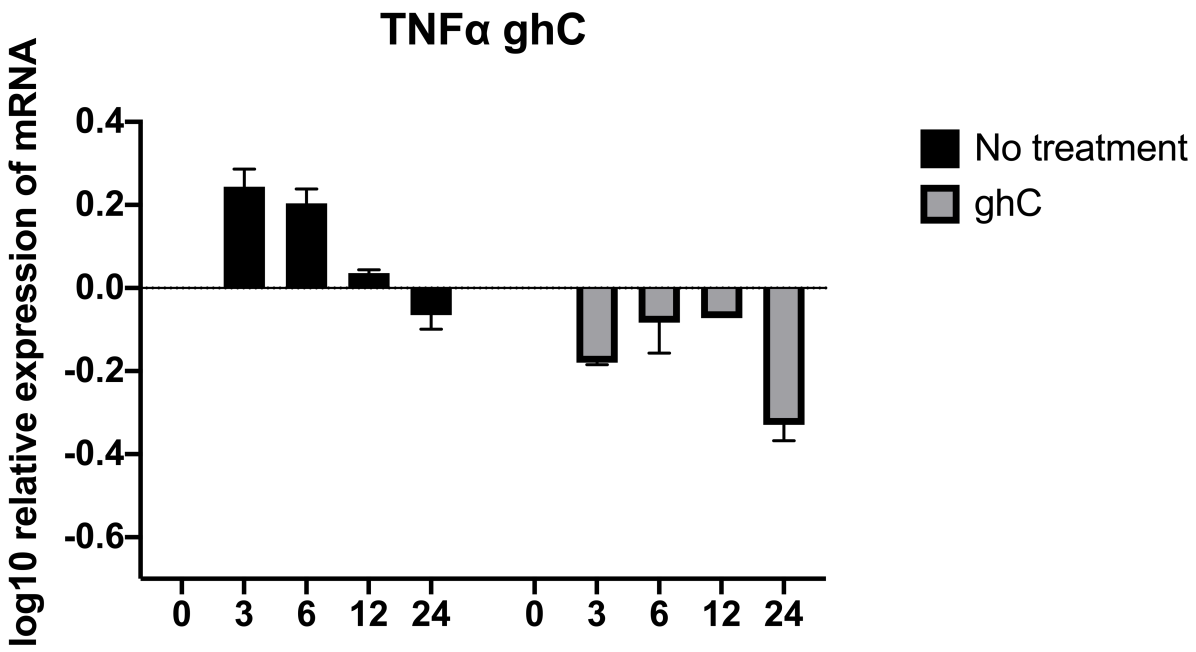

Fig 4:6 Composite Bar graph illustrating the effect of ghC on Amyloid Beta induced expression of TNF-α mRNA.
qPCR analysis of the expression of TNF α mRNA extracted from BV-2 microglia samples at 0, 3, 6, 12, 24hr. All samples were incubated with Aβ42 with or without ghC treatment. Graph plotted represents log10 relative expression levels of gene of interest normalised to an endogenous control of β-actin. Zero hr timepoint was used as the calibrator. Assays were conducted in triplicate. Error bars represent Mean ± standard deviation.

Statistical Analysis: A 2-way ANOVA was performed on the data to determine significant differences in expression between Amyloid Beta challenged BV-2 samples with or without ghC treatment.

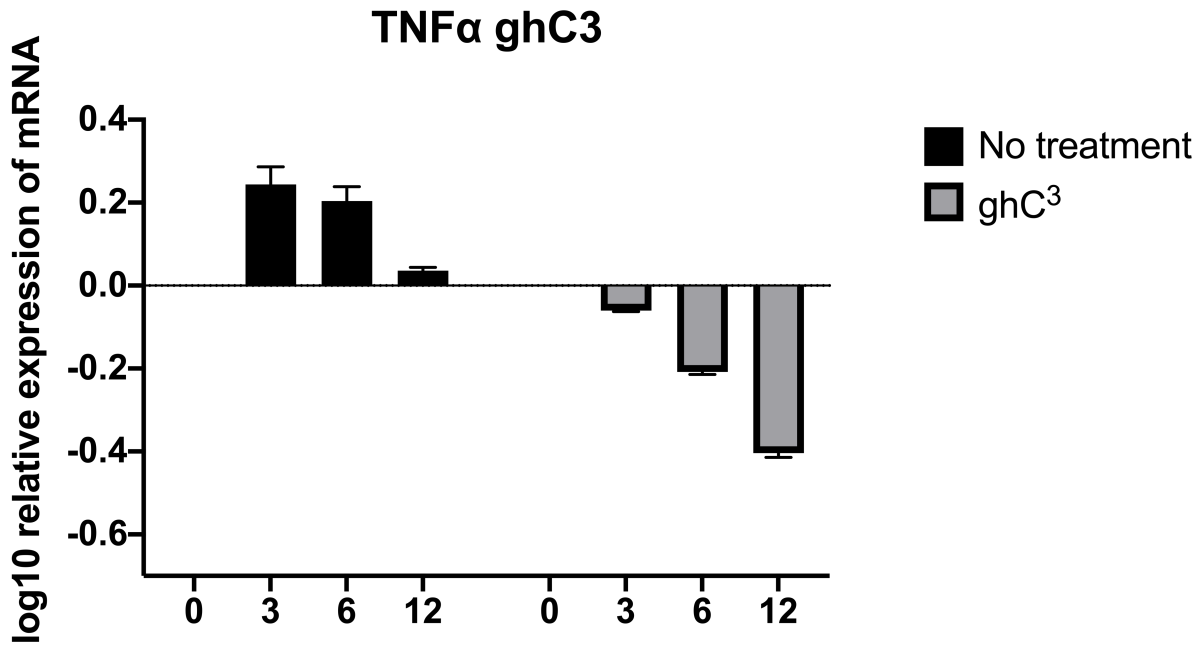

Fig 4:7 Composite Bar graph illustrating the effect of ghC^3 on Amyloid Beta induced expression of TNF-α mRNA.
qPCR analysis of the expression of TNF α mRNA extracted from BV-2 microglia samples at 0, 3, 6, 12 hr timepoints. All samples were incubated with Aβ42 with or without ghC^3 treatment. Graph plotted represents log10 relative expression levels of gene of interest normalised to an endogenous control of β-actin. Zero hr timepoint was used as the calibrator. Assays were conducted in triplicate. Error bars represent Mean ± standard deviation.

Statistical Analysis: A 2-way ANOVA was performed on the data to determine significant differences in expression between Amyloid Beta challenged BV-2 samples with or without ghC^3 treatment.

4.3.3 C1q recombinant fusion protein inhibits the expression of IL-1β mRNA.

Gene expression of BV-2 cells incubated with Aβ-42 were studied via qPCR following treatment with or without MBP fusion proteins. Primers as previously described were used. The data (ghA-Fig 4.8, ghB- Fig 4.10 and ghC- Fig 4.12) revealed a significant (*$p<0.05$) downregulation of IL-1β mRNA expression by MBP fusion protein treated BV-2 cells at 3 hr, 6h and 12 hr timepoints (no significant difference in expression at the ghA treated 12 hr timepoint Fig 4.8). The downregulation of IL-1β mRNA expression was more pronounced in ghB (Fig 4.10) treated BV-2 cells, and existed for up to 12 hrs. However, at the 24-hr time point there was a significant upregulation in expression of IL-1β in both the treated and non-treated groups. At this time point there was no significant difference in expression between, the treated and ghB treated groups Fig 4.10, whereas a significant (**$p<0.001$) downregulation of mRNA expression was still observed between the ghA (Fig 4.8) and ghC (Fig 4.12) groups when compared to the non-treated group. These graphs therefore reveal that the globular head proteins are capable of inhibiting the expression of the pro-inflammatory cytokine IL-1β, and the different patterns of inhibition are consistent their varied binding affinities to Aβ.

The globular head multimers ghB^3 (Fig 4.11), and ghC^3 (Fig 4.13) revealed a significant 2-fold downregulation of expression at all the 6 hr and the 12 hr time points compared to the untreated groups (***$p<0.001$) and the treated globular head monomer groups (**$p<0.01$). revealing that the multimers have a greater inhibitory effect on mRNA expression of the pro-inflammatory cytokine than the monomers. Moreover, ghB^3 (Fig 4.11) had the largest effect on the downregulation (3-fold) of IL-1β mRNA expression at the 12hr timepoint. This downregulation was also significant (*$p<0.05$) when compared to ghA^3 (Fig 4.3) and ghC^3 (Fig 4.7) at all time points, thus, indicating that ghB^3 may have a greater inhibitory effect on the expression of IL-1βmRNA than both the globular head multimers. Though there is precedence for cross species studies, the experiment needs to be confirmed or further investigated in a human microglial cell line due to potential cross species differences having an impact on the results. Raw data is included in Appendix sections (1-5).

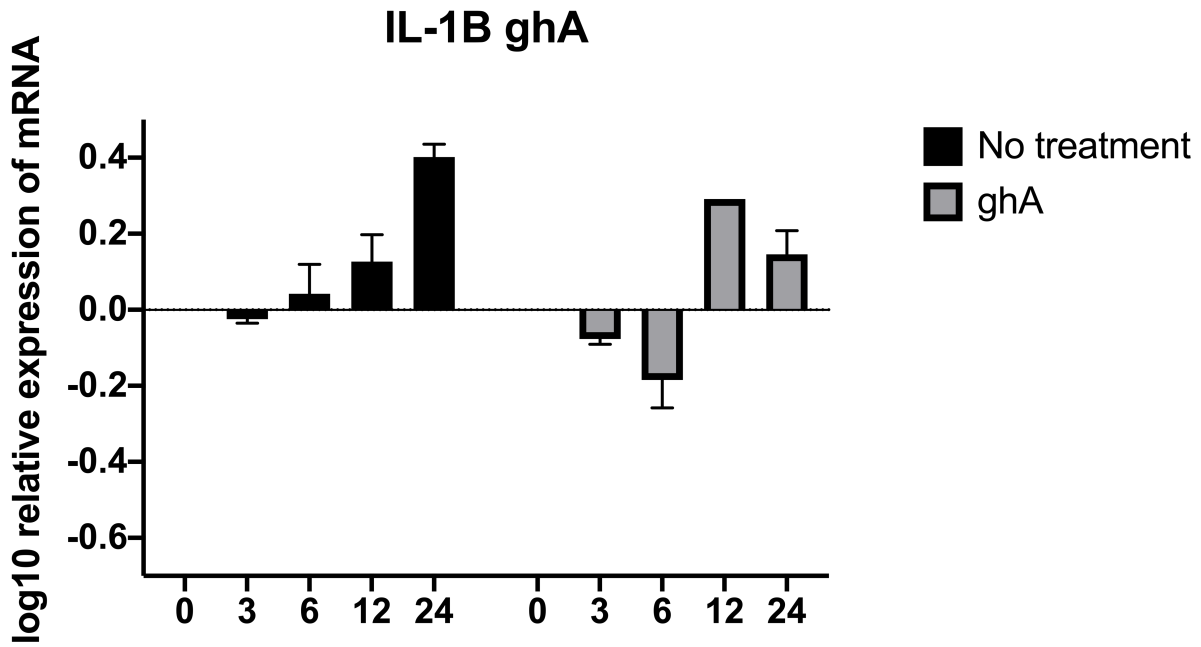

Fig 4:8 Composite Bar graph illustrating the effect of ghA on Amyloid Beta induced expression of IL-1β mRNA.
qPCR analysis of the expression of IL-1β mRNA extracted from BV-2 microglia samples at 0, 3, 6, 12, 24hr. All samples were incubated with Aβ42 with or without ghA treatment. Graph plotted represents log10 relative expression levels of gene of interest normalised to an endogenous control of β-actin. Zero hr timepoint was used as the calibrator. Assays were conducted in triplicate. Error bars represent Mean ± standard deviation.

Statistical Analysis: A 2-way ANOVA was performed on the data to determine significant differences in expression between Amyloid Beta challenged BV-2 samples with or without ghA treatment.

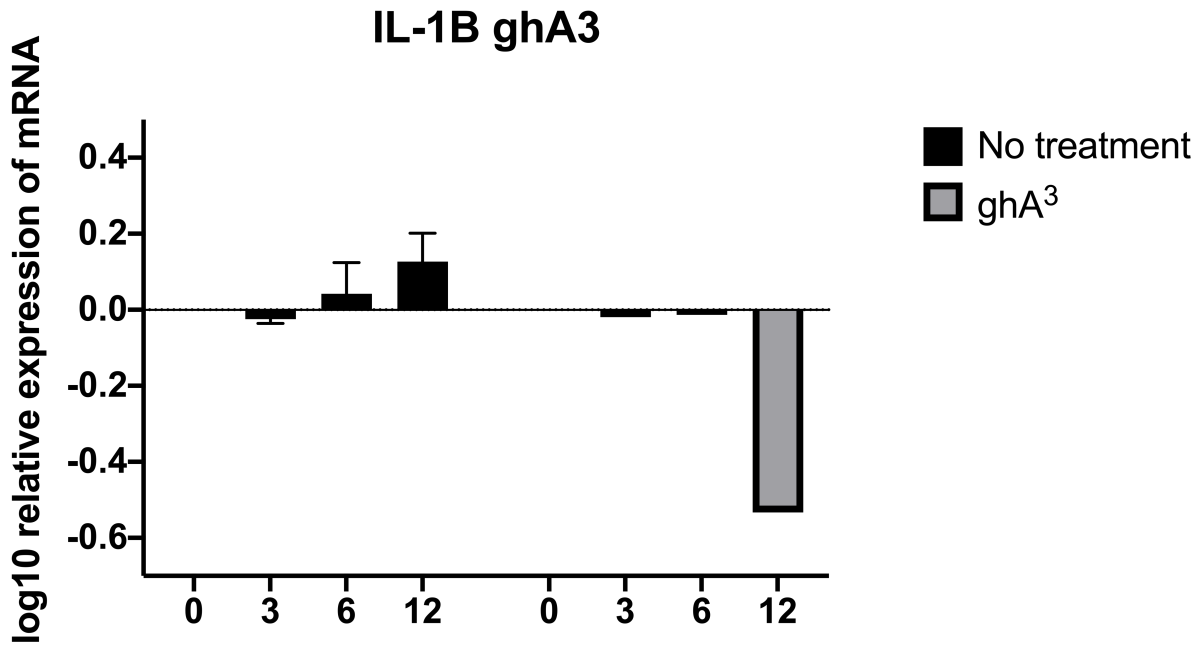

Fig 4:9 Composite Bar graph illustrating the effect of ghA^3 on Amyloid Beta induced expression of IL-1β mRNA.
qPCR analysis of the expression of IL-1β mRNA extracted from BV-2 microglia samples at 0, 3, 6, 12 hr timepoints. All samples were incubated with Aβ42 with or without ghA^3 treatment. Graph plotted represents log10 relative expression levels of gene of interest normalised to an endogenous control of β-actin. Zero hr timepoint was used as the calibrator. Assays were conducted in triplicate. Error bars represent Mean ± standard deviation. (n=3)

Statistical Analysis: A 2-way ANOVA was performed on the data to determine significant differences in expression between Amyloid Beta challenged BV-2 samples with or without ghA^3 treatment.

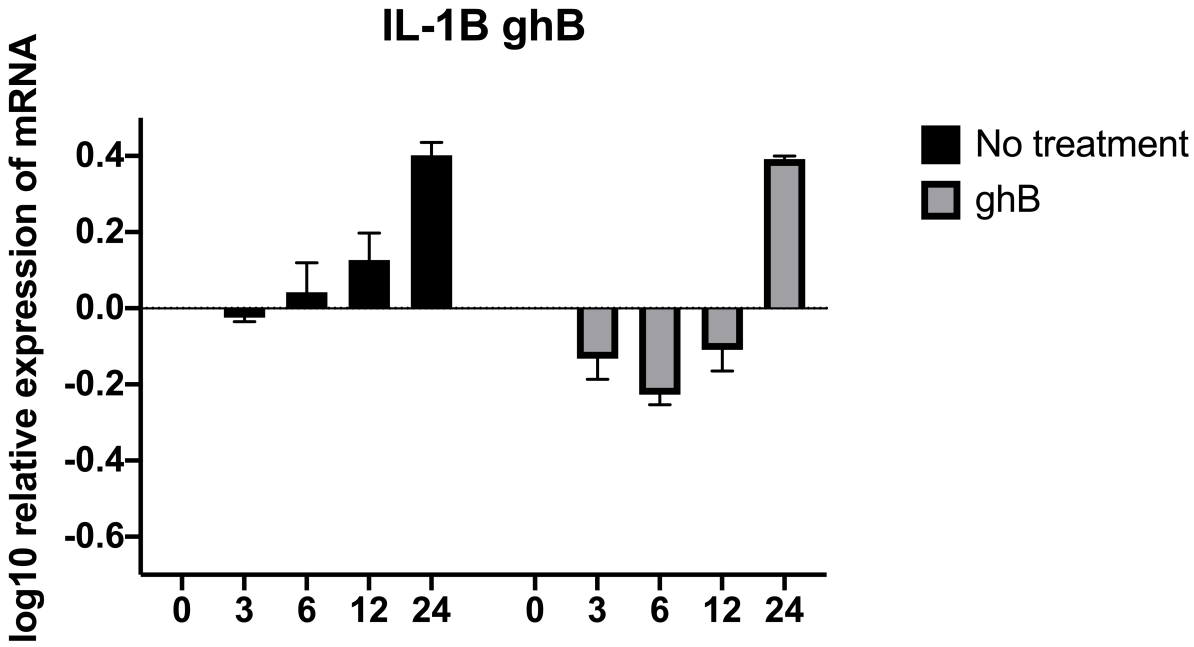

Fig 4:10 Composite Bar graph illustrating the effect of ghB on Amyloid Beta induced expression of IL-1β mRNA.
qPCR analysis of the expression of IL-1β mRNA extracted from BV-2 microglia samples at 0, 3, 6, 12, 24hr. All samples were incubated with Aβ42 with or without ghB treatment. Graph plotted represents log10 relative expression levels of gene of interest normalised to an endogenous control of β-actin. Zero hr timepoint was used as the calibrator. Assays were conducted in triplicate. Error bars represent Mean ± standard deviation. (n=3)

Statistical Analysis: A 2-way ANOVA was performed on the data to determine significant differences in expression between Amyloid Beta challenged BV-2 samples with or without ghB treatment.

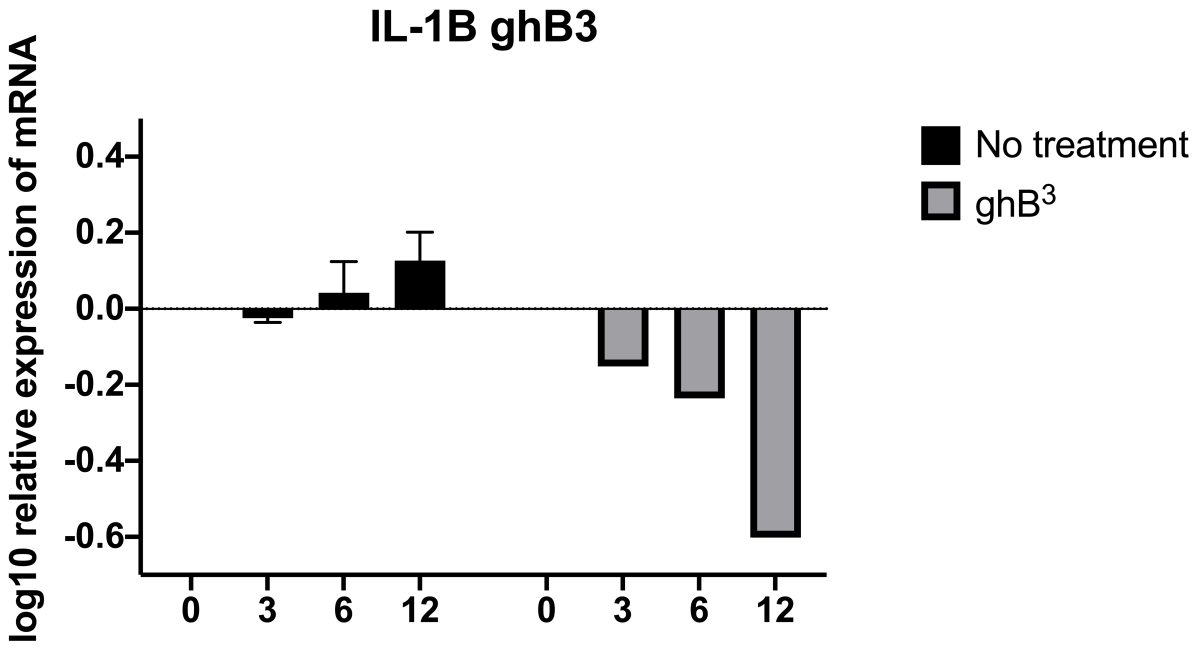

Fig 4:11 Composite Bar graph illustrating the effect of ghB^3 on Amyloid Beta induced expression of IL-1β mRNA.
qPCR analysis of the expression of IL-1β mRNA extracted from BV-2 microglia samples at 0, 3, 6, 12 hr timepoints. All samples were incubated with Aβ42 with or without ghB^3 treatment. Graph plotted represents log10 relative expression levels of gene of interest normalised to an endogenous control of β-actin. Zero hr timepoint was used as the calibrator. Assays were conducted in triplicate. Error bars represent Mean ± standard deviation.

Statistical Analysis: A 2-way ANOVA was performed on the data to determine significant differences in expression between Amyloid Beta challenged BV-2 samples with or without ghB^3 treatment.

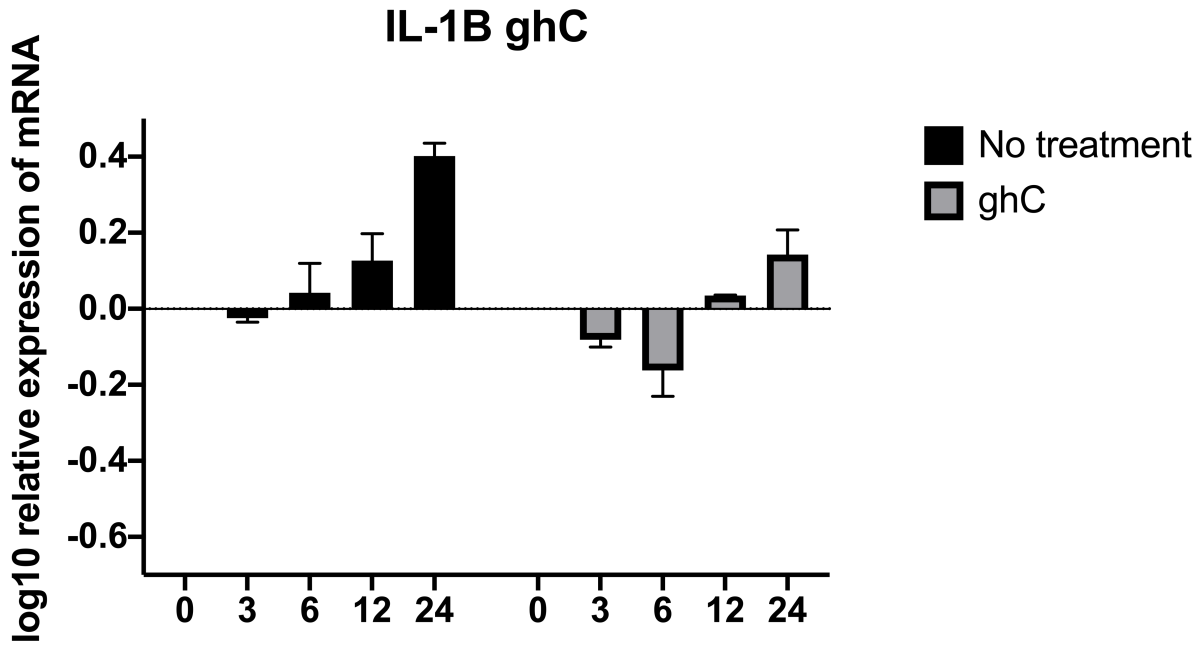

Fig 4:12 Composite Bar graph illustrating the effect of ghC on Amyloid Beta induced expression of IL-1β mRNA.
qPCR analysis of the expression of IL-1β mRNA extracted from BV-2 microglia samples at 0, 3, 6, 12, 24hr. All samples were incubated with Aβ42 with or without ghC treatment. Graph plotted represents log10 relative expression levels of gene of interest normalised to an endogenous control of β-actin. Zero hr timepoint was used as the calibrator. Assays were conducted in triplicate. Error bars represent Mean ± standard deviation.

Statistical Analysis: A 2-way ANOVA was performed on the data to determine significant differences in expression between Amyloid Beta challenged BV-2 samples with or without ghC treatment.

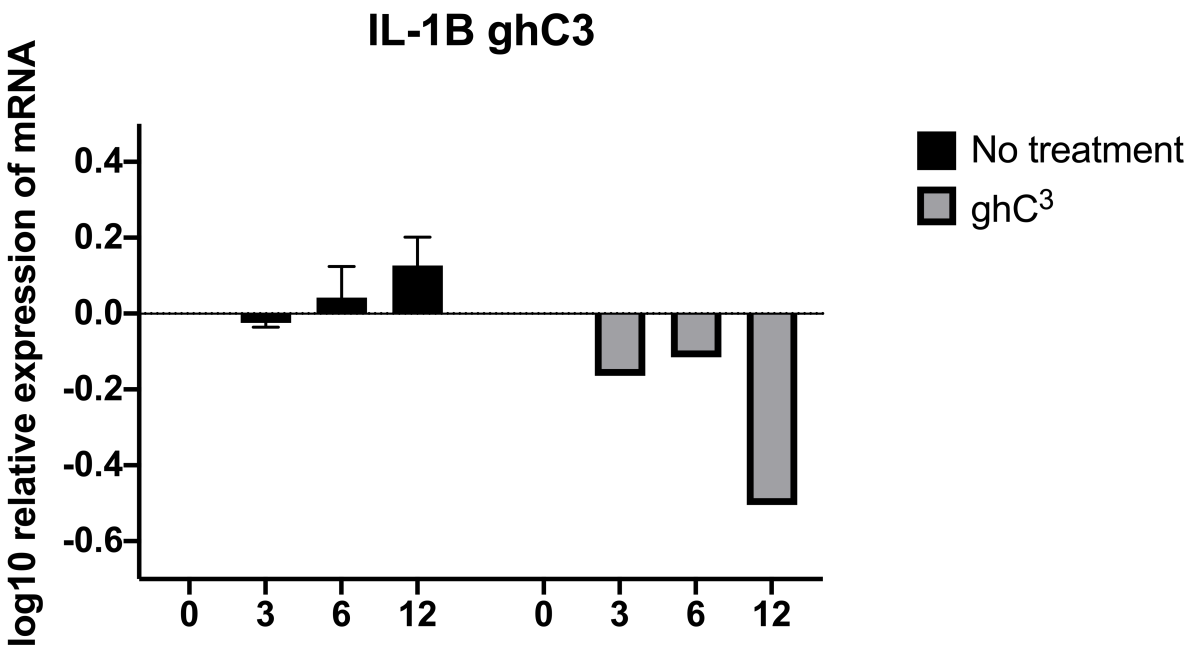

Fig 4:13 Composite Bar graph illustrating the effect of ghC^3 on Amyloid Beta induced expression of IL-1β mRNA.
qPCR analysis of the expression of IL-1β mRNA extracted from BV-2 microglia samples at 0, 3, 6, 12 hr timepoints. All samples were incubated with Aβ42 with or without ghC^3 treatment. Graph plotted represents log10 relative expression levels of gene of interest normalised to an endogenous control of β-actin. Zero hr timepoint was used as the calibrator. Assays were conducted in triplicate. Error bars represent Mean ± standard deviation.

Statistical Analysis: A 2-way ANOVA was performed on the data to determine significant differences in expression between Amyloid Beta challenged BV-2 samples with or without ghC^3 treatment.

4.3.4 C1q recombinant fusion proteins and the expression of IL-6 mRNA.

Gene expression of BV-2 cells incubated with Aβ-42 were studied via qPCR following treatment with or without MBP fusion proteins. Primers as previously described were used. The data (ghA-Fig 4.14, ghB- Fig 4.16 and ghC- Fig 4.18) revealed a significant (***$p<0.01$) upregulation of IL6 mRNA expression by MBP fusion protein treated BV-2 cells at 6 hr, 12h and 24 hr timepoints when compared with the non-treated groups. The upregulation (***$p<0.001$) of IL-6 mRNA expression was more pronounced in ghB (Fig 4.16) at the 24-hr time point when compared with the non-treated groups. At this time point there was a significant (**$p<0.001$) 20-fold difference in expression between, the non-treated and ghB treated groups Fig 4.16, whereas a significant (**$p<0.001$) 10-fold upregulation of mRNA expression was still observed between the ghA (Fig 4.14) and ghC (Fig 4.18) groups when compared to the non-treated group. These graphs therefore reveal that the globular head monomer proteins are not capable of inhibiting the expression of the pro-inflammatory cytokine IL-6.

The globular head multimers ghA^3 (Fig 4.15) ghB^3 (Fig 4.17), and ghC^3 (Fig 4.19) revealed a significant downregulation of expression at all the 6 hr and the 12 hr time points compared to the untreated groups (***$p<0.001$) and the treated globular head monomer groups (**$p<0.01$). There is no significant difference in downregulation of mRNA expression between the multimer groups. As shown previously, ghB^3 has the highest affinity to Aβ so a greater inhibition of mRNA expression of IL6 should be expected. However, none is revealed in the data, which indicates that IL6 has a different mode of activation and any inhibition observed by the multimers is an indirect effect of unavailable sites for the binding of Aβ. Raw data is included in Appendix sections (1-5).

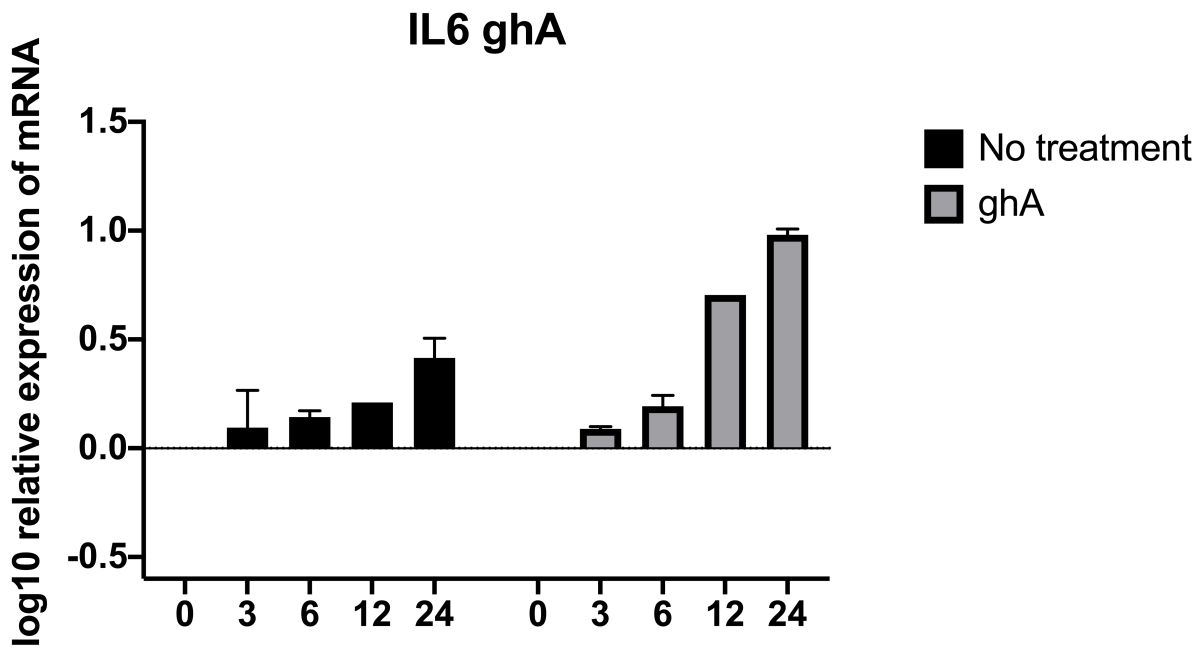

Fig 4:14 Composite Bar graph illustrating the effect of ghA on Amyloid Beta induced expression of IL6 mRNA.
qPCR analysis of the expression of IL6 mRNA extracted from BV-2 microglia samples at 0, 3, 6, 12, 24hr. All samples were incubated with Aβ42 with or without ghA treatment. Graph plotted represents log10 relative expression levels of gene of interest normalised to an endogenous control of β-actin. Zero hr timepoint was used as the calibrator. Assays were conducted in triplicate. Error bars represent Mean ± standard deviation.

Statistical Analysis: A 2-way ANOVA was performed on the data to determine significant differences in expression between Amyloid Beta challenged BV-2 samples with or without ghA treatment.

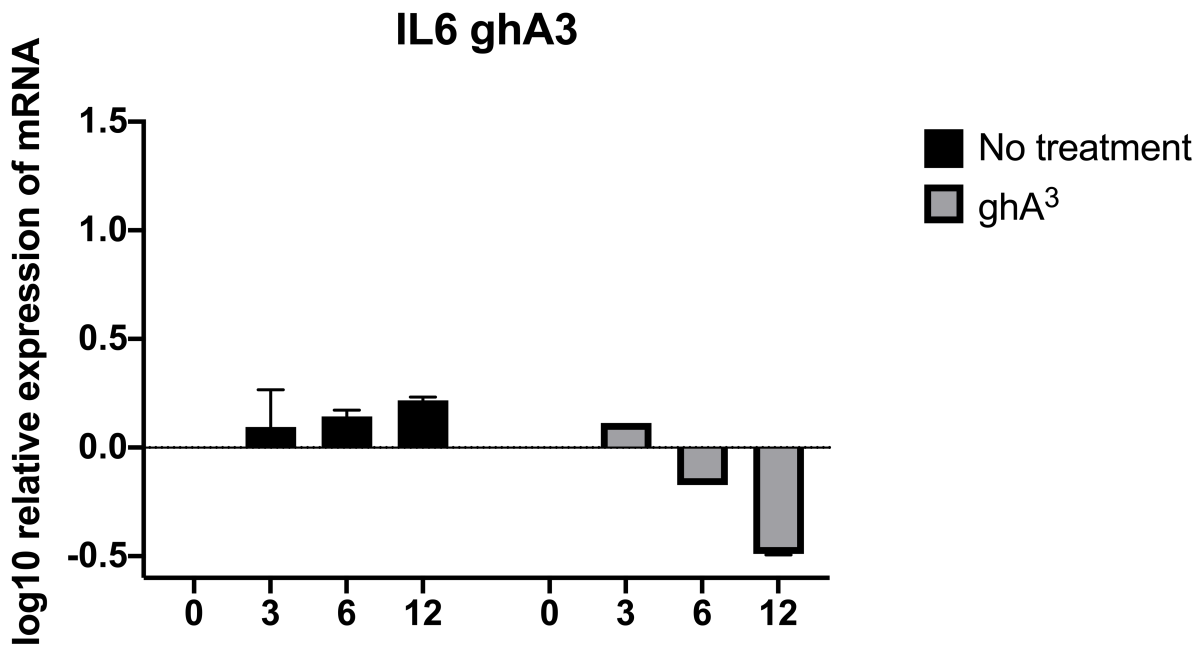

Fig 4:15 Composite Bar graph illustrating the effect of ghA^3 on Amyloid Beta induced expression of IL6 mRNA.
qPCR analysis of the expression of IL6 mRNA extracted from BV-2 microglia samples at 0, 3, 6, 12 hr timepoints. All samples were incubated with Aβ42 with or without ghA^3 treatment. Graph plotted represents log10 relative expression levels of gene of interest normalised to an endogenous control of β-actin. Zero hr timepoint was used as the calibrator. Assays were conducted in triplicate. Error bars represent Mean ± standard deviation. (n=3)

Statistical Analysis: A 2-way ANOVA was performed on the data to determine significant differences in expression between Amyloid Beta challenged BV-2 samples with or without ghA^3 treatment.

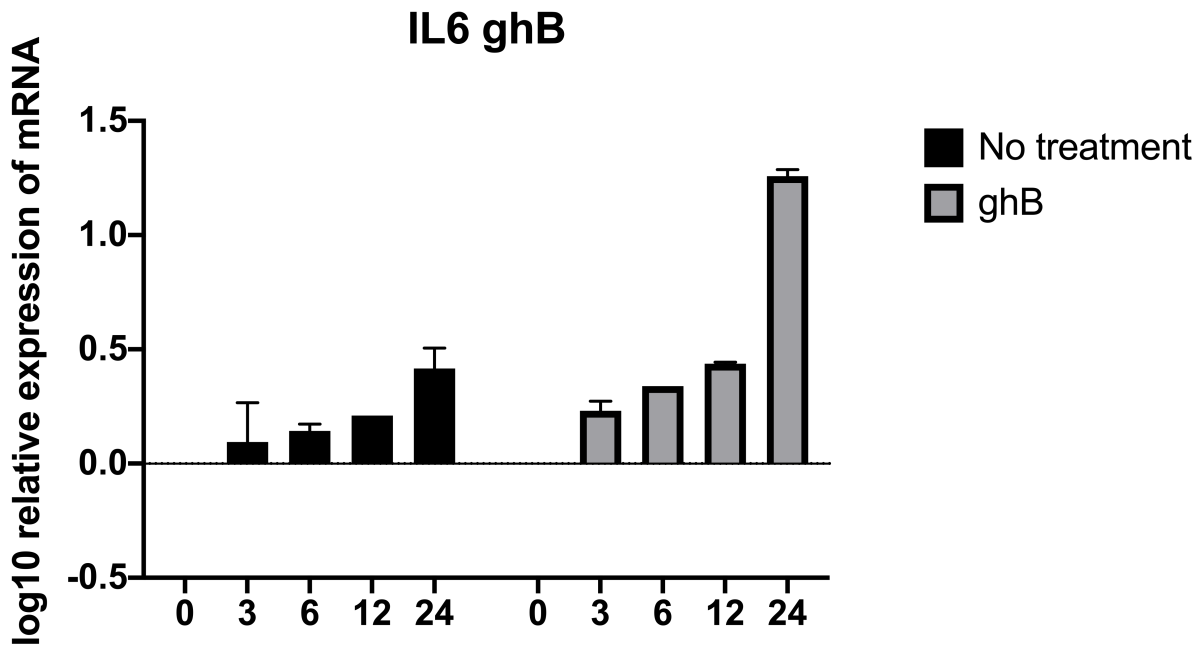

Fig 4:16 Composite Bar graph illustrating the effect of ghB on Amyloid Beta induced expression of IL6 mRNA.
qPCR analysis of the expression of IL6 mRNA extracted from BV-2 microglia samples at 0, 3, 6, 12, 24hr. All samples were incubated with Aβ42 with or without ghB treatment. Graph plotted represents log10 relative expression levels of gene of interest normalised to an endogenous control of β-actin. Zero hr timepoint was used as the calibrator. Assays were conducted in triplicate. Error bars represent Mean ± standard deviation. (n=3)

Statistical Analysis: A 2-way ANOVA was performed on the data to determine significant differences in expression between Amyloid Beta challenged BV-2 samples with or without ghB treatment.

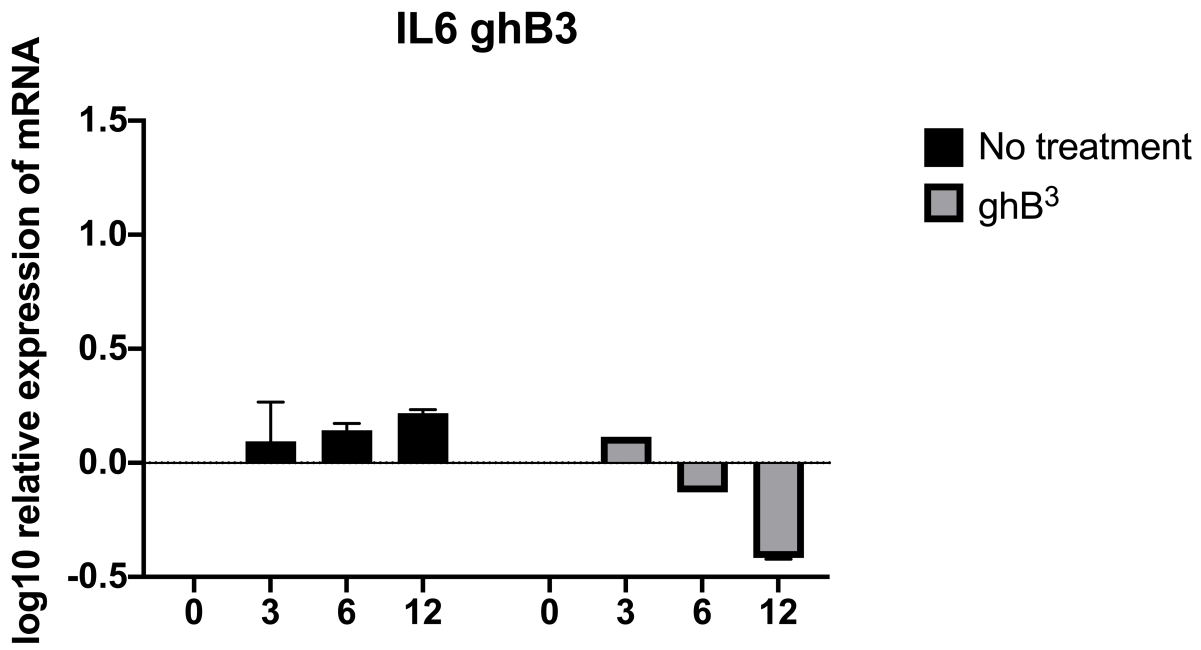

Fig 4:17 Composite Bar graph illustrating the effect of ghB^3 on Amyloid Beta induced expression of IL6 mRNA.
qPCR analysis of the expression of IL6 mRNA extracted from BV-2 microglia samples at 0, 3, 6, 12 hr timepoints. All samples were incubated with Aβ42 with or without ghB^3 treatment. Graph plotted represents log10 relative expression levels of gene of interest normalised to an endogenous control of β-actin. Zero hr timepoint was used as the calibrator. Assays were conducted in triplicate. Error bars represent Mean ± standard deviation.

Statistical Analysis: A 2-way ANOVA was performed on the data to determine significant differences in expression between Amyloid Beta challenged BV-2 samples with or without ghB^3 treatment.

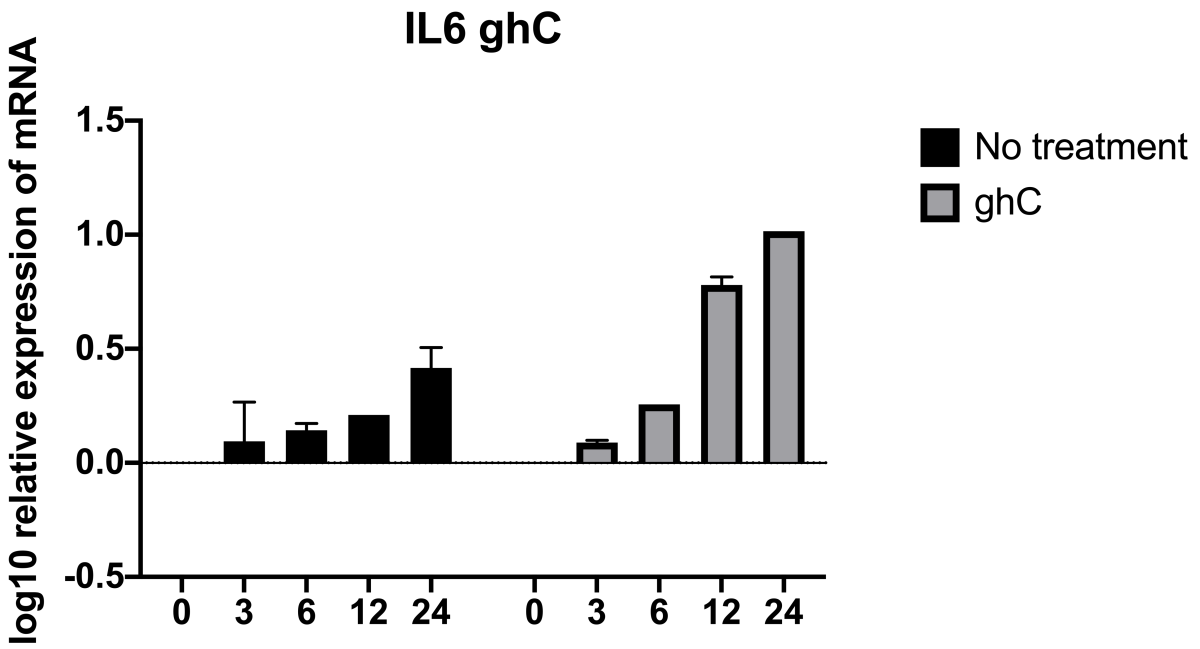

Fig 4:18 Composite Bar graph illustrating the effect of ghC on Amyloid Beta induced expression of IL6 mRNA.
qPCR analysis of the expression of IL6 mRNA extracted from BV-2 microglia samples at 0, 3, 6, 12, 24hr. All samples were incubated with Aβ42 with or without ghC treatment. Graph plotted represents log10 relative expression levels of gene of interest normalised to an endogenous control of β-actin. Zero hr timepoint was used as the calibrator. Assays were conducted in triplicate. Error bars represent Mean ± standard deviation.

Statistical Analysis: A 2-way ANOVA was performed on the data to determine significant differences in expression between Amyloid Beta challenged BV-2 samples with or without ghC treatment.

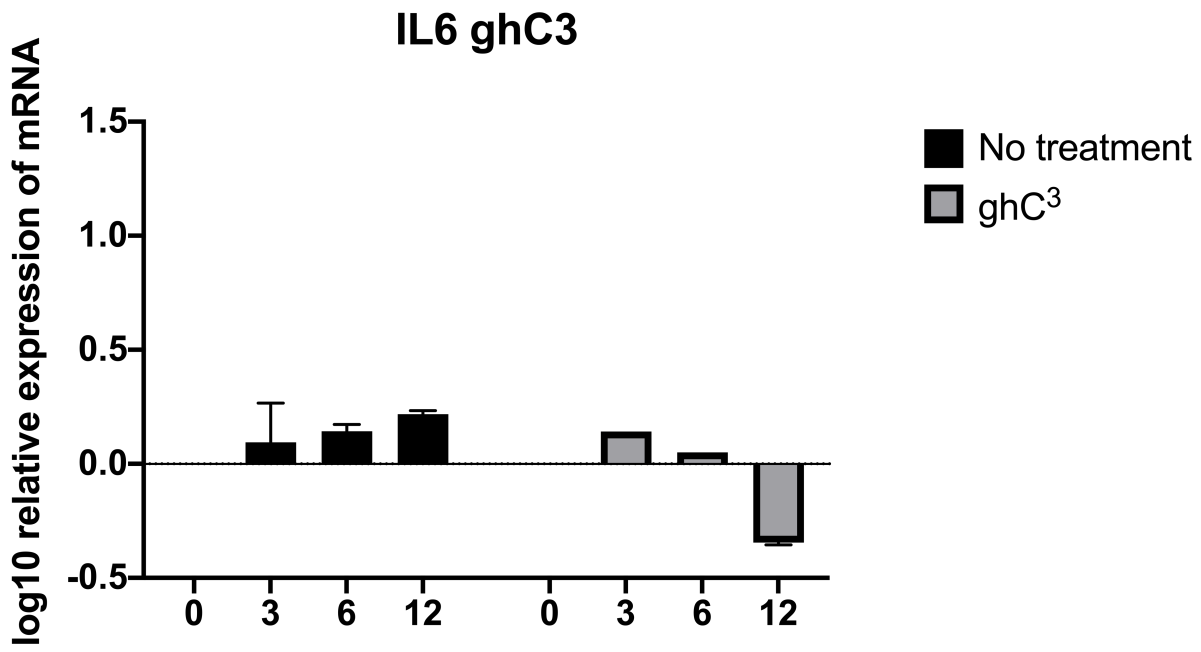

Fig 4:19 Composite Bar graph illustrating the effect of ghC^3 on Amyloid Beta induced expression of IL6 mRNA.
qPCR analysis of the expression of IL6 mRNA extracted from BV-2 microglia samples at 0, 3, 6, 12 hr timepoints. All samples were incubated with Aβ42 with or without ghC^3 treatment. Graph plotted represents log10 relative expression levels of gene of interest normalised to an endogenous control of β-actin. Zero hr timepoint was used as the calibrator. Assays were conducted in triplicate. Error bars represent Mean ± standard deviation.

Statistical Analysis: A 2-way ANOVA was performed on the data to determine significant differences in expression between Amyloid Beta challenged BV-2 samples with or without ghC^3 treatment.

4.3.5 C1q recombinant fusion proteins and the expression of IL-18 mRNA

Gene expression of BV-2 cells incubated with Aβ-42 were studied via qPCR following treatment with or without MBP fusion proteins. Primers as previously described were used. The data (ghA-Fig 4.20, ghB- Fig 4.22and ghC- Fig 4.24) revealed a significant (**p<0.01) downregulation of IL-18 mRNA expression by MBP fusion protein treated BV-2 cells predominantly at 3 hr, 6h and 12 hr timepoints (no significant difference in expression at the ghA treated 3 hr timepoint Fig 4.20). At the 6 hr and 24 hr time points there is an up-regulation of IL-18 when compared to the 0hr and 12 Hr time points. All treated groups indicate a slight visual downregulation in mRNA expression at the 24hr timepoint. However, the downregulation of IL-18 mRNA expression was more pronounced in ghB (Fig 4.10; *p<0.05) treated BV-2 cells, at the 24-hr time point when compared with the non-treated group.

The globular head multimers ghB^3 (Fig 4.23), and ghA^3 (Fig 4.21) revealed a significant downregulation of expression at all the 6 hr and the 12 hr time points compared to the untreated groups (***p<0.001) and the treated globular head monomer groups (**p<0.01). revealing that the multimers have a greater inhibitory effect on mRNA expression of the pro-inflammatory cytokine than the monomers. Moreover, ghB^3 (Fig 4) had the largest effect on the downregulation (2-fold) of IL-18 mRNA expression at the 12hr timepoint. This downregulation was only significant (*p<0.05) when compared to ghA^3 (Fig 4.3) and ghC^3 (Fig 4.7) at the 12 hr timepoint. Thus, indicating that ghB^3 has a greater inhibitory effect on the expression of IL-18 mRNA than both the globular head multimers. Raw data is included in Appendix sections (1-5).

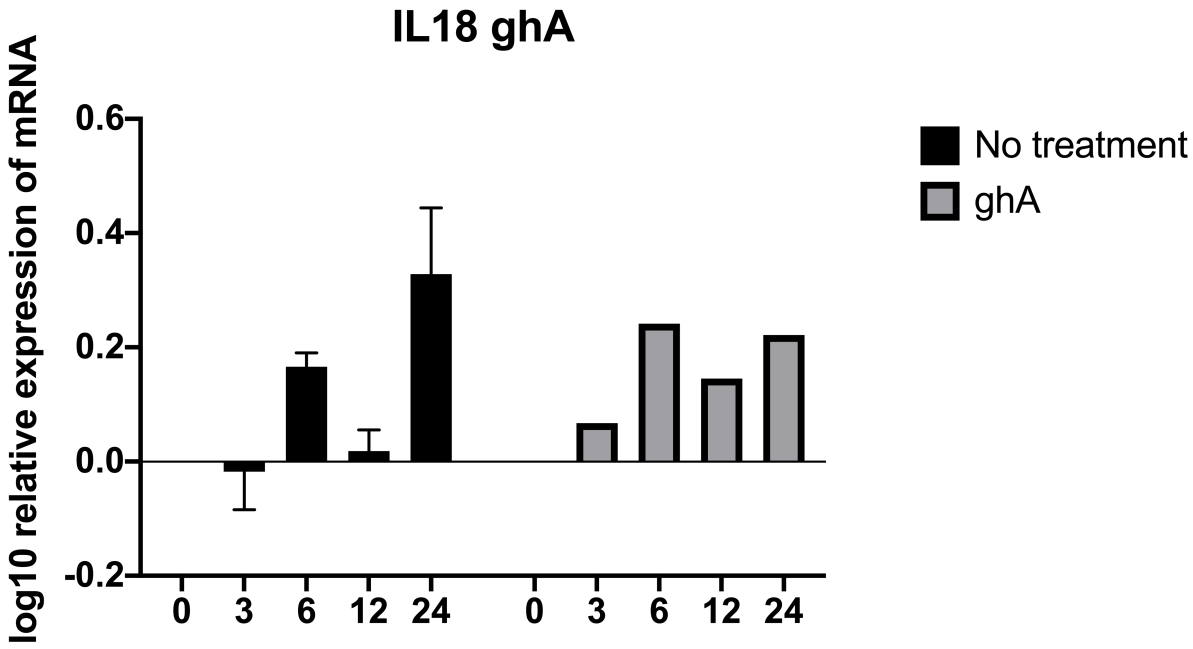

Fig 4:20 Composite Bar graph illustrating the effect of ghA on Amyloid Beta induced expression of IL-18 mRNA.
qPCR analysis of the expression of IL-18 mRNA extracted from BV-2 microglia samples at 0, 3, 6, 12, 24hr. All samples were incubated with Aβ42 with or without ghA treatment. Graph plotted represents log10 relative expression levels of gene of interest normalised to an endogenous control of β-actin. Zero hr timepoint was used as the calibrator. Assays were conducted in triplicate. Error bars represent Mean ± standard deviation.

Statistical Analysis: A 2-way ANOVA was performed on the data to determine significant differences in expression between Amyloid Beta challenged BV-2 samples with or without ghA treatment

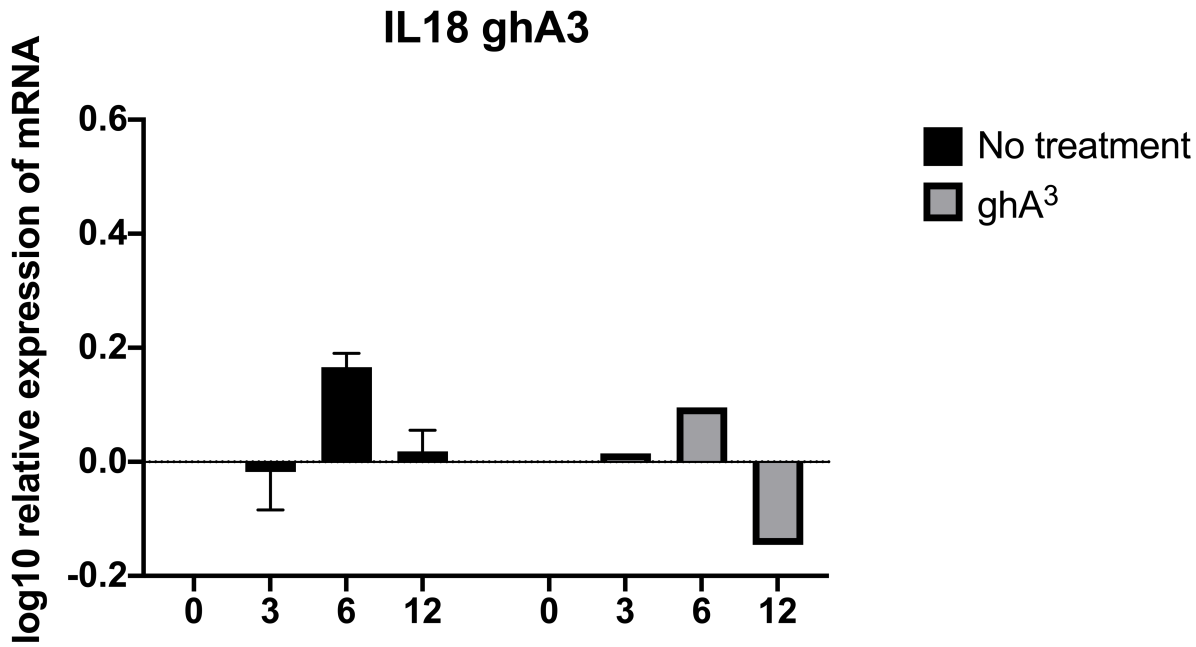

Fig 4:21 Composite Bar graph illustrating the effect of ghA^3 on Amyloid Beta induced expression of IL-18 mRNA.
qPCR analysis of the expression of IL-18 mRNA extracted from BV-2 microglia samples at 0, 3, 6, 12 hr timepoints. All samples were incubated with Aβ42 with or without ghA^3 treatment. Graph plotted represents log10 relative expression levels of gene of interest normalised to an endogenous control of β-actin. Zero hr timepoint was used as the calibrator. Assays were conducted in triplicate. Error bars represent Mean ± standard deviation. (n=3)

Statistical Analysis: A 2-way ANOVA was performed on the data to determine significant differences in expression between Amyloid Beta challenged BV-2 samples with or without ghA^3 treatment.

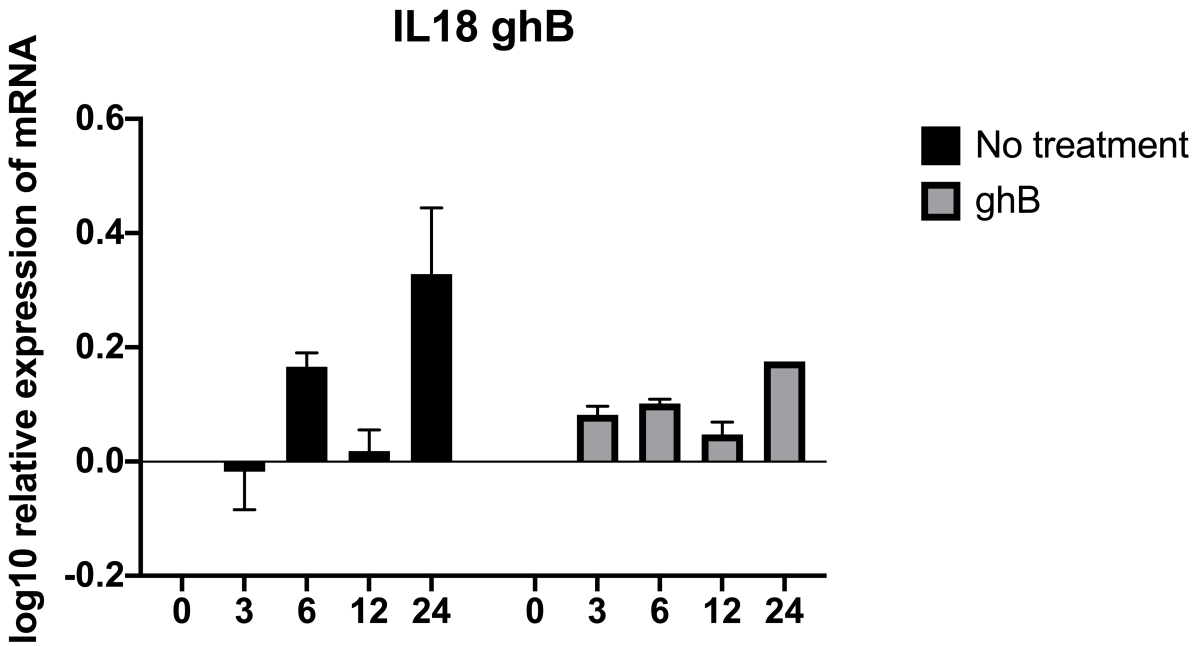

Fig 4:22 Composite Bar graph illustrating the effect of ghB on Amyloid Beta induced expression of IL-18 mRNA.
qPCR analysis of the expression of IL-18 mRNA extracted from BV-2 microglia samples at 0, 3, 6, 12, 24hr. All samples were incubated with Aβ42 with or without ghB treatment. Graph plotted represents log10 relative expression levels of gene of interest normalised to an endogenous control of β-actin. Zero hr timepoint was used as the calibrator. Assays were conducted in triplicate. Error bars represent Mean ± standard deviation. (n=3)

Statistical Analysis: A 2-way ANOVA was performed on the data to determine significant differences in expression between Amyloid Beta challenged BV-2 samples with or without ghB treatment.

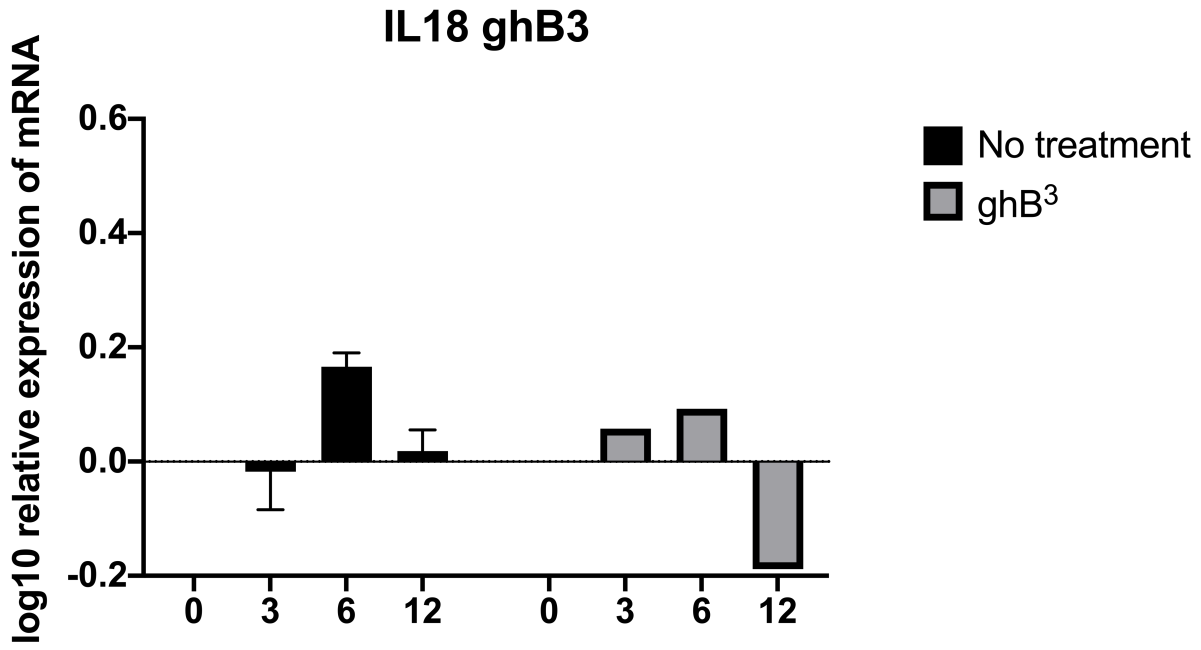

Fig 4:23 Composite Bar graph illustrating the effect of ghB^3 on Amyloid Beta induced expression of IL-18 mRNA.
qPCR analysis of the expression of IL-18 mRNA extracted from BV-2 microglia samples at 0, 3, 6, 12 hr timepoints. All samples were incubated with Aβ42 with or without ghB^3 treatment. Graph plotted represents log10 relative expression levels of gene of interest normalised to an endogenous control of β-actin. Zero hr timepoint was used as the calibrator. Assays were conducted in triplicate. Error bars represent Mean ± standard deviation.

Statistical Analysis: A 2-way ANOVA was performed on the data to determine significant differences in expression between Amyloid Beta challenged BV-2 samples with or without ghB^3 treatment.

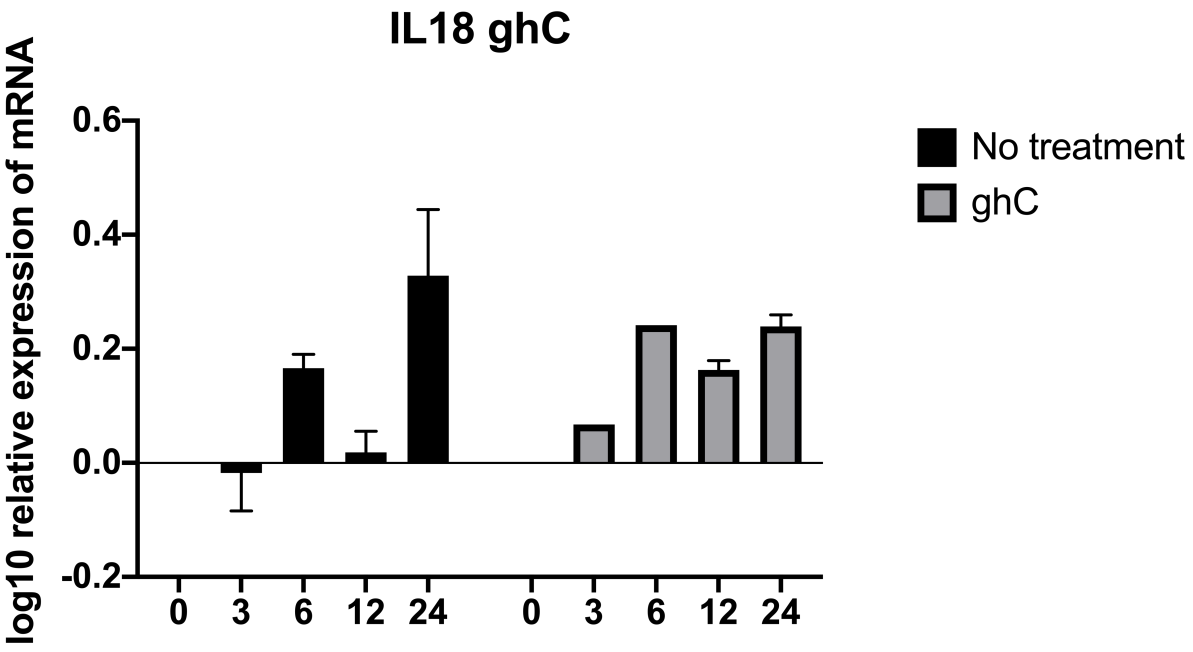

Fig 4:24 Composite Bar graph illustrating the effect of ghC on Amyloid Beta induced expression of IL-18 mRNA.
qPCR analysis of the expression of IL-18 mRNA extracted from BV-2 microglia samples at 0, 3, 6, 12, 24hr. All samples were incubated with Aβ42 with or without ghC treatment. Graph plotted represents log10 relative expression levels of gene of interest normalised to an endogenous control of β-actin. Zero hr timepoint was used as the calibrator. Assays were conducted in triplicate. Error bars represent Mean ± standard deviation.

Statistical Analysis: A 2-way ANOVA was performed on the data to determine significant differences in expression between Amyloid Beta challenged BV-2 samples with or without ghC treatment.

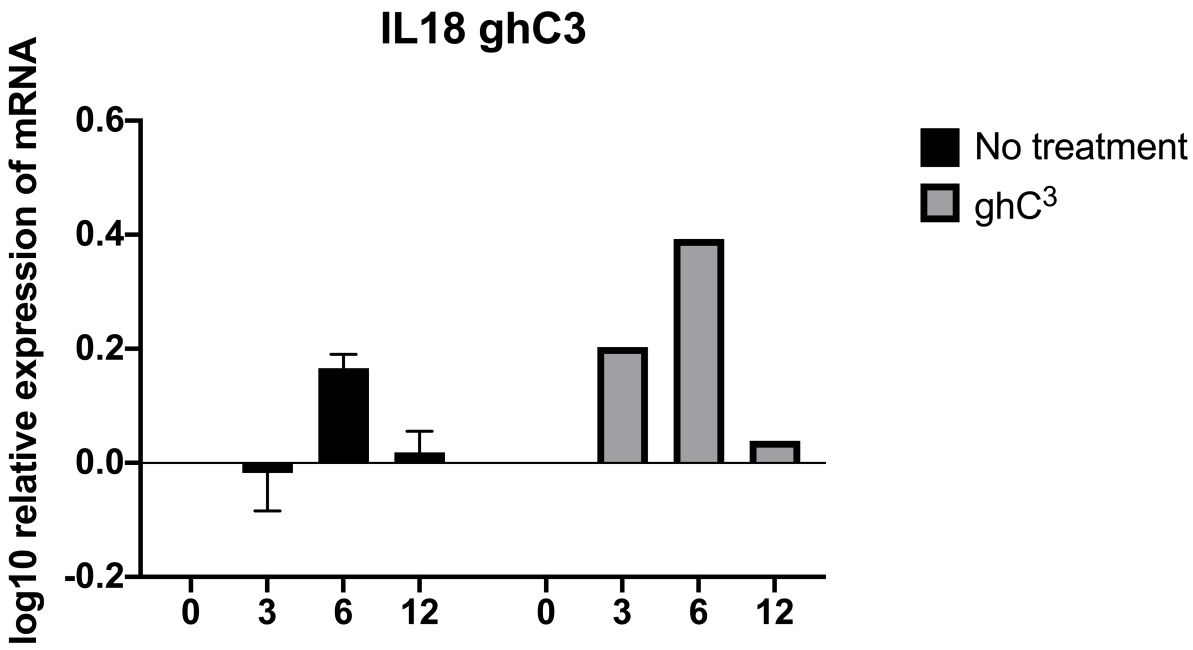

Fig 4:25 Composite Bar graph illustrating the effect of ghC^3 on Amyloid Beta induced expression of IL-18 mRNA.
qPCR analysis of the expression of IL-18 mRNA extracted from BV-2 microglia samples at 0, 3, 6, 12 hr timepoints. All samples were incubated with Aβ42 with or without ghC^3 treatment. Graph plotted represents log10 relative expression levels of gene of interest normalised to an endogenous control of β-actin. Zero hr timepoint was used as the calibrator. Assays were conducted in triplicate. Error bars represent Mean ± standard deviation.

Statistical Analysis: A 2-way ANOVA was performed on the data to determine significant differences in expression between Amyloid Beta challenged BV-2 samples with or without ghC^3 treatment.

4.3.5 C1q recombinant fusion proteins lead to an increase in the expression of TGF-β mRNA

Gene expression of BV-2 cells incubated with Aβ-42 were studied via qPCR following treatment with or without MBP fusion proteins. Primers as previously described were used. The data (ghA-Fig 4.26, ghB- Fig 4.28 and ghC- Fig 4.29) revealed a significant (between *p<0.05 and ***p<0.001)) up-regulation of TGF-β mRNA expression by MBP fusion protein treated BV-2 cells at 3 hr, 12 hr and 24hr timepoints when compared to non-treated groups. At the 24hr time point there is a 2-fold increase of TGF-β mRNA expression which is more pronounced in ghB (Fig 4.28) treated BV-2 cells. The expression of TGF-β mRNA increased over time in all treated groups. In the non-treated group there is an increase in TGF-β mRNA expression at the 3hr and 6hr timepoints when compared to the 0hr group. Which indicates that during the initial response, anti-inflammatory mediators are released by microglia. This anti-inflammatory response however decreases over time, whereas with the treatment groups an upregulation of mRNA expression of TGF-β persists up to 24 hrs post treatment. These graphs therefore reveal that the globular head proteins are capable of inhibiting Aβ induced inflammation, and therefore directly or indirectly stimulate the release of anti-inflammatory mediators.

Unlike the increased effect of downregulation observed across this study when the effect of globular head multimer treatments is compared to monomer treatments; TGF-β expression levels do not demonstrate a greater upregulation effect when multimers were compared with monomers. The globular head multimers ghA^3 (Fig 4.27), and ghC^3 (Fig 4.31) revealed a significant 2-fold downregulation of TGF-β expression at the 3 hr and the 6 hr time points compared to the untreated groups (***p<0.001) and the treated globular head monomer groups (***p<0.001). However, there was no significant difference observed between ghB^3 (Fig 4.29) and ghB upregulation of TGF-β expression at all time points. Raw data is included in Appendix sections (1-5).

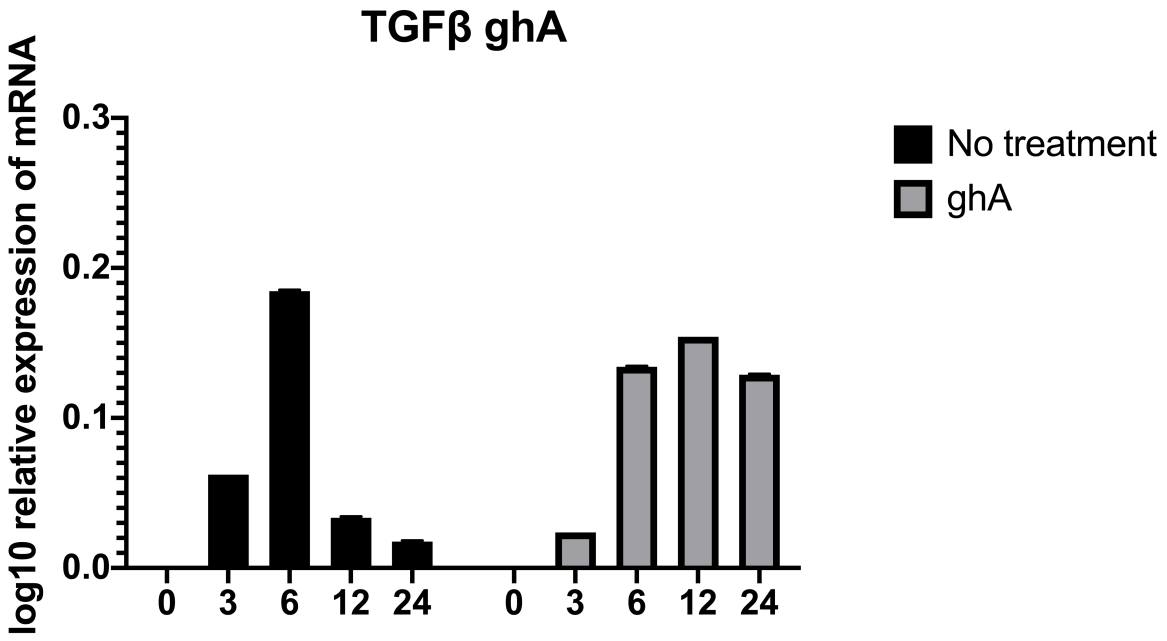

Fig 4:26 Composite Bar graph illustrating the effect of ghA on Amyloid Beta induced expression of TGF-β mRNA.
qPCR analysis of the expression of TGF-β mRNA extracted from BV-2 microglia samples at 0, 3, 6, 12, 24hr. All samples were incubated with Aβ42 with or without ghA treatment. Graph plotted represents log10 relative expression levels of gene of interest normalised to an endogenous control of β-actin. Zero hr timepoint was used as the calibrator. Assays were conducted in triplicate. Error bars represent Mean ± standard deviation.

Statistical Analysis: A 2-way ANOVA was performed on the data to determine significant differences in expression between Amyloid Beta challenged BV-2 samples with or without ghA treatment

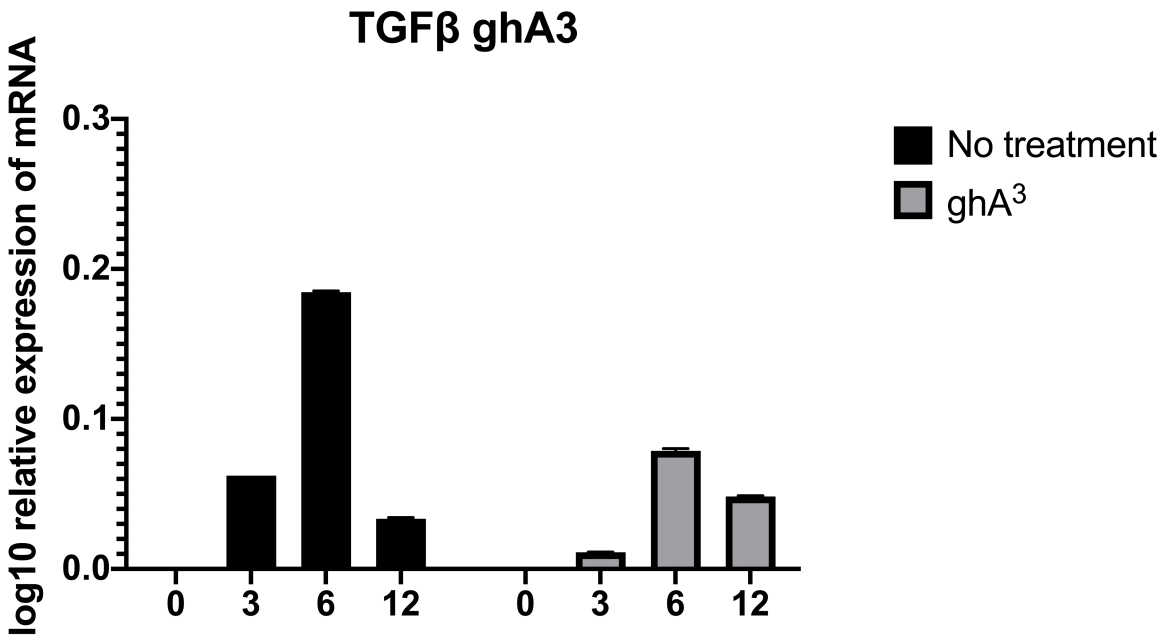

Fig 4:27 Composite Bar graph illustrating the effect of ghA^3 on Amyloid Beta induced expression of TGF-β mRNA.
qPCR analysis of the expression of TGF-β mRNA extracted from BV-2 microglia samples at 0, 3, 6, 12 hr timepoints. All samples were incubated with Aβ42 with or without ghA^3 treatment. Graph plotted represents log10 relative expression levels of gene of interest normalised to an endogenous control of β-actin. Zero hr timepoint was used as the calibrator. Assays were conducted in triplicate. Error bars represent Mean ± standard deviation. (n=3)

Statistical Analysis: A 2-way ANOVA was performed on the data to determine significant differences in expression between Amyloid Beta challenged BV-2 samples with or without ghA^3 treatment.

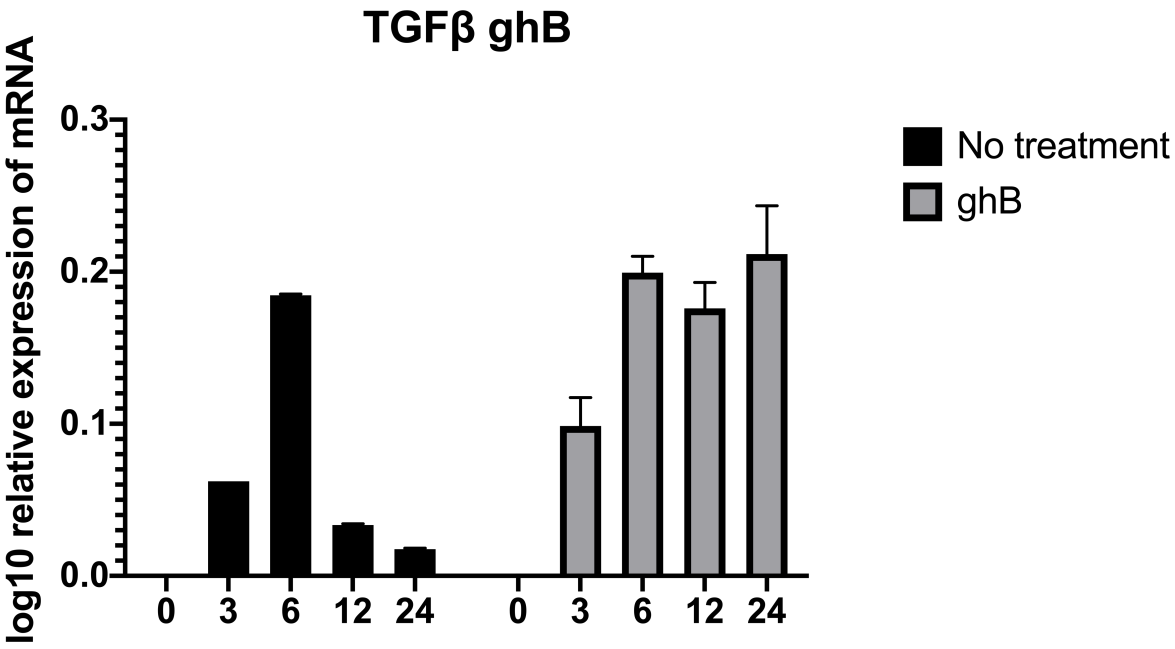

Fig 4:28 Composite Bar graph illustrating the effect of ghB on Amyloid Beta induced expression of TGF-β mRNA.
qPCR analysis of the expression of TGF-β mRNA extracted from BV-2 microglia samples at 0, 3, 6, 12, 24hr. All samples were incubated with Aβ42 with or without ghB treatment. Graph plotted represents log10 relative expression levels of gene of interest normalised to an endogenous control of β-actin. Zero hr timepoint was used as the calibrator. Assays were conducted in triplicate. Error bars represent Mean ± standard deviation. (n=3)

Statistical Analysis: A 2-way ANOVA was performed on the data to determine significant differences in expression between Amyloid Beta challenged BV-2 samples with or without ghB treatment.

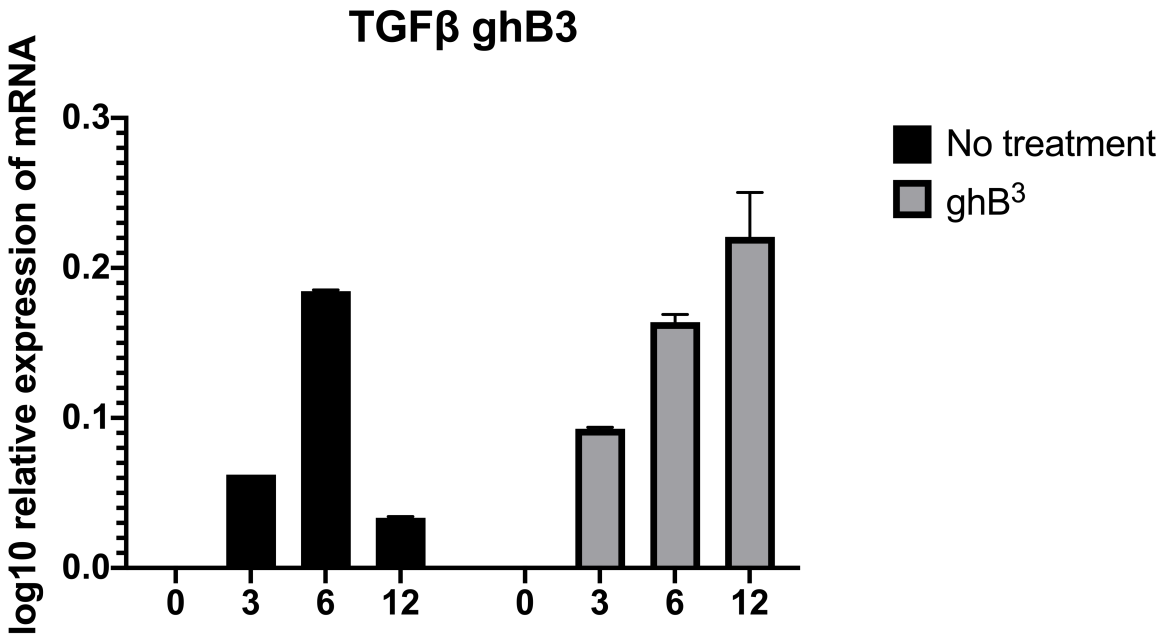

Fig 4:29 Composite Bar graph illustrating the effect of ghB^3 on Amyloid Beta induced expression of TGF-β mRNA.
qPCR analysis of the expression of TGF-β mRNA extracted from BV-2 microglia samples at 0, 3, 6, 12 hr timepoints. All samples were incubated with Aβ42 with or without ghB^3 treatment. Graph plotted represents log10 relative expression levels of gene of interest normalised to an endogenous control of β-actin. Zero hr timepoint was used as the calibrator. Assays were conducted in triplicate. Error bars represent Mean ± standard deviation.

Statistical Analysis: A 2-way ANOVA was performed on the data to determine significant differences in expression between Amyloid Beta challenged BV-2 samples with or without ghB^3 treatment.

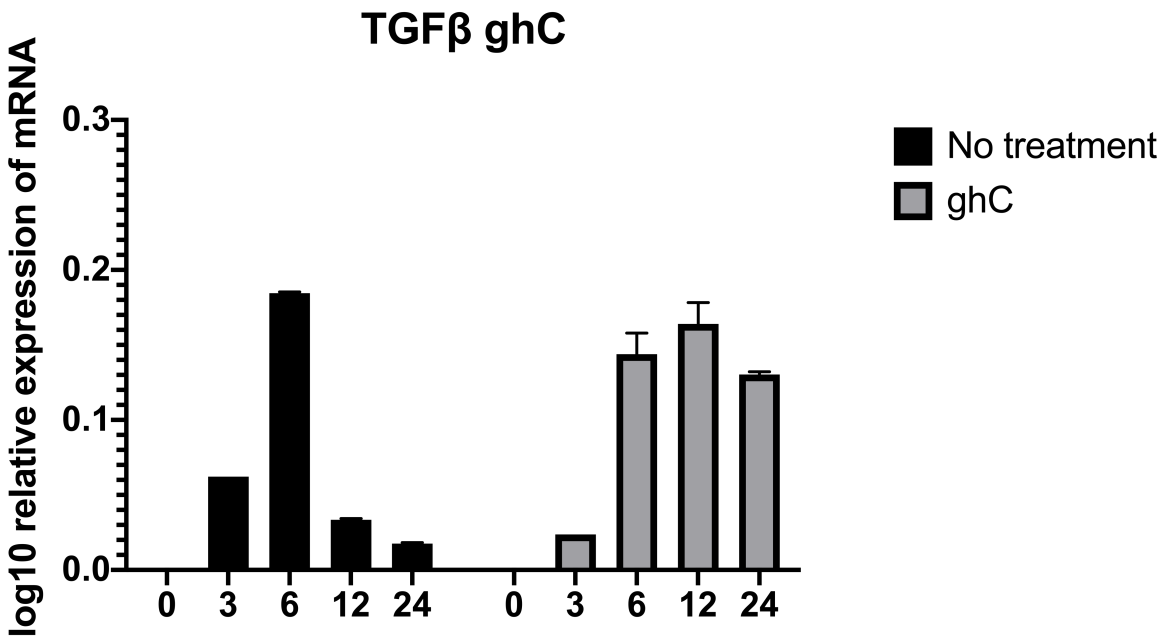

Fig 4:30 Composite Bar graph illustrating the effect of ghC on Amyloid Beta induced expression of TGF-β mRNA.
qPCR analysis of the expression of TGF-β mRNA extracted from BV-2 microglia samples at 0, 3, 6, 12, 24hr. All samples were incubated with Aβ42 with or without ghC treatment. Graph plotted represents log10 relative expression levels of gene of interest normalised to an endogenous control of β-actin. Zero hr timepoint was used as the calibrator. Assays were conducted in triplicate. Error bars represent Mean ± standard deviation.

Statistical Analysis: A 2-way ANOVA was performed on the data to determine significant differences in expression between Amyloid Beta challenged BV-2 samples with or without ghC treatment.

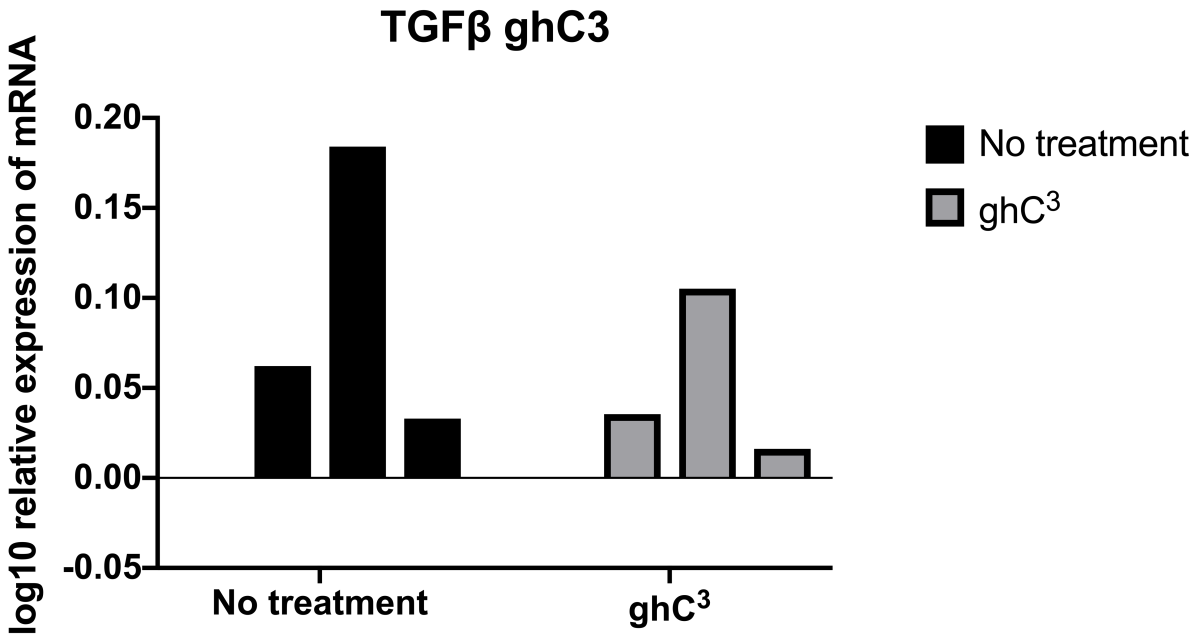

Fig 4:31 Composite Bar graph illustrating the effect of ghC^3 on Amyloid Beta induced expression of TGF-β mRNA.
qPCR analysis of the expression of TGF-β mRNA extracted from BV-2 microglia samples at 0, 3, 6, 12 hr timepoints. All samples were incubated with Aβ42 with or without ghC^3 treatment. Graph plotted represents log10 relative expression levels of gene of interest normalised to an endogenous control of β-actin. Zero hr timepoint was used as the calibrator. Assays were conducted in triplicate. Error bars represent Mean ± standard deviation.

Statistical Analysis: A 2-way ANOVA was performed on the data to determine significant differences in expression between Amyloid Beta challenged BV-2 samples with or without ghC^3 treatment.

4.3.6 Western blot to assess expression of NF-κB post ghB^3 treatment

We performed western blots on the cell lysates of BV-2 microglia 24 hrs post treatment to evaluate changes in NF-κB p65 protein expression post ghB^3 +1μM Aβ42 treatment compared to just 1 μM Aβ42 treatment. We observed a significant (***p<0.001) downregulation in NF-κB expression post ghB^3 treatment. Indicating that ghB^3 is capable of downregulating inflammatory mediator expression and release.

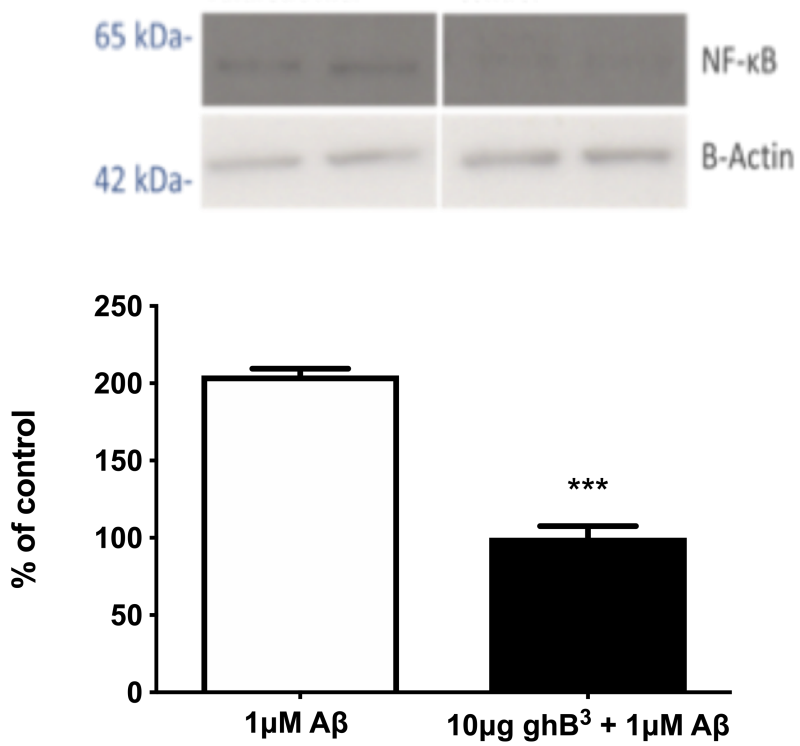

Fig 4:32 Far western blot of Bv-2 cell lysates
Western blot image illustrating the decrease in NF-κB protein expression indicate by expression at 65kDa. Densitometric analysis was conducted using image J and results were normalised to β-Actin.

Statistical Analysis: An unpaired t-test was performed on the data to determine significant differences in expression between Amyloid Beta challenged BV-2 samples with or without ghB^3 treatment. (***p<0.001) was considered significant

4.4 Discussion

C1q activation by pathogens, ligands and molecular complexes is of vital importance to the innate immune response. In most cases activation of the classical complement pathway leads to an acute response which promotes clearance either by opsonisation, activation of the CCP, recognition by phagocytes such as microglia, and subsequent phagocytic clearance (Trouw et al., 2007). However, in disease states such as Alzheimer's disease (AD), the ligand recognition and binding of C1q to Aβ, and thus the activation of the CCP perpetuates the chronic inflammatory profile observed in post mortem AD subjects. Studies conducted by Fonseca and colleagues (2004) demonstrated a significant reduction in inflammatory glial markers and mediators proximal to Aβ plaques when C1q null transgenic mice expressing an aberrant form of APP were compared to the APP transgenic mice with a fully functioning complement system. Neuronal integrity of APP C1q-/- when compared with APP mice was also improved despite there being no change in plaque deposition (Fonseca et al., 2004). Which therefore suggests that much - though not all - of the pro-inflammatory cascade that results in the release of neurotoxic cytokines, chemokines, reactive oxygen and nitrogen species is dependent on C1q's activation of the CCP.

Microglia are the effectors of the innate immune response in the CNS. Chemotactic agents such as C3a and C5a released by the activation of the CCP recruit microglia towards the site and lead to the secretion of pro-inflammatory mediators TNF-α, IL-1B, IL-6 and IL-18 (Sastre et al., 2006).

In this study we posited that C1q globular head recombinantly expressed proteins are capable of inhibiting the expression of pro-inflammatory mediators leading to a reduction in the long-term pathogenic effect of Aβ. First, we characterised the binding ability of each of the globular heads to Aβ. All globular head proteins bound in a dose dependent manner, albeit with different binding affinities. This correlates with findings from previous studies that $A\beta_{1-42}$ binds to C1q (Jiang et al., 1994); and that globular heads display different binding affinities to different proteins (Kishore et al., 1998; Kishore et al., 2003).

When Amyloid Beta incubated BV-2 cells were treated with recombinant proteins the recombinant globular heads there were significant changes in mRNA expression of various pro-inflammatory mediators. As hypothesised the mRNA

expression of pro-inflammatory genes for TNF-α, IL-1B, IL-6 and IL-18 was significantly downregulated across most time points whereas the expression of the anti-inflammatory mediator TGF-β was significantly upregulated at most time points when compared to Amyloid Beta incubated BV-2 microglia cells. The greater the binding affinity of the globular heads to Aβ, the greater their capacity for competitive inhibition of C1q and thus CCP activation. The ability of the globular heads to supress much of the pro-inflammatory response, as well as prolong the duration of an anti-inflammatory response gives credence to the theory that the role of the complement system in AD is highly significant but also detrimental.

CHAPTER 5:

Whole genome profiling to examine microglial gene response to challenge with Aβ42

5.1 Introduction

Alzheimer's disease is a complex multifactorial disorder characterised by a failure of normal regulatory processes in the CNS milieu. Much of the current AD research relies on elucidating the neuro-inflammatory pathogenesis induced by Aβ, or on Genome Wide Association studies to identify genetic polymorphisms that confer AD risk. Though much of the early causal processes in AD are due to an acute innate response to chronic activation by Aβ aggregates; the development of AD is largely directed by changes in the expression patterns of specific genes at various stages of disease progression (Matarin et al., 2015). In addition to their role as mediators of the acute inflammatory response to amyloid and/or tau deposition, microglial cells also upregulate and downregulate the expression of pro and anti-inflammatory genes, transcription factors, complement opsonin receptors such as CR1, anaphylatoxin receptors such as C3aR1 (Barnum et al., 1999). Though great strides been made in the past two decades, there are yet more pathways and gene expression changes in microglia that are yet to be observed. Without a whole genome characterisation of gene expression changes in response to dementia peptides, finding a therapeutic strategy to cure, stall or reverse AD disease progression will prove difficult. Moreover, testing the gene expression profile of Aβ induced cells and cells treated with therapeutic targets, will enable researchers to better understand the multifactorial causality of the disorder; and identify more suitable therapeutic targets.

With this background, we aim to determine the gene expression (transcriptome) signature response of BV-2 mouse microglial cells, challenged with human Aβ42, and whether this response can be salvaged by globular head proteins as competitive inhibitors.

5.2 Materials and methods

5.2.1 cDNA library preparation for RNA-Seq

BV-2 microglial cells are the primary model used for the study of microglial induced inflammation (refer to sections 4.2.6 and 4.2.7 for methodology). RNA was extracted from BV-2 cells incubated with 1μM oligomeric Amyloid Beta (Stine et al., 2013) with no globular head treatment; and BV-2 cells incubated with 1μM Amyloid Beta with ghB or ghB^3 treatment at 3hr, 6 hr, 12 and 24 hr timepoints respectively. RNA extraction was conducted with the Picopure RNA isolation Kit (Applied Biosciences) according to the manufacturer's instructions. Each RNA Library was quantified by Qubit RNA quantification assay (Invitrogen, UK) and run on an Agilent 2100 Bioanalyzer Instrument and analysed with TapeStation Analysis Software A.02.01 SR1 (Agilent) to assess fragment distribution and presence of artefacts. Samples with an RNA yield less than 30μg and RIN values below 8.5 were discarded. cDNA fragments were sequenced using an Illumina HiSeq4000 System (75bp reads, paired-end (PE) lane). Biological duplicate RNA sequencing was performed on independent RNA samples from the amyloid and globular head treated BV-2 cells.

The quality-checked reads for each condition were obtained as FASTQ files and processed using TopHat version 2.1.1 and Bowtie 2 version 2.2.3 scripts. Reads were mapped to the reference genome Mus musculus GRCm38, and the alignment files were generated as BAM files. Subsequently BAM files were set to -q30 via Samtools version 0.1.19 in order to filter out reads that do not uniquely map or are mapped in a repeat region. BAM-q30 files were then run through Cufflinks 2.1.1 software, in order to generate the transcriptome for each condition. The "fragments per kilobase per million map reads" (FPKM) values were calculated for each gene. The files were also run via the Cuffdiff tools within the Cufflinks 2.2.1 software package in order to quantify the differential expression levels between treatments and evaluate the statistical significance of the detected upregulated or downregulated genes. Values which had a p-value derived from the unpaired student T test of less than 0.05 compared to the control and with a fold change compared to the control more than 1.5 or less than 0.5 were included, all others were discounted as displaying no significance.

5.3 Results

5.3.1 Differential expression between exposure to Aβ42 and exposure to Aβ42 plus fusion protein at the 3 hr timepoints

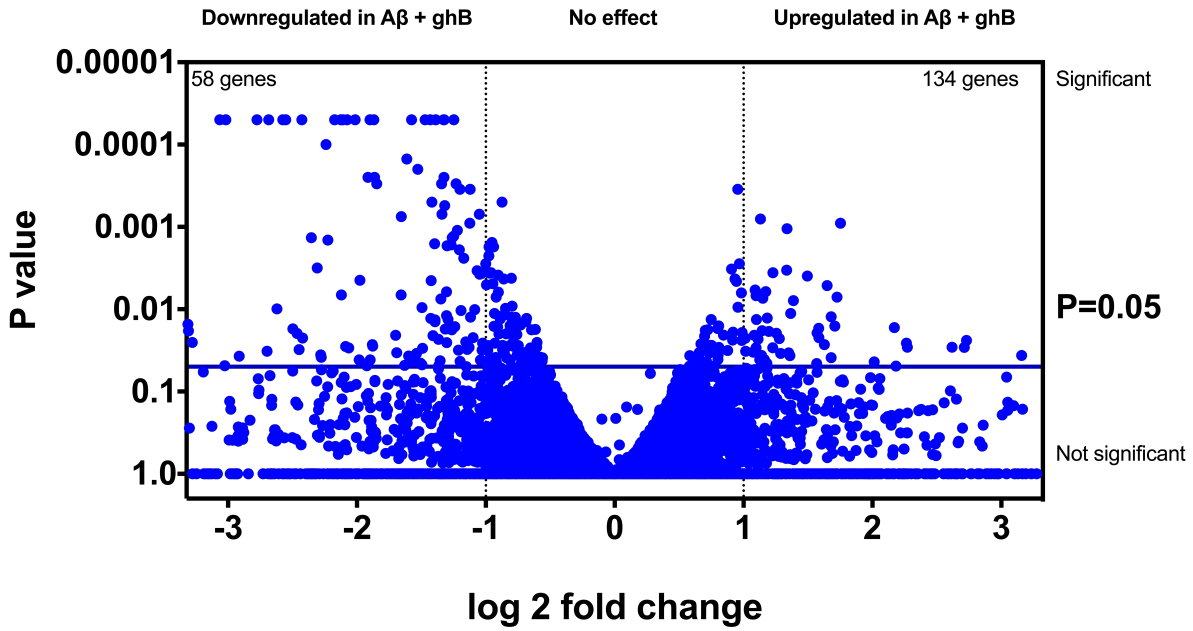

Fig 5.1 Volcano plot illustrating the distribution gene expression changes between Aβ and treatment with ghB at the 3hr timepoint.
Values were presented as log2fold change of PKBM values against p values. Fold change represents treatment values divided by control values. Control- 1 μM Aβ treated Bv-2 cells, Treatment- 10μg/ml ghB +1 μM Aβ. (P<0.05) is considered significant.

A total of 134 genes were upregulated and 58 were downregulated, all of which had statistically significant changes in expression level ($p < 0.05$). Gene expression levels of 54000 genes remained unchanged between the AD and ghB treated groups (Fig. 5.1). Overall, differential gene expression was skewed towards downregulation, i.e. transcriptional activity was much higher in the Aβ sample, possibly due to microglial response to Aβ. However, most was not considered significant. The top 10 up- and downregulated genes are listed in Table 5.1. Finally, we placed all significant upregulations through the string database and identified pathways of related networks that were upregulated (Table 5.2). mRNA expression of TNF -α and IL-1β in Table 5.1 is shown to be upregulated, which is at odds with the qPCR data obtained in Fig 4.4 (TNF -α) and 4.10 (IL-1β). It could be due to the different forms of AB42 used in both studies (refer to 4.2 and 5.2). Unfortunately, due to time contraints this study has been unable to explore the reasons for this discrepancy. IL6, IL18 and TGFβ however had no significant changes in mRNA expression.

	gene	FPKM Aβ	FPKM ghB	log2(fold_change)
1	Acod1	6.2796	169.671	4.75592
2	Hpn	0.040079	1.06895	4.7372
3	Il1b	0.58963	11.5404	4.29074
4	Slc10a7	11.3474	207.578	4.19322
5	Dusp8	0.0536948	0.944942	4.13737
6	Gpr84	1.69649	29.1028	4.10053
7	Tnip3	0.399314	6.79828	4.08958
8	Tfr2	0.0468616	0.759948	4.01942
9	Gdpd2	0.161719	2.43798	3.91413
10	Cxcl10	2.89663	42.5395	3.87636
11	Traf1	0.359053	4.87287	3.7625
12	Cacna1g	0.151872	1.95945	3.68952
13	Ccdc80	0.179293	2.16968	3.59709
14	Cxcl2	0.608822	6.83457	3.48876
15	Mturn	0.20587	2.08485	3.34014
16	Egr2	0.156575	1.554	3.31106
17	Fam71e1	0.337195	3.2691	3.27724
18	Hp	3.89713	32.5795	3.06348
19	Clec4a1	0.228028	1.857	3.02569
20	Saa3	17.601	142.421	3.01643
21	Marco	0.287041	2.16282	2.91358
22	Cybb	3.50291	23.9927	2.77597
23	Isg15	0.78309	5.08109	2.69789
24	Pou2f2	1.87845	12.0767	2.68461
25	Cdc42ep2	0.575759	3.53996	2.62019

26	Parp14	0.779031	4.64247	2.57514
27	Slfn2	10.2776	60.3019	2.55271
28	AC104921.1	0.353415	1.99554	2.49734
29	Vangl2	0.31068	1.7142	2.46403
30	Myl2	0.702211	3.83485	2.44919
31	Pde4b	1.87729	10.0961	2.42707
32	Ifit1	0.251833	1.34944	2.42182
33	Rsad2	0.742093	3.79102	2.35291
34	St3gal6	1.44215	7.1443	2.30857
35	Slfn8	0.284651	1.38373	2.2813
36	Ccl5	1.5048	7.28951	2.27625
37	Nod2	0.807531	3.81266	2.23921
38	Nfkbie	1.00225	4.68692	2.2254
39	Ikbke	5.6019	25.249	2.17224
40	Zc3h12a	4.18763	18.2555	2.12413
41	Tnf	19.5793	85.2281	2.122
42	Chst7	0.678567	2.9492	2.11976
43	Nfkbiz	4.8798	21.0491	2.10887
44	Lrrc25	5.15186	21.7218	2.07598
45	Magi2	0.204969	0.856814	2.06357
46	Nfkbia	31.4279	126.979	2.01447
47	Slc39a4	0.832083	3.27471	1.97657
48	Kynu	0.36611	1.38807	1.92273
49	Relb	5.91754	22.0688	1.89894
50	Rarg	0.589492	2.19601	1.89734
51	Adam3	2.8661	10.5536	1.88058

52	Tlr2	44.6968	163.182	1.86823
53	Tnfaip3	3.14991	11.4626	1.86356
54	Cd40	6.00924	21.5945	1.84541
55	Mgmt	0.505013	1.64053	1.69977
56	AC159257.6	1.67676	5.4124	1.69059
57	Pkd1l2	1.02432	3.23199	1.65776
58	Rassf4	14.7922	46.5931	1.65528
59	Cbr2	1.02264	3.16611	1.63041
60	Cd83	7.55376	23.117	1.61369
61	Irgm2	0.575908	1.74403	1.59851
62	Ccl4	31.1457	92.8362	1.57566
63	Tspan17	0.876565	2.59193	1.56409
64	Fcrls	0.746128	2.16564	1.5373
65	Spata13	2.70984	7.8119	1.52747
66	Csf3r	0.763604	2.16912	1.50621
67	Phlda1	0.707627	1.99495	1.49529
68	Vsig10	2.55818	7.21156	1.49519
69	H2-Oa	1.8162	5.10478	1.49092
70	Tnip1	24.5897	68.1716	1.47112
71	Lacc1	10.2563	27.6573	1.43115
72	Nsmf	1.98588	5.34015	1.4271
73	Cebpd	6.0033	16.1135	1.42444
74	Lsp1	14.0218	37.4658	1.41791
75	Clec12a	1.26342	3.35664	1.40969
76	Gdf15	5.7285	15.0879	1.39716
77	Hivep3	4.37574	11.4978	1.39375

78	Nlrp3	7.23603	18.9495	1.38889
79	Bcl2a1b	7.15232	18.4552	1.36755
80	Umad1	4.59218	11.8353	1.36585
81	Fyb	33.2914	85.1108	1.35419
82	Ksr1	2.14739	5.46763	1.34833
83	Hcar2	11.4484	29.0355	1.34267
84	Gsap	4.61237	11.6786	1.34029
85	Marcksl1	48.2629	121.11	1.32734
86	Zc3h12c	4.16772	10.4401	1.3248
87	Herpud1	20.0304	50.1195	1.32318
88	Icosl	5.12169	12.7729	1.3184
89	Igsf6	8.33354	20.7281	1.31459
90	Bcl3	2.61172	6.45115	1.30456
91	Lrrc16a	3.62877	8.95707	1.30355
92	Ralgds	5.01327	12.3452	1.30013
93	Igf1	14.3741	35.2242	1.29309
94	Filip1l	5.46812	13.3928	1.29234
95	Neurl3	5.08089	12.2428	1.26878
96	Zdhhc18	5.08572	12.2148	1.26411
97	Pim1	4.99177	11.9542	1.25989
98	Themis2	4.38152	10.4178	1.24955
99	Icam1	36.2266	85.9932	1.24717
100	Llgl2	3.18413	7.52567	1.24092
101	Slc2a6	42.5452	99.836	1.23057
102	Kcnj2	3.41741	7.96709	1.22115
103	Irf9	3.66524	8.4912	1.21206

104	Fam20c	45.6863	105.369	1.20562
105	Tmem176b	72.2675	166.169	1.20123
106	Slc2a4rg-ps	0.779663	1.79116	1.19997
107	Casp4	5.68007	12.9852	1.19288
108	Clec4e	49.182	110.796	1.17171
109	Gm10036	11.8587	26.4146	1.15539
110	Agrn	1.149	2.55195	1.15122
111	Mycbp	9.73042	21.2863	1.12935
112	Atf3	44.436	96.8131	1.12347
113	Nfkb1	39.9116	86.7935	1.12078
114	Rasa4	3.0935	6.71338	1.1178
115	Map3k8	2.08813	4.46988	1.09802
116	Socs3	6.4169	13.6204	1.08582
117	Neat1	10.1019	21.1616	1.06683
118	C3ar1	14.3494	29.7187	1.05038
119	Eri3	30.6326	63.3225	1.04765
120	Creb5	1.65432	3.40695	1.04224
121	Apobec3	22.4703	46.0553	1.03535
122	Ehd1	51.7348	105.853	1.03286
123	Ring1	6.43543	13.1269	1.02842
124	Cd5	3.44341	7.00502	1.02455
125	Folr1	1.22524	0.103476	-3.5657
126	Megf11	0.913331	0.0814538	-3.48708
127	Mdfi	1.47168	0.145686	-3.33652
128	Slc2a4	0.706436	0.07912	-3.15845
129	Gng8	4.55147	0.686077	-2.72989

130	Ccdc162	1.98919	0.303325	-2.71324
131	Il34	2.91109	0.474195	-2.61801
132	Uggt2	1.24953	0.258961	-2.27057
133	Il17c	0.729052	0.15177	-2.26414
134	Wwc1	0.827697	0.182326	-2.18258
135	Kif21a	1.50646	0.334848	-2.16959
136	Rufy4	1.05895	0.262213	-2.01383
137	Cyp11a1	8.64029	2.56532	-1.75194
138	Gda	2.29559	0.694354	-1.72512
139	Jakmip1	2.32016	0.709767	-1.70881
140	Map2k6	2.97531	0.928906	-1.67944
141	Hist1h2bh	2.21881	0.692854	-1.67916
142	Sbsn	17.6378	5.62735	-1.64814
143	Kdm5b	2.45631	0.795297	-1.62693
144	Cmbl	6.15438	2.05171	-1.58479
145	Pde7b	2.2149	0.738907	-1.58378
146	Nfia	7.03014	2.36663	-1.57072
147	Lhx6	1.17844	0.397427	-1.56812
148	Ifitm6	22.7856	8.08235	-1.49528
149	Scel	4.6302	1.7702	-1.38716
150	Nudt12	3.27682	1.27187	-1.36534
151	Hyal1	11.2164	4.36792	-1.36059
152	Rundc3a	2.99416	1.17477	-1.34978
153	Rps10	52.7959	20.8876	-1.33778
154	Rpl11	87.9858	34.8836	-1.33472
155	Il7r	10.9032	4.49553	-1.27818

156	Reps2	3.8797	1.62634	-1.25432
157	Mertk	5.45466	2.32919	-1.22766
158	Snx29	4.77916	2.04188	-1.22686
159	Tiam2	9.48145	4.13717	-1.19647
160	Rnf150	1.19224	0.524922	-1.1835
161	Akap3	1.87085	0.824847	-1.1815
162	Etv1	4.32277	1.91756	-1.17268
163	Ptpn22	5.43235	2.4296	-1.16086
164	Sorbs1	19.6048	8.83825	-1.14937
165	Vsir	27.8092	12.578	-1.14466
166	Zfp780b	2.44283	1.10832	-1.14018
167	Mical2	10.1301	4.62277	-1.13182
168	Zc3h11a	18.5654	8.50795	-1.12573
169	Nhej1	16.8015	7.83933	-1.09979
170	Wwtr1	4.52307	2.11371	-1.09753
171	Slc5a3	5.59797	2.61761	-1.09665
172	Naca	12.7564	5.9823	-1.09245
173	Tnfrsf26	27.3735	12.8649	-1.08934
174	Nedd4l	31.1143	14.6883	-1.08291
175	Ap1s3	17.5708	8.34647	-1.07394
176	Tmem245	5.84457	2.89106	-1.0155
177	Dusp11	35.9566	17.8223	-1.01258

Table 5.1 Differential expression was calculated using the ratio of the Aβ FPKM to the ghB treated FPKM. The FPKM values for each expressed gene is shown. Differentially expressed genes that were statistically significant were ranked by their fold changes, and the top upregulated (red) and downregulated (green) genes were shown here.

KEGG pathway	pathway description	observed gene count	false discovery rate	matching proteins in your network (labels)
4668	TNF signaling pathway	23	1.43E-13	Bcl3,Birc3,Ccl12,Ccl5,Creb3l4,Creb5,Csf2,Cxcl10,Cxcl2,Edn1,Fas,Icam1,Lta,Map3k8,Nfkb1,Nfkbia,No
4064	NF-kappa B signaling pathway	15	2.44E-07	Bcl2a1b,Birc3,Ccl4,Cd40,Cxcl2,Icam1,Lta,Nfkb1,Nfkbia,Relb,Tnfaip3,Tnfsf14,Traf1
4621	NOD-like receptor signaling pathway	12	3.99E-07	Birc3,Ccl12,Ccl5,Cxcl2, Nfkb1,Nfkbia,Nlrp3,Nod1,Nod2,Tnf,Tnfaip3
5168	Herpes simplex infection	21	3.99E-07	Ccl12,Ccl5,Fas,H2-M2,H2-Oa,H2-Q1,Ifih1,Ifit1,Ikbke,Irf7,Irf9,Lta,Nfkb1,Nfkbia,Nxf7,Socs3,Tlr2,Tnfsf
4060	Cytokine-cytokine receptor interaction	21	1.58E-05	Amh,Ccl12,Ccl4,Ccl5,Ccr4,Cd40,Csf2,Csf3r,Cx3cr1,Cxcl10,Cxcl2,Fas,Il1a,Il21r,Il4,Lta,Tnfrsf18,Tnfrsf4,
4620	Toll-like receptor signaling pathway	13	2.33E-05	Ccl4,Ccl5,Cd40,Cxcl10,Ikbke,Irf7,Map3k8,Nfkb1,Nfkbia,Tlr2,Tlr5
4623	Cytosolic DNA-sensing pathway	9	0.000316	Ccl4,Ccl5,Cxcl10,Ikbke,Il1b,Irf7,Nfkb1,Nfkbia,Ripk3
4622	RIG-I-like receptor signaling pathway	9	0.000686	Cxcl10,Ifih1,Ikbke,Irf7,Isg15,Nfkb1,Nfkbia,Nlrx1
4940	Type I diabetes mellitus	8	0.000686	Fas,H2-M2,H2-Oa,H2-Q1,Il1a,Lta
4660	T cell receptor signaling pathway	9	0.00691	Cd247,Csf2,Icos,Il4,Map3k8,Nfkb1,Nfkbia,Nfkbie
4672	Intestinal immune network for IgA production	5	0.0194	Cd40,H2-Oa,Icos,Icosl,Il4
4210	Apoptosis	7	0.0205	Birc3,Fas,Il1a,Nfkb1,Nfkbia
4020	Calcium signaling pathway	11	0.0208	Adora2a,Atp2b4,Cacna1g,Grin2d,Nos2,P2rx6,Plcd1,Plcd4,Ptger1,Ryr1,Sphk1
4062	Chemokine signaling pathway	11	0.0208	Ccl12,Ccl4,Ccl5,Ccr4,Cx3cr1,Cxcl10,Cxcl2,Gnb3,Gng3,Nfkb1,Nfkbia
5166	HTLV-I infection	14	0.0252	Atf3,Cd40,Csf2,Egr2,H2-M2,H2-Oa,H2-Q1,Icam1,Lta,Myc,Nfkb1,Nfkbia,Relb
4151	PI3K-Akt signaling pathway	16	0.0401	Col11a2,Col6a6,Creb3l4,Creb5,Csf3r,Fgf13,Gnb3,Gng3,Igf1,Il4,Itgb4,Itgb8,Lama5,Myc,Nfkb1,Tlr2

Table 5.2 KEGG Pathways associated with ghB treatment of Aβ42 incubated BV-2 cells.

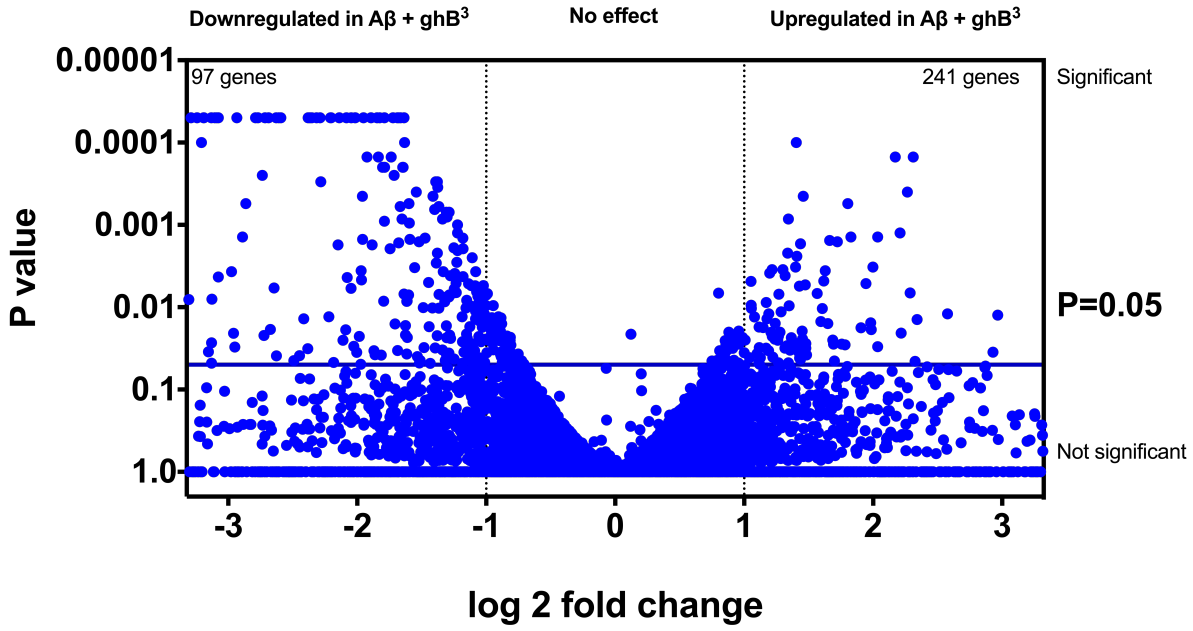

Fig 5.2 Volcano plot illustrating the distribution of gene expression changes between Aβ and treatment with ghB^3 at the 3hr timepoint.
Values were presented as log2fold change of PKBM values against p values. Fold change represents treatment values divided by control values. Control- 1 μM Aβ treated Bv-2 cells, Treatment- 10μg ghB^3 +1 μM Aβ. (P<0.05) is considered significant.

Incubation with the multimeric globular head protein led to an increase of almost 2-fold increase in the no of genes that are differentially expressed between the treatment groups. 241 genes were upregulated and 97 were downregulated, all of which had statistically significant changes in expression level ($p < 0.05$). Gene expression levels of 54000 genes remained unchanged between the AD and ghB treated groups (Fig. 5.2). We further presented the top 10 most upregulated and downregulated genes post treatment, by examining the log2 change in mRNA expression of the Fragments Per Kilobase of transcript per Million mapped reads (Table 5.2). Finally, we placed all significant upregulations through the string database and identified pathways of related networks that were upregulated (Table 5.4).

1	gene	FPKM Aβ	FPKM ghB3	log2(fold_change)
2	Gm26778	0.000723	0.992572	10.423
3	Cxcl2	0.591907	117.029	7.62728
4	Acod1	6.10514	705.688	6.85286
5	Cxcl10	2.81615	260.042	6.52887
6	Il1b	0.573248	44.4799	6.27785
7	Nos2	0.130305	8.52184	6.0312
8	Traf1	0.349078	21.6452	5.95435
9	Dusp8	0.052203	2.07733	5.31445
10	Ccl5	1.46299	41.7593	4.8351
11	Ntng2	0.0342466	0.971297	4.82588
12	Fas	0.337343	9.146	4.76085
13	Gbp3	0.0990347	2.35887	4.57402
14	Gpr84	1.64936	35.7894	4.43956
15	Tnip3	0.388223	8.32232	4.42203
16	Stmn4	0.0557163	1.04313	4.22667
17	Isg15	0.761333	14.0115	4.20194
18	Gdf15	5.56942	95.5478	4.10062
19	Ccl4	30.2804	506.562	4.06428
20	Tnf	19.0353	287.191	3.91526
21	Samd9l	0.117116	1.68438	3.84622
22	Rsad2	0.721475	10.3072	3.83656
23	Cdc42ep2	0.559763	7.9838	3.83419
24	Ccrl2	0.494698	6.7073	3.76111
25	Cmpk2	0.220409	2.75522	3.64391
26	Slfn2	9.99202	119.997	3.58608
27	Mmp12	2.22741	26.2047	3.55638
28	Mmp13	0.510616	5.74108	3.49101

29	Zc3h12a	4.07128	44.8021	3.46001
30	Pde4b	1.82513	19.7581	3.43637
31	Ccl7	7.9445	82.4807	3.37603
32	Ifit1	0.244836	2.42028	3.30529
33	Tnfaip3	3.06232	29.9196	3.28839
34	Ptgs2	6.49927	61.4646	3.2414
35	Nfkbie	0.974401	9.00419	3.20801
36	Nfkbiz	4.74422	43.2895	3.18977
37	Nod2	0.785096	7.16139	3.1893
38	Sema3b	0.0733033	0.652147	3.15325
39	Clec4e	47.8155	418.952	3.13123
40	Nat14	0.148721	1.30158	3.12958
41	Crip2	0.319564	2.79509	3.12872
42	Lcn2	0.506631	4.42632	3.1271
43	Cybb	3.40559	29.2724	3.10357
44	Parp14	0.757387	6.43873	3.08767
45	Ccl2	73.6828	621.672	3.07675
46	Ptpn14	0.277494	2.34029	3.07616
47	Mturn	0.200151	1.57274	2.97412
48	Cish	0.204492	1.58941	2.95837
49	Ttc23	0.178544	1.37855	2.94881
50	Nfkbia	30.553	233.381	2.9333
51	Phlda1	0.687978	5.09654	2.88908
52	Stx11	2.73023	19.8658	2.86319
53	Ikbke	5.44621	37.6113	2.78784
54	Ier3	80.5649	549.693	2.7704
55	Mab21l3	0.192281	1.26951	2.72298
56	Nlrp3	7.03502	46.1708	2.71435

57	Zc3h12c	4.05187	26.1055	2.68769
58	Cacna1g	0.147649	0.942052	2.67363
59	Myc	0.62525	3.9116	2.64526
60	Cd40	5.84228	36.1115	2.62786
61	Glcci1	0.266856	1.64768	2.62631
62	Serpine1	9.93268	60.5182	2.60711
63	Hp	3.78877	22.8568	2.59282
64	Cgnl1	0.123152	0.692774	2.49194
65	Prr5l	0.490349	2.67303	2.4466
66	Treml4	0.428816	2.28578	2.41426
67	Abcg2	0.182553	0.952868	2.38396
68	Tlr2	43.455	226.233	2.38021
69	Pim1	4.85308	25.0586	2.36833
70	Rab11fip1	2.42648	12.4984	2.36481
71	Icam1	35.2201	179.805	2.35196
72	Relb	5.75313	28.6266	2.31494
73	Ccl3	513.408	2507.68	2.28817
74	Slpi	14.2212	69.2136	2.28301
75	Rapgef2	4.31303	20.0858	2.2194
76	Tnip1	23.9065	110.39	2.20713
77	Slc7a11	6.52318	30.0294	2.20273
78	Pde6b	0.161941	0.735513	2.18328
79	Ampd3	8.05848	35.7426	2.14906
80	Il1rn	23.407	103.098	2.13901
81	Prdm1	0.260557	1.12502	2.11028
82	Ccdc15	0.626267	2.66547	2.08954
83	Plpp3	8.7765	37.2091	2.08394
84	Igsf6	8.102	34.2034	2.07779

85	Bcl2a1b	6.9536	28.7611	2.04828
86	Pdgfb	13.9526	57.6083	2.04575
87	Lamc2	4.13918	16.8708	2.02712
88	Plk2	23.1379	93.643	2.01691
89	Maff	9.42846	38.1263	2.01569
90	Mpp2	0.35745	1.41428	1.98426
91	Lif	0.217147	0.852452	1.97294
92	Hivep3	4.25402	16.6563	1.96917
93	Trim13	4.50481	17.6164	1.96738
94	Lrrc25	5.00873	19.4779	1.95932
95	Pou2f2	1.82626	7.09578	1.95807
96	Ralgds	4.87397	18.8395	1.95059
97	Slc11a2	16.2492	61.6569	1.92389
98	Marcksl1	46.922	174.218	1.89255
99	Creb5	1.60866	5.94096	1.88483
100	Mfsd7a	0.416902	1.52443	1.87049
101	AC162291.2	0.526232	1.91255	1.86172
102	Dusp16	3.83254	13.7834	1.84656
103	Fam20c	44.4169	158.597	1.83618
104	Ehd1	50.2957	178.338	1.82611
105	St3gal1	11.4484	39.9689	1.80374
106	Acp5	1.83538	6.36558	1.79422
107	Osgin2	5.92636	20.4903	1.78972
108	Ets2	18.4153	63.6262	1.78871
109	Icosl	4.97936	17.1873	1.78731
110	Rassf4	14.3809	48.1936	1.74469
111	Atf3	43.2014	144	1.73691
112	Tnfrsf1b	57.9738	191.324	1.72255

113	Mdm2	16.6529	54.6347	1.71404
114	Atf7ip	2.89982	9.46933	1.7073
115	Oasl1	25.7205	82.8668	1.68788
116	Casp4	5.52179	17.6816	1.67904
117	Sdc4	74.8426	239.58	1.67858
118	Lacc1	9.97136	31.6623	1.66691
119	Tnfrsf8	10.4171	33.0049	1.66373
120	Socs3	6.23861	19.6147	1.65264
121	Slc15a3	58.9079	184.531	1.64733
122	Hcar2	11.1303	34.7997	1.64458
123	Nfkb1	38.8026	120.699	1.63719
124	Plaur	31.7368	98.4216	1.63282
125	Met	4.61749	14.2558	1.62637
126	Slc39a4	0.808924	2.49693	1.62608
127	Calcrl	3.32786	10.1956	1.61528
128	Bcl3	2.53871	7.76573	1.61303
129	Btg2	1.74971	5.31197	1.60213
130	Cpd	29.6969	89.9447	1.59872
131	Itga5	28.7485	86.9421	1.59657
132	Neurl3	4.93966	14.8939	1.59223
133	Bcar1	2.82439	8.30032	1.55523
134	Spata13	2.63455	7.67056	1.54177
135	Lilr4b	21.7097	62.8198	1.53288
136	Gsap	4.48419	12.8637	1.52039
137	Dcbld2	1.5413	4.41487	1.51823
138	Gm26809	0.730165	2.08244	1.51198
139	Irak2	11.7843	33.0645	1.48842
140	Birc3	5.12804	14.33	1.48256

141	Lilrb4a	64.6132	179.447	1.47366
142	Src	6.55676	17.8756	1.44694
143	Tarm1	3.07522	8.35942	1.44271
144	Spsb4	2.37353	6.3363	1.4166
145	Rhbdf2	10.2875	27.3886	1.41269
146	Adamts1	17.9991	47.4796	1.39938
147	Filip1l	5.3162	13.9931	1.39625
148	Tnfaip2	86.73	227.571	1.39171
149	Rab20	10.881	28.4612	1.38718
150	Cebpd	5.83651	15.1843	1.3794
151	Nfkb2	31.1041	80.901	1.37905
152	Zswim4	3.78859	9.84565	1.37783
153	Ptprj	8.73443	22.6662	1.37576
154	Atp13a4	4.8025	12.3938	1.36777
155	Peli1	20.1793	52.0399	1.36674
156	Bcl2l11	16.137	41.5793	1.36549
157	Tet2	5.05654	12.7947	1.33932
158	Helz2	3.46233	8.75467	1.33831
159	Ripk2	5.13955	12.9472	1.33292
160	Nupr1	13.8967	34.7405	1.32188
161	Lzts3	2.31303	5.78159	1.32169
162	Rasa4	3.00742	7.45232	1.30916
163	Daam1	11.2107	27.7711	1.3087
164	Swt1	7.52391	18.6256	1.30773
165	Zdhhc18	4.9418	12.225	1.30673
166	Cd14	114.671	283.076	1.30369
167	Cd80	2.49174	6.08706	1.28859
168	Lrrc8d	26.9899	65.9316	1.28855

169	Jund	136.8	333.893	1.28732
170	Fam219a	4.34116	10.5889	1.2864
171	Akap13	12.269	29.8528	1.28285
172	H2-Q4	11.1243	26.9623	1.27722
173	Ptafr	1.69626	4.1072	1.2758
174	Znrf1	68.7177	163.887	1.25395
175	Pik3r5	32.8815	78.2363	1.25056
176	Gdpd1	8.19413	19.4547	1.24746
177	Hivep2	2.43769	5.77143	1.24342
178	Tmem2	3.26183	7.67294	1.2341
179	Kcnj2	3.32246	7.80568	1.23227
180	Herpud1	19.4733	45.6285	1.22844
181	Plxna2	3.9707	9.26532	1.22245
182	Mapkapk2	198.882	463.857	1.22177
183	Fgd3	20.1969	47.1041	1.22172
184	Tfec	6.61675	15.0565	1.18619
185	Aoah	5.01145	11.3904	1.18452
186	Agrn	1.11695	2.53693	1.18351
187	Sod2	33.7647	76.5411	1.18072
188	Pmp22	56.3805	127.668	1.17913
189	Rhoq	14.8142	33.5453	1.17913
190	Map3k8	2.03011	4.574	1.1719
191	Ell2	28.4365	63.4172	1.15713
192	Gm7334	8.80718	19.578	1.15249
193	Cdc42ep4	5.38401	11.9602	1.15148
194	Ksr1	2.08772	4.62852	1.14862
195	Kdm6b	2.16865	4.80061	1.14642
196	Ptgs2os2	3.38935	7.46972	1.14005

197	Lcp2	26.9953	59.3927	1.13758
198	Fzd5	1.44763	3.17883	1.1348
199	Slfn10-ps	3.65437	7.98208	1.12714
200	Sema4b	5.44936	11.837	1.11914
201	Pvr	19.1755	41.5505	1.1156
202	Nfe2l2	75.3881	162.587	1.10881
203	Usp35	1.30186	2.79778	1.1037
204	Adora2b	3.58522	7.68522	1.10002
205	Insig2	12.0893	25.7453	1.09058
206	C3	10.1013	21.4821	1.08859
207	Slc2a6	41.3629	87.8289	1.08636
208	Rsbn1	12.6728	26.8578	1.0836
209	Mcoln2	24.3034	51.4813	1.08289
210	Lrp12	25.1243	53.1672	1.08145
211	Abtb2	7.47316	15.7408	1.07472
212	Pip5k1b	19.3674	40.5044	1.06445
213	C3ar1	13.9507	29.1752	1.0644
214	Rnf19b	25.4829	53.2425	1.06304
215	Mtmr14	14.6407	30.4954	1.05861
216	Pdlim7	16.8419	35.0429	1.05707
217	Fosl1	25.4437	52.9404	1.05706
218	Osm	6.19537	12.8425	1.05167
219	Stk40	4.18466	8.60701	1.0404
220	Pdgfa	26.1084	53.4423	1.03347
221	Fam46c	10.9995	22.502	1.03262
222	Irf1	8.46374	17.2955	1.03103
223	Tank	32.6895	66.559	1.02581
224	Slc25a25	19.2851	39.1597	1.02188

225	Slc7a8	22.7001	46.0912	1.02179
226	Kctd12	13.0155	26.3642	1.01835
227	Gch1	12.3757	24.9895	1.01381
228	Plscr1	11.9417	23.9656	1.00496
229	Trip10	26.5099	53.0529	1.0009
230	Rnf43	1.50572	0.0874318	-4.10615
231	Ndrg2	0.792033	0.0605628	-3.70906
232	Vash2	1.53488	0.196399	-2.96627
233	C4b	0.852472	0.111944	-2.92888
234	Fut7	2.29983	0.38564	-2.5762
235	Ipcef1	1.71032	0.337631	-2.34074
236	Gpr183	12.2611	2.44711	-2.32494
237	Lbh	9.11001	1.83596	-2.31092
238	Rtn4rl1	1.95231	0.400111	-2.28671
239	Gpr157	4.26984	0.887764	-2.26593
240	Nr4a2	1.78021	0.382904	-2.217
241	Vsir	27.0366	5.84692	-2.20917
242	Ppia	44.3673	9.8464	-2.17183
243	Zfp799	2.02672	0.49447	-2.0352
244	Plekhg5	5.23664	1.2782	-2.03453
245	Thbd	2.95135	0.739097	-1.99754
246	Tpk1	7.92693	2.00291	-1.98466
247	Fggy	5.61733	1.42332	-1.98062
248	Cnr2	2.31687	0.602091	-1.94412
249	Mtus1	5.50693	1.46966	-1.90577
250	Rin2	22.9385	6.45964	-1.82825
251	Nfam1	11.344	3.25058	-1.80316
252	Jakmip1	2.2557	0.6675	-1.75673

253	Cytip	40.8994	12.3902	-1.72288
254	Ankrd13d	3.48777	1.07395	-1.69937
255	Rnasel	5.40311	1.67144	-1.6927
256	Frmd4b	13.0485	4.0524	-1.68704
257	Nudt12	3.18578	1.01614	-1.64855
258	Rgs2	62.9943	20.3739	-1.6285
259	Rubcnl	5.99842	1.95427	-1.61795
260	Nudt22	11.2896	3.70865	-1.60603
261	C5ar2	2.63422	0.872549	-1.59407
262	Slc26a11	5.54062	1.87112	-1.56615
263	Lpin1	2.41614	0.863656	-1.48418
264	Fan1	1.98664	0.71287	-1.47862
265	Zfp395	9.49502	3.40905	-1.4778
266	Tifab	6.91836	2.49132	-1.47352
267	Klhl6	43.7758	15.9333	-1.45809
268	Tmem86a	4.72346	1.72621	-1.45224
269	Tk2	6.33108	2.31865	-1.44917
270	Tmem194b	3.10409	1.14637	-1.4371
271	Sipa1l2	6.22173	2.29883	-1.43642
272	Akap3	1.81889	0.675382	-1.42928
273	Irf2	20.079	7.46085	-1.42827
274	Mlh3	1.79237	0.669877	-1.4199
275	Angel1	5.98017	2.24266	-1.41497
276	Dusp6	18.7802	7.07218	-1.40898
277	Ypel3	7.93343	2.99333	-1.4062
278	Mafb	50.5317	19.0855	-1.40471
279	Rab7b	33.4163	12.6817	-1.39781
280	Meis1	4.41163	1.71145	-1.3661

281	Dennd3	2.56171	1.0005	-1.35639
282	Rpl11	85.5413	33.5861	-1.34876
283	Uvssa	0.845923	0.333305	-1.34368
284	Nfatc2	10.831	4.2711	-1.34249
285	Sesn1	15.5042	6.13804	-1.33681
286	Cd200r1	4.93867	1.9615	-1.33217
287	Tnfaip8l2	42.4431	17.0294	-1.31751
288	Spice1	8.58993	3.45077	-1.31573
289	Rasa3	10.6059	4.30752	-1.29994
290	Mertk	5.30311	2.1742	-1.28635
291	Card14	7.10547	2.93093	-1.27757
292	Rab3il1	14.1352	5.86525	-1.26903
293	Asb10	4.92342	2.04592	-1.26691
294	P2ry1	5.91956	2.46146	-1.26598
295	Cdc14a	5.17629	2.15961	-1.26115
296	Lpar5	15.0744	6.3773	-1.24109
297	Tpra1	15.7828	6.69262	-1.23771
298	Dusp28	8.49141	3.64004	-1.22205
299	Ocstamp	4.86806	2.092	-1.21846
300	Sash3	27.8442	11.9764	-1.21719
301	Crot	7.16515	3.10188	-1.20786
302	St6gal1	14.784	6.44417	-1.19797
303	Pex11b	25.3656	11.1121	-1.19074
304	Fam122b	3.83815	1.68286	-1.1895
305	Chst10	15.2365	6.74217	-1.17625
306	Slc37a2	40.1981	17.8466	-1.17148
307	Mlycd	7.05182	3.1355	-1.1693
308	Klhl30	8.59408	3.88041	-1.14714

309	Cirbp	14.7942	6.78132	-1.12539
310	Rin1	3.60925	1.66235	-1.11848
311	Tmem119	7.89456	3.63937	-1.11717
312	Rassf2	28.5533	13.1836	-1.11491
313	Ephb2	3.42254	1.5809	-1.11432
314	Cbx4	18.9824	8.85186	-1.10061
315	Cxcr4	41.5532	19.6569	-1.07992
316	Etv5	12.8473	6.17968	-1.05586
317	Arhgap45	19.7442	9.50202	-1.05512
318	Mt2	587.826	283.165	-1.05375
319	Bmyc	22.346	10.8541	-1.04178
320	Orc5	43.1528	21.4731	-1.00692

Table 5.3 Differential expression was calculated using the ratio of the Aβ FPKM to the ghB[3] treated FPKM. The FPKM values for each expressed gene is shown. Differentially expressed genes that were statistically significant were ranked by their fold changes, and the top upregulated (red) and downregulated (green) genes were shown here.

KEGG pathways	pathway description	observed ger	false discovery rate	matching proteins in your network (labels)
4668	TNF signaling pathway	22	1.07E-20	Bcl3,Birc3,Ccl2,Ccl5,Creb5,Cxcl10,Cxcl2,Fas,Icam1,Il1b,Lif,Map3k8,Nfkb1,Nfkbia,Nod2,Pik3r5,Ptgs2,Socs3,Tnf,Tnfaip3,Tnfrsf1b,Traf1
4064	NF-kappa B signaling pathway	16	5.38E-14	Bcl2a1b,Birc3,Ccl4,Cd14,Cd40,Cxcl2,Icam1,Il1b,Nfkb1,Nfkb2,Nfkbia,Ptgs2,Relb,Tnf,Tnfaip3,Traf1
4620	Toll-like receptor signaling pathway	15	4.28E-12	Ccl3,Ccl4,Ccl5,Cd14,Cd40,Cd80,Cxcl10,Ikbke,Il1b,Map3k8,Nfkb1,Nfkbia,Pik3r5,Tlr2,Tnf
4621	NOD-like receptor signaling pathway	12	1.67E-11	Birc3,Ccl2,Ccl5,Cxcl2,Il1b,Nfkb1,Nfkbia,Nlrp3,Nod2,Ripk2,Tnf,Tnfaip3
4060	Cytokine-cytokine receptor interaction	18	1.53E-09	Ccl2,Ccl3,Ccl4,Ccl5,Ccl7,Cd40,Cxcl10,Cxcl2,Fas,Il1b,Lif,Met,Osm,Pdgfa,Pdgfb,Tnf,Tnfrsf1b,Tnfrsf8
4010	MAPK signaling pathway	17	1.37E-08	Cacna1g,Cd14,Dusp16,Dusp8,Fas,Il1b,Jund,Map3k8,Mapkapk2,Myc,Nfkb1,Nfkb2,Pdgfa,Pdgfb,Rapgef2,Relb,Tnf
4062	Chemokine signaling pathway	12	2.31E-06	Bcar1,Ccl2,Ccl3,Ccl4,Ccl5,Ccl7,Cxcl10,Cxcl2,Nfkb1,Nfkbia,Pik3r5,Src
4210	Apoptosis	8	1.39E-05	Birc3,Fas,Il1b,Irak2,Nfkb1,Nfkbia,Pik3r5,Tnf
4151	PI3K-Akt signaling pathway	13	0.000264	Bcl2l11,Creb5,Itga5,Lamc2,Mdm2,Met,Myc,Nfkb1,Osm,Pdgfa,Pdgfb,Pik3r5,Tlr2
4015	Rap1 signaling pathway	10	0.000319	Adora2b,Bcar1,Lcp2,Met,Pdgfa,Pdgfb,Pik3r5,Ralgds,Rapgef2,Src
4660	T cell receptor signaling pathway	7	0.000499	Lcp2,Map3k8,Nfkb1,Nfkbia,Nfkbie,Pik3r5,Tnf
4722	Neurotrophin signaling pathway	7	0.000998	Irak2,Mapkapk2,Nfkb1,Nfkbia,Nfkbie,Pik3r5,Ripk2
4810	Regulation of actin cytoskeleton	9	0.00153	Bcar1,Cd14,Fgd3,Itga5,Pdgfa,Pdgfb,Pik3r5,Pip5k1b,Src
4014	Ras signaling pathway	9	0.00193	Ets2,Ksr1,Met,Nfkb1,Pdgfa,Pdgfb,Pik3r5,Ralgds,Rasa4
4630	Jak-STAT signaling pathway	7	0.00371	Cish,Lif,Myc,Osm,Pik3r5,Pim1,Socs3
4610	Complement and coagulation cascades	4	0.028	C3,C3ar1,Plaur,Serpine1
4666	Fc gamma R-mediated phagocytosis	4	0.039	Marcksl1,Pik3r5,Pip5k1b,Ppap2b
4068	FoxO signaling pathway	5	0.0392	Bcl2l11,Mdm2,Pik3r5,Plk2,Sod2
5322	Systemic lupus erythematosus	4	0.0471	C3,Cd40,Cd80,Tnf

Table 5.4 KEGG Pathways associated with ghB^3 treatment of Aβ42 incubated BV-2 cells at the 3hr timepoint.

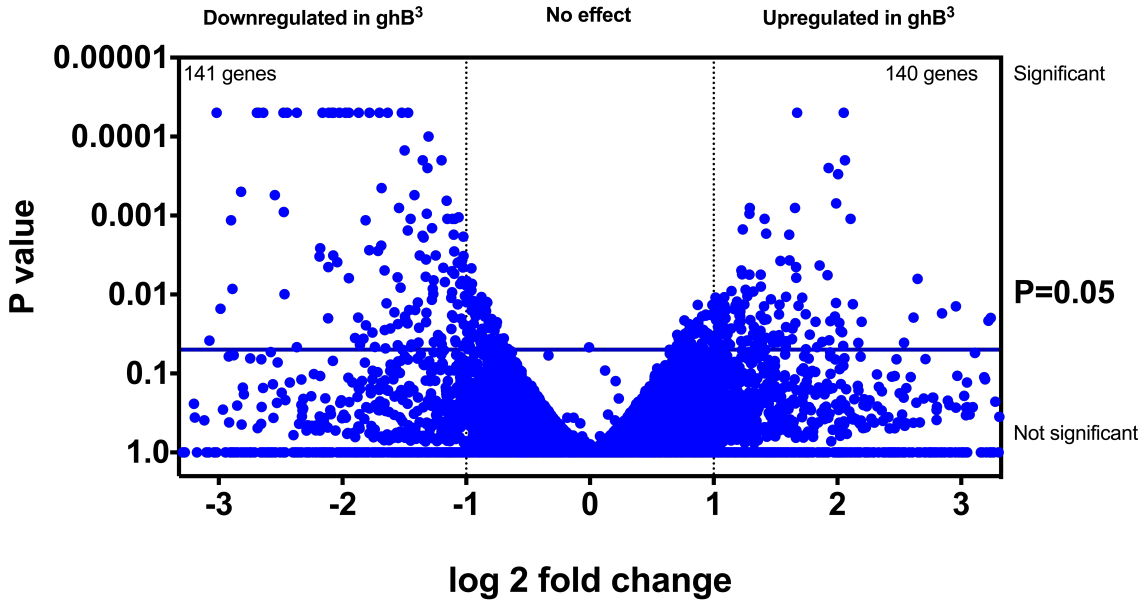

Fig 5.3 Volcano plot illustrating the distribution of gene expression changes between ghB and treatment with ghB^3 at the 3hr timepoint.
Values were presented as log2fold change of PKBM values against p values. Fold change represents treatment values divided by control values. Control- 10µg ghB +1 µM Aβ Bv-2 cells, Treatment- 10µg ghB^3 +1 µM Aβ. ($P<0.05$) is considered significant.

In order to identify the prominent mechanisms of mRNA changes as a result of globular head inhibition, differential expression analysis was also conducted between the ghB and ghB^3 groups at the 3hr timepoint. 140 genes were upregulated and 141 were downregulated, all of which had statistically significant changes in expression level ($p < 0.05$). Gene expression levels of 54000 genes remained unchanged between the AD and ghB treated groups (Fig. 5.3). We further presented all the upregulated and downregulated genes post treatment, by examining the log2 change in mRNA expression of the Fragments Per Kilobase of transcript per Million mapped reads (Table 5.5). Finally, we placed all significant upregulations through the string database and identified pathways of related networks that were upregulated (Table 5.6).

	Gene ID	FPKM ghB	FPKM ghB3	Fold change	Log 2 fold change
1	Gm26735	0.00002255	0.45939	20372.06208	14.3143044
2	Fxyd3	0.000005205	0.06406755	12308.84726	13.58740804
3	Gm26778	0.000344398	0.989782	2873.948165	11.48881833
5	Cacnb4	0.0113245	2.60576	230.0993421	7.846113049
6	RP24-103K4.5	0.024324	1.918635	78.87826838	6.301555975
7	Gm26695	0.003008155	0.1939975	64.49052659	6.011015345
8	RP23-105I10.5	0.001975285	0.1249025	63.23264744	5.982597719
9	AC114005.5	0.04608515	2.303245	49.9780298	5.643222124
10	Tmeff2	0.0309113	0.9783715	31.65093348	4.984176144
11	Ccr5	0.00970744	0.3070975	31.6352715	4.983462072
12	Lrrc14b	2.9894	0.0454945	0.015218606	-6.038019998
13	Ighm	3.30682	0.0441152	0.013340672	-6.228024882
14	Pet117	1.570115	0.01698025	0.010814654	-6.53086872
15	Sp9	0.4289385	0.00200657	0.00467799	-7.739895517
16	Nrg2	8.248195	0.0205467	0.002491054	-8.649027929
17	RP23-414K1.10	6.58537	0.00554081	0.000841382	-10.21495189
18	Pagr1a	13.0153	0.002325945	0.000178709	-12.45010396
19	RP23-325D10.3	2.77554	0.000449733	0.000162034	-12.59141212
20	RP24-252B21.2	0.04750125	0.000000554	1.16629E-05	-16.38771998
21	Lgi4	0.142075	9.775E-07	6.88017E-06	-17.14912458

Table 5.5 Differential expression was calculated using the ratio of the ghB FPKM to the ghB[3] treated FPKM. The FPKM values for each expressed gene is shown. Differentially expressed genes that were statistically significant were ranked by their fold changes, and the top 10 upregulated (red) and downregulated (green) genes were shown here.

KEGG Pathways	pathway description	observed ger	false discove	matching proteins in your network (labels)
4060	Cytokine-cytokine receptor interaction	29	7.50E-11	Ccl12,Ccl2,Ccl3,Ccl4,Ccl5,Ccl7,Ccr1,Ccr5,Csf3,Cxcl10,Cxcl2,Cxcr5,Fas,Il1a,Il1b,Il1r1,Il20rb,Il7,Il7r,Lif,Lta,Met,Osm,Pdgfb,Pdgfrb,Tnf,Tnfrsf1b,Tnfsf18,Xc
4062	Chemokine signaling pathway	20	2.96E-07	Adcy3,Bcar1,Ccl12,Ccl2,Ccl3,Ccl4,Ccl5,Ccl7,Ccr1,Ccr5,Cxcl10,Cxcl2,Cxcr5,Gng4,Gng8,Plcb4,Shc2,Src,Tiam1,Xcr1
4668	TNF signaling pathway	16	2.96E-07	Ccl12,Ccl2,Ccl5,Creb3l2,Cxcl10,Cxcl2,Fas,Icam1,Il1b,Lif,Lta,Ptgs2,Tnf,Tnfaip3,Tnfrsf1b,Traf1
4064	NF-kappa B signaling pathway	13	7.14E-06	Ccl4,Cd14,Cxcl2,Ddx58,Icam1,Il1b,Il1r1,Lat,Lta,Ptgs2,Tnf,Tnfaip3,Traf1
4010	MAPK signaling pathway	19	0.000122	Cacna1s,Cacnb4,Cd14,Dusp16,Dusp5,Dusp8,Fas,Flnb,Il1a,Il1b,Il1r1,Myc,Pdgfb,Pdgfrb,Pla2g4b,Pla2g4c,Prkcg,Rapgef2,Tnf
4621	NOD-like receptor signaling pathway	9	0.000126	Ccl12,Ccl2,Ccl5,Cxcl2,Il1b,Nlrp3,Ripk2,Tnf,Tnfaip3
5322	Systemic lupus erythematosus	11	0.000138	Actn3,Cd80,H2-DMa,Hist1h2bb,Hist1h2bj,Hist1h2bm,Hist1h2bp,Hist2h3c2,Hist4h4,Tnf,mCG_113416
4151	PI3K-Akt signaling pathway	21	0.000568	Col4a2,Creb3l2,Csf3,Epha2,Gng4,Gng8,Il7,Il7r,Itga10,Itgb3,Lamb1,Lamb3,Lamc2,Mdm2,Met,Myc,Nos3,Osm,Pdgfb,Pdgfrb,Thbs3
4540	Gap junction	9	0.00167	Adcy3,Htr2b,Pdgfb,Pdgfrb,Plcb4,Prkcg,Prkg2,Src,Tubb1
4014	Ras signaling pathway	15	0.00176	Epha2,Ets2,Gab1,Gng4,Gng8,Lat,Met,Pdgfb,Pdgfrb,Pla2g4b,Pla2g4c,Pld1,Prkcg,Shc2,Tiam1
4512	ECM-receptor interaction	9	0.00182	Col4a2,Gp5,Itga10,Itgb3,Lamb1,Lamb3,Lamc2,Sdc4,Thbs3
4514	Cell adhesion molecules (CAMs)	12	0.00184	Cd274,Cd80,Cldn15,H2-DMa,H2-Q6,Icam1,Jam3,Mpz,Ntng2,Pvr,Sdc4,Vcan
4750	Inflammatory mediator regulation of TRP channels	10	0.00323	Adcy3,Htr2b,Il1b,Il1r1,Pla2g4b,Pla2g4c,Plcb4,Prkcg,Src,Trpv4
4370	VEGF signaling pathway	7	0.00348	Nos3,Pla2g4b,Pla2g4c,Prkcg,Ptgs2,Shc2,Src
4912	GnRH signaling pathway	7	0.0193	Adcy3,Cacna1s,Pla2g4b,Pla2g4c,Plcb4,Pld1,Src
4725	Cholinergic synapse	8	0.0202	Adcy3,Cacna1s,Chrm4,Creb3l2,Gng4,Gng8,Plcb4,Prkcg
4622	RIG-I-like receptor signaling pathway	6	0.0225	Cxcl10,Ddx58,Ifih1,Isg15,Tank,Tnf
4610	Complement and coagulation cascades	6	0.0333	F10,F3,F5,Plaur,Serpine1,Serpinf2

Table 5.6 KEGG Pathways associated with ghB^3 treatment of Aβ42 incubated BV-2 cells when differentially compared with ghB expression at the 3hr timepoint.

5.3.2 Differential expression between exposure to Aβ42 and exposure to Aβ42 plus fusion protein at the 12 hr timepoints

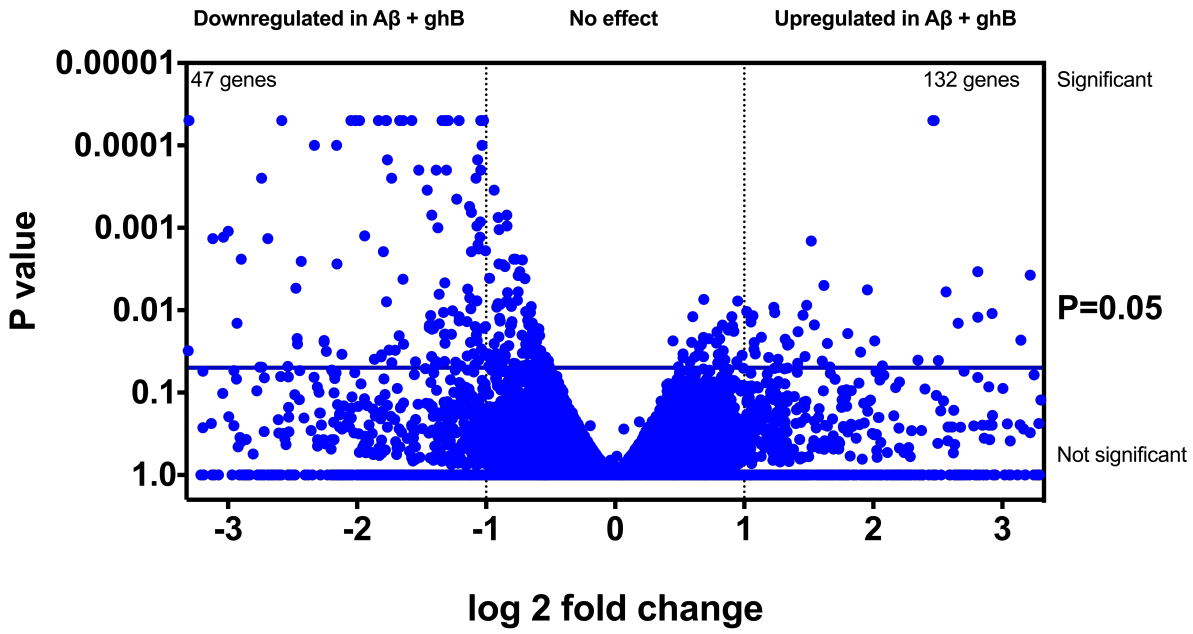

Fig 5.4 Volcano plot illustrating the distribution of gene expression changes between Aβ and treatment with ghB at the 12hr timepoint post treatment.
Values were presented as log2fold change of PKBM values against p values. Fold change represents treatment values divided by control values. Control- 10µg ghB +1 µM Aβ Bv-2 cells, Treatment- 10µg ghB +1 µM Aβ. (P<0.05) is considered significant.

A total of 132 genes were upregulated and 47 were downregulated, all of which had statistically significant changes in expression level ($p < 0.05$). Gene expression levels of 54,00 genes remained unchanged between the AD and ghB treated groups (Fig. 5.4). Overall, differential gene expression was skewed towards downregulation, i.e. transcriptional activity was much higher in the Aβ sample, possibly due to microglial response to Aβ. However, most was not considered significant.

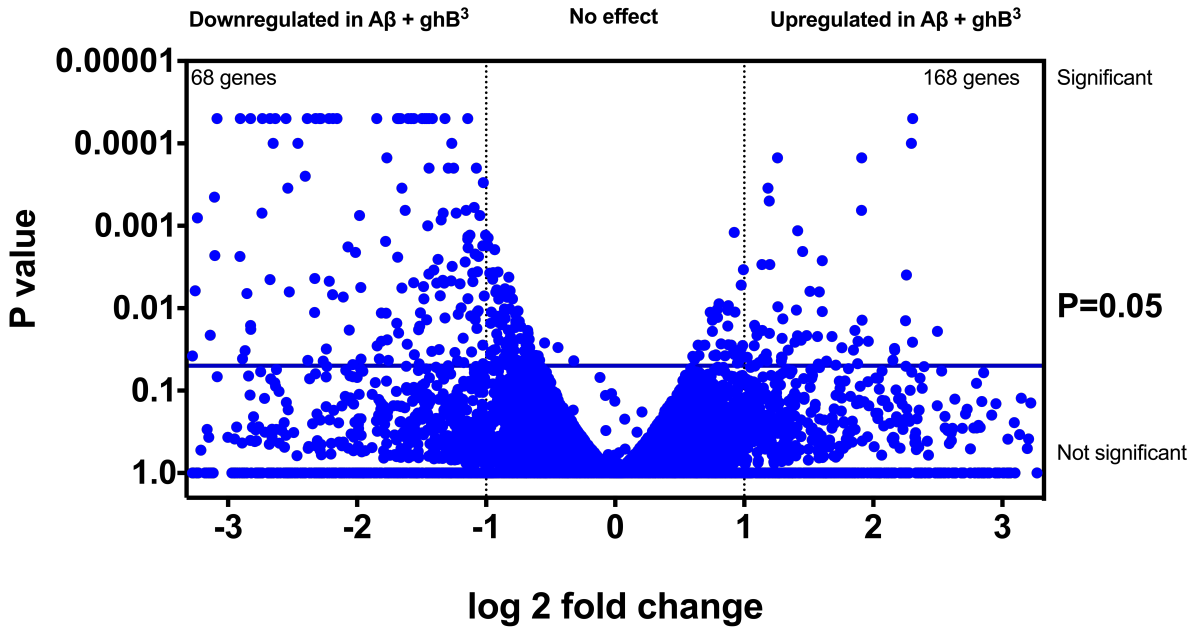

Fig 5.5 Volcano plot illustrating the distribution of gene expression changes between Aβ and treatment with ghB^3 at the 12 hr timepoint post treatment.
Values were presented as log2fold change of PKBM values against p values. Fold change represents treatment values divided by control values. Control- 10µg ghB +1 µM Aβ Bv-2 cells, Treatment- 10µg ghB^3 +1 µM Aβ. (P<0.05) is considered significant.

Incubation with the multimeric globular head protein led to an increase in the no of genes that are differentially expressed between the treatment groups. 168 genes were upregulated and 68 were downregulated, all of which had statistically significant changes in expression level ($p < 0.05$). Gene expression levels of 54000 genes remained unchanged between the AD and ghB treated groups (Fig. 5.5). Table 5.5 shows all the upregulated and downregulated genes. There was less differential expression of transcripts overall than in the 3hr timepoint

5.3.3 Complement Cascade: Differential Expression of mRNA

The transcriptome of BV-2 cells incubated with Aβ and no treatment was compared via cuffdiff software to BV-2 cells incubated with treatment (refer to sections 4.2.6, 4.2.7 and 5.2.1 for methodology).. This experiment was conducted so that we can examine the impact of exposure to globular head constructs on microglia cells exposed to AB42. We obtained log2 fold change values for each differentially expressed gene. Log2 fold change values greater than 1 (i.e. 2-fold upregulation) and less than -1 (2-fold downregulation) were considered significant.

C1qa component was upregulated >2-fold at 3hr post treatment with the weaker inhibitor of the CCP (Table 5.7 A). At 12hr post activation the upregulation increased to 4-fold. Treatment with ghB^3 on the hand showed a non-significant trend forC1q downregulation at the 3hr time point, and a 2-fold down regulation at the 12hr time point. Differential expression values between ghB and ghB^3 showed a downregulation of almost 3-fold at 3 hrs, 4-fold at 12 hrs and 3-fold at 24 hrs.

C1qb component (Table 5.7B) showed a slight though non-significant trend of upregulation at 3hrs and 12 hrs post treatment with ghB. Treatment with ghB^3 on the hand showed a non-significant trend for C1qb downregulation at the 3hr, and a 2-fold down regulation at the 12hr time point. Differential expression values between ghB and ghB^3 showed a downregulation of almost 3-fold at 3 hrs, 2-fold at 12 hrs and 3-fold at 24 hrs.

In Table 5.7C we observe no change in mRNA expression of the C1qc component at 3hrs and 12 hrs post treatment with ghB. Treatment with ghB^3 on the hand showed a non-significant trend for C1qc downregulation at the 3hr, and a 4-fold down regulation at the 12hr time point. Differential expression values between ghB and ghB^3 showed a downregulation of 2-fold at 3 hrs, 12 hrs post ghB^3 treatment.

We observed no change in mRNA expression of the C3 component at 3hrs and a 3-fold change at the 12hr time point post treatment with ghB. Whereas with ghB^3 treatment we observed a 2 and 3-fold upregulation in mRNA expression at 3hr and 12 hrs post treatment respectively. Differential expression values between ghB and ghB^3 showed a 3-fold downward trend at 24hrs post ghB^3 treatment. (Table 5.7 D)

The mRNA expression of the complement C3a receptor (C3ar1) showed a trend towards upregulation post treatment with ghB. mRNA expression was upregulated by 2-fold at 3 hr and 12hrs post ghB^3 treatment. Differential expression analysis

between both did not demonstrate any significant changes in upregulation (table 5.7E).

Complement protein C4b mRNA expression was downregulated by almost 2-fold at the 3hr time point post ghB treatment, which swung to a significant 2-fold upregulation at the 12 hr timepoint. Whereas, post ghB^3 treatment C4b expression was downregulated 8-fold at the 3-hr time point which recovered to a slight trend towards upregulation. No significant difference was observed between C4b mRNA expression profiles post ghB and ghB^3 treatment.

Expression of complement receptor for c5a, c5ar1 displayed no significant change in expression post ghB. There was a slight but non-significant trend towards upregulation post ghB treatment. Comparatively, there was a significant upregulation in C5ar1 expression post ghB^3 treatment when compared to ghB.

A

C1qa	Aβ + ghB 3hr	Aβ + ghB 12hr	Aβ + ghB3 3hr	Aβ + ghB3 12hr	Aβ + ghB3 24 hr
Aβ 3	1.4202043		-0.7950434		
Aβ12		2.1270488		-1.1671901	
Aβ + ghB 3hr			-1.5422514		
Aβ + ghB 12 hr				-2.4764785	
Aβ + ghB 24 hr					-1.5460161

B

C1qb	Aβ + ghB 3hr	Aβ + ghB 12hr	Aβ + ghB3 3hr	Aβ + ghB3 12hr	Aβ + ghB3 24 hr
Aβ 3	0.6116486		-0.5725205		
Aβ12		0.6048804		-1.1671901	
Aβ + ghB 3hr			-1.4252787		
Aβ + ghB 12 hr				-1.2639353	
Aβ + ghB 24 hr					-1.5308173

C

C1qc	Aβ + ghB 3hr	Aβ + ghB 12hr	Aβ + ghB3 3hr	Aβ + ghB3 12hr	Aβ + ghB3 24 hr
Aβ 3	0.1095852		-0.6003391		
Aβ12		0.2281372			
Aβ + ghB 3hr			-0.9510338		
Aβ + ghB 12 hr				-1.277224	
Aβ + ghB 24 hr					-1.3249407

D

C3	Aβ + ghB 3hr	Aβ + ghB 12hr	Aβ + ghB3 3hr	Aβ + ghB3 12hr	Aβ + ghB3 24 hr
Aβ 3	0.6675623		1.0624609		
Aβ12		1.7521640		1.6677398	
Aβ + ghB 3hr			0.0866433		
Aβ + ghB 12 hr				-0.3048594	
Aβ + ghB 24 hr					-1.685808

E

C3ar1	Aβ + ghB 3hr	Aβ + ghB 12hr	Aβ + ghB3 3hr	Aβ + ghB3 12hr	Aβ + ghB3 24 hr
Aβ 3	0.7425003		1.0383988		
Aβ12		0.6253042		1.0176524	
Aβ + ghB 3hr			-0.0123568		
Aβ + ghB 12 hr				0.1719129	
Aβ + ghB 24 hr					-0.1348657

F

C4	Aβ + ghB 3hr	Aβ + ghB 12hr	Aβ + ghB3 3hr	Aβ + ghB3 12hr	Aβ + ghB3 24 hr
Aβ 3	-0.7612706		-3.0220293		
Aβ12		1.2415635		0.8802149	
Aβ + ghB 3hr			-2.5018682		
Aβ + ghB 12 hr				0.5373046	
Aβ + ghB 24 hr					0.3588191

G

C5ar1	Aβ + ghB 3hr	Aβ + ghB 12hr	Aβ + ghB3 3hr	Aβ + ghB3 12hr	Aβ + ghB3 24 hr
Aβ 3	0.0881298		0.6071403		
Aβ12		-0.3776945		0.8802149	
Aβ + ghB 3hr			0.2779009		
Aβ + ghB 12 hr				1.0374742	
Aβ + ghB 24 hr					-0.6385602

Table 5.7 RNA Seq Differential expression of mRNA. Table presents log2 fold mRNA expression differences of complement cascade components at different time points post Amyloid Beta and globular head B variant treatments. **A-** Complement C1q chain A, **B-** Complement C1q chain B, **C-** Complement C1q chain C, **D-** Complement C3, **E-** Complement C3a receptor C3ar1, **F-**Complement C4, **G-** Complement C5a receptor (C5ar1).

5.3.5 Inflammatory mediators: Differential Expression of mRNA

The transcriptome of BV-2 cells incubated with Aβ and no treatment was compared via cuffdiff software to BV-2 cells incubated with treatment. We obtained log2 fold change values for the above differentially expressed inflammatory mediator genes. Log2 fold change values greater than 1 (i.e. 2-fold upregulation) and less than -1 (2-fold downregulation) were considered significant.

The TNF gene which codes for pro-inflammatory mediator TNF-α was upregulated >3-fold at 3hr post treatment with the weaker inhibitor of the CCP. The upregulation persisted at 3-fold at the 12hr time point. Treatment with ghB^3 on the hand showed a 13-fold upregulation at the 3hr time point, which decreased to 7-fold at 12hr post treatment. Differential expression values between ghB and ghB^3 showed a difference in upregulation of almost 4-fold at the 3-hr time point, 2-fold at the 12hr timepoint. However, no significant difference was observed at the 24 hr timepoint, indicating a sharp upregulation in inflammation which resolves more quickly with ghB^3 than which ghB (Table 5.8A).

Concurrently IL-1β mRNA expression was shown to be upregulated 16-fold more than Aβ, 3hr post treatment of ghB, and 13-fold 12 hrs post treatment. On the other hand, mRNA expression post ghB^3 treatment. ghB^3 expression was 4-fold more upregulated at 3 hrs, 2-fold more up regulated at 12 hrs and > 1-fold downregulated at the 24hr than ghB. (Table 5.8B)

IL-18 mRNA did not significantly change across any time points. However, comparison between ghB and ghB^3showed a slight trend towards upregulation at the 3hr and downregulation at the 24 hr time points. (Table 5.8 C)

Expression of CCL2 demonstrated a trend towards upregulation at the 3hr timepoint which became significant at the 12hr timepoint post ghB treatment. ghB^3 treatment elicited an 8-fold upregulation at the 3 point and a 4-fold upregulation at the 12-hr point. Comparative expression showed a 4-fold upregulation post ghB^3 treatment at the 3hr time point, 2-fold a 12 hrs and no significant difference at the 24-hr time point compared to ghB. Indicating a downregulation in upregulation of CCCL2 expression post 3hrs. (Table 5.8 D)

We further examined differential Transforming Growth Factor (TGF-β) mRNA expression between Aβ and ghB. At the 3hr and 12 hr time points there was no significant difference in expression. Similarly, there was no change in expression between Aβ and ghB^3, nor between the 2 globular head variants. Table 5.8 E

At the 3hr time point chemokine receptor type 4 (CXCR4) expression was significantly downregulated at the. Expression patterns for ghB^3 mirrored that of ghB and there was no significant in mRNA expression at any time point. Table 5.8 F

CXCL10 mRNA was upregulated 8-fold at 3hr and declined to 4-fold after 12 hr with ghB treatment. Similarly, mRNA expression was upregulated 64-fold at the 3hr timepoint and declined to 4-fold upregulation at the 12hr time point. Comparative expression showed a 4-fold difference in upregulation at 3hr, and a 4-fold downregulation at 24 hrs compared to ghB. Table 5.8 G

Expression of the C-X-C motif chemokine 2 (CXCL2) demonstrated an 8-fold upregulation at the 3hr timepoint which persisted at the 12hr time point post ghB treatment. However, ghB^3 treatment elicited a robust 128-fold upregulation at the 3 point which declined to a 16-fold upregulation at the 12-hr point. Comparative expression showed a 16-fold upregulation post ghB^3 treatment at the 3hr time point, 2-fold a 12 hrs and a 4-fold downregulation at the 24-hr time point compared to ghB. Indicating a downregulation in upregulation of CCCL2 expression post 3hrs. (Table 5.8 H).

Expression of CXCR3 demonstrated a trend towards upregulation at the 3hr timepoint which became significant at the 12hr timepoint post ghB treatment. Conversely ghB^3 treatment elicited an 8-fold upregulation at the 3 point and a 4-hr upregulation at the 24-hr point. Comparative expression showed a 4-fold upregulation post ghB^3 treatment at the 3hr time point, 2-fold a 12 hrs and no significant difference at the 24-hr time point compared to ghB. Indicating a downregulation in upregulation of CCCL2 expression post 3hrs. (Table 5.8I).

We further examined the expression profile of the nuclear factor of kappa light polypeptide gene enhancer in B-cells inhibitor-α (NFKBIA; Table 5.8J). Expression was upregulated >3 fold at 3hr and 2-fold at 12 hrs post ghB treatment. ghB^3 post treatment expression was up-regulated almost 8-fold at 3 hrs and almost 3-fold at 12 hrs post treatment. NFKB1 mRNA expression on the other hand showed a trend towards upregulation at the 3hr and 12 hr timepoints post ghB treatment. Upregulation was significant post treatment at 3hr, whilst the 2hr time point showed a decline but still a trend towards upregulation post treatment with ghB^3. At the 24-hr time point there was a comparative decline in NFKB activation post ghB^3treatment when compared to ghA treatment. Table 5.8 K

Finally, we examined expression of NOS-2 the gene for the inducible nitric oxide synthase. NOS2 expression was upregulated >3 fold at the 3hr time point and >* fold at the 12-hr time point post ghB treatment when compared to Aβ. NOS2 was more significantly upregulated post ghB[3]. Expression was 64-fold at the 3hr time point which declined to 32 at the 12hr point. At the 24-hr time point the post treatment expression of ghB[3] had downregulated comparatively when compared to that of ghB. Table 5.8L.

A

TNF	Aβ + ghB 3hr	Aβ + ghB 12hr	Aβ + ghB3 3hr	Aβ + ghB3 12hr	Aβ + ghB3 24 hr
Aβ 3	1.8141181		3.82210997		
Aβ12		1.6062128		2.89587558	
Aβ + ghB 3hr			1.76688235		
Aβ + ghB 12 hr				1.06922755	
Aβ + ghB 24 hr					0.22555128

B

IL-1β	Aβ + ghB 3hr	Aβ + ghB 12hr	Aβ + ghB3 3hr	Aβ + ghB3 12hr	Aβ + ghB3 24 hr
Aβ 3	3.9828602		6.18470021		
Aβ12		3.74486856		5.24155684	
Aβ + ghB 3hr			1.96073050		
Aβ + ghB 12 hr				1.27625305	
Aβ + ghB 24 hr					-0.68985624

C

IL-18	Aβ + ghB 3hr	Aβ + ghB 12hr	Aβ + ghB3 3hr	Aβ + ghB3 12hr	Aβ + ghB3 24 hr
Aβ 3	-0.3038712		0.30242641		
Aβ12		0.12863385		0.20081513	
Aβ + ghB 3hr			0.36518806		
Aβ + ghB 12 hr				-0.14825394	
Aβ + ghB 24 hr					-0.36709860

D

CCL2	Aβ + ghB 3hr	Aβ + ghB 12hr	Aβ + ghB3 3hr	Aβ + ghB3 12hr	Aβ + ghB3 24 hr
Aβ 3	0.5954572		2.98360317		
Aβ12		0.98046456		2.20795019	
Aβ + ghB 3hr			2.14703642		
Aβ + ghB 12 hr				1.00705040	
Aβ + ghB 24 hr					0.53450282

E

TGF-β	Aβ + ghB 3hr	Aβ + ghB 12hr	Aβ + ghB3 3hr	Aβ + ghB3 12hr	Aβ + ghB3 24 hr
Aβ 3	0.0454006		0.24792341		
Aβ12		0.27853645		0.27853645	
Aβ + ghB 3hr			-0.03858669		
Aβ + ghB 12 hr				-0.15459557	
Aβ + ghB 24 hr					-0.08078170

F

cXCr4	Aβ + ghB 3hr	Aβ + ghB 12hr	Aβ + ghB3 3hr	Aβ + ghB3 12hr	Aβ + ghB3 24 hr
Aβ 3	-1.0021922		-1.17309909		
Aβ12		-0.4569703		-0.32837295	
Aβ + ghB 3hr			-0.41201639		
Aβ + ghB 12 hr				-0.09183792	
Aβ + ghB 24 hr					-1.08115622

G

CXCL10	Aβ + ghB 3hr	Aβ + ghB 12hr	Aβ + ghB3 3hr	Aβ + ghB3 12hr	Aβ + ghB3 24 hr
Aβ 3	3.5684738		6.43572572		
Aβ12		2.46294498		2.31918511	
Aβ + ghB 3hr			2.86730576		
Aβ + ghB 12 hr				-0.36419508	
Aβ + ghB 24 hr					-1.83255200

H

CXCL2	Aβ + ghB 3hr	Aβ + ghB 12hr	Aβ + ghB3 3hr	Aβ + ghB3 12hr	Aβ + ghB3 24 hr

Aβ 3	3.1808759		7.53412630			
Aβ12		3.07906655		4.52559109		
ghB 3hr			4.35330429			
ghB 12 hr				1.22608931		
ghB 24 hr					-1.96292547	

I

CXCR3	**Aβ + ghB 3hr**	**Aβ + ghB 12hr**	**Aβ + ghB3 3hr**	**Aβ + ghB3 12hr**	**Aβ + ghB3 24 hr**
Aβ 3	0.8083830		-1.16137037		
Aβ12		1.67721247		0.94470921	
Aβ + ghB 3hr			-1.90266272		
Aβ + ghB 12 hr				-0.95293848	
Aβ + ghB 24 hr					-0.62997667

J

NFKBIA	**Aβ + ghB 3hr**	**Aβ + ghB 12hr**	**Aβ + ghB3 3hr**	**Aβ + ghB3 12hr**	**Aβ + ghB3 24 hr**
Aβ 3	1.7066309		2.84010863		
Aβ12		1.09013788		1.43397437	
Aβ + ghB 3hr			0.89236824		
Aβ + ghB 12 hr				0.12340126	
Aβ + ghB 24 hr					-0.2227243

K

NFKB	**Aβ + ghB 3hr**	**Aβ + ghB 12hr**	**Aβ + ghB3 3hr**	**Aβ + ghB3 12hr**	**Aβ + ghB3 24 hr**
Aβ 3	0.8128984		1.54403928		
Aβ12		0.60910791		0.84533722	
Aβ + ghB 3hr			0.49003137		
Aβ + ghB 12 hr				0.01579408	
Aβ + ghB 24 hr					-0.83474111

L

NOS2	Aβ + ghB 3hr	Aβ + ghB 12hr	Aβ + ghB3 3hr	Aβ + ghB3 12hr	Aβ + ghB3 24 hr
Aβ 3	1.7896468		5.93807098		
Aβ12		3.34573808		5.19449895	
Aβ + ghB 3hr			3.90731466		
Aβ + ghB 12 hr				1.62832564	
Aβ + ghB 24 hr					-0.60758867

Table 5.8 RNA Seq Differential expression of mRNA. Table presents log2 fold mRNA expression differences of inflammatory mediators at different time points post Amyloid Beta and globular head B variant treatments. **A-** Tumour Necrosis Factor (TNF), **B-** Interleukin 1β, **C-** Interleukin 18, **D-** chemokine (C-C motif) ligand 2 (CCL2), **E-** Transforming Growth Factor (TGF-β), **F-** chemokine receptor type 4 (CXCR-4), **G-** C-X-C motif chemokine 10 (CXCL10), **H;** C-X-C motif chemokine 2 (CXCL2), **I-** chemokine receptor type 3 (CXCR-3), **J-** nuclear factor of kappa light polypeptide gene enhancer in B-cells inhibitor-α (NFKBIA), **K-** nuclear factor kappa-light-chain-enhancer of activated B cells (NF-κB), **L-** Inducible nitric oxide synthase gene (NOS2)

5.4 Discussion

We performed a study to examine the combined effects of Amyloid Beta and recombinant globular head fusion proteins on the BV-2 mouse genome. With ghB and ghB^3 treatment we observed an upregulation in many genes involved in the inflammatory response and the production of cytokines and chemokines. Yet conversely, we also observed a significant increase in mRNA expression of many inhibitors and regulators of the chemokines, cytokines and transcription factors.

Previous studies have implicated the complement system and the classical complement pathway in AD. In regions of the brain with high amyloid LOAD, C1q expression is upregulated 80-fold (Yasojima et al., 1999). Webster and colleagues demonstrated an increase in amyloid beta aggregation on co-incubation with C1q (Webster et al., 1994), implicating C1q in the pathogenesis of AD and the resulting cognitive decline. C1q null APP transgenic mice demonstrated an improved neuronal integrity and reduction in inflammatory markers when compared to APP transgenic mice. Thus, these studies suggest that an inhibition of Aβ, will result in reduction of C1q mRNA expression. Correlating with the observations in previous studies, we observed, a significant 4-fold reduction in the mRNA expression of C1qa, C1b and C1qc chains when BV-2 cells were incubated with ghB^3 at both the 3 and 12 hr timepoints. Furthermore, there was a significant 8-fold decrease in the transcriptome expression of another CCP pathway protein, C4b when compared with Aβ. C4b is a crucial component of CCP C3 convertase which catalyses the hydrolysis of C3 through the cleavage of a single Arg-X bond in the α chains of C3 into the anaphylatoxin C3a, and C3b. C3b then hydrolyses C5 into the crucial component of the MAC C5b, and a glial recruiting chemotaxis agent C5a (Fig 5. Kishore et al., 2003). This all suggests that in addition to inhibiting the CCP, competitive inhibition of C1q-Aβ interaction will inhibit further activation of the CCP by reducing the expression of complement proteins. Therefore, we would posit that exposure to higher doses of ghB^3 will further reduce and possibility eradicate the upregulation of C1q expression in AD.

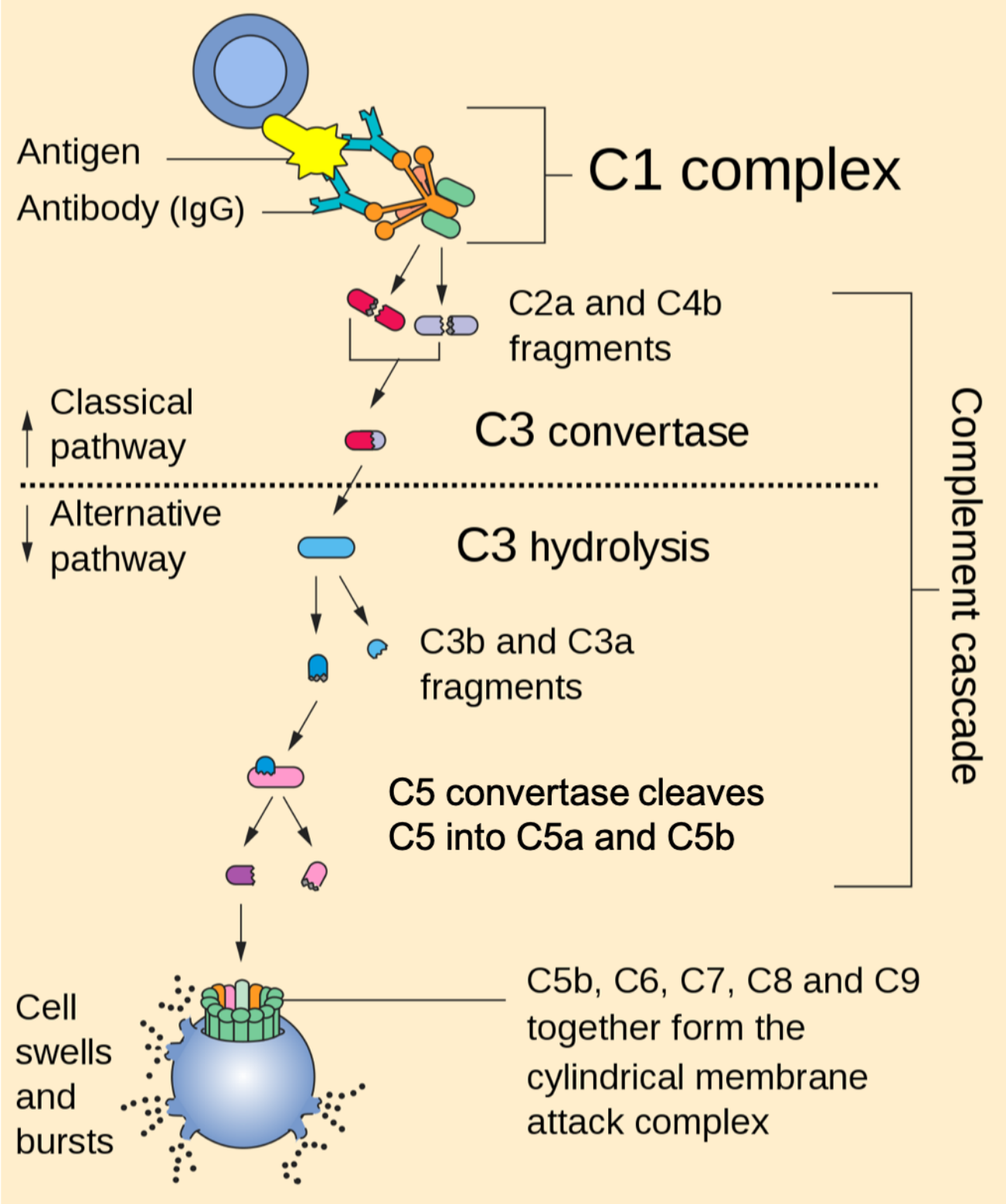

Fig 5.6: Diagram illustrating the complement cascade. Modified from original (https://en.wikipedia.org/wiki/Complement_system#/media/File:Complement_pathway.svg)

However, in this study we observed that with ghB^3 treatment genes from the complement and coagulation (Kyoto Encyclopedia of Genes and Genomes) KEGG pathway were activated. Expression of the Complement C3 protein, and its g protein coupled receptor (GPCR) C3aR1 (C3a receptor) were upregulated 2-fold post treatment with ghB and 3-fold post treatment with ghB^3 at the 3-hr time point. The downregulation of C4b, previously observed should concurrently lead to a downregulation of C3. However, an upregulation of C3 was observed, which suggests an activation of C3 and release of C3a. It is likely due to different mechanisms of binding by complement proteins to Aβ. C1q binds aa 1-11 on AB_{1-42} protein whereas C3 can bind via aa 25-35 (Cadman and Puttfarcken, 1997). Therefore, inhibition of the C1q binding is unlikely to inhibit the availability of the C3 component binding sites to Aβ.

The alternative pathway functions through a feedback loop through which the C3 hydrolysis, activates C3 convertase which leads to further C3 hydrolysis. The mechanism for its occurrence is likely due to a low “tickover” hydrolysis of C3b that is independent of the CCP. This allows for the subsequent formation of alternative pathway C3 convertase. Once C3 is cleaved C3b binds with C3 convertase to form C5 convertase (C3bBbP3b). A concurrent increase in mRNA expression of C5ar1 (the receptor for the C5a component) was also observed at the 12 hr timepoint, suggesting activation of the complement cascade, resulting in a release of the C5a chemotaxis agent and C5b the initiator of the MAC. Thus, from these observations we can infer that in the event of CCP inhibition, the alternative pathway functions as a biological compensatory mechanism for the activation of the complement cascade.

Indeed, the C3 component is essential toward the reduction of pathology in the CNS. Previous studies observed that Amyloid precursor protein (APP) transgenic mice with a C3 gene knockout showed a 2-fold increase in Amyloid load (Maier et al, 2012). However, APP transgenic mice lacking C1q had no change in Aβ plaque burden (Fonseca et.al, 2004). This suggests that the alternative pathway C3 though capable of complement cascade aggregation is rate limited. Rate limitation can occur by either limitation in activation of C3 or due to the instability and short half-life of C3b. To identify which is the case in this situation we checked for differential expression of Properdin a positive regulator of C3 (Kouser et al.,2015). At all time points, with both treatments we observed no increase in mRNA expression of CFB gene encoding Properdin. There was a slight 10% downregulation on incubation with

ghB^3 though not considered significant. Thus, upregulation of C3 by the inhibition of CCP activation route is more likely to perpetuate the feedback loop of C3a and C3b rather than the formation of the MAC. In this instance therefore, inhibition of the CCP may be protective to neurons from MAC induced cytolysis (Shen et al., 1997).

Previous studies demonstrated that congo red an inhibitor of Amyloid aggregation is capable of reducing C3 convertase activity on aggregated Aβ 1-42 (Emmerling et al., 1997). This decrease in activity was indicated by decreased C3a production. As C3aR1 expression was upregulated by ghB and ghB^3 it can be posited that C3a activity was also increased in this study. So conversely, increased C3a activity, indicates activation of C3 which in turn suggests the presence of Aβ aggregates. As the mRNA expression of C3 and C3ar1 increased by 2-fold after incubation with ghB and ghB^3 compared to just Aβ, it is likely that C1q ghB chain promotes the aggregation of Aβ. This theory is corroborated by earlier findings by Webster and colleagues (1994). Alternatively, it may be related to impaired degradation of Aβ aggregates. Serpine1 (complement and coagulation KEGG pathway) was observed to be upregulated in this study. Serpine1 encodes fast-acting clade E serine protease inhibitor (SERPIN) plasminogen activator inhibitor type-1 which inhibits tissue plasminogen actor (tPA) and thereby the production of Plasmin. Plasmin degrades Aβ aggregates, catalyses α- secretase proteolysis of APP, and increases mRNA expression of tPA thus reducing the production of Aβ (Kutz et al., 2012). So therefore, the upregulation of Serpin directly results in an impairment of Plasmin dependent degradation of Aβ. Plasmin has been suggested, to further act as an alternative pathway C5 convertase. Inhibition of its production may contribute to a reduction in alternative pathway activation of the MAC, and thereby bystander lysis. Thus, the complement cascade may be a negative regulator of degradation of Aβ via upregulation of Plasmin inhibitors. Conversely, at the 24 hr timepoint we observed an 8-fold tPA downregulation in mRNA expression with gHB^3 when compared to Aβ. Indicating that long term inactivation of the CCP results in diminished Aβ degradation. Hence like any homeostatic regulation system, disease states can be inititated by any form of persistent dysregulation.

The persistence of Aβ aggregates, may explain the upregulation of mRNA expression of chemotaxis agents such as CCL2 which recruits monocytes, and C3ar1 which promotes chemotaxis of microglia, Platelet derived growth factor a and b (PDGFA and b). PDGFA and B have recently been identified in GWAS studies as

loci that are implicated in Late onset Alzheimer' s disease (Wang et al., 2017). PDGFB is the gene for protein platelet-derived growth factor-β (PDGF-β), an active component of the PI3-K/Akt pathway which binds to PDGF-R and regulates proliferation, migration and recruitment of pericytes to the vascular wall (Bell et al. 2010a). Pericytes are an important part of the vasculature that surrounds the BBB (Sengillo et al., 2013). PDGFβ regulates clearance through the BBB. (Sagare et al. 2013). Corroborative evidence comes from studies of an APP and pericyte deficient transgenic mouse models which showed an increased deposition of Aβ40 and Aβ42 when compared to APP transgenic mice alone. (Sagare et al. 2013). Therefore PDGF-β is essential to clearance of aggregates of Aβ. As ghB and ghB^3 inhibition of amyloid Beta led to an upregulation in the mRNA expression of PDGFβ, inhibition of C1q-Aβ interaction may confer neuroprotection.

On the other spectrum, anaphylatoxins such as C3a and C5a which are upregulated in our study contribute largely towards the inflammatory milieu observed in the CNS in the presence of Aβ. They bind receptors on the surface of astrocytes, microglia, neurons and oligodendrocytes and recruit cells towards the site of aggregates and fibrils (Davoust et al., 1999). The normal function of these cells is to release pro-inflammatory mediators - such as IL-1β and TNF-α - and phagocytose opsonised pathogens or aberrant aggregates through activation of TLRs, lectins and complement receptors (Laudisi et al., 2013). However, in disease states such as AD the primary result of the recruitment of inflammatory cells is the further activation of cells proximal to the site either due to direct binding of Aβ or to ligand-receptor interactions with other chemoattractants. The result is a chronic activated state which promotes the release of inflammatory mediators and leads to the activation of transcription factors such as NF-kB. Nf-kB in turn promotes the further transcription and upregulation of inflammatory genes (Niederberger and Geisslinger, 2008).

NF-κB is composed of homo- and heterodimers of Rel family proteins (p65, RelB, c-Rel, p52, and p50), the most common of which is the p50/p65 heterodimer (Niederberger and Geisslinger, 2008). In the cell cytoplasm, NF-κB is bound by the inhibitor of NF-κB (I-κB). Upon activation of cell surface chemokine and cytokine receptors such as the tumour necrosis factor (TNF) receptor CD120 by cytokines, Interleukin-1β (IL-1β), or TNF-α, I-κB is phosphorylated by I-κB kinases (IKKs) in a classical canonical or alternative pathway (Fig 1.3), leading to ubiquitinylation and proteolysis of the complex. Subsequently, NF-κB is translocated into the nucleus and

binds to the promoter region of various genes such as COX-2, inducible Nitric Oxide-synthase (iNOS), IL-1β and TNF-α, thus inducing transcription of those genes (Niederberger and Geisslinger, 2008; Hayden and Ghosh, 2012). The primary role of TNFα is the regulation of immune cells, so activation of NF-κB results in an intracellular cascade which induces expression of IL1 & IL6 production and thus induces inflammation.

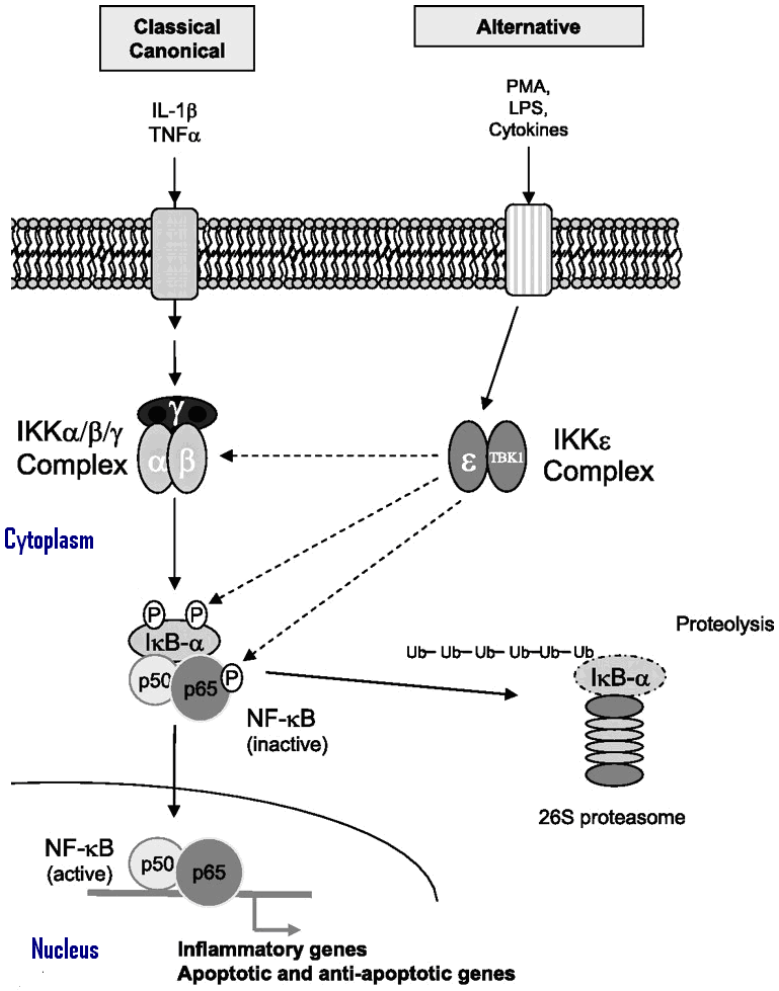

Fig 5.7 Schematic diagram illustrating the two main NF-κB activation pathways involved in the inflammatory response.

The classic canonical pathway can be induced by IL-1β and TNF-α, which triggers a subsequent activation of the IKKα,β,γ complex. In turn IKK phosphorylates I-κBα at serines 32 and 36. the pathway culminates in the release of p65 and its entry into the cell nucleus.

(Niederberger and Geisslinger, 2008).

Our original hypothesis was that inhibition of the CCP would lead to a reduction the inflammatory profile. Yet we observed a rather potent increase in expression of the genes for proinflammatory mediator's TNF, IL-1B, NF-kB, NOS2; chemokines such as CCL2 and chemokine receptors. this study we observed a trend towards upregulation of NF-kB post ghB treatment and a 3-fold upregulation of NF-kB post treatment with the more potent CCP inhibitor ghB^3. With ghB treatment, there is a reduction in CCP activation, though likely not a complete inactivation. We posit that

this creates the environment for both alternative pathway activation and a lower rate of CCP activation. We further posit that due to this inhibition induced persistence of Aβ, the alternative pathway loop will continue to generate C3a at a rate higher than that of just Aβ treatment. In this way complement pathway inhibition will increase release of inflammatory mediators and further lead to an upregulation in the mRNA expression of inflammatory mediator genes.

C1q opsonisation induced phagocytosis would likely also occur concurrently post ghB treatment but at a diminished rate, explaining why there was a slight decrease in the expression of IL-1B and TNF-α at the 12 hr time points post ghB treatment. Likewise, a more potent inhibition of the CCP by ghB^3 would lead to a more potent upregulation of NF-κB, IL-1β and TNF-α as observed in this study. Previous studies indicate that NF-κB activation is abolished in C3-deficient serum, which was recovered by reconstitution with C3 (Tam et al., 2014). Moreover, increased activation of the IKK complex was observed after a viral challenge only in the presence of C3. Tam et al., findings therefore corroborate with the upregulation demonstrated in this study, and the theory espoused above. Therefore, the possible mechanism of action is that activation of the alternative pathway by Aβ increases the hydrolysis of C3 into C3a and C3b. C3a then binds to its receptors (C3ar1, PRRs) on the surface of microglial cells and increases the activation of NF-kB. NF-κB in turn mediates the transcription of inflammatory mediators. Due to the fact that C3 promoter is also a target of NF-kB (Lian et al., 2015), this theory also explains the mode of upregulation of the C3 gene observed in this study at the 12hr timepoint.

Improbably the downregulation of NF-KB, TNF-α, IL-1β, NOS2 mRNA expression observed between the 3hr and 12hr timepoints was more prominent post ghB^3 treatment. There are two possibilities for this which may work concurrently. Firstly, opsonisation of Aβ by C3b may promote phagocytosis (Yamanaka et al., 2016). As C3 expression was significantly higher post ghB^3 treatment, elevated levels of C3b protein may speed up the opsonisation of aberrant aggregates more quickly than with just Aβ or ghB treatment. Alternatively, NF-κB promotes transcription of its inhibitor NFKBIA which produces IKKα (Pahl, 1999). A robust upregulation in NF-κB would therefore increase expression of its inhibitor, promote downregulation of the classically canonical pathway of NF-κB activation and thus modulate and inhibit the expression of inflammatory mediators. We observed such an effect in this study with a significant downregulation of inflammatory mediators by

ghB^3 at 12 hrs post treatment. However, this process may not occur so robustly in AD. Therefore, this study suggests that the role of the Classical complement pathway is beneficial at early stages of AD and promotes clearance. Whereas that of the alternative pathway, though it may compensate and contribute towards clearance, is largely a generator of anaphylatoxins which in turn generate inflammatory mediators and their regulators. The 24hr recovery of a non-inflammatory milieu by ghB^3 suggests that large changes in the expression of pro-inflammatory mediators do not confer AD risk. Conversely, it indicates that more controlled activation of the CCP is likely to perpetuate chronic activation. We posit that this persistent activated state induced by C1q-Aβ interaction is the cause of chronic inflammation and amyloid Beta induced pathogenesis. It could also explain why Aβ pathology precedes development of AD by decades.

CHAPTER 6:

Conclusion and Future Studies

6.1 Conclusion

Alzheimer's disease is multifactorial disorder with a complex causality. A chronic neuroinflammatory state, which is a hallmark of Aβ induced microglial activation has been identified as the point at which disease progression occurs in AD. As a result, many avenues of research have been targeted towards inhibiting the actions, or downstream pathways of these regulators of immune function. The research presented in this thesis examined the ability of recombinant fusion proteins globular heads ghA^3, ghB^3, ghC^3, ghA, ghB and ghC, to inhibit Aβ-microglia induced neuroinflammation. We further examined whether this role was beneficial or detrimental.

We first observed a decrease in mRNA expression of inflammatory mediators IL-6, IL-1β, TNF-α and IL-18, and a concurrent increase in expression of TGF-β´ on incubation of BV-2 Aβ (unaggregated) treated cells with globular heads. mRNA expression downregulation of inflammatory mediators was far more prominent with globular heads A^3, B^3 and C$^{3.}$ Indicating that inhibition of the Classical complement pathway can confer neuroprotection and inhibition of Inflammation.

However, subsequent RNA Seq results which showed up regulation in mRNA expression of the same genes at some time points appeared incongruous with this downregulation. Unaggregated Aβ was utilised for the initial qPCR experiments in order to identify whether there was an inhibitory effect. Once established, we utilised oligomer preparations of Aβ to conduct RNA Seq experiments. This is due to the fact that the oligomeric form is 10-fold more neurotoxic than fibrillar amyloid and 40-fold more toxic than the unaggregated form (Stine et al., 2013). Thus, we endeavoured to identify the ability of the globular heads to inhibit CCP activation of the more toxic form of Aβ and thus the production of more inflammatory mediators

Transcriptome analysis of BV-2 cells incubated with oligomeric amyloid and treated with ghB or ghB^3 demonstrated an inhibition of the classical complement pathway. It further suggested that the CCP inhibition and alternative pathway activation promotes early potent upregulation in the mRNA expression of inflammatory mediators which at latter stages may prove to be more neuroprotective than neurodetrimental. We further observed that the compensatory activation of the complement cascade via the alternative pathway results in sharp upregulation of expression of pro-inflammatory mediators, and activation of inflammatory cascades.

This in turn triggers a larger compensatory response that mediates the reduction in transcription of proinflammatory mediators. This silencing and recovery of a homeostatic environment is more potent with ghB^3 than with ghB. It is therefore possible that the chronic inflammation observed in AD is due to a constant activation, that increases expression of inflammatory mediators over time, but is unable to mount a response large enough to trigger the expression of modulators of the anti-inflammatory mediators.

6.2 Limitations of the study and future work

We would like to acknowledge that our study has a number of limitations. Primarily was the inability to express ghA^3, ghB^3 and ghC^3 as functional homotrimers, in their fully characterised cleaved morphology. So, we will endeavor in future to express globular head trimer via a different vector. The full characterization of globular heads as homotrimers will enable researchers to study the full inhibitory effects. Moreover, it will enable researchers to directly test its effects against those of recombinant C1q when both are incubated together. Secondly, we did not compare dose dependent effects of BV-2 treatments, nor did we explore beyond 24 hrs post treatment. This would enable researchers to characterise the dose at which inhibition becomes neuroprotective or neurodetrimental.

We characterised the upregulation in neuroprotective effects of ghB3 via transcriptome analysis. Many of the pathways involved, such as the pi3/akt pathway are implicated in neuronal survival and long-term potentiation. One avenue of further research is to assess the ability of recombinant ghA, ghB and ghC monomeric and trimeric variants to protect cultured neuronal cells from the C1q-Aβ interaction. This can be conducted in a couple of ways. Microglia and neurons, co-incubated together will be challenged with Aβ and globular head variants. Neurons will be assessed via cell staining and microscopy to identify any damage to neurons. Secondly, we will challenge neurons separately with medium obtained from microglial cells, challenged with dementia peptides and treated with globular head peptides. We will assess the ability of secreted proteins in the medium to either protect or degenerate the neurons. We will also assess of the ability of recombinant ghA, ghB and ghC variants to protect the neuronal cell directly. We will do this by incubating neurons with dementia peptides and globular head variants. CCP activation will be assessed. Cell death assay and degeneration of neuronal processes will also be assessed.

BIBLIOGRAPHY

REFERENCES

1. Abbott, N. J., Ronnback, L. and Hansson, E. (2006) 'Astrocyte-endothelial interactions at the blood-brain barrier', *Nat Rev Neurosci,* 7(1), pp. 41-53.
2. Ager, R. R., Fonseca, M. I., Chu, S. H., Sanderson, S. D., Taylor, S. M., Woodruff, T. M. and Tenner, A. J. (2010) 'Microglial C5aR (CD88) expression correlates with amyloid-beta deposition in murine models of Alzheimer's disease', *J Neurochem,* 113(2), pp. 389-401.
3. Aisen, P. S., Schafer, K. A., Grundman, M., Pfeiffer, E., Sano, M., Davis, K. L., Farlow, M. R., Jin, S., Thomas, R. G. and Thal, L. J. (2003) 'Effects of rofecoxib or naproxen vs placebo on Alzheimer disease progression: a randomized controlled trial', *Jama,* 289(21), pp. 2819-26.
4. Akiyama, H., Barger, S., Barnum, S., Bradt, B., Bauer, J., Cole, G. M., Cooper, N. R., Eikelenboom, P., Emmerling, M., Fiebich, B. L., Finch, C. E., Frautschy, S., Griffin, W. S., Hampel, H., Hull, M., Landreth, G., Lue, L., Mrak, R., Mackenzie, I. R., McGeer, P. L., O'Banion, M. K., Pachter, J., Pasinetti, G., Plata-Salaman, C., Rogers, J., Rydel, R., Shen, Y., Streit, W., Strohmeyer, R., Tooyoma, I., Van Muiswinkel, F. L., Veerhuis, R., Walker, D., Webster, S., Wegrzyniak, B., Wenk, G. and Wyss-Coray, T. (2000) 'Inflammation and Alzheimer's disease', *Neurobiol Aging,* 21(3), pp. 383-421.
5. Amariglio, R. E., Becker, J. A., Carmasin, J., Wadsworth, L. P., Lorius, N., Sullivan, C., Maye, J. E., Gidicsin, C., Pepin, L. C., Sperling, R. A., Johnson, K. A. and Rentz, D. M. (2012) 'Subjective cognitive complaints and amyloid burden in cognitively normal older individuals', *Neuropsychologia,* 50(12), pp. 2880-6.
6. Barnum, S. R. (1999) 'Inhibition of complement as a therapeutic approach in inflammatory central nervous system (CNS) disease', *Mol Med,* 5(9), pp. 569-82.
7. Bayly-Jones, C., Bubeck, D. and Dunstone, M. A. (2017) 'The mystery behind membrane insertion: a review of the complement membrane attack complex', *Philos Trans R Soc Lond B Biol Sci,* 372(1726).
8. Bermejo, P., Martin-Aragon, S., Benedi, J., Susin, C., Felici, E., Gil, P., Ribera, J. M. and Villar, A. M. (2008) 'Differences of peripheral inflammatory markers between mild cognitive impairment and Alzheimer's disease', *Immunol Lett,* 117(2), pp. 198-202.
9. Bertram, L. and Tanzi, R. E. (2005) 'The genetic epidemiology of neurodegenerative disease', *J Clin Invest,* 115(6), pp. 1449-57.
10. Bertram, L., Lill, C. M. and Tanzi, R. E. (2010) 'The genetics of Alzheimer disease: back to the future', *Neuron,* 68(2), pp. 270-81.
11. Bird, T. D. (2008) 'Genetic aspects of Alzheimer disease', *Genet Med,* 10(4), pp. 231-9.

12. Birks, J. S. and Harvey, R. J. (2018) 'Donepezil for dementia due to Alzheimer's disease', *Cochrane Database Syst Rev,* 6, pp. Cd001190.
13. Blasko, I., Stampfer-Kountchev, M., Robatscher, P., Veerhuis, R., Eikelenboom, P. and Grubeck-Loebenstein, B. (2004) 'How chronic inflammation can affect the brain and support the development of Alzheimer's disease in old age: the role of microglia and astrocytes', *Aging Cell,* 3(4), pp. 169-76.
14. Bonifati, D. M. and Kishore, U. (2007) 'Role of complement in neurodegeneration and neuroinflammation', *Mol Immunol,* 44(5), pp. 999-1010.
15. Botto, M. and Walport, M. J. (2002) 'C1q, autoimmunity and apoptosis', *Immunobiology,* 205(4-5), pp. 395-406.
16. Botto, M., Dell'Agnola, C., Bygrave, A. E., Thompson, E. M., Cook, H. T., Petry, F., Loos, M., Pandolfi, P. P. and Walport, M. J. (1998) 'Homozygous C1q deficiency causes glomerulonephritis associated with multiple apoptotic bodies', *Nat Genet,* 19(1), pp. 56-9.
17. Bourgeat, P., Chetelat, G., Villemagne, V. L., Fripp, J., Raniga, P., Pike, K., Acosta, O., Szoeke, C., Ourselin, S., Ames, D., Ellis, K. A., Martins, R. N., Masters, C. L., Rowe, C. C. and Salvado, O. (2010) 'Beta-amyloid burden in the temporal neocortex is related to hippocampal atrophy in elderly subjects without dementia', *Neurology,* 74(2), pp. 121-7.
18. Bowen, D. M., Smith, C. B., White, P. and Davison, A. N. (1976) 'Neurotransmitter-related enzymes and indices of hypoxia in senile dementia and other abiotrophies', *Brain,* 99(3), pp. 459-96.
19. Braak, H. and Braak, E. (1991) 'Neuropathological stageing of Alzheimer-related changes', *Acta Neuropathol,* 82(4), pp. 239-59.
20. Breitner, J. C., Haneuse, S. J., Walker, R., Dublin, S., Crane, P. K., Gray, S. L. and Larson, E. B. (2009) 'Risk of dementia and AD with prior exposure to NSAIDs in an elderly community-based cohort', *Neurology,* 72(22), pp. 1899-905.
21. Brinkmann, B. G., Agarwal, A., Sereda, M. W., Garratt, A. N., Muller, T., Wende, H., Stassart, R. M., Nawaz, S., Humml, C., Velanac, V., Radyushkin, K., Goebbels, S., Fischer, T. M., Franklin, R. J., Lai, C., Ehrenreich, H., Birchmeier, C., Schwab, M. H. and Nave, K. A. (2008) 'Neuregulin-1/ErbB signaling serves distinct functions in myelination of the peripheral and central nervous system', *Neuron,* 59(4), pp. 581-95.
22. Brookmeyer, R., Corrada, M. M., Curriero, F. C. and Kawas, C. (2002) 'Survival following a diagnosis of Alzheimer disease', *Arch Neurol,* 59(11), pp. 1764-7.
23. Brookmeyer, R., Johnson, E., Ziegler-Graham, K. and Arrighi, H. M. (2007) 'Forecasting the global burden of Alzheimer's disease', *Alzheimers Dement,* 3(3), pp. 186-91.

24. Bruggink, K. A., Muller, M., Kuiperij, H. B. and Verbeek, M. M. (2012) 'Methods for analysis of amyloid-beta aggregates', *J Alzheimers Dis,* 28(4), pp. 735-58.
25. Bushong, E. A., Martone, M. E., Jones, Y. Z. and Ellisman, M. H. (2002) 'Protoplasmic astrocytes in CA1 stratum radiatum occupy separate anatomical domains', *J Neurosci,* 22(1), pp. 183-92.
26. Cadman, E. D. and Puttfarcken, P. S. (1997) 'Beta-amyloid peptides initiate the complement cascade without producing a comparable effect on the terminal pathway in vitro', *Exp Neurol,* 146(2), pp. 388-94.
27. Castellano, J. M., Kim, J., Stewart, F. R., Jiang, H., DeMattos, R. B., Patterson, B. W., Fagan, A. M., Morris, J. C., Mawuenyega, K. G., Cruchaga, C., Goate, A. M., Bales, K. R., Paul, S. M., Bateman, R. J. and Holtzman, D. M. (2011) 'Human apoE isoforms differentially regulate brain amyloid-beta peptide clearance', *Sci Transl Med,* 3(89), pp. 89ra57.
28. Chen, Y., Khanna, S., Goodyear, C. S., Park, Y. B., Raz, E., Thiel, S., Gronwall, C., Vas, J., Boyle, D. L., Corr, M., Kono, D. H. and Silverman, G. J. (2009) 'Regulation of dendritic cells and macrophages by an anti-apoptotic cell natural antibody that suppresses TLR responses and inhibits inflammatory arthritis', *J Immunol,* 183(2), pp. 1346-59.
29. Cirrito, J. R., Deane, R., Fagan, A. M., Spinner, M. L., Parsadanian, M., Finn, M. B., Jiang, H., Prior, J. L., Sagare, A., Bales, K. R., Paul, S. M., Zlokovic, B. V., Piwnica-Worms, D. and Holtzman, D. M. (2005) 'P-glycoprotein deficiency at the blood-brain barrier increases amyloid- beta deposition in an Alzheimer disease mouse model', *J Clin Invest,* 115(11), pp. 3285-90.
30. Citron, M. (2002) 'Emerging Alzheimer's disease therapies: inhibition of beta-secretase', *Neurobiol Aging,* 23(6), pp. 1017-22.
31. Clarke, L. E. and Barres, B. A. (2013) 'Glia keep synapse distribution under wraps', *Cell,* 154(2), pp. 267-8.
32. Corder, E. H., Saunders, A. M., Strittmatter, W. J., Schmechel, D. E., Gaskell, P. C., Small, G. W., Roses, A. D., Haines, J. L. and Pericak-Vance, M. A. (1993) 'Gene dose of apolipoprotein E type 4 allele and the risk of Alzheimer's disease in late onset families', *Science,* 261(5123), pp. 921-3.
33. Crews, L. and Masliah, E. (2010) 'Molecular mechanisms of neurodegeneration in Alzheimer's disease', *Hum Mol Genet,* 19(R1), pp. R12-20.
34. Cummings, J. L., Cohen, S., van Dyck, C. H., Brody, M., Curtis, C., Cho, W., Ward, M., Friesenhahn, M., Rabe, C., Brunstein, F., Quartino, A., Honigberg, L. A., Fuji, R. N., Clayton, D., Mortensen, D., Ho, C. and Paul, R. (2018) 'ABBY: A phase 2 randomized trial of crenezumab in mild to moderate Alzheimer disease', *Neurology,* 90(21), pp. e1889-e1897.
35. Cummings, J., Lai, T. J., Hemrungrojn, S., Mohandas, E., Yun Kim, S., Nair, G. and Dash, A. (2016) 'Role of Donepezil in the Management of

Neuropsychiatric Symptoms in Alzheimer's Disease and Dementia with Lewy Bodies', *CNS Neurosci Ther,* 22(3), pp. 159-66.
36. Davoust, N., Jones, J., Stahel, P. F., Ames, R. S. and Barnum, S. R. (1999) 'Receptor for the C3a anaphylatoxin is expressed by neurons and glial cells', *Glia,* 26(3), pp. 201-11.
37. Deane, R., Du Yan, S., Submamaryan, R. K., LaRue, B., Jovanovic, S., Hogg, E., Welch, D., Manness, L., Lin, C., Yu, J., Zhu, H., Ghiso, J., Frangione, B., Stern, A., Schmidt, A. M., Armstrong, D. L., Arnold, B., Liliensiek, B., Nawroth, P., Hofman, F., Kindy, M., Stern, D. and Zlokovic, B. (2003) 'RAGE mediates amyloid-beta peptide transport across the blood-brain barrier and accumulation in brain', *Nat Med,* 9(7), pp. 907-13.
38. Donahue, J. E., Flaherty, S. L., Johanson, C. E., Duncan, J. A., 3rd, Silverberg, G. D., Miller, M. C., Tavares, R., Yang, W., Wu, Q., Sabo, E., Hovanesian, V. and Stopa, E. G. (2006) 'RAGE, LRP-1, and amyloid-beta protein in Alzheimer's disease', *Acta Neuropathol,* 112(4), pp. 405-15.
39. Drachman, D. A. and Leavitt, J. (1974) 'Human memory and the cholinergic system. A relationship to aging?', *Arch Neurol,* 30(2), pp. 113-21.
40. Edbauer, D., Winkler, E., Regula, J. T., Pesold, B., Steiner, H. and Haass, C. (2003) 'Reconstitution of gamma-secretase activity', *Nat Cell Biol,* 5(5), pp. 486-8.
41. Edison, P., Archer, H. A., Hinz, R., Hammers, A., Pavese, N., Tai, Y. F., Hotton, G., Cutler, D., Fox, N., Kennedy, A., Rossor, M. and Brooks, D. J. (2007) 'Amyloid, hypometabolism, and cognition in Alzheimer disease: an [11C]PIB and [18F]FDG PET study', *Neurology,* 68(7), pp. 501-8.
42. Edison, P., Brooks, D. J., Turkheimer, F. E., Archer, H. A. and Hinz, R. (2009) 'Strategies for the generation of parametric images of [11C]PIB with plasma input functions considering discriminations and reproducibility', *Neuroimage,* 48(2), pp. 329-38.
43. Ekdahl, C. T. (2012) 'Microglial activation - tuning and pruning adult neurogenesis', *Front Pharmacol,* 3, pp. 41.
44. Engelhart, M. J., Geerlings, M. I., Meijer, J., Kiliaan, A., Ruitenberg, A., van Swieten, J. C., Stijnen, T., Hofman, A., Witteman, J. C. and Breteler, M. M. (2004) 'Inflammatory proteins in plasma and the risk of dementia: the rotterdam study', *Arch Neurol,* 61(5), pp. 668-72.
45. Engler, H., Forsberg, A., Almkvist, O., Blomquist, G., Larsson, E., Savitcheva, I., Wall, A., Ringheim, A., Langstrom, B. and Nordberg, A. (2006) 'Two-year follow-up of amyloid deposition in patients with Alzheimer's disease', *Brain,* 129(Pt 11), pp. 2856-66.
46. Eriksen, J. L., Sagi, S. A., Smith, T. E., Weggen, S., Das, P., McLendon, D. C., Ozols, V. V., Jessing, K. W., Zavitz, K. H., Koo, E. H. and Golde, T. E. (2003) 'NSAIDs and enantiomers of flurbiprofen target gamma-secretase and lower Abeta 42 in vivo', *J Clin Invest,* 112(3), pp. 440-9.

47. Etminan, M., Gill, S. and Samii, A. (2003) 'Effect of non-steroidal anti-inflammatory drugs on risk of Alzheimer's disease: systematic review and meta-analysis of observational studies', *Bmj,* 327(7407), pp. 128.
48. Fiala, M., Liu, Q. N., Sayre, J., Pop, V., Brahmandam, V., Graves, M. C. and Vinters, H. V. (2002) 'Cyclooxygenase-2-positive macrophages infiltrate the Alzheimer's disease brain and damage the blood-brain barrier', *Eur J Clin Invest,* 32(5), pp. 360-71.
49. Fonseca, M. I., Ager, R. R., Chu, S. H., Yazan, O., Sanderson, S. D., LaFerla, F. M., Taylor, S. M., Woodruff, T. M. and Tenner, A. J. (2009) 'Treatment with a C5aR antagonist decreases pathology and enhances behavioral performance in murine models of Alzheimer's disease', *J Immunol,* 183(2), pp. 1375-83.
50. Fonseca, M. I., Chu, S. H., Berci, A. M., Benoit, M. E., Peters, D. G., Kimura, Y. and Tenner, A. J. (2011) 'Contribution of complement activation pathways to neuropathology differs among mouse models of Alzheimer's disease', *J Neuroinflammation,* 8(1), pp. 4.
51. Fonseca, M. I., Kawas, C. H., Troncoso, J. C. and Tenner, A. J. (2004a) 'Neuronal localization of C1q in preclinical Alzheimer's disease', *Neurobiol Dis,* 15(1), pp. 40-6.
52. Fonseca, M. I., Zhou, J., Botto, M. and Tenner, A. J. (2004b) 'Absence of C1q leads to less neuropathology in transgenic mouse models of Alzheimer's disease', *J Neurosci,* 24(29), pp. 6457-65.
53. Forsberg, A., Engler, H., Almkvist, O., Blomquist, G., Hagman, G., Wall, A., Ringheim, A., Langstrom, B. and Nordberg, A. (2008) 'PET imaging of amyloid deposition in patients with mild cognitive impairment', *Neurobiol Aging,* 29(10), pp. 1456-65.
54. Fraser, D. A., Pisalyaput, K. and Tenner, A. J. (2010) 'C1q enhances microglial clearance of apoptotic neurons and neuronal blebs, and modulates subsequent inflammatory cytokine production', *J Neurochem,* 112(3), pp. 733-43.
55. Gaboriaud, C., Juanhuix, J., Gruez, A., Lacroix, M., Darnault, C., Pignol, D., Verger, D., Fontecilla-Camps, J. C. and Arlaud, G. J. (2003) 'The crystal structure of the globular head of complement protein C1q provides a basis for its versatile recognition properties', *J Biol Chem,* 278(47), pp. 46974-82.
56. Garcia-Osta, A. and Alberini, C. M. (2009) 'Amyloid beta mediates memory formation', *Learn Mem,* 16(4), pp. 267-72.
57. Gasque, P., Dean, Y. D., McGreal, E. P., VanBeek, J. and Morgan, B. P. (2000) 'Complement components of the innate immune system in health and disease in the CNS', *Immunopharmacology,* 49(1-2), pp. 171-86.
58. Giasson, B. I., Lee, V. M. and Trojanowski, J. Q. (2003) 'Interactions of amyloidogenic proteins', *Neuromolecular Med,* 4(1-2), pp. 49-58.
59. Glenner, G. G., Wong, C. W., Quaranta, V. and Eanes, E. D. (1984) 'The amyloid deposits in Alzheimer's disease: their nature and pathogenesis', *Appl Pathol,* 2(6), pp. 357-69.

60. Goate, A., Chartier-Harlin, M. C., Mullan, M., Brown, J., Crawford, F., Fidani, L., Giuffra, L., Haynes, A., Irving, N., James, L. and et al. (1991) 'Segregation of a missense mutation in the amyloid precursor protein gene with familial Alzheimer's disease', *Nature,* 349(6311), pp. 704-6.
61. Golby, A., Silverberg, G., Race, E., Gabrieli, S., O'Shea, J., Knierim, K., Stebbins, G. and Gabrieli, J. (2005) 'Memory encoding in Alzheimer's disease: an fMRI study of explicit and implicit memory', *Brain,* 128(Pt 4), pp. 773-87.
62. Goldin, A., Beckman, J. A., Schmidt, A. M. and Creager, M. A. (2006) 'Advanced glycation end products: sparking the development of diabetic vascular injury', *Circulation,* 114(6), pp. 597-605.
63. Gomez-Isla, T., West, H. L., Rebeck, G. W., Harr, S. D., Growdon, J. H., Locascio, J. J., Perls, T. T., Lipsitz, L. A. and Hyman, B. T. (1996) 'Clinical and pathological correlates of apolipoprotein E epsilon 4 in Alzheimer's disease', *Ann Neurol,* 39(1), pp. 62-70.
64. Grossman, M. and Rhee, J. (2001) 'Cognitive resources during sentence processing in Alzheimer's disease', *Neuropsychologia,* 39(13), pp. 1419-31.
65. Guillot-Sestier, M. V. and Town, T. (2013) 'Innate immunity in Alzheimer's disease: a complex affair', *CNS Neurol Disord Drug Targets,* 12(5), pp. 593-607.
66. Hampel, H., Mesulam, M. M., Cuello, A. C., Farlow, M. R., Giacobini, E., Grossberg, G. T., Khachaturian, A. S., Vergallo, A., Cavedo, E., Snyder, P. J. and Khachaturian, Z. S. (2018) 'The cholinergic system in the pathophysiology and treatment of Alzheimer's disease', *Brain,* 141(7), pp. 1917-1933.
67. Hansson, O., Strom, K., Guner, N., Wierup, N., Sundler, F., Hoglund, P. and Holm, C. (2006) 'Inflammatory response in white adipose tissue in the non-obese hormone- sensitive lipase null mouse model', *J Proteome Res,*5(7), pp. 1701-10.
68. Hardy, J. and Allsop, D. (1991) 'Amyloid deposition as the central event in the aetiology of Alzheimer's disease', *Trends Pharmacol Sci,* 12(10), pp. 383-8.
69. Haughey, N. J. and Mattson, M. P. (2003) 'Alzheimer's amyloid beta-peptide enhances ATP/gap junction-mediated calcium-wave propagation in astrocytes', *Neuromolecular Med,* 3(3), pp. 173-80.
70. Hayden, M. S. and Ghosh, S. (2012) 'NF-kappaB, the first quarter-century: remarkable progress and outstanding questions', *Genes Dev,* 26(3), pp. 203-34.
71. Heneka, M. T., Landreth, G. E. and Hull, M. (2007) 'Drug insight: effects mediated by peroxisome proliferator-activated receptor-gamma in CNS disorders', *Nat Clin Pract Neurol,* 3(9), pp. 496-504.
72. Heneka, M. T., O'Banion, M. K., Terwel, D. and Kummer, M. P. (2010) 'Neuroinflammatory processes in Alzheimer's disease', *J Neural Transm (Vienna),* 117(8), pp. 919-47.

73. Heneka, M. T., Sastre, M., Dumitrescu-Ozimek, L., Dewachter, I., Walter, J., Klockgether, T. and Van Leuven, F. (2005) 'Focal glial activation coincides with increased BACE1 activation and precedes amyloid plaque deposition in APP[V717I] transgenic mice', *J Neuroinflammation,* 2, pp. 22.
74. Heneka, M. T., Wiesinger, H., Dumitrescu-Ozimek, L., Riederer, P., Feinstein, D. L. and Klockgether, T. (2001) 'Neuronal and glial coexpression of argininosuccinate synthetase and inducible nitric oxide synthase in Alzheimer disease', *J Neuropathol Exp Neurol,* 60(9), pp. 906-16.
75. Hernandez, M. X., Jiang, S., Cole, T. A., Chu, S. H., Fonseca, M. I., Fang, M. J., Hohsfield, L. A., Torres, M. D., Green, K. N., Wetsel, R. A., Mortazavi, A. and Tenner, A. J. (2017a) 'Prevention of C5aR1 signaling delays microglial inflammatory polarization, favors clearance pathways and suppresses cognitive loss', *Mol Neurodegener,* 12(1), pp. 66.
76. Hernandez, M. X., Namiranian, P., Nguyen, E., Fonseca, M. I. and Tenner, A. J. (2017b) 'C5a Increases the Injury to Primary Neurons Elicited by Fibrillar Amyloid Beta', *ASN Neuro,* 9(1), pp. 1759091416687871.
77. Ho, L., Purohit, D., Haroutunian, V., Luterman, J. D., Willis, F., Naslund, J., Buxbaum, J. D., Mohs, R. C., Aisen, P. S. and Pasinetti, G. M. (2001) 'Neuronal cyclooxygenase 2 expression in the hippocampal formation as a function of the clinical progression of Alzheimer disease', *Arch Neurol,* 58(3), pp. 487-92.
78. Holmes, C., Cunningham, C., Zotova, E., Woolford, J., Dean, C., Kerr, S., Culliford, D. and Perry, V. H. (2009) 'Systemic inflammation and disease progression in Alzheimer disease', *Neurology,* 73(10), pp. 768-74.
79. https://www.alz.org/espanol/about/brain/10.asp
80. https://www.alz.org/espanol/about/brain/12.asp
81. Huang, Y. and Mucke, L. (2012) 'Alzheimer mechanisms and therapeutic strategies', *Cell,* 148(6), pp. 1204-22.
82. Huber, G., Martin, J. R., Loffler, J. and Moreau, J. L. (1993) 'Involvement of amyloid precursor protein in memory formation in the rat: an indirect antibody approach', *Brain Res,* 603(2), pp. 348-52.
83. Hultman, K., Strickland, S. and Norris, E. H. (2013) 'The APOE varepsilon4/varepsilon4 genotype potentiates vascular fibrin(ogen) deposition in amyloid-laden vessels in the brains of Alzheimer's disease patients', *J Cereb Blood Flow Metab,* 33(8), pp. 1251-8.
84. Iqbal, K., Alonso Adel, C., El-Akkad, E., Gong, C. X., Haque, N., Khatoon, S., Pei, J. J., Tanimukai, H., Tsujio, I., Wang, J. Z. and Grundke-Iqba, I. (2003) 'Alzheimer neurofibrillary degeneration: therapeutic targets and high- throughput assays', *J Mol Neurosci,* 20(3), pp. 425-9.
85. Irani, D. N., Lin, K. I. and Griffin, D. E. (1996) 'Brain-derived gangliosides regulate the cytokine production and proliferation of activated T cells', *J Immunol,* 157(10), pp. 4333-40.
86. Jack, C. R., Jr. (2011) 'Alliance for aging research AD biomarkers work group: structural MRI', *Neurobiol Aging,* 32 Suppl 1, pp. S48-57.

87. Jack, C. R., Jr., Lowe, V. J., Weigand, S. D., Wiste, H. J., Senjem, M. L., Knopman, D. S., Shiung, M. M., Gunter, J. L., Boeve, B. F., Kemp, B. J., Weiner, M. and Petersen, R. C. (2009) 'Serial PIB and MRI in normal, mild cognitive impairment and Alzheimer's disease: implications for sequence of pathological events in Alzheimer's disease', *Brain,* 132(Pt 5), pp. 1355-65.
88. Jack, C. R., Jr., Petersen, R. C., Xu, Y. C., O'Brien, P. C., Smith, G. E., Ivnik, R. J., Boeve, B. F., Waring, S. C., Tangalos, E. G. and Kokmen, E. (1999) 'Prediction of AD with MRI-based hippocampal volume in mild cognitive impairment', *Neurology,* 52(7), pp. 1397-403.
89. Jack, C. R., Jr., Vemuri, P., Wiste, H. J., Weigand, S. D., Aisen, P. S., Trojanowski, J. Q., Shaw, L. M., Bernstein, M. A., Petersen, R. C., Weiner, M. W. and Knopman, D. S. (2011) 'Evidence for ordering of Alzheimer disease biomarkers', *Arch Neurol,* 68(12), pp. 1526-35.
90. Jack, C. R., Jr., Weigand, S. D., Shiung, M. M., Przybelski, S. A., O'Brien, P. C., Gunter, J. L., Knopman, D. S., Boeve, B. F., Smith, G. E. and Petersen, R. C. (2008) 'Atrophy rates accelerate in amnestic mild cognitive impairment', *Neurology,* 70(19 Pt 2), pp. 1740-52.
91. Kamenetz, F., Tomita, T., Hsieh, H., Seabrook, G., Borchelt, D., Iwatsubo, T., Sisodia, S. and Malinow, R. (2003) 'APP processing and synaptic function', *Neuron,* 37(6), pp. 925-37.
92. Kamer, A. R., Craig, R. G., Dasanayake, A. P., Brys, M., Glodzik-Sobanska, L. and de Leon, M. J. (2008) 'Inflammation and Alzheimer's disease: possible role of periodontal diseases', *Alzheimers Dement,* 4(4), pp. 242-50.
93. Kandiah, N., Pai, M. C., Senanarong, V., Looi, I., Ampil, E., Park, K. W., Karanam, A. K. and Christopher, S. (2017) 'Rivastigmine: the advantages of dual inhibition of acetylcholinesterase and butyrylcholinesterase and its role in subcortical vascular dementia and Parkinson's disease dementia', *Clin Interv Aging,* 12, pp. 697-707.
94. Kaneko, H., Kakita, A., Kasuga, K., Nozaki, H., Ishikawa, A., Miyashita, A., Kuwano, R., Ito, G., Iwatsubo, T., Takahashi, H., Nishizawa, M., Onodera, O., Sisodia, S. S. and Ikeuchi, T. (2007) 'Enhanced accumulation of phosphorylated alpha-synuclein and elevated beta-amyloid 42/40 ratio caused by expression of the presenilin-1 deltaT440 mutant associated with familial Lewy body disease and variant Alzheimer's disease', *J Neurosci,*27(48), pp. 13092-7.
95. Kang, D. E., Pietrzik, C. U., Baum, L., Chevallier, N., Merriam, D. E., Kounnas, M. Z., Wagner, S. L., Troncoso, J. C., Kawas, C. H., Katzman, R. and Koo, E. H. (2000) 'Modulation of amyloid beta-protein clearance and Alzheimer's disease susceptibility by the LDL receptor-related protein pathway', *J Clin Invest,* 106(9), pp. 1159-66.
96. Karch, C. M. and Goate, A. M. (2015) 'Alzheimer's disease risk genes and mechanisms of disease pathogenesis', *Biol Psychiatry,* 77(1), pp. 43-51.

97. Karran, E., Mercken, M. and De Strooper, B. (2011) 'The amyloid cascade hypothesis for Alzheimer's disease: an appraisal for the development of therapeutics', *Nat Rev Drug Discov,* 10(9), pp. 698-712.
98. Kemppainen, N. M., Aalto, S., Karrasch, M., Nagren, K., Savisto, N., Oikonen, V., Viitanen, M., Parkkola, R. and Rinne, J. O. (2008) 'Cognitive reserve hypothesis: Pittsburgh Compound B and fluorodeoxyglucose positron emission tomography in relation to education in mild Alzheimer's disease', *Ann Neurol,* 63(1), pp. 112-8.
99. Kerchner, G. A. and Boxer, A. L. (2010) 'Bapineuzumab', *Expert Opin Biol Ther,* 10(7), pp. 1121-30.
100. Kim, J., Castellano, J. M., Jiang, H., Basak, J. M., Parsadanian, M., Pham, V., Mason, S. M., Paul, S. M. and Holtzman, D. M. (2009) 'Overexpression of low-density lipoprotein receptor in the brain markedly inhibits amyloid deposition and increases extracellular A beta clearance', *Neuron,* 64(5), pp. 632-44.
101. Kishi, T., Matsunaga, S., Oya, K., Nomura, I., Ikuta, T. and Iwata, N. (2017) 'Memantine for Alzheimer's Disease: An Updated Systematic Review and Meta- analysis', *J Alzheimers Dis,* 60(2), pp. 401-425.
102. Kishore, U. and Reid, K. B. (1999) 'Modular organization of proteins containing C1q-like globular domain', *Immunopharmacology,* 42(1-3), pp. 15-21.
103. Kishore, U., Gaboriaud, C., Waters, P., Shrive, A.K., Greenhough, T.J., Reid, K.B., Sim, R.B. and Arlaud, G.J. (2004) "C1q and tumor necrosis factor superfamily: modularity and versatility", *Trends in immunology,* vol. 25, no. 10, pp. 551-561.
104. Kishore, U., Ghai, R., Greenhough, T. J., Shrive, A. K., Bonifati, D. M., Gadjeva, M. G., Waters, P., Kojouharova, M. S., Chakraborty, T. and Agrawal, A. (2004) 'Structural and functional anatomy of the globular domain of complement protein C1q', *Immunol Lett,* 95(2), pp. 113-28.
105. Kishore, U., Gupta, S. K., Perdikoulis, M. V., Kojouharova, M. S., Urban, B. C. and Reid, K. B. (2003) 'Modular organization of the carboxyl-terminal, globular head region of human C1q A, B, and C chains', *J Immunol,*171(2), pp. 812-20.
106. Klunk, W. E., Engler, H., Nordberg, A., Wang, Y., Blomqvist, G., Holt, D. P., Bergstrom, M., Savitcheva, I., Huang, G. F., Estrada, S., Ausen, B., Debnath, M. L., Barletta, J., Price, J. C., Sandell, J., Lopresti, B. J., Wall, A., Koivisto, P., Antoni, G., Mathis, C. A. and Langstrom, B. (2004) 'Imaging brain amyloid in Alzheimer's disease with Pittsburgh Compound-B', *Ann Neurol,* 55(3), pp. 306-19.
107. Klunk, W. E., Mathis, C. A., Price, J. C., Lopresti, B. J. and DeKosky, S. T. (2006) 'Two-year follow-up of amyloid deposition in patients with Alzheimer's disease', *Brain,* 129(Pt 11), pp. 2805-7.
108. Krych-Goldberg, M., Moulds, J. M. and Atkinson, J. P. (2002) 'Human complement receptor type 1 (CR1) binds to a major malarial adhesin', *Trends Mol Med,* 8(11), pp. 531-7.

109. Kukar, T. L., Ladd, T. B., Bann, M. A., Fraering, P. C., Narlawar, R., Maharvi, G. M., Healy, B., Chapman, R., Welzel, A. T., Price, R. W., Moore, B., Rangachari, V., Cusack, B., Eriksen, J., Jansen-West, K., Verbeeck, C., Yager, D., Eckman, C., Ye, W., Sagi, S., Cottrell, B. A., Torpey, J., Rosenberry, T. L., Fauq, A., Wolfe, M. S., Schmidt, B., Walsh, D. M., Koo, E. H. and Golde, T. E. (2008) 'Substrate-targeting gamma-secretase modulators', *Nature,* 453(7197), pp. 925-9.
110. Kukar, T., Murphy, M. P., Eriksen, J. L., Sagi, S. A., Weggen, S., Smith, T. E., Ladd, T., Khan, M. A., Kache, R., Beard, J., Dodson, M., Merit, S., Ozols, V. V., Anastasiadis, P. Z., Das, P., Fauq, A., Koo, E. H. and Golde, T. E. (2005) 'Diverse compounds mimic Alzheimer disease-causing mutations by augmenting Abeta42 production', *Nat Med,* 11(5), pp. 545-50.
111. Lacombe, P., Meric, P. and Seylaz, J. (1980) 'Validity of cerebral blood flow measurements obtained with quantitative tracer techniques', *Brain Res,* 203(2), pp. 105-69.
112. Lacombe, P., Sercombe, R., Vaucher, E. and Seylaz, J. (1997) 'Reduced cortical vasodilatory response to stimulation of the nucleus basalis of Meynert in the aged rat and evidence for a control of the cerebral circulation', *Ann N Y Acad Sci,* 826, pp. 410-5.
113. Laudisi, F., Spreafico, R., Evrard, M., Hughes, T. R., Mandriani, B., Kandasamy, M., Morgan, B. P., Sivasankar, B. and Mortellaro, A. (2013) 'Cutting edge: the NLRP3 inflammasome links complement-mediated inflammation and IL-1beta release', *J Immunol,* 191(3), pp. 1006-10.
114. Lee, J. H., Jeong, S. K., Kim, B. C., Park, K. W. and Dash, A. (2015) 'Donepezil across the spectrum of Alzheimer's disease: dose optimization and clinical relevance', *Acta Neurol Scand,* 131(5), pp. 259-67.
115. Levy-Lahad, E., Lahad, A., Wijsman, E. M., Bird, T. D. and Schellenberg, G. D. (1995) 'Apolipoprotein E genotypes and age of onset in early-onset familial Alzheimer's disease', *Ann Neurol,* 38(4), pp. 678-80.
116. Li, Y., Rinne, J. O., Mosconi, L., Pirraglia, E., Rusinek, H., DeSanti, S., Kemppainen, N., Nagren, K., Kim, B. C., Tsui, W. and de Leon, M. J. (2008) 'Regional analysis of FDG and PIB-PET images in normal aging, mild cognitive impairment, and Alzheimer's disease', *Eur J Nucl Med Mol Imaging,* 35(12), pp. 2169-81.
117. Lian, H., Yang, L., Cole, A., Sun, L., Chiang, A. C., Fowler, S. W., Shim, D. J., Rodriguez-Rivera, J., Taglialatela, G., Jankowsky, J. L., Lu, H. C. and Zheng, H. (2015) 'NFkappaB-activated astroglial release of complement C3 compromises neuronal morphology and function associated with Alzheimer's disease', *Neuron,* 85(1), pp. 101-115.
118. Luterman, J. D., Haroutunian, V., Yemul, S., Ho, L., Purohit, D., Aisen, P. S., Mohs, R. and Pasinetti, G. M. (2000) 'Cytokine gene expression as a function of the clinical progression of Alzheimer disease dementia', *Arch Neurol,* 57(8), pp. 1153-60.

119. Maibaum, M. A., Haywood, M. E., Walport, M. J. and Morley, B. J. (2000) 'Lupus susceptibility loci map within regions of BXSB derived from the SB/Le parental strain', *Immunogenetics,* 51(4-5), pp. 370-2.
120. Mangialasche, F., Kivipelto, M., Solomon, A. and Fratiglioni, L. (2012) 'Dementia prevention: current epidemiological evidence and future perspective', *Alzheimers Res Ther,* 4(1), pp. 6.
121. Marques, F., Sousa, J. C., Sousa, N. and Palha, J. A. (2013) 'Blood-brain-barriers in aging and in Alzheimer's disease', *Mol Neurodegener,* 8, pp. 38.
122. Marques, G., Anton, L. C., Barrio, E., Sanchez, A., Ruiz, S., Gavilanes, F. and Vivanco, F. (1993) 'Arginine residues of the globular regions of human C1q involved in the interaction with immunoglobulin G', *J Biol Chem,*268(14), pp. 10393-402.
123. Marsland, A. L., Gianaros, P. J., Abramowitch, S. M., Manuck, S. B. and Hariri, A. R. (2008a) 'Interleukin-6 covaries inversely with hippocampal grey matter volume in middle-aged adults', *Biol Psychiatry,* 64(6), pp. 484-90.
124. Marsland, A. L., Prather, A. A., Petersen, K. L., Cohen, S. and Manuck, S. B. (2008b) 'Antagonistic characteristics are positively associated with inflammatory markers independently of trait negative emotionality', *Brain Behav Immun,* 22(5), pp. 753-61.
125. Mashta, O. (2007) 'Number of people in UK with dementia will more than double by 2050', *Bmj: Vol. 7591.* England, pp. 447.
126. Matarin, M., Salih, D. A., Yasvoina, M., Cummings, D. M., Guelfi, S., Liu, W., Nahaboo Solim, M. A., Moens, T. G., Paublete, R. M., Ali, S. S., Perona, M., Desai, R., Smith, K. J., Latcham, J., Fulleylove, M., Richardson, J. C., Hardy, J. and Edwards, F. A. (2015) 'A genome-wide gene-expression analysis and database in transgenic mice during development of amyloid or tau pathology', *Cell Rep,* 10(4), pp. 633-44.
127. Mayeux, R. and Stern, Y. (2012) 'Epidemiology of Alzheimer disease', *Cold Spring Harb Perspect Med,* 2(8).
128. McGeer, P. L. and McGeer, E. G. (2013) 'The amyloid cascade-inflammatory hypothesis of Alzheimer disease: implications for therapy', *Acta Neuropathol,* 126(4), pp. 479-97.
129. Meda, L., Cassatella, M. A., Szendrei, G. I., Otvos, L., Jr., Baron, P., Villalba, M., Ferrari, D. and Rossi, F. (1995) 'Activation of microglial cells by beta-amyloid protein and interferon- gamma', *Nature,* 374(6523), pp. 647-50.
130. Mesulam, M. (1976) 'A horseradish peroxidase method for the identification of the efferents of acetyl cholinesterase-containing neurons', *J Histochem Cytochem,* 24(12), pp. 1281-5.
131. Mintun, M. A., Larossa, G. N., Sheline, Y. I., Dence, C. S., Lee, S. Y., Mach, R. H., Klunk, W. E., Mathis, C. A., DeKosky, S. T. and Morris, J.

C. (2006) '[11C]PIB in a nondemented population: potential antecedent marker of Alzheimer disease', *Neurology,* 67(3), pp. 446-52.
132. Monk, P. N., Scola, A. M., Madala, P. and Fairlie, D. P. (2007) 'Function, structure and therapeutic potential of complement C5a receptors', *Br J Pharmacol,* 152(4), pp. 429-48.
133. Murphy, E. A., Davis, J. M. and Carmichael, M. D. (2010) 'Immune modulating effects of beta-glucan', *Curr Opin Clin Nutr Metab Care,* 13(6), pp. 656-61.
134. Murphy, K. (2012), "Innate Immunity: The First Lines of Defense", *Janeway's Immunobiology*, Garland Science, Taylor & Francis Group, Abingdon, UK, 8th edition, pp. 37-73.
135. Narita, M., Holtzman, D. M., Schwartz, A. L. and Bu, G. (1997) 'Alpha2-macroglobulin complexes with and mediates the endocytosis of beta- amyloid peptide via cell surface low-density lipoprotein receptor-related protein', *J Neurochem,* 69(5), pp. 1904-11.
136. Navratil, J. S. and Ahearn, J. M. (2001) 'Apoptosis, clearance mechanisms, and the development of systemic lupus erythematosus', *Curr Rheumatol Rep,* 3(3), pp. 191-8.
137. Nayak, A., Ferluga, J., Tsolaki, A. G. and Kishore, U. (2010) 'The non-classical functions of the classical complement pathway recognition subcomponent C1q', *Immunol Lett,* 131(2), pp. 139-50.
138. Niederberger, E. and Geisslinger, G. (2008) 'The IKK-NF-kappaB pathway: a source for novel molecular drug targets in pain therapy?', *Faseb j,* 22(10), pp. 3432-42.
139. Nordberg, A., Rinne, J. O., Kadir, A. and Langstrom, B. (2010) 'The use of PET in Alzheimer disease', *Nat Rev Neurol,* 6(2), pp. 78-87.
140. Nunomura, A., Perry, G., Aliev, G., Hirai, K., Takeda, A., Balraj, E. K., Jones, P. K., Ghanbari, H., Wataya, T., Shimohama, S., Chiba, S., Atwood, C. S., Petersen, R. B. and Smith, M. A. (2001) 'Oxidative damage is the earliest event in Alzheimer disease', *J Neuropathol Exp Neurol,* 60(8), pp. 759-67.
141. Oberheim, N. A., Takano, T., Han, X., He, W., Lin, J. H., Wang, F., Xu, Q., Wyatt, J. D., Pilcher, W., Ojemann, J. G., Ransom, B. R., Goldman, S. A. and Nedergaard, M. (2009) 'Uniquely hominid features of adult human astrocytes', *J Neurosci,* 29(10), pp. 3276-87.
142. Okello, A., Koivunen, J., Edison, P., Archer, H. A., Turkheimer, F. E., Nagren, K., Bullock, R., Walker, Z., Kennedy, A., Fox, N. C., Rossor, M. N., Rinne, J. O. and Brooks, D. J. (2009) 'Conversion of amyloid positive and negative MCI to AD over 3 years: an 11C-PIB PET study', *Neurology,* 73(10), pp. 754-60.
143. Pahl, H. L. (1999) 'Activators and target genes of Rel/NF-kappaB transcription factors', *Oncogene,* 18(49), pp. 6853-66.
144. Pasinetti, G. M. (2001) 'Cyclooxygenase and Alzheimer's disease: implications for preventive initiatives to slow the progression of clinical dementia', *Arch Gerontol Geriatr,* 33(1), pp. 13-28.

145. Petersen, R. C. and Negash, S. (2008) 'Mild cognitive impairment: an overview', *CNS Spectr,* 13(1), pp. 45-53.
146. Petersen, R. C., Doody, R., Kurz, A., Mohs, R. C., Morris, J. C., Rabins, P. V., Ritchie, K., Rossor, M., Thal, L. and Winblad, B. (2001) 'Current concepts in mild cognitive impairment', *Arch Neurol,* 58(12), pp. 1985-92.
147. Petersen, R. C., Smith, G. E., Waring, S. C., Ivnik, R. J., Tangalos, E. G. and Kokmen, E. (1999) 'Mild cognitive impairment: clinical characterization and outcome', *Arch Neurol,* 56(3), pp. 303-8.
148. Petrou, M., Bohnen, N. I., Muller, M. L., Koeppe, R. A., Albin, R. L. and Frey, K. A. (2012) 'Abeta-amyloid deposition in patients with Parkinson disease at risk for development of dementia', *Neurology,* 79(11), pp. 1161-7.
149. Philipson, O., Lord, A., Lalowski, M., Soliymani, R., Baumann, M., Thyberg, J., Bogdanovic, N., Olofsson, T., Tjernberg, L. O., Ingelsson, M., Lannfelt, L., Kalimo, H. and Nilsson, L. N. (2012) 'The Arctic amyloid-beta precursor protein (AbetaPP) mutation results in distinct plaques and accumulation of N- and C-truncated Abeta', *Neurobiol Aging,* 33(5), pp. 1010.e1-13.
150. Plant, L. D., Boyle, J. P., Smith, I. F., Peers, C. and Pearson, H. A. (2003) 'The production of amyloid beta peptide is a critical requirement for the viability of central neurons', *J Neurosci,* 23(13), pp. 5531-5.
151. Pluta, R. (2007) 'Role of ischemic blood-brain barrier on amyloid plaques development in Alzheimer's disease brain', *Curr Neurovasc Res,* 4(2), pp. 121-9.
152. Qiu, C., Kivipelto, M. and von Strauss, E. (2009) 'Epidemiology of Alzheimer's disease: occurrence, determinants, and strategies toward intervention', *Dialogues Clin Neurosci,* 11(2), pp. 111-28.
153. Ramirez-Bermudez, J. (2012) 'Alzheimer's disease: critical notes on the history of a medical concept', *Arch Med Res,* 43(8), pp. 595-9.
154. Ramos-Rodriguez, J. J., Pacheco-Herrero, M., Thyssen, D., Murillo-Carretero, M. I., Berrocoso, E., Spires-Jones, T. L., Bacskai, B. J. and Garcia-Alloza, M. (2013) 'Rapid beta-amyloid deposition and cognitive impairment after cholinergic denervation in APP/PS1 mice', *J Neuropathol Exp Neurol,* 72(4), pp. 272-85.
155. Reitz, C., Brayne, C. and Mayeux, R. (2011) 'Epidemiology of Alzheimer disease', *Nat Rev Neurol,* 7(3), pp. 137-52.
156. Risacher, S. L., McDonald, B. C., Tallman, E. F., West, J. D., Farlow, M. R., Unverzagt, F. W., Gao, S., Boustani, M., Crane, P. K., Petersen, R. C., Jack, C. R., Jr., Jagust, W. J., Aisen, P. S., Weiner, M. W. and Saykin, A. J. (2016) 'Association Between Anticholinergic Medication Use and Cognition, Brain Metabolism, and Brain Atrophy in Cognitively Normal Older Adults', *JAMA Neurol,* 73(6), pp. 721-32.
157. Rogers, J., Li, R., Mastroeni, D., Grover, A., Leonard, B., Ahern, G., Cao, P., Kolody, H., Vedders, L., Kolb, W. P. and Sabbagh, M. (2006)

'Peripheral clearance of amyloid beta peptide by complement C3-dependent adherence to erythrocytes', *Neurobiol Aging,* 27(12), pp. 1733-9.
158. Rohan de Silva, H. A., Jen, A., Wickenden, C., Jen, L. S., Wilkinson, S. L. and Patel, A. J. (1997) 'Cell-specific expression of beta-amyloid precursor protein isoform mRNAs and proteins in neurons and astrocytes', *Brain Res Mol Brain Res,* 47(1-2), pp. 147-56.
159. Roumenina, L. T., Kantardjiev, A. A., Atanasov, B. P., Waters, P., Gadjeva, M., Reid, K. B., Mantovani, A., Kishore, U. and Kojouharova, M. S. (2005) 'Role of Ca2+ in the electrostatic stability and the functional activity of the globular domain of human C1q', *Biochemistry,* 44(43), pp. 14097-109.
160. Sagare, A. P., Bell, R. D., Zhao, Z., Ma, Q., Winkler, E. A., Ramanathan, A. and Zlokovic, B. V. (2013) 'Pericyte loss influences Alzheimer-like neurodegeneration in mice', *Nat Commun,* 4, pp. 2932.
161. Salloway, S., Sperling, R., Fox, N. C., Blennow, K., Klunk, W., Raskind, M., Sabbagh, M., Honig, L. S., Porsteinsson, A. P., Ferris, S., Reichert, M., Ketter, N., Nejadnik, B., Guenzler, V., Miloslavsky, M., Wang, D., Lu, Y., Lull, J., Tudor, I. C., Liu, E., Grundman, M., Yuen, E., Black, R. and Brashear, H. R. (2014) 'Two phase 3 trials of bapineuzumab in mild-to-moderate Alzheimer's disease', *N Engl J Med,* 370(4), pp. 322-33.
162. Sassin, I., Schultz, C., Thal, D. R., Rub, U., Arai, K., Braak, E. and Braak, H. (2000) 'Evolution of Alzheimer's disease-related cytoskeletal changes in the basal nucleus of Meynert', *Acta Neuropathol,* 100(3), pp. 259-69.
163. Sato, A. and Sato, Y. (1990) 'Cerebral cortical vasodilatation in response to stimulation of cholinergic fibres originating in the nucleus basalis of Meynert', *J Auton Nerv Syst,* 30 Suppl, pp. S137-40.
164. Savonenko, A. V., Melnikova, T., Laird, F. M., Stewart, K. A., Price, D. L. and Wong, P. C. (2008) 'Alteration of BACE1-dependent NRG1/ErbB4 signaling and schizophrenia-like phenotypes in BACE1-null mice', *Proc Natl Acad Sci U S A,* 105(14), pp. 5585-90.
165. Schaefer, T. L., Lingrel, J. B., Moseley, A. E., Vorhees, C. V. and Williams, M. T. (2011) 'Targeted mutations in the Na,K-ATPase alpha 2 isoform confer ouabain resistance and result in abnormal behavior in mice', *Synapse,* 65(6), pp. 520-31.
166. Schellenberg, G. D. and Montine, T. J. (2012) 'The genetics and neuropathology of Alzheimer's disease', *Acta Neuropathol,* 124(3), pp. 305-23.
167. Selkoe, D. J. (1996) 'Amyloid beta-protein and the genetics of Alzheimer's disease', *J Biol Chem,* 271(31), pp. 18295-8.
168. Semmler, A., Widmann, C. N., Okulla, T., Urbach, H., Kaiser, M., Widman, G., Mormann, F., Weide, J., Fliessbach, K., Hoeft, A., Jessen, F., Putensen, C. and Heneka, M. T. (2013) 'Persistent cognitive impairment,

hippocampal atrophy and EEG changes in sepsis survivors', *J Neurol Neurosurg Psychiatry,* 84(1), pp. 62-9.
169. Sengillo, J. D., Winkler, E. A., Walker, C. T., Sullivan, J. S., Johnson, M. and Zlokovic, B. V. (2013) 'Deficiency in mural vascular cells coincides with blood-brain barrier disruption in Alzheimer's disease', *Brain Pathol,*23(3), pp. 303-10.
170. Serrano-Pozo, A., Frosch, M. P., Masliah, E. and Hyman, B. T. (2011) 'Neuropathological alterations in Alzheimer disease', *Cold Spring Harb Perspect Med,* 1(1), pp. a006189.
171. Sharma, H. S., Castellani, R. J., Smith, M. A. and Sharma, A. (2012) 'The blood-brain barrier in Alzheimer's disease: novel therapeutic targets and nanodrug delivery', *Int Rev Neurobiol,* 102, pp. 47-90.
172. Shastri, A., Bonifati, D. M. and Kishore, U. (2013) 'Innate immunity and neuroinflammation', *Mediators Inflamm,* 2013, pp. 342931.
173. Sherrington, R., Rogaev, E. I., Liang, Y., Rogaeva, E. A., Levesque, G., Ikeda, M., Chi, H., Lin, C., Li, G., Holman, K., Tsuda, T., Mar, L., Foncin, J. F., Bruni, A. C., Montesi, M. P., Sorbi, S., Rainero, I., Pinessi, L., Nee, L., Chumakov, I., Pollen, D., Brookes, A., Sanseau, P., Polinsky, R. J., Wasco, W., Da Silva, H. A., Haines, J. L., Perkicak-Vance, M. A., Tanzi, R. E., Roses, A. D., Fraser, P. E., Rommens, J. M. and St George-Hyslop, P. H. (1995) 'Cloning of a gene bearing missense mutations in early-onset familial Alzheimer's disease', *Nature,* 375(6534), pp. 754-60.
174. Shibata, M., Yamada, S., Kumar, S. R., Calero, M., Bading, J., Frangione, B., Holtzman, D. M., Miller, C. A., Strickland, D. K., Ghiso, J. and Zlokovic, B. V. (2000) 'Clearance of Alzheimer's amyloid-ss(1-40) peptide from brain by LDL receptor-related protein-1 at the blood-brain barrier', *J Clin Invest,* 106(12), pp. 1489-99.
175. Siemers, E. R., Sundell, K. L., Carlson, C., Case, M., Sethuraman, G., Liu-Seifert, H., Dowsett, S. A., Pontecorvo, M. J., Dean, R. A. and Demattos, R. (2016) 'Phase 3 solanezumab trials: Secondary outcomes in mild Alzheimer's disease patients', *Alzheimers Dement,* 12(2), pp. 110-120.
176. Sim, R. B. and Malhotra, R. (1994) 'Interactions of carbohydrates and lectins with complement', *Biochem Soc Trans,* 22(1), pp. 106-11.
177. Sofroniew, M. V. and Vinters, H. V. (2010) 'Astrocytes: biology and pathology', *Acta Neuropathol,* 119(1), pp. 7-35.
178. Stine, W. B., Jr., Dahlgren, K. N., Krafft, G. A. and LaDu, M. J. (2003) 'In vitro characterization of conditions for amyloid-beta peptide oligomerization and fibrillogenesis', *J Biol Chem,* 278(13), pp. 11612-22.
179. Storck, S. E., Meister, S., Nahrath, J., Meissner, J. N., Schubert, N., Di Spiezio, A., Baches, S., Vandenbroucke, R. E., Bouter, Y., Prikulis, I., Korth, C., Weggen, S., Heimann, A., Schwaninger, M., Bayer, T. A. and Pietrzik, C. U. (2016) 'Endothelial LRP1 transports amyloid-beta(1-42) across the blood-brain barrier', *J Clin Invest,* 126(1), pp. 123-36.

180. Strle, K., Zhou, J. H., Shen, W. H., Broussard, S. R., Johnson, R. W., Freund, G. G., Dantzer, R. and Kelley, K. W. (2001) 'Interleukin-10 in the brain', *Crit Rev Immunol,* 21(5), pp. 427-49.
181. Tam, J. C., Bidgood, S. R., McEwan, W. A. and James, L. C. (2014) 'Intracellular sensing of complement C3 activates cell autonomous immunity', *Science,* 345(6201), pp. 1256070.
182. Tan, Z. S., Beiser, A., Vasan, R. S., Au, R., Auerbach, S., Kiel, D. P., Wolf, P. A. and Seshadri, S. (2008) 'Thyroid function and the risk of Alzheimer disease: the Framingham Study', *Arch Intern Med,* 168(14), pp. 1514-20.
183. Tenner, A. J. and Fonseca, M. I. (2006) 'The double-edged flower: roles of complement protein C1q in neurodegenerative diseases', *Adv Exp Med Biol,* 586, pp. 153-76.
184. Terry, R. D. and Wisniewski, H. M. (1975) 'Structural and chemical changes of the aged human brain', *Psychopharmacol Bull,* 11(4), pp. 46.
185. Ting, J. T., Kelley, B. G., Lambert, T. J., Cook, D. G. and Sullivan, J. M. (2007) 'Amyloid precursor protein overexpression depresses excitatory transmission through both presynaptic and postsynaptic mechanisms', *Proc Natl Acad Sci U S A,* 104(1), pp. 353-8.
186. Tocco, G., Musleh, W., Sakhi, S., Schreiber, S. S., Baudry, M. and Pasinetti, G. M. (1997) 'Complement and glutamate neurotoxicity. Genotypic influences of C5 in a mouse model of hippocampal neurodegeneration', *Mol Chem Neuropathol,* 31(3), pp. 289-300.
187. Trouw, L. A., Bengtsson, A. A., Gelderman, K. A., Dahlback, B., Sturfelt, G. and Blom, A. M. (2007) 'C4b-binding protein and factor H compensate for the loss of membrane- bound complement inhibitors to protect apoptotic cells against excessive complement attack', *J Biol Chem,* 282(39), pp. 28540-8.
188. Trouw, L. A., Nielsen, H. M., Minthon, L., Londos, E., Landberg, G., Veerhuis, R., Janciauskiene, S. and Blom, A. M. (2008) 'C4b-binding protein in Alzheimer's disease: binding to Abeta1-42 and to dead cells', *Mol Immunol,* 45(13), pp. 3649-60.
189. Uzunhisarcikli, M. and Kalender, Y. (2011) 'Protective effects of vitamins C and E against hepatotoxicity induced by methyl parathion in rats', *Ecotoxicol Environ Saf,* 74(7), pp. 2112-8.
190. Vassar, R. and Citron, M. (2000) 'Abeta-generating enzymes: recent advances in beta- and gamma-secretase research', *Neuron,* 27(3), pp. 419-22.
191. Verghese, P. B., Castellano, J. M., Garai, K., Wang, Y., Jiang, H., Shah, A., Bu, G., Frieden, C. and Holtzman, D. M. (2013) 'ApoE influences amyloid-beta (Abeta) clearance despite minimal apoE/Abeta association in physiological conditions', *Proc Natl Acad Sci U S A,* 110(19), pp. E1807-16.
192. Vlassara, H., Cai, W., Crandall, J., Goldberg, T., Oberstein, R., Dardaine, V., Peppa, M. and Rayfield, E. J. (2002) 'Inflammatory mediators

are induced by dietary glycotoxins, a major risk factor for diabetic angiopathy', *Proc Natl Acad Sci U S A,* 99(24), pp. 15596-601.
193. Weggen, S., Eriksen, J. L., Das, P., Sagi, S. A., Wang, R., Pietrzik, C. U., Findlay, K. A., Smith, T. E., Murphy, M. P., Bulter, T., Kang, D. E., Marquez-Sterling, N., Golde, T. E. and Koo, E. H. (2001) 'A subset of NSAIDs lower amyloidogenic Abeta42 independently of cyclooxygenase activity', *Nature,* 414(6860), pp. 212-6.
194. Winblad, B., Palmer, K., Kivipelto, M., Jelic, V., Fratiglioni, L., Wahlund, L. O., Nordberg, A., Backman, L., Albert, M., Almkvist, O., Arai, H., Basun, H., Blennow, K., de Leon, M., DeCarli, C., Erkinjuntti, T., Giacobini, E., Graff, C., Hardy, J., Jack, C., Jorm, A., Ritchie, K., van Duijn, C., Visser, P. and Petersen, R. C. (2004) 'Mild cognitive impairment--beyond controversies, towards a consensus: report of the International Working Group on Mild Cognitive Impairment', *J Intern Med,* 256(3), pp. 240-6.
195. Wisniewski, H. M. and Wegiel, J. (1991) 'Spatial relationships between astrocytes and classical plaque components', *Neurobiol Aging,* 12(5), pp. 593-600.
196. Wyss-Coray, T., Yan, F., Lin, A. H., Lambris, J. D., Alexander, J. J., Quigg, R. J. and Masliah, E. (2002) 'Prominent neurodegeneration and increased plaque formation in complement- inhibited Alzheimer's mice', *Proc Natl Acad Sci U S A,* 99(16), pp. 10837-42.
197. Xu, Z. Q., Zhang, L. Q., Wang, Q., Marshall, C., Xiao, N., Gao, J. Y., Wu, T., Ding, J., Hu, G. and Xiao, M. (2013) 'Aerobic exercise combined with antioxidative treatment does not counteract moderate- or mid-stage Alzheimer-like pathophysiology of APP/PS1 mice', *CNS Neurosci Ther,* 19(10), pp. 795-803.
198. Yaffe, K., Clemons, T. E., McBee, W. L. and Lindblad, A. S. (2004a) 'Impact of antioxidants, zinc, and copper on cognition in the elderly: a randomized, controlled trial', *Neurology,* 63(9), pp. 1705-7.
199. Yaffe, K., Kanaya, A., Lindquist, K., Simonsick, E. M., Harris, T., Shorr, R. I., Tylavsky, F. A. and Newman, A. B. (2004b) 'The metabolic syndrome, inflammation, and risk of cognitive decline', *Jama,* 292(18), pp. 2237-42.
200. Yamanaka, K., Kakuta, Y., Miyagawa, S., Nakazawa, S., Kato, T., Abe, T., Imamura, R., Okumi, M., Maeda, A., Okuyama, H., Mizuno, M. and Nonomura, N. (2016) 'Depression of Complement Regulatory Factors in Rat and Human Renal Grafts Is Associated with the Progress of Acute T-Cell Mediated Rejection', *PLoS One,* 11(2), pp. e0148881.
201. Yan, P., Hu, X., Song, H., Yin, K., Bateman, R. J., Cirrito, J. R., Xiao, Q., Hsu, F. F., Turk, J. W., Xu, J., Hsu, C. Y., Holtzman, D. M. and Lee, J. M. (2006) 'Matrix metalloproteinase-9 degrades amyloid-beta fibrils in vitro and compact plaques in situ', *J Biol Chem,* 281(34), pp. 24566-74.

202. Yasojima, K., Schwab, C., McGeer, E. G. and McGeer, P. L. (1999) 'Up-regulated production and activation of the complement system in Alzheimer's disease brain', *Am J Pathol,* 154(3), pp. 927-36.
203. Zhang, C. and Saunders, A. J. (2007) 'Therapeutic targeting of the alpha-secretase pathway to treat Alzheimer's disease', *Discov Med,* 7(39), pp. 113-7.
204. Zilka, N. and Novak, M. (2006) 'The tangled story of Alois Alzheimer', *Bratisl Lek Listy,* 107(9-10), pp. 343-5.
205. Zipser, B. D., Johanson, C. E., Gonzalez, L., Berzin, T. M., Tavares, R., Hulette, C. M., Vitek, M. P., Hovanesian, V. and Stopa, E. G. (2007) 'Microvascular injury and blood-brain barrier leakage in Alzheimer's disease', *Neurobiol Aging,* 28(7), pp. 977-86.
206. Zlokovic, B. V., Deane, R., Sagare, A. P., Bell, R. D. and Winkler, E. A. (2010) 'Low-density lipoprotein receptor-related protein-1: a serial clearance homeostatic mechanism controlling Alzheimer's amyloid beta-peptide elimination from the brain', *J Neurochem,* 115(5), pp. 1077-89.

APPENDIX

Raw qPCR data

1. ghA qPCR results

Sample	Target	CT	CT Mean	ΔCT Mean	ΔCT SE	RQ Max	log10 RQ
A-24	B-Actin	14.397	14.422				
A-24	B-Actin	14.411	14.422				
A-24	B-Actin	14.452	14.422				
A-24	B-Actin	14.426	14.422				
A-6	B-Actin	14.342	14.434				
A-6	B-Actin	14.338	14.434				
A-6	B-Actin	14.590	14.434				
A-6	B-Actin	14.466	14.434				
A-3	B-Actin	13.874	13.886				
A-3	B-Actin	13.873	13.886				
A-3	B-Actin	13.912	13.886				
A-3	B-Actin	13.883	13.886				
A-0	B-Actin	13.807	13.819				
A-0	B-Actin	13.913	13.819				
A-0	B-Actin	13.735	13.819				
A-24	IL-18	26.021	26.066	11.644	0.049	1.665	0.2214142
A-24	IL-18	25.962	26.066	11.644	0.049	1.665	0.2214142
A-24	IL-18	26.101	26.066	11.644	0.049	1.665	0.2214142
A-24	IL-18	26.180	26.066	11.644	0.049	1.665	0.2214142
A-3	IL-18	25.959	25.976	12.090	0.022	1.168	0.0674428
A-3	IL-18	25.930	25.976	12.090	0.022	1.168	0.0674428
A-3	IL-18	25.994	25.976	12.090	0.022	1.168	0.0674428
A-3	IL-18	26.021	25.976	12.090	0.022	1.168	0.0674428
A-0	IL-18	26.126	26.078	12.260	0.063	1.118	0.0484418
A-0	IL-18	25.974	26.078	12.260	0.063	1.118	0.0484418
A-0	IL-18	26.120	26.078	12.260	0.063	1.118	0.0484418
A-0	IL-18	26.094	26.078	12.260	0.063	1.118	0.0484418
A-6	IL-18	26.038	26.170	11.736	0.113	1.743	0.2412974
A-6	IL-18	26.045	26.170	11.736	0.113	1.743	0.2412974
A-6	IL-18	26.449	26.170	11.736	0.113	1.743	0.2412974
A-6	IL-18	26.148	26.170	11.736	0.113	1.743	0.2412974
A-6	IL-1B	24.695	24.763	10.329	0.065	0.586	-0.232102
A-6	IL-1B	24.770	24.763	10.329	0.065	0.586	-0.232102
A-6	IL-1B	24.767	24.763	10.329	0.065	0.586	-0.232102
A-6	IL-1B	24.820	24.763	10.329	0.065	0.586	-0.232102
A-3	IL-1B	23.626	23.611	9.726	0.018	0.821	-0.085657

A-3	IL-1B	23.616	23.611	9.726	0.018	0.821	-0.085657
A-3	IL-1B	23.634	23.611	9.726	0.018	0.821	-0.085657
A-3	IL-1B	23.568	23.611	9.726	0.018	0.821	-0.085657
A-0	IL-1B	23.230	23.217	9.399	0.055	1.104	0.0429691
A-0	IL-1B	23.251	23.217	9.399	0.055	1.104	0.0429691
A-0	IL-1B	23.158	23.217	9.399	0.055	1.104	0.0429691
A-0	IL-1B	23.230	23.217	9.399	0.055	1.104	0.0429691
A-24	IL-1B	23.504	23.531	9.109	0.026	1.276	0.1058507
A-24	IL-1B	23.490	23.531	9.109	0.026	1.276	0.1058507
A-24	IL-1B	23.592	23.531	9.109	0.026	1.276	0.1058507
A-24	IL-1B	23.539	23.531	9.109	0.026	1.276	0.1058507
A-6	IL-6	28.291	28.526	14.092	0.102	1.453	0.1622656
A-6	IL-6	28.675	28.526	14.092	0.102	1.453	0.1622656
A-6	IL-6	28.561	28.526	14.092	0.102	1.453	0.1622656
A-6	IL-6	28.578	28.526	14.092	0.102	1.453	0.1622656
A-3	IL-6	27.986	28.062	14.177	0.028	1.209	0.0824263
A-3	IL-6	28.072	28.062	14.177	0.028	1.209	0.0824263
A-3	IL-6	28.081	28.062	14.177	0.028	1.209	0.0824263
A-3	IL-6	28.110	28.062	14.177	0.028	1.209	0.0824263
A-0	IL-6	28.252	28.200	14.381	0.097	1.189	0.0751819
A-0	IL-6	28.408	28.200	14.381	0.097	1.189	0.0751819
A-0	IL-6	28.037	28.200	14.381	0.097	1.189	0.0751819
A-0	IL-6	28.104	28.200	14.381	0.097	1.189	0.0751819
A-24	IL-6	25.652	25.688	11.266	0.035	9.206	0.964071
A-24	IL-6	25.617	25.688	11.266	0.035	9.206	0.964071
A-24	IL-6	25.714	25.688	11.266	0.035	9.206	0.964071
A-24	IL-6	25.768	25.688	11.266	0.035	9.206	0.964071
A-6	TGF-B	21.466	21.448	7.014	0.062	1.361	0.1338581
A-6	TGF-B	21.482	21.448	7.014	0.062	1.361	0.1338581
A-6	TGF-B	21.423	21.448	7.014	0.062	1.361	0.1338581
A-6	TGF-B	21.423	21.448	7.014	0.062	1.361	0.1338581
A-24	TGF-B	21.365	21.475	7.053	0.071	1.346	0.129045
A-24	TGF-B	21.373	21.475	7.053	0.071	1.346	0.129045
A-24	TGF-B	21.663	21.475	7.053	0.071	1.346	0.129045
A-24	TGF-B	21.499	21.475	7.053	0.071	1.346	0.129045
A-3	TGF-B	21.170	21.170	7.285	0.023	1.056	0.0236639
A-3	TGF-B	21.119	21.170	7.285	0.023	1.056	0.0236639
A-3	TGF-B	21.171	21.170	7.285	0.023	1.056	0.0236639
A-3	TGF-B	21.222	21.170	7.285	0.023	1.056	0.0236639
A-0	TGF-B	21.173	21.127	7.308	0.061	1.125	0.0511525
A-0	TGF-B	21.144	21.127	7.308	0.061	1.125	0.0511525
A-0	TGF-B	21.062	21.127	7.308	0.061	1.125	0.0511525

A-0	TGF-B	-	21.127	7.308	0.061	1.125	0.0511525
A-24	TNF-A	21.788	21.829	7.407	0.025	0.477	-0.321482
A-24	TNF-A	21.810	21.829	7.407	0.025	0.477	-0.321482
A-24	TNF-A	21.891	21.829	7.407	0.025	0.477	-0.321482
A-24	TNF-A	21.828	21.829	7.407	0.025	0.477	-0.321482
A-0	TNF-A	20.101	20.096	6.277	0.052	1.098	0.0406024
A-0	TNF-A	20.074	20.096	6.277	0.052	1.098	0.0406024
A-0	TNF-A	20.092	20.096	6.277	0.052	1.098	0.0406024
A-0	TNF-A	20.116	20.096	6.277	0.052	1.098	0.0406024
A-3	TNF-A	20.741	20.786	6.900	0.022	0.673	-0.171985
A-3	TNF-A	20.782	20.786	6.900	0.022	0.673	-0.171985
A-3	TNF-A	20.785	20.786	6.900	0.022	0.673	-0.171985
A-3	TNF-A	20.836	20.786	6.900	0.022	0.673	-0.171985
A-6	TNF-A	21.256	21.285	6.851	0.062	0.747	-0.126679
A-6	TNF-A	21.272	21.285	6.851	0.062	0.747	-0.126679
A-6	TNF-A	21.332	21.285	6.851	0.062	0.747	-0.126679
A-6	TNF-A	21.281	21.285	6.851	0.062	0.747	-0.126679

Sample	Target Name	Cт	Cт Mean	ΔCт Mean	ΔCт SE	RQ	log 10 RQ
A6	B-ACTIN	13.415	13.587				
A6	B-ACTIN	13.759	13.587				
A24	B-ACTIN	14.395	14.352				
A24	B-ACTIN	14.310	14.352				
A3	B-ACTIN	Undetermined	13.028				
A3	B-ACTIN	13.028	13.028				
A0	B-ACTIN	12.928	12.937				
A0	B-ACTIN	12.946	12.937				
A12	B-ACTIN	13.471	13.500				
A12	B-ACTIN	13.529	13.500				
A6	IL-1B	23.601	23.625	10.038	0.174	0.486	-0.3133637
A6	IL-1B	23.649	23.625	10.038	0.174	0.486	-0.3133637
A24	IL-1B	22.779	22.781	8.428	0.043	1.482	0.1708482
A24	IL-1B	22.783	22.781	8.428	0.043	1.482	0.1708482
A3	IL-1B	22.283	22.218	9.190		0.874	-0.0584886
A3	IL-1B	22.153	22.218	9.190		0.874	-0.0584886
A0	IL-1B	21.835	21.933	8.996	0.099	1.000	0
A0	IL-1B	22.031	21.933	8.996	0.099	1.000	0
A12	IL-1B	21.716	21.691	8.191	0.038	1.746	0.24204425
A12	IL-1B	21.667	21.691	8.191	0.038	1.746	0.24204425

A12	IL-6	25.986	25.980	12.480	0.030	4.635	0.66604976
A12	IL-6	25.974	25.980	12.480	0.030	4.635	0.66604976
A3	IL-6	27.385	27.382	14.355		1.264	0.10174709
A3	IL-6	27.380	27.382	14.355		1.264	0.10174709
A0	IL-6	27.652	27.630	14.693	0.024	1.000	0
A0	IL-6	27.608	27.630	14.693	0.024	1.000	0
A24	IL-6	25.937	26.000	11.648	0.076	8.254	0.91666445
A24	IL-6	26.063	26.000	11.648	0.076	8.254	0.91666445
A6	IL-6	28.158	28.230	14.643	0.186	1.035	0.01494034
A6	IL-6	28.302	28.230	14.643	0.186	1.035	0.01494034
A0	TNF ALPHA	19.076	19.020	6.083	0.057	1.000	0
A0	TNF ALPHA	18.964	19.020	6.083	0.057	1.000	0
A3	TNF ALPHA	19.622	19.693	6.666		0.668	-0.1752235
A3	TNF ALPHA	19.765	19.693	6.666		0.668	-0.1752235
A6	TNF ALPHA	20.824	20.644	7.057	0.249	0.509	-0.2932822
A6	TNF ALPHA	20.465	20.644	7.057	0.249	0.509	-0.2932822
A24	TNF ALPHA	21.513	21.517	7.165	0.043	0.472	-0.326058
A24	TNF ALPHA	21.521	21.517	7.165	0.043	0.472	-0.326058
A12	TNF ALPHA	19.746	19.674	6.175	0.077	0.938	-0.0277972
A12	TNF ALPHA	19.603	19.674	6.175	0.077	0.938	-0.0277972

2. ghA[3] qPCR results

Sample	Target	CT	CT Mean	ΔCT Mean	ΔCT SE	RQ	log10 RQ
A3-12	B-Actin	14.094	14.078				
A3-12	B-Actin	14.016	14.078				
A3-12	B-Actin	14.081	14.078				
A3-12	B-Actin	14.120	14.078				
A3-3	B-Actin	13.061	13.122				
A3-3	B-Actin	13.176	13.122				
A3-3	B-Actin	13.157	13.122				
A3-3	B-Actin	13.095	13.122				
A3-6	B-Actin	15.540	15.543				
A3-6	B-Actin	15.517	15.543				
A3-6	B-Actin	15.580	15.543				
A3-6	B-Actin	15.534	15.543				
A3-0	B-Actin	15.104	15.090				
A3-0	B-Actin	15.083	15.090				
A3-0	B-Actin	15.109	15.090				
A3-0	B-Actin	15.067	15.090				
A3-0	IL-18	26.974	27.101	12.011	0.062	1.000	0
A3-0	IL-18	27.172	27.101	12.011	0.062	1.000	0
A3-0	IL-18	27.234	27.101	12.011	0.062	1.000	0
A3-0	IL-18	27.026	27.101	12.011	0.062	1.000	0
A3-6	IL-18	27.292	27.274	11.732	0.015	1.214	0.084219
A3-6	IL-18	27.255	27.274	11.732	0.015	1.214	0.084219
A3-6	IL-18	27.269	27.274	11.732	0.015	1.214	0.084219
A3-6	IL-18	27.281	27.274	11.732	0.015	1.214	0.084219
A3-3	IL-18	25.237	25.170	12.048	0.035	0.975	-0.011
A3-3	IL-18	25.160	25.170	12.048	0.035	0.975	-0.011
A3-3	IL-18	25.148	25.170	12.048	0.035	0.975	-0.011
A3-3	IL-18	25.134	25.170	12.048	0.035	0.975	-0.011
A3-12	IL-18	26.838	26.708	12.630	0.055	0.651	-0.18642
A3-12	IL-18	26.630	26.708	12.630	0.055	0.651	-0.18642
A3-12	IL-18	26.625	26.708	12.630	0.055	0.651	-0.18642
A3-12	IL-18	26.738	26.708	12.630	0.055	0.651	-0.18642
A3-12	IL-1B	21.830	21.856	7.778	0.026	0.280	-0.55284
A3-12	IL-1B	21.887	21.856	7.778	0.026	0.280	-0.55284
A3-12	IL-1B	21.839	21.856	7.778	0.026	0.280	-0.55284
A3-12	IL-1B	21.869	21.856	7.778	0.026	0.280	-0.55284
A3-6	IL-1B	21.569	21.566	6.023	0.014	0.946	-0.02411
A3-6	IL-1B	21.579	21.566	6.023	0.014	0.946	-0.02411

A3-6	IL-1B	21.564	21.566	6.023	0.014	0.946	-0.02411
A3-6	IL-1B	21.553	21.566	6.023	0.014	0.946	-0.02411
A3-3	IL-1B	19.239	19.210	6.088	0.033	0.905	-0.04335
A3-3	IL-1B	19.247	19.210	6.088	0.033	0.905	-0.04335
A3-3	IL-1B	19.188	19.210	6.088	0.033	0.905	-0.04335
A3-3	IL-1B	19.167	19.210	6.088	0.033	0.905	-0.04335
A3-0	IL-1B	21.001	21.034	5.944	0.040	1.000	0
A3-0	IL-1B	20.979	21.034	5.944	0.040	1.000	0
A3-0	IL-1B	21.151	21.034	5.944	0.040	1.000	0
A3-0	IL-1B	21.006	21.034	5.944	0.040	1.000	0
A3-12	IL-6	25.549	25.606	11.528	0.043	0.303	-0.51856
A3-12	IL-6	25.559	25.606	11.528	0.043	0.303	-0.51856
A3-12	IL-6	25.605	25.606	11.528	0.043	0.303	-0.51856
A3-12	IL-6	25.710	25.606	11.528	0.043	0.303	-0.51856
A3-0	IL-6	24.915	24.895	9.804	0.027	1.000	0
A3-0	IL-6	24.955	24.895	9.804	0.027	1.000	0
A3-0	IL-6	24.857	24.895	9.804	0.027	1.000	0
A3-0	IL-6	24.852	24.895	9.804	0.027	1.000	0
A3-6	IL-6	25.965	25.989	10.447	0.029	0.640	-0.19382
A3-6	IL-6	25.967	25.989	10.447	0.029	0.640	-0.19382
A3-6	IL-6	26.067	25.989	10.447	0.029	0.640	-0.19382
A3-6	IL-6	25.958	25.989	10.447	0.029	0.640	-0.19382
A3-3	IL-6	22.618	22.633	9.511	0.034	1.226	0.08849
A3-3	IL-6	22.677	22.633	9.511	0.034	1.226	0.08849
A3-3	IL-6	22.654	22.633	9.511	0.034	1.226	0.08849
A3-3	IL-6	22.583	22.633	9.511	0.034	1.226	0.08849
A3-3	TGF-B	19.955	20.013	6.891	0.044	0.952	-0.02136
A3-3	TGF-B	19.988	20.013	6.891	0.044	0.952	-0.02136
A3-3	TGF-B	20.116	20.013	6.891	0.044	0.952	-0.02136
A3-3	TGF-B	19.993	20.013	6.891	0.044	0.952	-0.02136
A3-6	TGF-B	22.194	22.159	6.617	0.025	1.151	0.061075
A3-6	TGF-B	22.197	22.159	6.617	0.025	1.151	0.061075
A3-6	TGF-B	22.127	22.159	6.617	0.025	1.151	0.061075
A3-6	TGF-B	22.118	22.159	6.617	0.025	1.151	0.061075
A3-12	TGF-B	20.810	20.802	6.724	0.026	1.068	0.028571
A3-12	TGF-B	20.759	20.802	6.724	0.026	1.068	0.028571
A3-12	TGF-B	20.820	20.802	6.724	0.026	1.068	0.028571
A3-12	TGF-B	20.818	20.802	6.724	0.026	1.068	0.028571
A3-0	TGF-B	21.893	21.910	6.819	0.017	1.000	0
A3-0	TGF-B	21.896	21.910	6.819	0.017	1.000	0
A3-0	TGF-B	21.950	21.910	6.819	0.017	1.000	0

A3-0	TGF-B	21.900	21.910	6.819	0.017	1.000	0
A3-6	TNF-A	20.047	20.056	4.514	0.016	0.426	-0.37059
A3-6	TNF-A	20.047	20.056	4.514	0.016	0.426	-0.37059
A3-6	TNF-A	20.050	20.056	4.514	0.016	0.426	-0.37059
A3-6	TNF-A	20.081	20.056	4.514	0.016	0.426	-0.37059
A3-12	TNF-A	19.086	19.084	5.006	0.034	0.303	-0.51856
A3-12	TNF-A	19.150	19.084	5.006	0.034	0.303	-0.51856
A3-12	TNF-A	19.075	19.084	5.006	0.034	0.303	-0.51856
A3-12	TNF-A	19.026	19.084	5.006	0.034	0.303	-0.51856
A3-0	TNF-A	18.339	18.372	3.282	0.030	1.000	0
A3-0	TNF-A	18.339	18.372	3.282	0.030	1.000	0
A3-0	TNF-A	18.353	18.372	3.282	0.030	1.000	0
A3-0	TNF-A	18.458	18.372	3.282	0.030	1.000	0
A3-3	TNF-A	16.648	16.692	3.570	0.039	0.819	-0.08672
A3-3	TNF-A	16.658	16.692	3.570	0.039	0.819	-0.08672
A3-3	TNF-A	16.689	16.692	3.570	0.039	0.819	-0.08672
A3-3	TNF-A	16.775	16.692	3.570	0.039	0.819	-0.08672

3. ghB qPCr results

Sample	Target	Cт	Cт Mean	ΔCт Mean	ΔCт SE	RQ	log10 RQ
B-12	B-Actin	14.252	14.220				
B-12	B-Actin	14.187	14.220				
B-0	B-Actin	13.854	13.921				
B-0	B-Actin	13.989	13.921				
B-6	B-Actin	15.493	15.527				
B-6	B-Actin	15.561	15.527				
B-3	B-Actin	14.164	14.122				
B-3	B-Actin	14.079	14.122				
B-24	B-Actin	14.773	14.633				
B-24	B-Actin	14.494	14.633				
B-6	IL-18	27.752	27.675	12.148	0.084	1.006	0.002598
B-6	IL-18	27.598	27.675	12.148	0.084	1.006	0.002598
B-3	IL-18	26.471	26.406	12.284	0.077	0.916	-0.0381045
B-3	IL-18	26.341	26.406	12.284	0.077	0.916	-0.0381045
B-0	IL-18	26.141	26.078	12.157	0.092	1.000	0
B-0	IL-18	26.016	26.078	12.157	0.092	1.000	0
B-12	IL-18	26.694	26.861	12.641	0.171	0.715	-0.145694
B-12	IL-18	27.029	26.861	12.641	0.171	0.715	-0.145694
B-24	IL-18	26.592	26.702	12.068	0.178	1.063	0.02653325
B-24	IL-18	26.811	26.702	12.068	0.178	1.063	0.02653325
B-24	IL-1B	23.033	23.052	8.419	0.141	1.658	0.21958452
B-24	IL-1B	23.071	23.052	8.419	0.141	1.658	0.21958452
B-0	IL-1B	23.104	23.069	9.148	0.076	1.000	0
B-0	IL-1B	23.034	23.069	9.148	0.076	1.000	0
B-3	IL-1B	24.123	24.125	10.003	0.043	0.553	-0.2572749
B-3	IL-1B	24.127	24.125	10.003	0.043	0.553	-0.2572749
B-12	IL-1B	24.105	24.108	9.888	0.032	0.599	-0.2225732
B-12	IL-1B	24.110	24.108	9.888	0.032	0.599	-0.2225732
B-6	IL-1B	25.707	25.737	10.210	0.046	0.479	-0.3196645
B-6	IL-1B	25.768	25.737	10.210	0.046	0.479	-0.3196645
B-12	IL-6	27.181	27.270	13.050	0.094	2.027	0.30685374
B-12	IL-6	27.358	27.270	13.050	0.094	2.027	0.30685374
B-3	IL-6	28.413	28.195	14.074	0.222	0.997	-0.0013049
B-3	IL-6	27.978	28.195	14.074	0.222	0.997	-0.0013049
B-6	IL-6	28.742	28.700	13.173	0.054	1.861	0.26974636
B-6	IL-6	28.658	28.700	13.173	0.054	1.861	0.26974636
B-0	IL-6	28.006	27.990	14.069	0.070	1.000	0
B-0	IL-6	27.975	27.990	14.069	0.070	1.000	0
B-24	IL-6	24.993	25.007	10.374	0.141	12.953	1.11237037
B-24	IL-6	25.021	25.007	10.374	0.141	12.953	1.11237037
B-6	TGF-B	22.191	22.132	6.605	0.068	1.334	0.12515583

B-6	TGF-B	22.073	22.132	6.605	0.068	1.334	0.12515583
B-24	TGF-B	21.404	21.421	6.788	0.141	1.175	0.07003785
B-24	TGF-B	21.438	21.421	6.788	0.141	1.175	0.07003785
B-3	TGF-B	21.119	21.098	6.977	0.047	1.031	0.01325867
B-3	TGF-B	21.078	21.098	6.977	0.047	1.031	0.01325867
B-0	TGF-B	20.959	20.942	7.021	0.070	1.000	0
B-0	TGF-B	20.926	20.942	7.021	0.070	1.000	0
B-12	TGF-B	20.873	20.893	6.673	0.038	1.273	0.1048284
B-12	TGF-B	20.913	20.893	6.673	0.038	1.273	0.1048284
B-6	TNF-A	22.232	22.250	6.723	0.039	0.715	-0.145694
B-6	TNF-A	22.269	22.250	6.723	0.039	0.715	-0.145694
B-0	TNF-A	20.153	20.160	6.238	0.068	1.000	0
B-0	TNF-A	20.166	20.160	6.238	0.068	1.000	0
B-3	TNF-A	20.696	20.670	6.549	0.050	0.806	-0.093665
B-3	TNF-A	20.645	20.670	6.549	0.050	0.806	-0.093665
B-24	TNF-A	21.708	21.731	7.098	0.142	0.551	-0.2588484
B-24	TNF-A	21.755	21.731	7.098	0.142	0.551	-0.2588484
B-12	TNF-A	21.230	21.240	7.020	0.034	0.582	-0.235077
B-12	TNF-A	21.250	21.240	7.020	0.034	0.582	-0.235077

Sample	Target	Cт	Cт Mean	ΔCт Mean	ΔCт SE	RQ	log10 RQ
B-12	B-Actin	14.308	14.171				
B-12	B-Actin	14.186	14.171				
B-12	B-Actin	14.128	14.171				
B-12	B-Actin	14.061	14.171				
B-0	B-Actin	13.526	13.668				
B-0	B-Actin	13.570	13.668				
B-0	B-Actin	13.726	13.668				
B-0	B-Actin	13.851	13.668				
B-6	B-Actin	15.420	15.423				

B-6	B-Actin	15.472	15.423				
B-6	B-Actin	15.366	15.423				
B-6	B-Actin	15.433	15.423				
B-3	B-Actin	13.863	13.985				
B-3	B-Actin	14.048	13.985				
B-3	B-Actin	14.039	13.985				
B-3	B-Actin	13.989	13.985				
B-24	B-Actin	14.194	14.347				
B-24	B-Actin	14.178	14.347				
B-24	B-Actin	14.646	14.347				
B-24	B-Actin	14.368	14.347				
B-6	IL-18	27.895	27.646	12.223	0.110	1.011	0.00475117
B-6	IL-18	27.636	27.646	12.223	0.110	1.011	0.00475117
B-6	IL-18	27.602	27.646	12.223	0.110	1.011	0.00475117
B-6	IL-18	27.450	27.646	12.223	0.110	1.011	0.00475117
B-3	IL-18	26.099	26.230	12.245	0.112	0.995	-0.0021769
B-3	IL-18	26.314	26.230	12.245	0.112	0.995	-0.0021769
B-3	IL-18	26.320	26.230	12.245	0.112	0.995	-0.0021769
B-3	IL-18	26.189	26.230	12.245	0.112	0.995	-0.0021769
B-0	IL-18	25.813	25.907	12.238	0.071	1.000	0
B-0	IL-18	25.933	25.907	12.238	0.071	1.000	0
B-0	IL-18	25.987	25.907	12.238	0.071	1.000	0
B-0	IL-18	25.893	25.907	12.238	0.071	1.000	0
B-12	IL-18	26.640	26.741	12.570	0.160	0.795	-0.0996329
B-12	IL-18	26.873	26.741	12.570	0.160	0.795	-0.0996329
B-12	IL-18	26.544	26.741	12.570	0.160	0.795	-0.0996329
B-12	IL-18	26.905	26.741	12.570	0.160	0.795	-0.0996329
B-24	IL-18	26.165	26.351	12.004	0.126	1.176	0.07040732
B-24	IL-18	26.141	26.351	12.004	0.126	1.176	0.07040732
B-24	IL-18	26.439	26.351	12.004	0.126	1.176	0.07040732
B-24	IL-18	26.659	26.351	12.004	0.126	1.176	0.07040732
B-24	IL-1B	22.616	22.753	8.406	0.099	2.011	0.30341205
B-24	IL-1B	22.602	22.753	8.406	0.099	2.011	0.30341205
B-24	IL-1B	22.876	22.753	8.406	0.099	2.011	0.30341205
B-24	IL-1B	22.917	22.753	8.406	0.099	2.011	0.30341205
B-0	IL-1B	23.420	23.082	9.414	0.132	1.000	0
B-0	IL-1B	23.077	23.082	9.414	0.132	1.000	0
B-0	IL-1B	22.950	23.082	9.414	0.132	1.000	0
B-0	IL-1B	22.881	23.082	9.414	0.132	1.000	0
B-3	IL-1B	24.194	24.022	10.038	0.108	0.649	-0.1877553
B-3	IL-1B	23.956	24.022	10.038	0.108	0.649	-0.1877553
B-3	IL-1B	23.967	24.022	10.038	0.108	0.649	-0.1877553
B-3	IL-1B	23.973	24.022	10.038	0.108	0.649	-0.1877553
B-12	IL-1B	24.140	24.014	9.843	0.066	0.743	-0.1290112
B-12	IL-1B	24.014	24.014	9.843	0.066	0.743	-0.1290112

B-12	IL-1B	23.947	24.014	9.843	0.066	0.743	-0.1290112
B-12	IL-1B	23.955	24.014	9.843	0.066	0.743	-0.1290112
B-6	IL-1B	25.755	25.641	10.218	0.039	0.573	-0.2418454
B-6	IL-1B	25.727	25.641	10.218	0.039	0.573	-0.2418454
B-6	IL-1B	25.509	25.641	10.218	0.039	0.573	-0.2418454
B-6	IL-1B	25.574	25.641	10.218	0.039	0.573	-0.2418454
B-12	IL-6	27.411	27.284	13.113	0.102	2.270	0.35602585
B-12	IL-6	27.230	27.284	13.113	0.102	2.270	0.35602585
B-12	IL-6	27.159	27.284	13.113	0.102	2.270	0.35602585
B-12	IL-6	27.336	27.284	13.113	0.102	2.270	0.35602585
B-3	IL-6	28.081	28.091	14.106	0.175	1.141	0.05728566
B-3	IL-6	27.938	28.091	14.106	0.175	1.141	0.05728566
B-3	IL-6	28.388	28.091	14.106	0.175	1.141	0.05728566
B-3	IL-6	27.955	28.091	14.106	0.175	1.141	0.05728566
B-6	IL-6	28.956	28.780	13.357	0.068	1.918	0.2828486
B-6	IL-6	28.806	28.780	13.357	0.068	1.918	0.2828486
B-6	IL-6	28.720	28.780	13.357	0.068	1.918	0.2828486
B-6	IL-6	28.636	28.780	13.357	0.068	1.918	0.2828486
B-0	IL-6	27.974	27.964	14.296	0.049	1.000	0
B-0	IL-6	27.947	27.964	14.296	0.049	1.000	0
B-0	IL-6	27.984	27.964	14.296	0.049	1.000	0
B-0	IL-6	27.952	27.964	14.296	0.049	1.000	0
B-24	IL-6	24.587	24.804	10.457	0.102	14.308	1.15557892
B-24	IL-6	24.658	24.804	10.457	0.102	14.308	1.15557892
B-24	IL-6	24.971	24.804	10.457	0.102	14.308	1.15557892
B-24	IL-6	25.000	24.804	10.457	0.102	14.308	1.15557892
B-6	TGF-B	22.237	22.177	6.754	0.052	1.408	0.14860265
B-6	TGF-B	22.208	22.177	6.754	0.052	1.408	0.14860265
B-6	TGF-B	22.191	22.177	6.754	0.052	1.408	0.14860265
B-6	TGF-B	22.073	22.177	6.754	0.052	1.408	0.14860265
B-24	TGF-B	21.081	21.239	6.893	0.100	1.280	0.10720996
B-24	TGF-B	21.033	21.239	6.893	0.100	1.280	0.10720996
B-24	TGF-B	21.404	21.239	6.893	0.100	1.280	0.10720996
B-24	TGF-B	21.438	21.239	6.893	0.100	1.280	0.10720996
B-3	TGF-B	21.024	21.059	7.074	0.070	1.129	0.05269392
B-3	TGF-B	21.014	21.059	7.074	0.070	1.129	0.05269392
B-3	TGF-B	21.119	21.059	7.074	0.070	1.129	0.05269392
B-3	TGF-B	21.078	21.059	7.074	0.070	1.129	0.05269392
B-0	TGF-B	20.915	20.916	7.248	0.051	1.000	0
B-0	TGF-B	20.866	20.916	7.248	0.051	1.000	0
B-0	TGF-B	20.959	20.916	7.248	0.051	1.000	0

B-0	TGF-B	20.926	20.916	7.248	0.051	1.000	0
B-12	TGF-B	20.979	20.945	6.774	0.053	1.389	0.14270226
B-12	TGF-B	21.016	20.945	6.774	0.053	1.389	0.14270226
B-12	TGF-B	20.873	20.945	6.774	0.053	1.389	0.14270226
B-12	TGF-B	20.913	20.945	6.774	0.053	1.389	0.14270226
B-24	TNF-a	20.855	21.142	6.796	0.105	0.708	-0.1499667
B-24	TNF-a	20.939	21.142	6.796	0.105	0.708	-0.1499667
B-24	TNF-a	21.359	21.142	6.796	0.105	0.708	-0.1499667
B-24	TNF-a	21.416	21.142	6.796	0.105	0.708	-0.1499667
B-3	TNF-a	20.248	20.301	6.316	0.072	0.987	-0.0056829
B-3	TNF-a	20.303	20.301	6.316	0.072	0.987	-0.0056829
B-3	TNF-a	20.344	20.301	6.316	0.072	0.987	-0.0056829
B-3	TNF-a	20.307	20.301	6.316	0.072	0.987	-0.0056829
B-12	TNF-a	21.183	21.067	6.896	0.050	0.660	-0.180456
B-12	TNF-a	21.197	21.067	6.896	0.050	0.660	-0.180456
B-12	TNF-a	20.931	21.067	6.896	0.050	0.660	-0.180456
B-12	TNF-a	20.957	21.067	6.896	0.050	0.660	-0.180456
B-0	TNF-a	20.344	19.966	6.297	0.199	1.000	0
B-0	TNF-a	19.796	19.966	6.297	0.199	1.000	0
B-0	TNF-a	19.855	19.966	6.297	0.199	1.000	0
B-0	TNF-a	19.868	19.966	6.297	0.199	1.000	0
B-6	TNF-a	22.320	22.065	6.642	0.112	0.787	-0.1040253
B-6	TNF-a	22.020	22.065	6.642	0.112	0.787	-0.1040253
B-6	TNF-a	21.936	22.065	6.642	0.112	0.787	-0.1040253
B-6	TNF-a	21.985	22.065	6.642	0.112	0.787	-0.1040253

4. ghB[3] qPCr results

Sample	Target	Cт	Cт Mean	ΔCт Mean	ΔCт SE	RQ
B3-12	IL-18	26.765	26.760	13.292	0.039	0.607
B3-12	IL-18	26.742	26.760	13.292	0.039	0.607
B3-12	IL-18	26.673	26.760	13.292	0.039	0.607
B3-12	IL-18	26.858	26.760	13.292	0.039	0.607
B3-12	IL-1B	22.217	22.197	8.730	0.013	0.244
B3-12	IL-1B	22.164	22.197	8.730	0.013	0.244
B3-12	IL-1B	22.207	22.197	8.730	0.013	0.244
B3-12	IL-1B	22.202	22.197	8.730	0.013	0.244
B3-3	TGF-B	20.722	20.775	7.061	0.044	1.007
B3-3	TGF-B	20.746	20.775	7.061	0.044	1.007
B3-3	TGF-B	20.788	20.775	7.061	0.044	1.007
B3-3	TGF-B	20.844	20.775	7.061	0.044	1.007
B3-3	TNF-Alpha	18.301	18.256	4.541	0.042	0.707
B3-3	TNF-Alpha	18.287	18.256	4.541	0.042	0.707
B3-3	TNF-Alpha	18.202	18.256	4.541	0.042	0.707
B3-3	TNF-Alpha	18.233	18.256	4.541	0.042	0.707
B3-3	IL-1B	21.021	21.014	7.300	0.040	0.659
B3-3	IL-1B	21.064	21.014	7.300	0.040	0.659
B3-3	IL-1B	21.001	21.014	7.300	0.040	0.659
B3-3	IL-1B	20.970	21.014	7.300	0.040	0.659
B3-6	B-Actin	14.358	14.437			
B3-6	B-Actin	14.319	14.437			
B3-6	B-Actin	14.368	14.437			
B3-6	B-Actin	14.703	14.437			
B3-6	TNF-Alpha	20.108	20.103	5.666	0.099	0.325
B3-6	TNF-Alpha	20.047	20.103	5.666	0.099	0.325
B3-6	TNF-Alpha	20.222	20.103	5.666	0.099	0.325
B3-6	TNF-Alpha	20.033	20.103	5.666	0.099	0.325
B3-0	TGF-B	22.118	22.085	7.071	0.034	1.000
B3-0	TGF-B	22.018	22.085	7.071	0.034	1.000
B3-0	TGF-B	22.139	22.085	7.071	0.034	1.000
B3-0	TGF-B	22.066	22.085	7.071	0.034	1.000
B3-0	TNF-Alpha	18.986	19.057	4.042	0.035	1.000
B3-0	TNF-Alpha	19.069	19.057	4.042	0.035	1.000
B3-0	TNF-Alpha	19.049	19.057	4.042	0.035	1.000
B3-0	TNF-Alpha	19.122	19.057	4.042	0.035	1.000
B3-0	B-Actin	15.006	15.015			
B3-0	B-Actin	15.071	15.015			
B3-0	B-Actin	15.007	15.015			
B3-0	B-Actin	14.975	15.015			
B3-6	IL-1B	22.132	22.138	7.701	0.090	0.499
B3-6	IL-1B	22.159	22.138	7.701	0.090	0.499

B3-6	IL-1B	22.150	22.138	7.701	0.090	0.499
B3-6	IL-1B	22.111	22.138	7.701	0.090	0.499
B3-3	B-Actin	13.673	13.714			
B3-3	B-Actin	13.808	13.714			
B3-3	B-Actin	13.727	13.714			
B3-3	B-Actin	13.650	13.714			
B3-12	B-Actin	13.475	13.467			
B3-12	B-Actin	13.474	13.467			
B3-12	B-Actin	13.471	13.467			
B3-12	B-Actin	13.449	13.467			
B3-0	IL-18	27.843	27.586	12.571	0.094	1.000
B3-0	IL-18	27.503	27.586	12.571	0.094	1.000
B3-0	IL-18	27.580	27.586	12.571	0.094	1.000
B3-0	IL-18	27.418	27.586	12.571	0.094	1.000
B3-6	TGF-B	21.368	21.377	6.940	0.089	1.095
B3-6	TGF-B	21.383	21.377	6.940	0.089	1.095
B3-6	TGF-B	21.369	21.377	6.940	0.089	1.095
B3-6	TGF-B	21.388	21.377	6.940	0.089	1.095
B3-6	IL-6	26.704	26.716	12.279	0.090	0.636
B3-6	IL-6	26.686	26.716	12.279	0.090	0.636
B3-6	IL-6	26.738	26.716	12.279	0.090	0.636
B3-6	IL-6	26.738	26.716	12.279	0.090	0.636
B3-12	IL-6	26.498	26.589	13.122	0.047	0.355
B3-12	IL-6	26.554	26.589	13.122	0.047	0.355
B3-12	IL-6	26.584	26.589	13.122	0.047	0.355
B3-12	IL-6	26.719	26.589	13.122	0.047	0.355
B3-0	IL-6	26.746	26.642	11.627	0.041	1.000
B3-0	IL-6	26.634	26.642	11.627	0.041	1.000
B3-0	IL-6	26.605	26.642	11.627	0.041	1.000
B3-0	IL-6	26.583	26.642	11.627	0.041	1.000
B3-0	IL-1B	21.766	21.713	6.698	0.030	1.000
B3-0	IL-1B	21.734	21.713	6.698	0.030	1.000
B3-0	IL-1B	21.670	21.713	6.698	0.030	1.000
B3-0	IL-1B	21.681	21.713	6.698	0.030	1.000
B3-3	IL-6	25.103	25.234	11.519	0.111	1.078
B3-3	IL-6	25.128	25.234	11.519	0.111	1.078
B3-3	IL-6	25.154	25.234	11.519	0.111	1.078
B3-3	IL-6	25.550	25.234	11.519	0.111	1.078
B3-12	TNF-Alpha	19.678	19.719	6.251	0.018	0.216
B3-12	TNF-Alpha	19.706	19.719	6.251	0.018	0.216
B3-12	TNF-Alpha	19.732	19.719	6.251	0.018	0.216
B3-12	TNF-Alpha	19.758	19.719	6.251	0.018	0.216
B3-12	TGF-B	20.490	20.549	7.081	0.027	0.993
B3-12	TGF-B	20.535	20.549	7.081	0.027	0.993
B3-12	TGF-B	20.614	20.549	7.081	0.027	0.993
B3-12	TGF-B	20.556	20.549	7.081	0.027	0.993
B3-6	IL-18	26.886	26.927	12.490	0.092	1.058
B3-6	IL-18	26.892	26.927	12.490	0.092	1.058
B3-6	IL-18	26.986	26.927	12.490	0.092	1.058
B3-6	IL-18	26.945	26.927	12.490	0.092	1.058

B3-3	IL-18	26.180	26.217	12.503	0.050	1.049
B3-3	IL-18	26.262	26.217	12.503	0.050	1.049
B3-3	IL-18	26.135	26.217	12.503	0.050	1.049
B3-3	IL-18	26.291	26.217	12.503	0.050	1.049

5. ghC[3] qPCR results

Sample	Target	Cт	Cт Mean	ΔCт Mean	ΔCт SE	RQ	log10 RQ
C3-6	B-Actin	13.584	13.796				
C3-6	B-Actin	13.655	13.796				
C3-6	B-Actin	13.937	13.796				
C3-6	B-Actin	14.010	13.796				
C3-3	B-Actin	14.477	14.638				
C3-3	B-Actin	14.595	14.638				
C3-3	B-Actin	14.751	14.638				
C3-3	B-Actin	14.728	14.638				
C3-12	B-Actin	14.643	14.664				
C3-12	B-Actin	14.636	14.664				
C3-12	B-Actin	14.725	14.664				
C3-12	B-Actin	14.650	14.664				
C3-0	B-Actin	20.256	20.360				
C3-0	B-Actin	20.198	20.360				
C3-0	B-Actin	20.518	20.360				
C3-0	B-Actin	20.469	20.360				
C3-6	IL-18	25.584	25.705	11.908	0.150	1.916	0.28239551
C3-6	IL-18	25.503	25.705	11.908	0.150	1.916	0.28239551
C3-6	IL-18	25.742	25.705	11.908	0.150	1.916	0.28239551
C3-6	IL-18	25.990	25.705	11.908	0.150	1.916	0.28239551
C3-12	IL-18	27.486	27.611	12.947	0.094	0.932	-0.0305841
C3-12	IL-18	27.526	27.611	12.947	0.094	0.932	-0.0305841
C3-12	IL-18	27.551	27.611	12.947	0.094	0.932	-0.0305841
C3-12	IL-18	27.882	27.611	12.947	0.094	0.932	-0.0305841
C3-3	IL-18	26.953	27.143	12.505	0.136	1.267	0.1027766
C3-3	IL-18	27.054	27.143	12.505	0.136	1.267	0.1027766
C3-3	IL-18	27.069	27.143	12.505	0.136	1.267	0.1027766
C3-3	IL-18	27.496	27.143	12.505	0.136	1.267	0.1027766
C3-0	IL-18	32.488	33.206	12.846	0.458	1.000	0
C3-0	IL-18	32.878	33.206	12.846	0.458	1.000	0
C3-0	IL-18	32.933	33.206	12.846	0.458	1.000	0
C3-0	IL-18	34.527	33.206	12.846	0.458	1.000	0
C3-6	IL-1B	20.834	20.871	7.075	0.106	0.641	-0.193142
C3-6	IL-1B	20.849	20.871	7.075	0.106	0.641	-0.193142
C3-6	IL-1B	20.898	20.871	7.075	0.106	0.641	-0.193142
C3-6	IL-1B	20.902	20.871	7.075	0.106	0.641	-0.193142
C3-3	IL-1B	21.784	21.774	7.136	0.064	0.614	-0.2118316
C3-3	IL-1B	21.752	21.774	7.136	0.064	0.614	-0.2118316
C3-3	IL-1B	21.797	21.774	7.136	0.064	0.614	-0.2118316
C3-3	IL-1B	21.763	21.774	7.136	0.064	0.614	-0.2118316
C3-0	IL-1B	26.672	26.793	6.432	0.101	1.000	0
C3-0	IL-1B	26.746	26.793	6.432	0.101	1.000	0
C3-0	IL-1B	26.783	26.793	6.432	0.101	1.000	0
C3-0	IL-1B	26.970	26.793	6.432	0.101	1.000	0
C3-12	IL-1B	22.833	22.840	8.176	0.027	0.299	-0.5243288
C3-12	IL-1B	22.888	22.840	8.176	0.027	0.299	-0.5243288
C3-12	IL-1B	22.801	22.840	8.176	0.027	0.299	-0.5243288
C3-12	IL-1B	22.839	22.840	8.176	0.027	0.299	-0.5243288
C3-3	IL-6	25.216	25.244	10.606	0.068	1.235	0.09166696
C3-3	IL-6	25.234	25.244	10.606	0.068	1.235	0.09166696
C3-3	IL-6	25.212	25.244	10.606	0.068	1.235	0.09166696

C3-3	IL-6	25.315	25.244	10.606	0.068	1.235	0.09166696
C3-6	IL-6	24.741	24.809	11.012	0.110	0.932	-0.0305841
C3-6	IL-6	24.756	24.809	11.012	0.110	0.932	-0.0305841
C3-6	IL-6	24.870	24.809	11.012	0.110	0.932	-0.0305841
C3-6	IL-6	24.868	24.809	11.012	0.110	0.932	-0.0305841
C3-0	IL-6	31.069	31.272	10.911	0.169	1.000	0
C3-0	IL-6	31.463	31.272	10.911	0.169	1.000	0
C3-0	IL-6	31.587	31.272	10.911	0.169	1.000	0
C3-0	IL-6	30.968	31.272	10.911	0.169	1.000	0
C3-12	IL-6	26.932	26.842	12.178	0.056	0.416	-0.3809067
C3-12	IL-6	26.832	26.842	12.178	0.056	0.416	-0.3809067
C3-12	IL-6	26.905	26.842	12.178	0.056	0.416	-0.3809067
C3-12	IL-6	26.697	26.842	12.178	0.056	0.416	-0.3809067
C3-3	TGF-B	21.901	21.930	7.292	0.072	1.094	0.03901731
C3-3	TGF-B	21.857	21.930	7.292	0.072	1.094	0.03901731
C3-3	TGF-B	21.946	21.930	7.292	0.072	1.094	0.03901731
C3-3	TGF-B	22.017	21.930	7.292	0.072	1.094	0.03901731
C3-0	TGF-B	27.709	27.783	7.423	0.098	1.000	0
C3-0	TGF-B	27.662	27.783	7.423	0.098	1.000	0
C3-0	TGF-B	27.919	27.783	7.423	0.098	1.000	0
C3-0	TGF-B	27.842	27.783	7.423	0.098	1.000	0
C3-6	TGF-B	20.896	20.966	7.169	0.123	1.192	0.07627627
C3-6	TGF-B	20.849	20.966	7.169	0.123	1.192	0.07627627
C3-6	TGF-B	20.975	20.966	7.169	0.123	1.192	0.07627627
C3-6	TGF-B	21.143	20.966	7.169	0.123	1.192	0.07627627
C3-12	TGF-B	21.467	21.531	6.867	0.053	1.469	0.16702179
C3-12	TGF-B	21.430	21.531	6.867	0.053	1.469	0.16702179
C3-12	TGF-B	21.623	21.531	6.867	0.053	1.469	0.16702179
C3-12	TGF-B	21.605	21.531	6.867	0.053	1.469	0.16702179
C3-12	TNF-Alpha	20.419	20.294	5.631	0.060	0.361	-0.4424928
C3-12	TNF-Alpha	20.358	20.294	5.631	0.060	0.361	-0.4424928
C3-12	TNF-Alpha	20.180	20.294	5.631	0.060	0.361	-0.4424928
C3-12	TNF-Alpha	20.220	20.294	5.631	0.060	0.361	-0.4424928
C3-6	TNF-Alpha	18.977	18.909	5.113	0.108	0.516	-0.2873503
C3-6	TNF-Alpha	18.908	18.909	5.113	0.108	0.516	-0.2873503
C3-6	TNF-Alpha	18.831	18.909	5.113	0.108	0.516	-0.2873503
C3-6	TNF-Alpha	18.920	18.909	5.113	0.108	0.516	-0.2873503
C3-0	TNF-Alpha	24.485	24.520	4.159	0.082	1.000	0
C3-0	TNF-Alpha	24.520	24.520	4.159	0.082	1.000	0
C3-0	TNF-Alpha	24.491	24.520	4.159	0.082	1.000	0
C3-0	TNF-Alpha	24.583	24.520	4.159	0.082	1.000	0
C3-3	TNF-Alpha	19.116	19.161	4.523	0.068	0.777	-0.109579

C3-3	TNF-Alpha	19.225	19.161	4.523	0.068	0.777	-0.109579
C3-3	TNF-Alpha	19.138	19.161	4.523	0.068	0.777	-0.109579
C3-3	TNF-Alpha	19.165	19.161	4.523	0.068	0.777	-0.109579

Full-length mouse C1q A chain

ATGGAGACCTCTCAGGGATGGCTGGTGGCCTGTGTGCTGACCATGACCCTAGTATGGACAGTGGCTGAAGA
TGTCTGCCGAGCACCCAACGGGAAGGATGGGGCTCCAGGAAATCCTGGCCGCCCGGGGAGGCCGGGTCTCA
AAGGAGAGAGAGGGGAGCCAGGAGCTGCTGGCATCCGGACTGGTATCCGAGGTTTTAAAGGAGACCCAGGG
GAATCTGGCCCCCCTGGCAAACCTGGCAATGTGGGGCTCCCAGGTCCCAGTGGTCCCCTGGGGGACAGCGG
CCCCCAAGGACTGAAGGGCGTGAAAGGCAATCCAGGCAATATCAGGGACCAGCCCCGGCCAGCTTTCTCAG
CCATTCGGCAGAACCCAATGACGCTTGGCAACGTGGTTATCTTTGACAAGGTCCTCACCAACCAGGAGAGT
CCATACCAGAACCACACGGGTCGCTTCATCTGTGCAGTGCCCGGCTTCTATTACTTCAACTTCCAAGTGAT
CTCCAAGTGGGACCTTTGTCTGTTTATCAAGTCTTCCTCCGGGGGCCAGCCCAGGGATTCCCTGAGTTTCT
CTAACACCAACAACAAGGGGCTCTTTCAGGTGTTAGCAGGGGGCACCGTGCTTCAGCTGCGACGAGGGGAC
GAGGTGTGGATCGAAAAGGACCCCGCAAAGGGTCGCATTTACCAGGGCACTGAAGCCGACAGCATCTTCAG
CGGATTCCTCATTTTCCCCTCGGCCTGA

Full-length C1q B chain

ATGAAGACACAGTGGGGTGAGGTCTGGACACACCTGTTACTGCTGCTTCTAGGTTTTCTCCATGTGTCCT
GGGCCCAAAGCAGCTGCACCGGGCCCCCTGGCATCCCTGGCATCCCTGGGGTCCCTGGGGTTCCTGGCTC
TGATGGCCAACCAGGCACTCCAGGGATAAAGGGGGAGAAAGGGCTCCCTGGACTGGCTGGAGACCTTGGT
GAGTTTGGAGAGAAAGGGGACCCAGGGATCCCTGGGACTCCAGGCAAAGTTGGCCCTAAGGGTCCCGTCG
GCCCTAAGGGTACTCCAGGCCCCTCTGGACCCCGCGGTCCCAAAGGCGATTCTGGGGACTACGGGGCTAC
ACAGAAAGTCGCCTTCTCTGCCCTGAGGACCATCAACAGCCCCTTGCGACCGAACCAGGTCATTCGCTTC
GAAAAGGTGATCACCAACGCGAACGAGAACTATGAGCCACGCAACGGCAAGTTCACCTGCAAGGTGCCTG
GCCTCTACTACTTCACCTATCATGCCAGCTCCCGGGGCAACCTGTGTGTGAATCTCGTTCGTGGCCGCGA
TCGGGACAGCATGCAGAAAGTAGTCACCTTCTGTGACTATGCCCAGAACACCTTCCAGGTGACCACAGGT
GGGGTAGTCTTGAAGCTAGAGCAAGAGGAGGTTGTTCACCTGCAGGCCACAGACAAGAACTCCCTCCTGG
GCATTGAGGGTGCCAACAGCATCTTCACTGGCTTTCTGCTTTTCCCTGACATGGATGCGTAA

Full length C1q C chain

ATGGTCGTTGGACCCAGTTGCCAGCCTCCATGTGGACTTTGCCTGCTGCTGCTGTTTCTTCTGGCCCTAC
CACTCAGGAGCCAGGCCAGCGCTGGCTGCTATGGGATCCCAGGGATGCCAGGCATGCCGGGGGCCCCTGG
GAAGGACGGGCATGATGGACTCCAGGGGCCCAAGGGAGAGCCAGGAATCCCAGCCGTCCCTGGGACCCGA
GGACCCAAGGGTCAGAAGGGCGAGCCTGGCATGCCTGGCCACCGTGGGAAAAATGGCCCCAGGGGGACCT
CAGGGTTGCCAGGGGACCCAGGCCCCAGGGGGCCTCCGGGGGAGCCAGGTGTGGAGGGCCGATACAAACA
GAAGCACCAGTCGGTATTCACAGTCACCCGGCAGACCACCCAGTACCCAGAGGCCAACGCCCTCGTCAGG
TTCAACTCTGTGGTCACCAACCCTCAGGGGCATTACAACCCAAGCACAGGGAAGTTCACCTGTGAAGTGC
CGGGCCTCTACTACTTCGTCTACTACACATCGCATACGGCCAACCTGTGCGTGCACCTGAACCTCAACCT
TGCCAGGGTGGCCAGCTTCTGCGACCACATGTTCAACAGCAAGCAGGTCAGCTCCGGAGGAGTCCTCCTG
CGGCTCCAGAGGGGCGATGAGGTGTGGCTATCAGTCAATGACTACAATGGCATGGTGGGCATAGAGGGCT
CCAACAGCGTCTTCTCTGGTTTCCTACTGTTTCCCGACTAG